High-Order Spatial Discretization Methods for the Shallow Water Equations

by

Anita W. Tam

A thesis submitted in conformity with the requirements
for the degree of Doctor of Philosophy
Graduate Department of Computer Science
University of Toronto

Abstract

High-Order Spatial Discretization Methods for the

Shallow Water Equations

Anita W. Tam

Doctor of Philosophy

Graduate Department of Computer Science

University of Toronto

2001

We present new numerical methods for the shallow water equations on a sphere in spherical coordinates. In our implementation, the equations are discretized in time with the two-level semi-Lagrangian semi-implicit (SLSI) method, and in space on a staggered grid with the quadratic spline Galerkin (QSG) and the optimal quadratic spline collocation (OQSC) methods. When discretized on a uniform spatial grid, the solutions are shown through numerical experiments to be fourth-order in space locally at the nodes and midpoints of the spatial grids, and third-order globally.

We also show that, when applied to a simplified version of the shallow water equations, each of our algorithms yields a neutrally stable solution for the meteorologically significant Rossby waves. Moreover, we demonstrate that the Helmholtz equation associated with the shallow water equations should be derived algebraically rather than analytically in order for the algorithms to be stable with respect to the Rossby waves. These results are verified numerically using Boyd's equatorial wave equations with initial conditions to generate a soliton.

We then analyze the performance of our methods on various staggered grids — the A-, B-, and C-grids. From an eigenvalue analysis of our simplified version of the shallow water equations, we conclude that, when discretized on the C-grid, our algorithms faithfully capture the group velocity of inertia-gravity waves. Our analysis suggests that neither the A- nor B-grids will produce such good results. Our theoretical results are supported by numerical experiments, in which we discretize Boyd's equatorial wave equations using different staggered grids and set the initial conditions for the problem to generate gravitation modes instead of a soliton. With both the A- and B-grids, some waves are observed to travel in the wrong direction, whereas, with the C-grid, gravity waves of all wavelengths propagate in the correct direction.

Acknowledgements

There are so many lucky stars around me that, at times, I am at a loss as to where to begin to count!

I am *extremely* grateful to my supervisors, Professors Christina Christara and Ken Jackson, who, throughout the course of my dissertation, have been supportive and patient, and offered me valuable advice and guidance. When I joined the numerical analysis group three years ago as a PhD candidate, I had forgotten most of what I had learned, or should have learned, in my undergraduate numerical analysis courses. So, even though I was supposed to embark on a doctoral project, I could hardly remember how an ODE solver worked, or what it meant for a matrix to have nonzero eigenvalues. (For the numerically-challenged reader, to a numerical analyst, these two topics are like swimming to a fish.) Christina and Ken helped me out of my predicament with their patience and guidance. Despite their busy schedules, they were, and still are, always available when I needed help (which happened quite often). Christina's work on optimal quadratic spline collocation methods lays the foundation for this project. Ken's strong mathematical background and insights have added much to the strength and quality of this dissertation.

Besides numerical techniques, I have also learned from my supervisors the virtue of being persistent and meticulous. The report I wrote for my depth exam, which is the first technical report required in our doctoral program, was full of inaccuracies and careless mistakes, and it took us half a year of revision after revision for it to take on an acceptable form. Though the process was tedious and at times frustrating, I learned a lot, and (hopefully) my technical writing and research skills have improved since!

I am thankful to Dr. Steve Thomas, who introduced us to the semi-Lagrangian integration method, and kept us informed of ongoing research at NCAR. Steve has been enthusiastic, encouraging, and extremely helpful. He has shared his shallow water code with us, pointed out to me potential pitfalls in various formulations, and helped me understand how the results of my project may be useful to the atmospheric modeling community.

I am also thankful to Professors Wayne Enright, Robert Almgren and Rudi Mathon for serving on my thesis committee and for their comments on the dissertation, and to Professor John Boyd of the University of Michigan for serving as the external examiner on my committee and for his very insightful comments and suggestions.

I am grateful to my parents, without whom the thought of attending graduate school might never have crossed my mind. My father has always stressed the importance of education, and sent me to the best schools, even when it meant additional financial burden for him. As for my mother, I fondly remember how she used to take me to the library and read to me when I was little. After I started school, she checked my homework every day to make sure that it was perfect. Now that my work has become too mathematical for her to comprehend, my mother is still willing to listen, and frequently enquires about my progress.

I am also thankful to my husband, Harold Layton, whose unflagging support and encouragement have made my months of dissertation writing aspirin-free, caffeine-free, and relatively stress-free. Being an academic, he totally understands the obsession one sometimes feels when engaged in a research project, and has never once complained about the long hours I spent in the office. Through his own work, he has inspired in me a desire to strive for excellence. When I am rewarded by research results after weeks of toiling, he shares my joy and excitement. When I feel discouraged, he tells me that every research project has its setbacks, and that even the best scientists feel discouraged at times; and he lets me know that he believes in me. I also wish to thank Harold for introducing LaTeX to me several years ago when I was still an undergraduate.

My two younger siblings, Helen and Eric, are my spring of joy. Helen has been supportive and understanding, as always, while Eric, who is twelve years old at the time of writing, shows his support by asking "So, how was school?" every night when I come home. Even though he was not sure how to pronounce the Greek letter ϕ, he tried to read my thesis, and made the intelligent observation that the shallow water equations must be hard to solve because there are so many variables! It is my possibly biased prediction that my brother will grow up to be a great scientist.

Very warm thanks to my colleagues and friends — Jin Lee, Wayne Hayes, Vincent Gogan — for their support; I give them my best wishes. Special thanks to Francois Pitt, the LaTeX expert in our department, who helped me with many tricky typesetting techniques.

Finally, I could not possibly have completed this thesis if it were not for the helpful staff and excellent facilities at the Department of Computer Science of the University of Toronto. The financial support provided by the Ontario Graduate Scholarships in Science and Technology (OGSST), the Open Doctoral Fellowship, and the University of Toronto Fellowship is gratefully acknowledged.

Contents

List of Tables

List of Figures

Chapter 1

Introduction

Weather prediction is a science with a long history. Its objective is the description and prediction of the behaviour of the atmosphere, ocean water and sea ice. Climate modeling, which predicts statistical meteorological quantities averaged over time and space through simulations, is also important inasmuch as it helps us understand, for example, the mechanisms of atmospheric and oceanic circulation, as well as the effects of technological advancements on the atmosphere. The accuracy of weather prediction and climate modeling depends on many factors, among which are the accuracy with which the state of the atmosphere is known at the initial time, the numerical methods applied, and the resolution used in these methods. Weather prediction computations are known to be very time-consuming. Therefore there is much interest in the scientific community in studying accurate and efficient methods for weather prediction. One way to achieve high accuracy in weather prediction computations is to consider high-order discretization methods.

The spatial discretization schemes that are commonly used in meteorological simulations are finite difference schemes, spectral schemes and finite element schemes. Currently there is some controversy over which of the three approaches is preferable for the integration of weather models. For instance, the model at the National Center for Atmospheric

Research (NCAR) incorporates the spectral transform method [32], while the model developed by the Canadian Meteorological Centre in partnership with the Meteorological Research Branch (CMC-MRB) adopts a variable-resolution cell-integrated finite element scheme [10, 11].

The spectral transform method represents the solution of a problem in spherical coordinates in terms of spherical harmonics. Since the spherical harmonics are the natural representation of the solution of a two-dimensional problem on the sphere, the spectral approach provides a natural solution to a technical aspect of the *pole problem*, which is that some variables may not be well defined at the poles. Also, since the spherical harmonics are eigenfunctions of the Laplacian on the sphere, the semi-implicit Helmholtz problem is relatively trivial to solve in spectral space. Another advantage of the spectral method is that, provided that the solution is sufficiently smooth, the method generates numerical approximations with exponential convergence and thus with accuracy higher than most other methods (e.g., finite-difference methods) for the same spatial resolution.

Although the spectral transform method seems ideal for the spherical domain, it also has some disadvantages. Assuming an optimal solver is applied for the solution of the linear system arising from the Helmholtz problem, the computational cost of finite-difference and finite-element methods applied to the shallow water equations on the sphere increases quadratically with the number of gridpoints in one dimension (i.e., $\mathcal{O}(N^2)$, where N is the number of spatial subintervals in one dimension). However, the cost of performing spectral transforms increases more rapidly. In the case of Fourier transforms in the longitudinal direction, fast Fourier Transforms (FFTs) may be used and their computational cost increases as $\mathcal{O}(N^2 \log(N))$. An efficient method for performing Legendre transforms, analogous to FFTs, has not yet been developed. Thus, the Legendre transforms in the the latitudinal direction are often performed by summation and their costs escalate rapidly with increased resolution. Moreover, the spectral method is formally equivalent to a least squares approximation that minimizes the mean square error over the global domain. This implies that the size of the error is likely to be the same everywhere. This may be a serious disadvantage in more comprehensive atmospheric models for a field, such as water vapour, for which the average value varies greatly over the globe. In the case of water vapour, for example, a small absolute error may be insignificant in equatorial regions, but it may completely alter the character of the field in polar regions [35]. Thus, there is interest in the atmospheric community in developing alternative high-order numerical methods.

In this thesis, we present new numerical methods for the shallow water equations on the sphere in spherical coordinates. The shallow water equations, which describe the inviscid flow of a thin layer of fluid in two dimensions, have been used for many years by the atmospheric modeling community as a vehicle for testing promising numerical methods for solving weather prediction and climate modeling problems. In our implementation, the shallow water equations are discretized in time with the semi-Lagrangian semi-implicit (SLSI) scheme, which allows large timesteps while maintaining stability, and in space on a staggered grid with the quadratic spline Galerkin (QSG) and the two optimal quadratic spline collocation (OQSC) methods. In order to properly capture small-scale energy propagation, staggered grids are employed in the spatial discretization. We extend current work on OQSC and QSG methods to systems of partial differential equations discretized on staggered grids, and then combine these methods with the semi-Lagrangian semi-implicit time integration scheme. We show through numerical experiments that on a uniform spatial grid the resulting errors of the numerical solutions are fourth-order locally at the nodes and midpoints of the grid.

The next chapter contains background material for this work. We present a description of the shallow water equations and their discretization in time with the SLSI method. The rest of the thesis details our contributions. In Chapter 3, we show how a generic weighted residual method can be incorporated into a SLSI scheme, and derive the associated Helmholtz equation. In Chapters 4 and 5, we focus on three weighted residual methods — the QSG and the two OQSC methods — and discuss how these methods should be modified to solve problems discretized on staggered grids. We also derive the procedures with which these methods can be applied to the shallow water equations in conjunction with the SLSI scheme. In Chapter 6, we present numerical results illustrating the convergence behaviour of both methods and compare their efficiency. In Chapter 7, using an eigenvalue analysis, we show that, when applied to a simplified version of the shallow water equations, both methods yield stable and accurate representations of the meteorologically important Rossby waves. Moreover, we demonstrate that the Helmholtz equation associated with the shallow water equations should be derived algebraically rather than analytically in order for the algorithms to be stable with respect to the Rossby waves. These results are supported by our numerical results for Boyd's equatorial soliton test problem. The mathematical analysis and the soliton test problem are done in spherical coordinates. This distinguishes our results from previous work based on Cartesian coordinates. In Chapter 8, we analyze the performance of the methods on various staggered grids when applied to a simplified version of the shallow water equations, and conclude that, when applied to the Arakawa C-type grid, our methods faithfully capture the group velocity of inertia-gravity waves. Our analysis suggests that neither the A- nor the B-grids produce such good results. This conclusion is supported by our numerical results in which we discretize Boyd's equatorial wave equations using the A-, B- and C-grids and set the initial conditions for the problem to generate gravitational modes instead of a soliton. It is generally agreed in the atmospheric modeling community that the C-grid is the most accurate for short gravity waves. However, our literature search indicates that ours is the first detailed analysis of the performance of the three staggering schemes for the shallow water equations. Finally, in Chapter 9, we summarize our results and discuss possible directions for future work.

Chapter 2

The Shallow Water Equations and Time Discretization

2.1 The Shallow Water Equations

The shallow water equations serve well as a testbed for new numerical methods for weather prediction and climate modeling as they contain the essential features of more complete models. For example, both the slowly propagating Rossby modes and the fast-moving gravitational oscillations are present. Let u and v be the wind velocity components in the x- and y-directions, respectively, and ϕ be the geopotential, which is related to the atmospheric pressure. The shallow water equations in Cartesian coordinates are

$$\frac{du}{dt} - fv + \phi_x = 0 \tag{2.1}$$

$$\frac{dv}{dt} + fu + \phi_y = 0 \tag{2.2}$$

$$\frac{d\phi}{dt} + \phi(u_x + v_y) = 0 \tag{2.3}$$

where f is the Coriolis parameter, and the subscripts x and y denote spatial derivatives in the respective directions. The first two equations are derived from Newton's second law of motion, and are commonly known as the *motion equations*. The third equation is the *continuity equation*, which enforces the law of conservation of mass. The Lagrangian derivative is defined by

$$\frac{d}{dt} = \frac{\partial}{\partial t} + u\frac{\partial}{\partial x} + v\frac{\partial}{\partial y} \tag{2.4}$$

Because the Earth is spherical, most global atmospheric models in use today are based on spherical coordinates. To define the equations on the sphere, let λ be longitude, θ be latitude, R be the radius of the Earth, Ω be its rotational speed, and $f = 2\Omega\sin\theta$ be the Coriolis parameter, where R and Ω are assumed to be constant. Redefine $u = R\cos\theta d\lambda/dt$ and $v = Rd\theta/dt$, the curvilinear wind velocity components towards the east and the north, respectively. In spherical coordinates, the shallow water equations take the form

$$\frac{du}{dt} - \left(f + \frac{u\tan\theta}{R}\right)v + \frac{\phi_\lambda}{R\cos\theta} = 0 \tag{2.5}$$

$$\frac{dv}{dt} + \left(f + \frac{u\tan\theta}{R}\right)u + \frac{\phi_\theta}{R} = 0 \tag{2.6}$$

$$\frac{d\phi}{dt} + \frac{\phi}{R\cos\theta}[u_\lambda + (v\cos\theta)_\theta] = 0 \tag{2.7}$$

where the Lagrangian derivative in spherical coordinates is

$$\frac{d}{dt} = \frac{\partial}{\partial t} + \frac{u}{R\cos\theta}\frac{\partial}{\partial\lambda} + \frac{v}{R}\frac{\partial}{\partial\theta} \tag{2.8}$$

and the subscripts λ and θ denote the spatial derivatives in the respective directions. The general development of the shallow water equations can be found in standard texts such as Haltiner [17] and Holton [19]. Since u and v are multi-valued at the poles, we adopt the approach of Côté and Staniforth [13] and compute the components of the so-called *wind images* instead:

$$U \equiv \frac{u\cos\theta}{R}, \qquad V \equiv \frac{v\cos\theta}{R}$$

To this end, we multiply the motion equations (2.5) and (2.6) by $\cos\theta/R$, and rewrite them in terms of U and V as

$$\frac{dU}{dt} - fV + \frac{\phi_\lambda}{R^2} = 0 \tag{2.9}$$

$$\frac{dV}{dt} + fU + \frac{\cos\theta}{R^2}\phi_\theta + \frac{\sin\theta}{\cos^2\theta}(U^2 + V^2) \quad = \quad 0 \tag{2.10}$$

Isolating the nonlinearity of the continuity equation (2.7) in a logarithmic term, and multiplying through by $\cos\theta$, we have

$$\cos\theta \frac{d}{dt}\log\phi + \left[\frac{U_\lambda}{\cos\theta} + V_\theta\right] = 0 \tag{2.11}$$

Along the longitude, U and V are assumed periodic, whereas, at the poles ($\theta = \pm\pi/2$), homogeneous Dirichlet boundary conditions are imposed: $U(\lambda, \pm\pi/2) = V(\lambda, \pm\pi/2) = 0$.

The semi-periodic boundary conditions on ϕ are designed to mimic the behaviour of its spherical harmonic expansions [13]. Along the longitude, ϕ is assumed periodic, while at the poles ϕ has zero derivative. To understand the derivation of the boundary conditions for ϕ at the poles, we expand it in terms of spherical harmonics as

$$\phi(\lambda, \theta) = \sum_{m,n} a_{m,n}(\lambda) P_{m,n}(\sin\theta)$$

The associated Legendre functions $P_{m,n}(\mu)$ are generated from the Legendre polynomials

$$P_n(\mu) = \frac{1}{2^n n!}\frac{d^n}{d\mu^n}\left[(\mu^2 - 1)^n\right]$$

using the relation

$$P_{m,n}(\mu) = \left[\frac{2n+1}{2}\frac{(n-m)!}{(n+m)!}\right]^{\frac{1}{2}} (1-\mu^2)^{\frac{m}{2}} \frac{d^m}{d\mu^m} P_n(\mu)$$

Now note that

$$\begin{aligned} \frac{\partial\phi}{\partial\theta} &= \sum_{m,n} a_{m,n} \frac{\partial P_{m,n}(\sin\theta)}{\partial\sin\theta}\frac{d\sin\theta}{d\theta} \\ &= \sum_{m,n} a_{m,n} \frac{\partial P_{m,n}(\sin\theta)}{\partial\sin\theta}\cos\theta \end{aligned}$$

vanishes at the poles. Therefore, we impose the homogeneous Neumann condition $\partial\phi/\partial\theta = 0$ at $\theta = \pm\pi/2$.

Some of our mathematical analysis in Chapters 4 to 8 is done on the simplified shallow water equations, obtained by linearizing (2.5) to (2.7) and assuming constant values for the coefficient $f + u\tan\theta/R(= f^*)$ associated with the Coriolis terms, for $u(= u^*)$ and $v(= v^*)$ in the Lagrangian derivative, and for the coefficients $\phi(= \Phi^*)$ and $\theta(= \Theta^*)$ associated with the gradient terms. The simplified equations are

$$\frac{du}{dt} - f^* v + \frac{\phi_\lambda}{R\cos\Theta^*} = 0 \tag{2.12}$$

$$\frac{dv}{dt} + f^* u + \frac{\phi_\theta}{R} = 0 \tag{2.13}$$

$$\frac{d\phi}{dt} + \frac{\Phi^*}{R}\left(\frac{u_\lambda}{\cos\Theta^*} + v_\theta\right) = 0 \tag{2.14}$$

where

$$\frac{d}{dt} = \frac{\partial}{\partial t} + \frac{u^*}{R\cos\Theta^*}\frac{\partial}{\partial\lambda} + \frac{v^*}{R}\frac{\partial}{\partial\theta} \tag{2.15}$$

In the associated simplified problem, we use periodic boundary conditions in both the longitudinal and latitudinal directions.

Equations (2.12) to (2.14) can also be obtained by linearizing (2.9) to (2.11), since, with $\cos\Theta^*$ assumed to be constant, U and V are simply constant multiples of u and v.

2.2 Notation for Discretization

Before discussing discretization, we introduce some notation used in this thesis. Let $\psi(\lambda, \theta)$ be an arbitrary function. Throughout, bold letters (e.g. $\boldsymbol{\psi}$) are used for vectors of values of functions, distinguishing them from the original functions (e.g. ψ). A superscript (e.g. ψ^n) indicates the time-level at which the function is evaluated. A subscript I (e.g. ψ_I) denotes the biquadratic spline interpolant of a function, whereas a subscript Δ (e.g. ψ_Δ) indicates the biquadratic spline approximation obtained by the collocation or Galerkin method. We illustrate this notation for the geopotential function ϕ.

$\phi = \phi(\lambda, \theta, t)$ is the geopotential function, which, together with the wind velocity functions u and v, satisfies the original shallow water equations (2.5) to (2.7).

$\phi^n = \phi^n(\lambda, \theta)$ denotes the solution of the time-discretized equations (see Section 2.6) at time t_n and is a function of λ and θ, but not t.

$\phi^n_\Delta = \phi^n_\Delta(\lambda, \theta)$ is the biquadratic spline approximation to $\phi^n(\lambda, \theta)$ by the collocation or Galerkin method. In our formulation, the shallow water equations are discretized first in time, then in space. While ϕ^n satisfies the time-discretized and spatially-continuous equations, ϕ^n_Δ is the solution of the time- and spatially-discretized equations.

$\boldsymbol{\phi^n_\Delta}$ is a vector of values of ϕ^n_Δ, $(\boldsymbol{\phi^n_\Delta})_{i,j} = \phi^n_\Delta(\tau_{\lambda_i}, \tau_{\theta_j})$, evaluated at the midpoints $(\tau_{\lambda_i}, \tau_{\theta_j})$ of the grid associated with the discretization for ϕ.

$\phi^n_I = \phi^n_I(\lambda, \theta)$ is the biquadratic spline interpolant of ϕ^n, used in the mathematical derivation of the optimal quadratic spline collocation method (see Chapter 5).

2.3 The Semi-Lagrangian Scheme

Discretization schemes based on a semi-Lagrangian treatment of advection have generated considerable interest in the past decade for the efficient integration of atmospheric models, since they offer the promise of larger timesteps, with no loss in accuracy, in comparison to the Eulerian-based advection schemes, in which the timestep size is limited by more severe stability restrictions.

In an Eulerian-based advection scheme, the observer stays at a fixed geographical point as the world (or the fluid) evolves around him. This scheme retains the regularity of the mesh as the observer stays fixed, but requires small timesteps in order to maintain stability. In a Lagrangian-based scheme, on the other hand, the observer watches the world evolve while traveling with a fluid particle. This technique is less restricted by stability requirements and allows larger timesteps. However, since the fluid particles move with time, the initially regularly-spaced set of fluid particles usually becomes irregularlyspaced as the system evolves.

The semi-Lagrangian advection scheme attempts to combine the advantages of both schemes — the regularity of the Eulerian scheme and the enhanced stability of the Lagrangian scheme. We briefly describe the semi-Lagrangian method. Consider a simple one-dimensional advection equation in Cartesian coordinates,

$$\frac{dF}{dt} \equiv \frac{\partial F}{\partial t} + w\frac{\partial F}{\partial x} = 0 \tag{2.16}$$

where $w(x,t)$ is a given function representing the wind speed. Let $x(t)$ satisfy the differential equation

$$\frac{dx}{dt} = w(x,t) \tag{2.17}$$

As is well-known, it follows easily from (2.16) and (2.17) that $F(x(t),t)$ is constant along any characteristic $x(t)$ satisfying (2.17).

We assume that the values of F are known at all spatial mesh points x_m at time t_n, where x_m denotes the m-th gridpoint ($x_m \equiv m\Delta x$) and t_n is the n-th time-level ($t_n \equiv n\Delta t$). The objective is to compute F at time $t_{n+1} = t_n + \Delta t$ at the same spatial mesh points. This is done by integrating equation (2.17) backward from the arrival point x_m at time t_{n+1} to the departure point $x_m - \delta x_m^{*n+1}$ at time t_n and taking $F(x_m, t_{n+1}) = F(x_m - \delta x_m^{*n+1}, t_n)$, where δx_m^{*n+1} is the displacement of a fluid particle in the time interval t_n to t_{n+1}.

In Figure 2.1, the exact trajectory $x(t)$ along which the function F is constant is denoted by the solid curve AC, where A and C are the departure and arrival points respectively. The exact trajectory is approximated by the straight dashed line A'BC. In the semi-Lagrangian method, we approximately integrate the advection equation along the approximated fluid trajectory. Equation (2.16) implies that F is approximately constant along A'BC. In other words, if we let δx_m^{n+1} be an approximation to δx_m^{*n+1}, then we have

$$F(x_m, t_{n+1}) \approx F(x_m - \delta x_m^{n+1}, t_n) \tag{2.18}$$

This is a two-level semi-Lagrangian scheme since two time-levels are used to approximate the Lagrangian derivative.

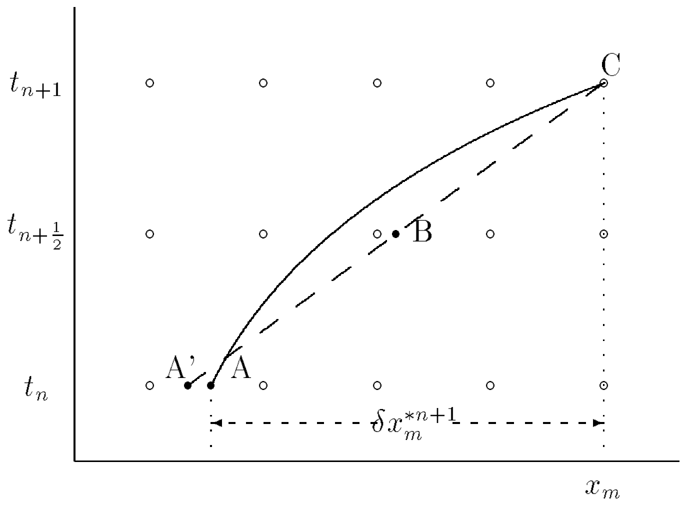

Figure 2.1: An illustration of the semi-Lagrangian method for one-dimensional advection. The solid line is the actual trajectory and the dashed line is the approximate trajectory along which the advection function F is integrated.

From equation (2.18), if we know the value of $F(x_m - \delta x_m^{n+1}, t_n)$, then we have an approximation to $F(x_m, t_{n+1})$. To compute the value of $F(x_m - \delta x_m^{n+1}, t_n)$, we need (a) the approximate displacement δx_m^{n+1}, and (b) if $x_m - \delta x_m^{n+1}$ is not one of the gridpoints, we need to interpolate F between gridpoints.

Since $1/w$ evaluated at the midpoint B of $A'BC$ is roughly the slope of the approximated fluid trajectory, the displacement δx_m^{*n+1} can be approximated by δx_m^{n+1} computed by the midpoint rule:

$$\delta x_m^{n+1} = \Delta t w \left(x_m - \frac{\delta x_m^{n+1}}{2}, t_{n+\frac{1}{2}} \right) \tag{2.19}$$

Equation (2.19) is solved via fixed-point iteration

$$\delta x_m^{n+1,[k]} = \Delta t w \left(x_m - \frac{\delta x_m^{n+1,[k-1]}}{2}, t_{n+\frac{1}{2}} \right) \tag{2.20}$$

using wind speed values from the previous timestep as the initial guess:

$$\delta x_m^{n+1,[0]} = \Delta t w(x_m, t_n) \tag{2.21}$$

When (2.21) is used as the initial guess, two fixed-point iterations (2.20) normally suffice to attain the suitable accuracy.

If the values of w at time-level $t_{n+\frac{1}{2}}$ are not known, then they can be extrapolated from known values at previous timesteps. For example, linear extrapolation gives

$$\boldsymbol{w}^{n+\frac{1}{2}} = \frac{3}{2}\boldsymbol{w}^n - \frac{1}{2}\boldsymbol{w}^{n-1} \tag{2.22}$$

where $\boldsymbol{w}^n$ represents the vector of values of w evaluated at gridpoints at time-level t_n. If $x_m - \delta x_m^{n+1}/2$ is not one of the gridpoints, then spatial interpolation using gridpoint values in $\boldsymbol{w}^{n+\frac{1}{2}}$ is used to approximate $w(x_m - \delta x_m^{n+1}/2, t_{n+\frac{1}{2}})$ between gridpoints.

Once δx_m^{n+1} is known, an approximation to F at the departure point $(x_m - \delta x_m^{n+1}, t_n)$ can be computed by interpolation. Then we set $F(x_m, t_{n+1}) = F(x_m - \delta x_m^{n+1}, t_n)$.

The semi-Lagrangian advection scheme is summarized below.

1. Use extrapolation, such as equation (2.22), to approximate $w(x_m, t_{n+\frac{1}{2}})$ at each gridpoint x_m.

2. Apply the fixed-point iteration (2.20) to solve equation (2.19) iteratively for the displacement δx_m^{n+1}. At the k-th iteration, use spatial interpolation to approximate $w(x_m - \delta x_m^{n+1,[k]}/2, t_{n+\frac{1}{2}})$.

3. If $x_m - \delta x_m^{n+1}$ is not a gridpoint, then use spatial interpolation to approximate $F(x_m - \delta x_m^{n+1}, t_n)$.

4. Set $F(x_m, t_{n+1}) = F(x_m - \delta x_m^{n+1}, t_n)$.

2.4 Trajectory Calculation in Spherical Coordinates

The Eulerian approach of discretizing the shallow water equations on a sphere suffers from the *pole problem* if the gridpoints are distributed evenly over the sphere. Due to the convergence of the meridians near the poles, physical distance between adjacent nodes on the same latitude circle decreases as one moves towards either pole. As a result, the CFL condition becomes far more restrictive near the poles. The semi-Lagrangian semi-implicit method solves this aspect of the pole problem by removing the CFL condition. That is, near either pole, a departure point may be many grid intervals away from its arrival point without causing a stability problem.

However, care should still be taken in computing a trajectory near the poles, where the λ spherical coordinate unit vector varies rapidly in space. In spherical coordinates, a semi-Lagrangian time discretization scheme approximates the Lagrangian derivative (2.8) along particle trajectories defined by the velocity vector with components

$$\frac{d\lambda}{dt} = \frac{u(\lambda,\theta,t)}{R\cos\theta} = \frac{U(\lambda,\theta,t)}{\cos^2\theta}, \quad \frac{d\theta}{dt} = \frac{v(\lambda,\theta,t)}{R} = \frac{V(\lambda,\theta,t)}{\cos\theta} \tag{2.23}$$

If, for instance, in computing the departure points, the midpoint rule (2.19) is used to integrate the velocity equations (2.23), then by expanding $\lambda(t_{n+1})$ and $\lambda(t_n)$ as Taylor's series around $\lambda(t_{n+\frac{1}{2}})$, we can obtain the error of the midpoint rule for the λ-component:

$$\lambda(t_{n+1}) - \lambda(t_n) = \Delta t \lambda'(t_{n+\frac{1}{2}}) + \frac{\Delta t^3}{24}\lambda^{(3)}(t_{n+\frac{1}{2}}) + \mathcal{O}(\Delta t^5) \tag{2.24}$$

The error term may become large near the pole, since it contains the third derivative of λ, which can be obtained by taking the total derivative of the λ-equation in (2.23) twice. The same problem may be encountered in computing the latitudinal component of the departure points. As a result, the assumption that the velocity components at the midpoint of the trajectory represent a good approximation to the flow along the entire trajectory may break down.

This problem can be solved by transforming to another coordinate system when calculating the trajectory. We adopt the approach of Côté and Staniforth [12], and compute the trajectory in three-dimensional Cartesian geometry with the restriction that the trajectory is confined on the surface of the sphere. The algorithm is outlined below.

Consider a sphere of radius R. Let $\vec{r} = (x, y, z)$ be a point on the sphere in a Cartesian frame of reference fixed at the center of the sphere. The Cartesian coordinates x, y and z are related to the spherical coordinates λ and θ by

$$\begin{aligned} x &= R\cos\lambda\cos\theta \\ y &= R\sin\lambda\cos\theta \\ z &= R\sin\theta \end{aligned} \tag{2.25}$$

Let $\dot{\vec{r}} = (\dot{x}, \dot{y}, \dot{z})$ be the wind velocity in Cartesian coordinates. The components of the wind velocity in Cartesian coordinates are related to those in spherical coordinates by

$$\begin{aligned} \dot{x} &= -RU\frac{\sin\lambda}{\cos\theta} - RV\cos\lambda\tan\theta \\ \dot{y} &= RU\frac{\cos\lambda}{\cos\theta} - RV\sin\lambda\tan\theta \\ \dot{z} &= RV \end{aligned} \tag{2.26}$$

Note that, unlike $d\lambda/dt$, which varies rapidly near the poles because of the $\cos\theta$ term in the denominator, none of the velocity components in Cartesian coordinates ($\dot{x}$, $\dot{y}$, or $\dot{z}$) has an "essential" $\cos\theta$ term in the denominator after we have cancelled the "apparent" $\cos\theta$ terms in the denominators with those implicit in the U and V variables. (Recall that $U \equiv u\cos\theta/R$ and $V \equiv v\cos\theta/R$.)

The trajectory is approximated by a geodesic[1] (see Figure 2.2) using the midpoint rule. The general idea is to iteratively compute a midpoint position vector $\vec{r}^0$ from the midpoint velocity $\dot{\vec{r}}^0$, which in turn depends on $\vec{r}^0$. At the end of the iteration, the departure position vector $\vec{\tilde{r}}$ can be computed from $\vec{r}$ and $\vec{r}^0$.

We begin by calculating the Cartesian coordinates x, y and z of each gridpoint $\vec{r}$, given in spherical coordinates, using (2.25). Each midpoint position $\vec{r}^{0,[0]} = (\lambda^{0,[0]}, \theta^{0,[0]})$

[1] A *geodesic* is the shortest line between two points on any mathematically derived surface — a sphere in this case.

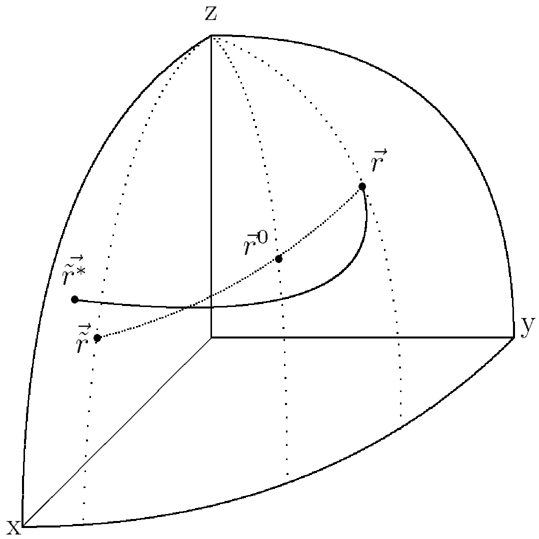

Figure 2.2: The actual trajectory (solid), which starts at $\tilde{\vec{r}}^*$ and ends at $\vec{r}$, is approximated by the geodesic (dotted) that passes through $\tilde{\vec{r}}$ and $\vec{r}$. The midpoint of the geodesic is denoted by $\vec{r}^0$.

is initialized by setting it equal to the associated midpoint position of the previous time-level. Then the midpoint wind image components $U^{n+\frac{1}{2}}(\lambda^{0,[0]}, \theta^{0,[0]})$ and $V^{n+\frac{1}{2}}(\lambda^{0,[0]}, \theta^{0,[0]})$ are also initialized. The wind image components $U^{n+\frac{1}{2}}$ and $V^{n+\frac{1}{2}}$ are first estimated at gridpoints by a linear extrapolation of wind images at time-levels t_n and t_{n-1} as in (2.22), then approximated at the initial midpoint position $(\lambda^{0,[0]}, \theta^{0,[0]})$ through spatial interpolation. At the k-th iteration, the wind velocity

$$\dot{\vec{r}}^{0,[k]} = \dot{\vec{r}}\left(\vec{r}^{0,[k-1]}, t_{n+\frac{1}{2}}\right) \tag{2.27}$$

at the midpoint of the trajectory is computed from $(\lambda^{0,[k-1]}, \theta^{0,[k-1]})$, $U^{n+\frac{1}{2}}(\lambda^{0,[k-1]}, \theta^{0,[k-1]})$ and $V^{n+\frac{1}{2}}(\lambda^{0,[k-1]}, \theta^{0,[k-1]})$ using (2.26). Then the midpoint position vector is calculated by

$$\Theta^{[k]} = \frac{\Delta t|\dot{\vec{r}}^{0,[k]}|}{2R} \tag{2.28}$$

$$\vec{r}^{0,[k]} = \cos\Theta^{[k]}\vec{r} + \sin\Theta^{[k]}\ \vec{r}\times\frac{\vec{r}\times\dot{\vec{r}}^{0,[k]}}{|\vec{r}\times\dot{\vec{r}}^{0,[k]}|} \tag{2.29}$$

Relation (2.28), depicted in Figure 2.3, can be viewed as an application of the midpoint rule to calculating the arc length from $\tilde{\vec{r}}$ to $\vec{r}$ (i.e. $2R\Theta^{[k]}$) assuming that the particle remains on the surface of the sphere and has a constant velocity of magnitude $|\dot{\vec{r}}^{0,[k]}|$. A schematic diagram describing the computation (2.29) is shown in Figure 2.4. Once the midpoint vector $\vec{r}^{0,[k]}$ is computed by (2.29), it is used to compute $(\lambda^{0,[k]}, \theta^{0,[k]})$, which is then used to update the wind image components $U^{n+\frac{1}{2}}(\lambda^{0,[k]}, \theta^{0,[k]})$ and $V^{n+\frac{1}{2}}(\lambda^{0,[k]}, \theta^{0,[k]})$ by interpolating gridpoint values of $U^{n+\frac{1}{2}}$ and $V^{n+\frac{1}{2}}$. The above procedure is repeated. In our implementation, two iterations suffice to yield the desired level of accuracy.

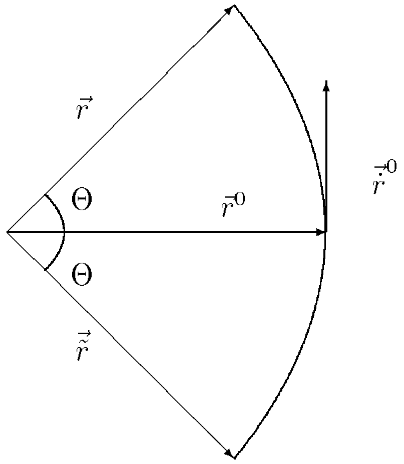

Figure 2.3: A schematic diagram for the geometry of the trajectory calculation.

The departure position vector $\tilde{\vec{r}}$ is given by

$$\tilde{\vec{r}} = 2\cos\Theta\vec{r}^0 - \vec{r} \tag{2.30}$$

which can then be translated back into spherical coordinates. A schematic diagram describing the computation in (2.30) is found in Figure 2.5.

The algorithm for calculating the trajectory is summarized below.

1. Translate each gridpoint $\vec{r}$ from spherical to Cartesian coordinates using (2.25).

2. Initialize each midpoint position vector $\vec{r}^{0,[0]}$ using its value at time-level t_n, and the midpoint wind image components $U^{n+\frac{1}{2}}(\lambda^{0,[0]}, \theta^{0,[0]})$ and $V^{n+\frac{1}{2}}(\lambda^{0,[0]}, \theta^{0,[0]})$, using linear extrapolation at time-levels t_n and t_{n-1} and spatial interpolation.

3. For $k = 1, 2, \cdots$, compute each $\vec{r}^{0,[k]}$ by the following iteration.

   (a) Compute each midpoint velocity $\dot{\vec{r}}^{0,[k]}$ from $\vec{r}^{0,[k-1]}$, $(\lambda^{0,[k-1]}, \theta^{0,[k-1]})$, $U^{n+\frac{1}{2}}(\lambda^{0,[k-1]}, \theta^{0,[k-1]})$ and $V^{n+\frac{1}{2}}(\lambda^{0,[k-1]}, \theta^{0,[k-1]})$, using (2.26) and (2.27).

   (b) Compute each angular displacement $\Theta^{[k]}$ from $\dot{\vec{r}}^{0,[k]}$ using the midpoint rule (2.28).

   (c) Compute each midpoint position $\vec{r}^{0,[k]}$ from $\vec{r}$, $\Theta^{[k]}$ and $\dot{\vec{r}}^{0,[k]}$ using (2.29).

4. Compute each departure position $\ddot{\vec{r}}$ by (2.30).

5. Translate each $\ddot{\vec{r}}$ back to spherical coordinates.

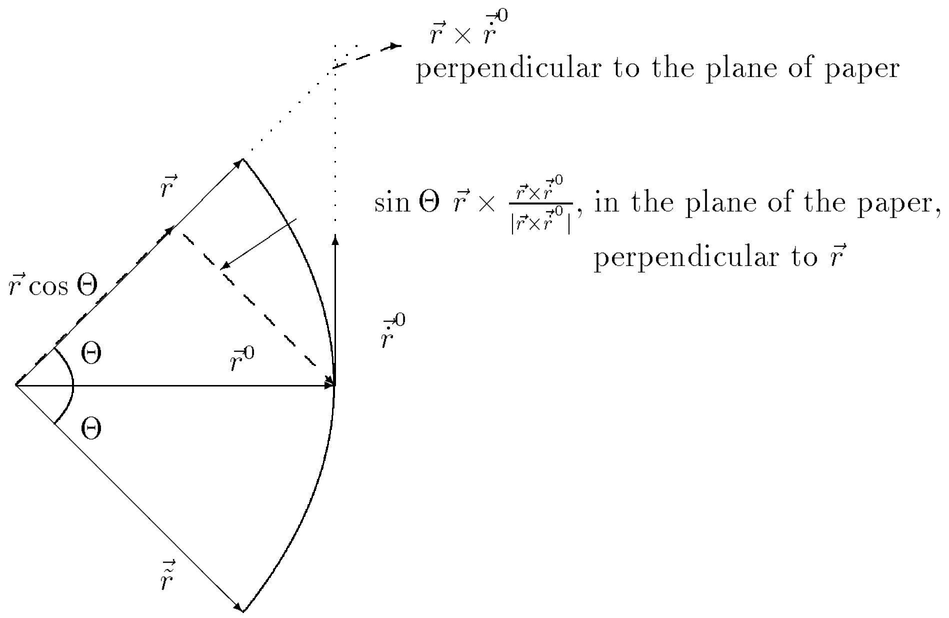

Figure 2.4: A schematic diagram that illustrates how $\vec{r}^0$ is computed from $\vec{r}$ and $\dot{\vec{r}}^0$ in equation (2.29).

2.5 Spatial Interpolation

Departure points usually fall between gridpoints and spatial interpolation is required to evaluate function values at departure points. In this section we compare the amount

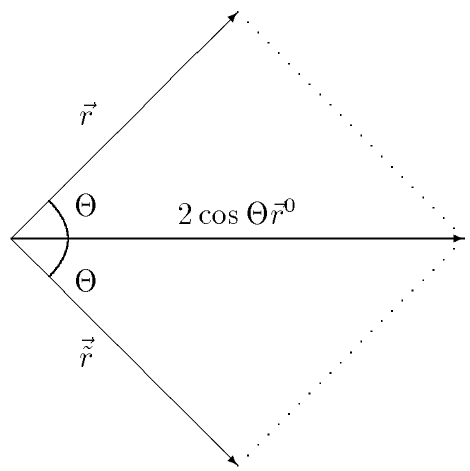

Figure 2.5: A schematic diagram that illustrates how the departure position vector $\vec{\tilde{r}}$ is computed from the arrival position $\vec{r}$ and the midpoint $\vec{r}^0$. According to the parallelogram rule, $\vec{r} + \vec{\tilde{r}} = 2\cos\Theta\vec{r}^0$, which results in equation (2.30).

of damping and phase errors introduced by the linear, quadratic and cubic Lagrange interpolation schemes.

Consider again the one-dimensional advection equation (2.16) and assume a constant wind speed of $w^* > 0$. Let $x^*_m \equiv x_m - w^*\Delta t$ be the m-th departure point. Let p denote the integer offset to the grid interval in which the departure point falls:

$$x_{m-p} \leq x^*_m < x_{m-p+1} \tag{2.31}$$

Denote the fraction of the grid interval between the departure point and the gridpoint to its left by α,

$$\alpha = \frac{x^*_m - x_{m-p}}{\Delta x} \tag{2.32}$$

where $\Delta x = x_{m-p+1} - x_{m-p}$ is the meshsize. Note that by definition $0 \leq \alpha < 1$. The solution $F(x,t)$ is assumed to be the waveform

$$F(x,t) = F_0 e^{\imath(kx+\nu t)} \tag{2.33}$$

where $\imath \equiv \sqrt{-1}$, k denotes the *wave number* and ν the *phase*, also known as the *frequency*. Note that the true frequency ν^* can be obtained by substituting (2.33) into (2.16):

$$\frac{\partial F}{\partial t} = -w^* \frac{\partial F}{\partial x} \Rightarrow \nu^* = -kw^* \tag{2.34}$$

2.5.1 Linear Lagrange Interpolation

With linear Lagrange interpolation, the value of F^n at the departure point is approximated by linear interpolation between x_{m-p} and x_{m-p+1}:

$$F^{n+1}(x_m) = F^n(x_m^*) \approx (1-\alpha)F^n(x_{m-p}) + \alpha F^n(x_{m-p+1}) \tag{2.35}$$

Substituting the solution (2.33) into (2.35) and canceling out the common factor $F_0 e^{\imath(k(m-p)\Delta x + \nu n \Delta t)}$ gives

$$\begin{aligned} e^{\imath(kp\Delta x + \nu\Delta t)} &\approx 1 - \alpha + \alpha e^{\imath k\Delta x} \\ &= 1 - \alpha(1 - \cos k\Delta x) + \imath\alpha \sin k\Delta x \end{aligned} \tag{2.36}$$

which is useful in analyzing the amplitude and phase error introduced by linear interpolation. The stability of the numerical solution can be assessed by taking the absolute value of each side of (2.36):

$$\begin{aligned} 1 = \left|e^{\imath(kp\Delta x + \nu\Delta t)}\right| &\approx |1 - \alpha(1 - \cos k\Delta x) + \imath\alpha \sin k\Delta x| \\ &= \sqrt{1 - 2\alpha(1-\alpha)(1 - \cos k\Delta x)} \end{aligned} \tag{2.37}$$

Since $0 \leq \alpha < 1$, we have $\sqrt{1 - 2\alpha(1-\alpha)(1 - \cos k\Delta x)} \leq 1$, with equality at $\alpha = 0$. Although by definition $\alpha \in [0, 1)$, it is useful to note that equality holds also when $\alpha = 1$. Therefore the numerical method is stable for any combination of Δt and Δx, but the amplitude damps if $\alpha \neq 0$ or 1.

Now we study the phase of the numerical solution. Taking the ratio of the imaginary to the real components of each side of (2.36) gives

$$\tan(kp\Delta x + \nu\Delta t) \approx \frac{\alpha \sin k\Delta x}{1 - \alpha(1 - \cos k\Delta x)} \tag{2.38}$$

which yields

$$\nu \approx -kp\frac{\Delta x}{\Delta t} + \frac{1}{\Delta t}\arctan\left[\frac{\alpha \sin k\Delta x}{1-\alpha(1-\cos k\Delta x)}\right] \equiv \bar{\nu} \tag{2.39}$$

where $\bar{\nu}$ represents the phase of the numerical solution.

From the definition of x_m^* and equation (2.32), we obtain the relation

$$p\frac{\Delta x}{\Delta t} = w^* + \alpha\frac{\Delta x}{\Delta t} \tag{2.40}$$

which can be combined with (2.39) to yield

$$\bar{\nu} = -kw^* - k\alpha\frac{\Delta x}{\Delta t} + \frac{1}{\Delta t}\arctan\left[\frac{\alpha \sin k\Delta x}{1-\alpha(1-\cos k\Delta x)}\right] \tag{2.41}$$

If $\alpha = 0$ or $\alpha = 1$, then $\bar{\nu} = -kw^* = \nu^*$. Therefore, the phase of the numerical solution is correct in this case. However, if $\alpha \in (0,1)$, then normally $k\alpha\Delta x \neq \arctan\left[\frac{\alpha \sin k\Delta x}{1-\alpha(1-\cos k\Delta x)}\right]$, in which case $\bar{\nu} \neq \nu^*$, implying that the numerical solution suffers from phase error.

2.5.2 Quadratic Lagrange Interpolation

With quadratic Lagrange interpolation, $F^{n+1}(x_m)$ is approximated as follows:

$$\begin{aligned} F^{n+1}(x_m) &= F^n(x_m^*) \\ &\approx -\frac{1}{2}\alpha(1-\alpha)F^n(x_{m-p-1}) + (1-\alpha)(1+\alpha)F^n(x_{m-p}) \\ &\quad +\frac{1}{2}\alpha(1+\alpha)F^n(x_{m-p+1}) \end{aligned} \tag{2.42}$$

Substituting the solution (2.33) into (2.42) and canceling the common factor $F_0 e^{\imath(k(m-p)\Delta x + \nu n\Delta t)}$ yields

$$e^{\imath(kp\Delta x + \nu\Delta t)} \approx 1 - \alpha^2(1-\cos k\Delta x) + \imath\alpha \sin k\Delta x \tag{2.43}$$

from which the amplitude of the numerical solution can be obtained. More specifically, it follows from (2.43) that

$$1 = |e^{\imath(kp\Delta x + \nu\Delta t)}| \approx \sqrt{1 - \alpha^2(1-\cos k\Delta x)^2 + \alpha^4(1-\cos k\Delta x)^2}$$

$$= \sqrt{1-\alpha^2(1-\alpha^2)(1-\cos(k\Delta x))^2} \tag{2.44}$$

Since $0 \le \alpha < 1$, $\sqrt{1-\alpha^2(1-\alpha^2)(1-\cos(k\Delta x))^2} \le 1$ with equality at $\alpha = 0$. Although by definition $\alpha \in [0,1)$, it is useful to note that equality holds also when $\alpha = 1$. Therefore, the numerical solution is stable for any combination of Δt and Δx, but the solution damps if $\alpha \ne 0$ or 1. The phase of the numerical solution is

$$\bar{\nu} = -kw^* - k\alpha\frac{\Delta x}{\Delta t} + \frac{1}{\Delta t}\arctan\left[\frac{\alpha \sin k\Delta x}{1-\alpha^2(1-\cos k\Delta x)}\right] \tag{2.45}$$

If $\alpha = 0$ or $\alpha = 1$, then $\bar{\nu} = -kw^* = \nu^*$. Therefore, the phase of the numerical solution is correct in this case. However, if $\alpha \in (0,1)$, then normally $k\alpha\Delta x \ne \arctan\left[\frac{\alpha \sin k\Delta x}{1-\alpha^2(1-\cos k\Delta x)}\right]$, in which case $\bar{\nu} \ne \nu^*$, implying that the numerical solution suffers from phase error.

2.5.3 Cubic Lagrange Interpolation

Cubic Lagrange interpolation approximates $F^{n+1}(x_m)$ using the relations

$$\begin{aligned} F^{n+1}(x_m) &= F^n(x_m^*) \\ &\approx -\frac{1}{6}\alpha(1-\alpha)(2-\alpha)F^n_{m-p-1} + \frac{1}{2}(1+\alpha)(1-\alpha)(2-\alpha)F^n_{m-p} \\ &\quad +\frac{1}{2}(1+\alpha)\alpha(2-\alpha)F^n_{m-p+1} - \frac{1}{6}(1+\alpha)\alpha(1-\alpha)F^n_{m-p+2} \end{aligned} \tag{2.46}$$

Substituting the solution (2.33) into (2.46) and canceling the common factor $F_0 e^{\imath(k(m-p)\Delta x + \nu n\Delta t)}$ yields

$$e^{\imath(kp\Delta x + \nu\Delta t)} \approx A + \imath B \tag{2.47}$$

where

$$\begin{aligned} A &= \frac{1}{3}(\alpha-1)(\alpha-3)(\alpha+1) - \frac{1}{3}\alpha(2\alpha+1)(\alpha-2)\cos k\Delta x + \frac{1}{3}\alpha(\alpha+1)(\alpha-1)\cos^2 k\Delta x \\ B &= \frac{1}{3}\alpha \sin k\Delta x\left[-(\alpha^2-4) + (\alpha^2-1)\cos k\Delta x\right] \end{aligned}$$

The stability of the numerical solution can be assessed by taking the absolute value of each side of (2.47):

$$1 = |e^{\imath(kp\Delta x+\nu\Delta t)}| \approx \sqrt{A^2+B^2} \tag{2.48}$$

By plotting $\sqrt{A^2+B^2}$ as a function of α and $k\Delta x$, we observe that $\sqrt{A^2+B^2} \leq 1$, with equality at $\alpha = 0$ and or $\alpha = 1$. Therefore the numerical solution is stable, but normally damps. The phase of the numerical solution is

$$\bar{\nu} = -kw^* - k\alpha\frac{\Delta x}{\Delta t} + \frac{1}{\Delta t}\arctan\left[\frac{B}{A}\right] \tag{2.49}$$

As in the case of linear and quadratic Lagrange interpolation, if $\alpha = 0$ or $\alpha = 1$, then $\bar{\nu} = -kw^* = \nu^*$. Therefore, the phase of the numerical solution is correct in this case. However, if $\alpha \in (0,1)$, then normally $k\alpha\Delta x \neq \arctan\left[\frac{B}{A}\right]$, in which case $\bar{\nu} \neq \nu^*$, implying that the numerical solution suffers from phase error.

2.5.4 Comparison of Interpolation Schemes

In this section, we compare and analyze the amplitude and phase errors of the numerical solutions obtained by the linear, quadratic and cubic Lagrange interpolation methods.

The amplitude of the numerical solution depends on $k\Delta x$. Because of aliasing for values of $k\Delta x > \pi$, it is standard practice to consider values of $k\Delta x \in [0,\pi]$ only [15, 17]. Although the amplitude error is largest at $k\Delta x = \pi$, which corresponds to the shortest resolvable wave, longer waves are numerically more relevant. Therefore, in Figure 2.6, we plot the normalized amplitudes of the wave solutions with $k\Delta x = \pi/2$ for all permissible values of α for the three interpolation methods. Similar results have been obtained for other values of $k\Delta x$. Linear Lagrange interpolation has excessive damping, with a maximum damping factor of $\sqrt{2}/2 \approx 0.7071$, at $\alpha = 1/2$. Quadratic Lagrange interpolation has less damping, with a maximum damping factor of $\sqrt{3}/2 \approx 0.8660$ at $\alpha = 1/\sqrt{2}$. Even better performance is obtained with cubic Lagrange interpolation, which has its largest damping factor of $5\sqrt{2}/8 \approx 0.8839$ at $\alpha = 1/2$.

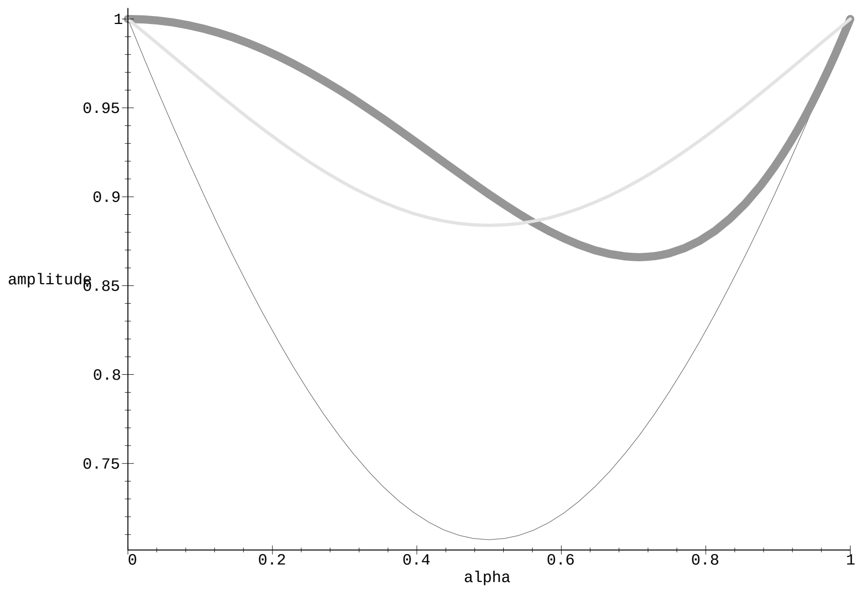

Figure 2.6: Normalized amplitude for the wave solution (2.33) with $k\Delta x = \pi/2$ as a function of α, the relative location of the departure point with respect to the nearest gridpoint, for linear (solid, thin), quadratic (thick) and cubic (light, medium) Lagrange interpolations.

The advantage of the cubic scheme over its linear and quadratic counterparts is more obvious when we consider the phase error of the three methods. We express the phase error accumulated in one time interval relative to $k\Delta x$ as

$$\frac{(\bar{\nu} - \nu^*)\Delta t}{k\Delta x} = \frac{1}{k\Delta x}\arctan[\,\cdot\,] - \alpha \tag{2.50}$$

where $\bar{\nu}$ is the numerical phase, $\nu^* = -kw^*$ is the true phase, and the $[\,\cdot\,]$ contains the quantities in the square brackets in (2.41), (2.45) and (2.49) for the linear, quadratic and cubic cases, respectively. The phase errors are plotted as functions of α in Figure 2.7 for $k\Delta x = \pi/2$. The absolute values of the phase errors of the linear and cubic methods have maxima at $\alpha = 0.25$ and $\alpha = 0.75$ and are zero at $\alpha = 0.5$, while the absolute value of the phase error of the quadratic method has a maximum at $\alpha = 0.5$. The magnitudes of the largest phase errors of the linear, quadratic and cubic methods are found to be approximately 0.0452, 0.1257 and 0.0178, respectively. Among the three interpolation methods, the cubic method introduces the smallest phase error. Similar results have also been obtained for other values of $k\Delta x$.

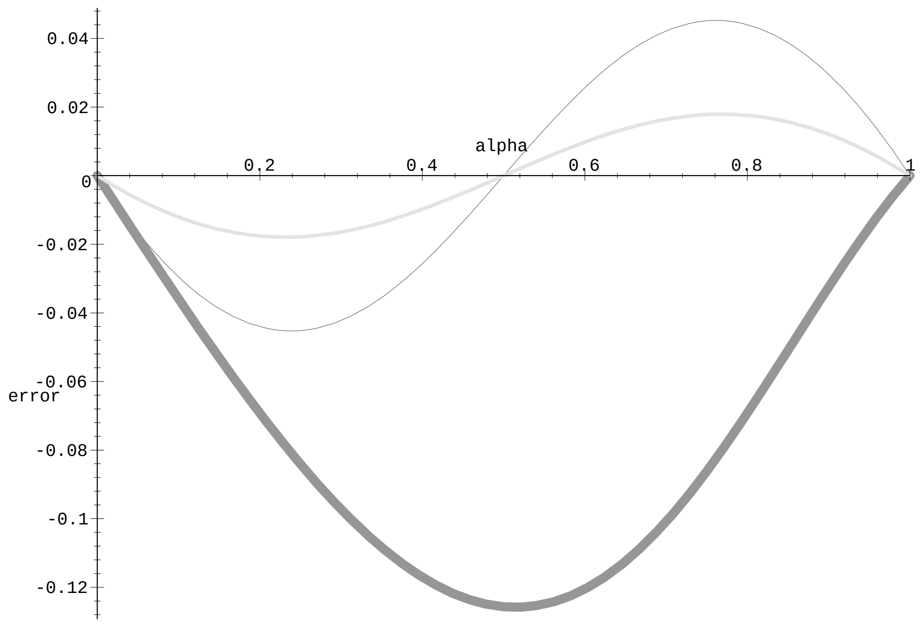

Figure 2.7: Phase error expressed as a fraction of $k\Delta x$, plotted above as a function of α, for linear (solid, thin), quadratic (thick) and cubic (light, medium) Lagrange interpolations.

To summarize our results, which agree with the numerical experiments in [2], we found that cubic interpolation gives small phase error with very little damping. Moreover, it is known that cubic interpolation gives fourth-order spatial truncation errors. Thus, it offers a good compromise between accuracy and computational cost, and is the method of choice in our implementation. Linear and quadratic interpolations, though less expensive, cause excessive damping and phase errors, whereas higher-order interpolants are more expensive and the rule of diminishing returns ultimately applies.

2.6 The Semi-Lagrangian Semi-Implicit Time Discretization

We are now ready to discretize the shallow water equations (2.9) to (2.11) in time using the SLSI method. In Section 2.3, departure points are defined in terms of trajectories with gridpoints as downstream points. But in fact, the downstream points can be points other than gridpoints. In particular, in our formulation, the downstream point (λ, θ) may be a midpoint, a Gauss point of the spatial partition or one of the poles. Therefore, we generalize the definition of the displacement and the associated departure point as follows. Let $(\delta\lambda^{n+1}, \delta\theta^{n+1})$ be the displacement of a fluid particle in the time interval t_n to t_{n+1}, ending at the downstream point (λ, θ) at time t_{n+1}. The associated departure point is $(\lambda - \delta\lambda^{n+1}, \theta - \delta\theta^{n+1})$ at time t_n. For an arbitrary function $\psi(\lambda, \theta, t)$, let the *upstream function* $\tilde{\psi}^n(\lambda, \theta)$ denote $\psi(\lambda - \delta\lambda^{n+1}, \theta - \delta\theta^{n+1}, t_n)$, the value of the function ψ at the associated departure point at time t_n. The Lagrangian derivative is approximated by

$$\frac{d\tilde{\psi}^{n+\frac{1}{2}}}{dt} \approx \frac{\psi^{n+1} - \tilde{\psi}^n}{\Delta t} \tag{2.51}$$

Fast moving waves may impose timestep restrictions for stability. In the semi-implicit time integration formulation, the fast and slow moving waves are treated differently. The high frequency (i.e., fast moving) modes are discretized implicitly, while the low frequency ones explicitly. To be specific, we treat the gravity and Coriolis terms implicitly by averaging in time along particle trajectories:

$$\tilde{\psi}^{n+\frac{1}{2}} \approx \frac{\psi^{n+1} + \tilde{\psi}^n}{2} \tag{2.52}$$

When discretized in time only using the two-level semi-Lagrangian semi-implicit scheme, the shallow water equations take the following form:

$$\frac{U^{n+1}-\tilde{U}^{n}}{\Delta t}-\frac{\tilde{f}^{n+\frac{1}{2}}}{2}(V^{n+1}+\tilde{V}^{n})+\frac{1}{2R^{2}}(\phi_{\lambda}^{n+1}+\tilde{\phi}_{\lambda}^{n})=0 \quad (2.53)$$

$$\frac{V^{n+1}-\tilde{V}^{n}}{\Delta t}+\frac{\tilde{f}^{n+\frac{1}{2}}}{2}(U^{n+1}+\tilde{U}^{n})+\frac{\cos\tilde{\theta}^{n+\frac{1}{2}}}{2R^{2}}(\phi_{\theta}^{n+1}+\tilde{\phi}_{\theta}^{n})+\tilde{\delta}^{n+\frac{1}{2}}=0 \quad (2.54)$$

$$\cos\tilde{\theta}^{n+\frac{1}{2}}\left(\frac{\log\phi^{n+1}-\log\tilde{\phi}^{n}}{\Delta t}\right)+\frac{1}{2}\left[\frac{1}{\cos\tilde{\theta}^{n+\frac{1}{2}}}(U_{\lambda}^{n+1}+\tilde{U}_{\lambda}^{n})+(V_{\theta}^{n+1}+\tilde{V}_{\theta}^{n})\right]=0 \quad (2.55)$$

where the correction term, $\tilde{\delta}^{n+\frac{1}{2}} \approx [(\tilde{U}^{n+\frac{1}{2}})^2+(\tilde{V}^{n+\frac{1}{2}})^2]\sin\tilde{\theta}^{n+\frac{1}{2}}/\cos^2\tilde{\theta}^{n+\frac{1}{2}}$, is evaluated at trajectory midpoints and computed explicitly using quadratic extrapolation in time of the form

$$\boldsymbol{\delta}^{n+\frac{1}{2}}=\frac{15}{8}\boldsymbol{\delta}^{n}-\frac{5}{4}\boldsymbol{\delta}^{n-1}+\frac{3}{8}\boldsymbol{\delta}^{n-2}$$

on gridpoints, followed by spatial interpolation to obtain trajectory midpoint values. In equations (2.53) to (2.55), functions at time-level t_{n+1} are evaluated at gridpoints; those at time-level $t_{n+\frac{1}{2}}$ are evaluated at approximate trajectory midpoints $(\lambda_l-\delta\lambda_l^{n+1}/2, \theta_m-\delta\theta_m^{n+1}/2)$; and those at time-level t_n are evaluated at approximate departure points $(\lambda_l-\delta\lambda_l^{n+1}, \theta_m-\delta\theta_m^{n+1})$. For brevity, let $\tilde{f}\equiv\tilde{f}^{n+\frac{1}{2}}$ and $\tilde{\theta}\equiv\tilde{\theta}^{n+\frac{1}{2}}$ from now on. The time-discretized shallow water equations can be rearranged into predictive form for each timestep by moving the known quantities to the right sides as follows:

$$U^{n+1}-\frac{\Delta t\tilde{f}}{2}V^{n+1}+\frac{\Delta t}{2R^{2}}\phi_{\lambda}^{n+1} = \tilde{U}^{n}+\frac{\Delta t\tilde{f}}{2}\tilde{V}^{n}-\frac{\Delta t}{2R^{2}}\tilde{\phi}_{\lambda}^{n} \quad (2.56)$$

$$V^{n+1}+\frac{\Delta t\tilde{f}}{2}U^{n+1}+\frac{\Delta t\cos\tilde{\theta}}{2R^{2}}\phi_{\theta}^{n+1} = \tilde{V}^{n}-\frac{\Delta t\tilde{f}}{2}\tilde{U}^{n}-\frac{\Delta t\cos\tilde{\theta}}{2R^{2}}\tilde{\phi}_{\theta}^{n}-\Delta t\tilde{\delta}^{n+\frac{1}{2}} \quad (2.57)$$

$$\cos\tilde{\theta}\log\phi^{n+1}+\frac{\Delta t}{2}\left[\frac{U_{\lambda}^{n+1}}{\cos\tilde{\theta}}+V_{\theta}^{n+1}\right] = \cos\tilde{\theta}\log\tilde{\phi}^{n}-\frac{\Delta t}{2}\left[\frac{\tilde{U}_{\lambda}^{n}}{\cos\tilde{\theta}}+\tilde{V}_{\theta}^{n}\right] \quad (2.58)$$

To solve the time discretized shallow water equations (2.56) to (2.58), the equations are discretized in space, followed by the elimination of the wind images U and V from the system to yield a nonlinear Helmholtz equation for the pressure ϕ only. To this end, we move the ϕ_λ^{n+1} and ϕ_θ^{n+1} terms of the motion equations (2.56) and (2.57) to the right side and rewrite the motion equations in matrix form

$$
\begin{aligned}
\begin{bmatrix} U^{n+1} \\ V^{n+1} \end{bmatrix} &= \begin{bmatrix} 1 & -\frac{\Delta t\tilde{f}}{2} \\ \frac{\Delta t\tilde{f}}{2} & 1 \end{bmatrix}^{-1} \left\{ \begin{bmatrix} 1 & \frac{\Delta t\tilde{f}}{2} \\ -\frac{\Delta t\tilde{f}}{2} & 1 \end{bmatrix} \begin{bmatrix} \tilde{U}^n \\ \tilde{V}^n \end{bmatrix} \right. \\
&\qquad \left. - \left(\frac{\Delta t}{2R^2}\right) \begin{bmatrix} \phi_\lambda^{n+1} + \tilde{\phi}_\lambda^n \\ \cos\tilde{\theta}(\phi_\theta^{n+1} + \tilde{\phi}_\theta^n) + 2R^2\tilde{\delta}^{n+\frac{1}{2}} \end{bmatrix} \right\} \\
&= \begin{bmatrix} a & b \\ -b & a \end{bmatrix} \begin{bmatrix} \tilde{U}^n \\ \tilde{V}^n \end{bmatrix} \\
&\quad - \left(\frac{\Delta t}{2R^2}\right) \begin{bmatrix} c & d \\ -d & c \end{bmatrix} \begin{bmatrix} \phi_\lambda^{n+1} + \tilde{\phi}_\lambda^n \\ \cos\tilde{\theta}(\phi_\theta^{n+1} + \tilde{\phi}_\theta^n) + 2R^2\tilde{\delta}^{n+\frac{1}{2}} \end{bmatrix}
\end{aligned} \tag{2.59}
$$

$$
\begin{aligned}
\Rightarrow \begin{bmatrix} U^{n+1} \\ V^{n+1} \end{bmatrix} + \left(\frac{\Delta t}{2R^2}\right) \begin{bmatrix} c & d \\ -d & c \end{bmatrix} \begin{bmatrix} \phi_\lambda^{n+1} \\ \cos\tilde{\theta}\phi_\theta^{n+1} \end{bmatrix} \\
= \begin{bmatrix} a & b \\ -b & a \end{bmatrix} \begin{bmatrix} \tilde{U}^n \\ \tilde{V}^n \end{bmatrix} - \left(\frac{\Delta t}{2R^2}\right) \begin{bmatrix} c & d \\ -d & c \end{bmatrix} \begin{bmatrix} \tilde{\phi}_\lambda^n \\ \cos\tilde{\theta}\tilde{\phi}_\theta^n + 2R^2\tilde{\delta}^{n+\frac{1}{2}} \end{bmatrix}
\end{aligned} \tag{2.60}
$$

where a, b, c and d are functions of θ and are defined as follows:

$$
\begin{aligned}
a &= \frac{1 - \left(\frac{\Delta t\tilde{f}}{2}\right)^2}{1 + \left(\frac{\Delta t\tilde{f}}{2}\right)^2} \qquad b = \frac{\Delta t\tilde{f}}{1 + \left(\frac{\Delta t\tilde{f}}{2}\right)^2} \\
c &= \frac{1}{1 + \left(\frac{\Delta t\tilde{f}}{2}\right)^2} \qquad d = \frac{\frac{\Delta t}{2}\tilde{f}}{1 + \left(\frac{\Delta t\tilde{f}}{2}\right)^2}
\end{aligned} \tag{2.61}
$$

Equations (2.58) and (2.60) are then spatially discretized and the divergence terms are then eliminated from the spatially discretized equations corresponding to (2.58) using the respective equations corresponding to (2.60) to result in a Helmholtz equation for ϕ. The details of the above procedure are described in Chapter 3.

It should be mentioned that higher-order multi-level semi-Lagrangian schemes can be constructed. Our decision to focus on the two-level scheme is motivated by the general agreement that the time-truncation error is dominated by the space-truncation error. Consequently, it seems reasonable to combine a simple second-order time integration scheme with high-order spatial discretization methods.

Chapter 3

Weighted Residual and Semi-Lagrangian Methods

In this chapter, we develop the procedures with which a generic weighted residual method can be applied to equations that are discretized with the semi-Lagrangian semi-implicit method, which proceeds in time by integrating along fluid trajectories. In particular, we explain how the upstream functions are represented in the biquadratic spline approximation space, and derive the Helmholtz equation associated with the shallow water equations.

3.1 Background

As will be explained in Chapter 7, the discretized Helmholtz equation is derived from the spatially discretized form of (2.58) and (2.60), in order to preserve the phase velocity of Rossby waves. Furthermore, the correct direction for energy propagation is maintained by discretizing on a staggered grid. In Chapter 8 we compare three types of staggering schemes and conclude that the Arakawa C-type grid [17] has superior performance. Therefore, in our implementation, the shallow water equations are discretized on a C-grid. The steps according to which this is done, and how the equations are subsequently solved with the weighted residual method are outlined in this section.

3.1.1 Spatial Discretization

Along the longitude, we define two uniform partitions that are staggered with respect to each other by

$$\begin{aligned}\Delta_\lambda &\equiv \{0 = \lambda_0 < \lambda_1 < \cdots < \lambda_{N_\lambda} = 2\pi\} \\ \hat{\Delta}_\lambda &\equiv \left\{-\frac{\Delta\lambda}{2} = \hat{\lambda}_{-1} < \hat{\lambda}_0 < \cdots < \hat{\lambda}_{N_\lambda} = 2\pi + \frac{\Delta\lambda}{2}\right\}\end{aligned}$$

where $\Delta\lambda = 2\pi/N_\lambda$ denotes the meshsize in the λ-direction. The gridpoints in Δ_λ and $\hat{\Delta}_\lambda$ are chosen so that $\lambda_i = i\Delta\lambda$ for $i = 0, \cdots, N_\lambda$, and $\hat{\lambda}_i = (i+1/2)\Delta\lambda$ for $i = -1, \cdots, N_\lambda$, respectively. Similarly, staggered partitions Δ_θ and $\hat{\Delta}_\theta$ are defined in the θ-direction by

$$\begin{aligned}\Delta_\theta &\equiv \left\{-\frac{\pi}{2} = \theta_0 < \theta_1 < \cdots < \theta_{N_\theta} = \frac{\pi}{2}\right\} \\ \hat{\Delta}_\theta &\equiv \left\{-\frac{\pi}{2} - \frac{\Delta\theta}{2} = \hat{\theta}_{-1} < \hat{\theta}_0 < \cdots < \hat{\theta}_{N_\theta} = \frac{\pi}{2} + \frac{\Delta\theta}{2}\right\}\end{aligned}$$

where $\Delta\theta = \pi/N_\theta$, $\theta_j = -\pi/2 + j\Delta\theta$ for $j = 0, \cdots, N_\theta$, and $\hat{\theta}_j = -\pi/2 + (j+1/2)\Delta\theta$ for $j = -1, \cdots, N_\theta$. Figure 3.1 shows the gridpoints associated with Δ_θ and $\hat{\Delta}_\theta$. Let $\{\tau_{\lambda_i} = (\lambda_{i-1} + \lambda_i)/2\}_{i=1}^{N_\lambda}$ and $\{\hat{\tau}_{\lambda_i} = (\hat{\lambda}_{i-1} + \hat{\lambda}_i)/2\}_{i=0}^{N_\lambda}$ be the midpoints and collocation points of Δ_λ and $\hat{\Delta}_\lambda$, respectively, and $\{\tau_{\theta_j} = (\theta_{j-1} + \theta_j)/2\}_{j=1}^{N_\theta}$ and $\{\hat{\tau}_{\theta_j} = (\hat{\theta}_{j-1} + \hat{\theta}_j)/2\}_{j=1}^{N_\theta - 1}$ be the midpoints of Δ_θ and $\hat{\Delta}_\theta$, respectively. Let $\{\tau_{\theta_j}\}_{j=1}^{N_\theta} \bigcup \{\tau_{\theta_0} \equiv \theta_0, \tau_{N_\theta+1} \equiv \theta_{N_\theta}\}$ and $\{\hat{\tau}_{\theta_j}\}_{j=1}^{N_\theta-1} \bigcup \{\hat{\tau}_{\theta_{-1}} \equiv -\pi/2, \hat{\tau}_{\theta_0} \equiv \hat{\theta}_0, \hat{\tau}_{\theta_{N_\theta}} \equiv \hat{\theta}_{N_\theta - 1}, \hat{\tau}_{\theta_{N_\theta+1}} \equiv \pi/2\}$ be the collocation points of Δ_θ and $\hat{\Delta}_\theta$, respectively. Note that the τ_{λ_i}'s and $\hat{\lambda}_i$'s almost coincide, as do the $\hat{\tau}_{\lambda_i}$'s and λ_i's, τ_{θ_j} and $\hat{\theta}_j$'s, and $\hat{\tau}_{\theta_j}$ and θ_j's, but for consistency with literature, these notations are adopted.

The target functions belong to two-dimensional approximation spaces, chosen to be tensor products of the associated one-dimensional approximation spaces. Let $\{\beta_i(\lambda) = \frac{1}{2}\psi(\frac{\lambda}{\Delta\lambda} - i + 2)\}_{i=0}^{N_\lambda+1}$ and $\{\hat{\beta}_i(\lambda) = \frac{1}{2}\psi(\frac{\lambda}{\Delta\lambda} - i + \frac{3}{2})\}_{i=-1}^{N_\lambda+1}$ be the sets of basis functions for the one-dimensional quadratic spline approximation spaces corresponding to partitions

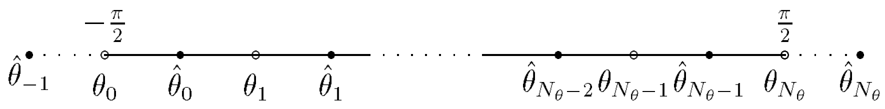

Figure 3.1: A diagram of the gridpoints of Δ_θ and $\hat{\Delta}_\theta$.

Δ_λ and $\hat{\Delta}_\lambda$, respectively, where the model quadratic spline function ψ is defined by

$$\psi(\lambda) = \begin{cases} \lambda^2 & 0 \leq \lambda \leq 1 \\ \lambda^2 - 3(\lambda-1)^2 & 1 \leq \lambda \leq 2 \\ \lambda^2 - 3(\lambda-1)^2 + 3(\lambda-2)^2 & 2 \leq \lambda \leq 3 \\ 0 & \text{otherwise} \end{cases}$$

For the partitions Δ_θ and $\hat{\Delta}_\theta$, let $\{\beta_j(\theta) = \frac{1}{2}\psi(\frac{\theta+\pi/2}{\Delta\theta} - j + 2)\}_{j=0}^{N_\theta+1}$ and $\{\hat{\beta}_j(\theta) = \frac{1}{2}\psi(\frac{\theta+\pi/2}{\Delta\theta} - j + \frac{3}{2})\}_{j=-1}^{N_\theta+1}$ be the corresponding basis functions, respectively. Figure 3.2 shows a diagram of the latitudinal staggered grids together with the associated basis functions. There are $N_\lambda + 2$ basis functions associated with Δ_λ, $N_\lambda + 3$ with $\hat{\Delta}_\lambda$, $N_\theta + 2$ with Δ_θ, and $N_\theta + 3$ with $\hat{\Delta}_\theta$. Note that the latitudinal boundary points (i.e. the poles) are not gridpoints in $\hat{\Delta}_\theta$.

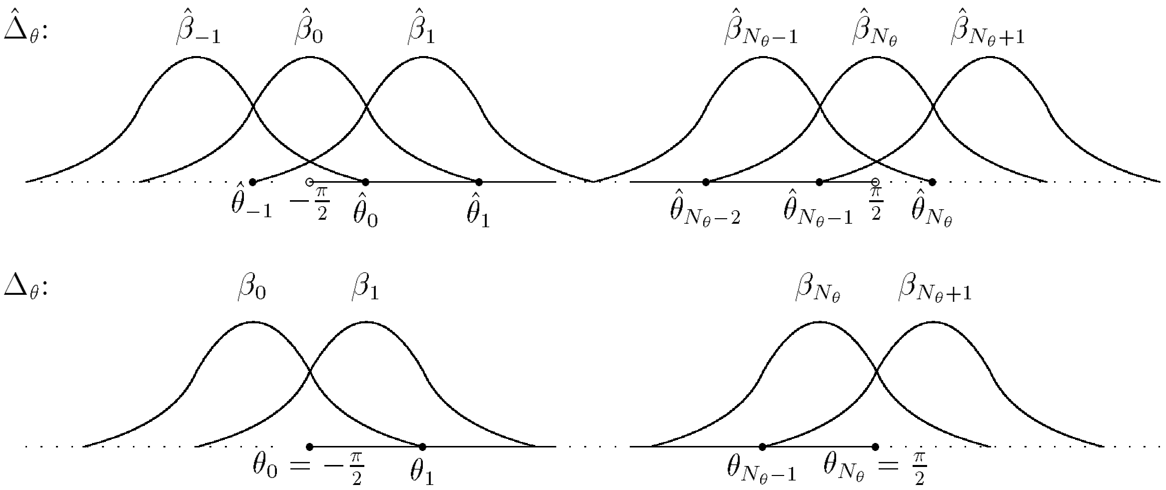

Figure 3.2: A diagram of the latitudinal staggered grids and associated basis functions.

Discretized on a C-grid [17], the target functions, U, V and ϕ, appearing in equations

(2.58) and (2.60) are approximated in the biquadratic spline spaces defined on the induced grid partitions $\Delta_1 \equiv \hat{\Delta}_\lambda \times \Delta_\theta$, $\Delta_2 \equiv \Delta_\lambda \times \hat{\Delta}_\theta$ and $\Delta_3 \equiv \Delta_\lambda \times \Delta_\theta$, respectively, by the basis functions $\{\hat{\beta}_i(\lambda)\beta_j(\theta)\}_{i=-1,j=0}^{N_\lambda+1,N_\theta+1}$, $\{\beta_i(\lambda)\hat{\beta}_j(\theta)\}_{i=0,j=-1}^{N_\lambda+1,N_\theta+1}$, and $\{\beta_i(\lambda)\beta_j(\theta)\}_{i=0,j=0}^{N_\lambda+1,N_\theta+1}$, respectively. That is, U^{n+1}, V^{n+1}, ϕ^{n+1} and the associated upstream functions are approximated by

$$U_\Delta^{n+1}(\lambda,\theta) = \sum_{i=-1,j=0}^{N_\lambda+1,N_\theta+1} \mathsf{U}_{i,j}^{n+1}\hat{\beta}_i(\lambda)\beta_j(\theta), \qquad \tilde{U}_\Delta^{n}(\lambda,\theta) = \sum_{i=-1,j=0}^{N_\lambda+1,N_\theta+1} \tilde{\mathsf{U}}_{i,j}^{n}\hat{\beta}_i(\lambda)\beta_j(\theta) \quad (3.1)$$

$$V_\Delta^{n+1}(\lambda,\theta) = \sum_{i=0,j=-1}^{N_\lambda+1,N_\theta+1} \mathsf{V}_{i,j}^{n+1}\beta_i(\lambda)\hat{\beta}_j(\theta), \qquad \tilde{V}_\Delta^{n}(\lambda,\theta) = \sum_{i=0,j=-1}^{N_\lambda+1,N_\theta+1} \tilde{\mathsf{V}}_{i,j}^{n}\beta_i(\lambda)\hat{\beta}_j(\theta) \quad (3.2)$$

$$\phi_\Delta^{n+1}(\lambda,\theta) = \sum_{i=0,j=0}^{N_\lambda,N_\theta} \Phi_{i,j}^{n+1}\beta_i(\lambda)\beta_j(\theta), \qquad \tilde{\phi}_\Delta^{n}(\lambda,\theta) = \sum_{i=0,j=0}^{N_\lambda,N_\theta} \tilde{\Phi}_{i,j}^{n}\beta_i(\lambda)\beta_j(\theta) \quad (3.3)$$

Furthermore, we define $\zeta^{n+1} \equiv \log \phi^{n+1}$ and approximate it and its upstream function by

$$\zeta_\Delta^{n+1}(\lambda,\theta) = \sum_{i=0,j=0}^{N_\lambda,N_\theta} \Gamma_{i,j}^{n+1}\beta_i(\lambda)\beta_j(\theta), \qquad \tilde{\zeta}_\Delta^{n}(\lambda,\theta) = \sum_{i=0,j=0}^{N_\lambda,N_\theta} \tilde{\Gamma}_{i,j}^{n}\beta_i(\lambda)\beta_j(\theta) \quad (3.4)$$

3.2 Incorporation of Boundary Conditions

In our analysis and implementation, the basis functions are adjusted so that they satisfy the boundary conditions by construction. In this way, the approximations defined in (3.1) to (3.4) also satisfy the boundary conditions. In this section, we explain how the basis functions are adjusted to incorporate the boundary conditions. For a standard one-dimensional grid partition with $N+1$ gridpoints, there are $N+2$ degrees of freedom in representing a function in terms of the quadratic spline basis functions. However, for the non-standard $\hat{\Delta}_\theta$, for example, there are $N_\theta+3$ degrees of freedom. By incorporating the boundary conditions, two or three degrees of freedom can be eliminated. In our case, the "outermost" basis functions are removed and the neighbouring ones are modified. How this is done depends on the boundary conditions.

3.2.1 Longitudinal Boundary Conditions

Since the longitude "wraps around" the sphere, all the functions in (3.1) to (3.4) are periodic in the longitudinal dimension — a stronger condition than the periodic boundary conditions. In order to form the periodic basis functions along the longitude, we drop $\beta_0(\lambda)$, $\hat\beta_{-1}(\lambda)$, $\hat\beta_0(\lambda)$, $\beta_{N_\lambda+1}(\lambda)$ and $\hat\beta_{N_\lambda+1}(\lambda)$, and modify the definitions of $\beta_j(\lambda)$ and $\hat\beta_j(\lambda)$ for $j = 1, \cdots, N_\lambda$ to be

$$\beta_1^P(\lambda) \equiv \begin{cases} \beta_1(\lambda) & \lambda \in [\lambda_0, \lambda_2] \\ \beta_{N_\lambda+1}(\lambda) & \lambda \in [\lambda_{N_\lambda-1}, \lambda_{N_\lambda}] \\ 0 & \text{otherwise} \end{cases} \qquad \hat\beta_1^P(\lambda) \equiv \begin{cases} \hat\beta_1(\lambda) & \lambda \in [0, \hat\lambda_2] \\ \hat\beta_{N_\lambda+1}(\lambda) & \lambda \in [\hat\lambda_{N_\lambda-1}, 2\pi] \\ 0 & \text{otherwise} \end{cases}$$

$$\beta_j^P(\lambda) \equiv \beta_j(\lambda), \qquad \hat\beta_j^P(\lambda) \equiv \hat\beta_j(\lambda), \qquad j = 2, \cdots, N_\lambda - 2$$

$$\beta_{N_\lambda-1}^P(\lambda) \equiv \beta_{N_\lambda-1}(\lambda), \qquad \hat\beta_{N_\lambda-1}^P(\lambda) \equiv \begin{cases} \hat\beta_{-1}(\lambda) & \lambda \in [0, \hat\lambda_0] \\ \hat\beta_{N_\lambda-1}(\lambda) & \lambda \in [\hat\lambda_{N_\lambda-3}, 2\pi] \\ 0 & \text{otherwise} \end{cases}$$

$$\beta_{N_\lambda}^P(\lambda) \equiv \begin{cases} \beta_0(\lambda) & \lambda \in [\lambda_0, \lambda_1] \\ \beta_{N_\lambda}(\lambda) & \lambda \in [\lambda_{N_\lambda-2}, \lambda_{N_\lambda}] \\ 0 & \text{otherwise} \end{cases} \qquad \hat\beta_{N_\lambda}^P(\lambda) \equiv \begin{cases} \hat\beta_0(\lambda) & \lambda \in [0, \hat\lambda_1] \\ \hat\beta_{N_\lambda}(\lambda) & \lambda \in [\hat\lambda_{N_\lambda-2}, 2\pi] \\ 0 & \text{otherwise} \end{cases}$$

When periodic boundary conditions are applied in the latitudinal dimension, the basis functions $\beta_j^P(\theta)$ and $\hat\beta_j^P(\theta)$ for $j = 1, \cdots, N_\theta$ are defined similarly.

3.2.2 Latitudinal Boundary Conditions — U_Δ^{n+1}

At the poles, U_Δ^{n+1} vanishes: $U_\Delta^{n+1}(\lambda, \pm\pi/2) = 0$. To impose the homogeneous Dirichlet boundary conditions for U_Δ^{n+1}, the modified basis functions $\beta_i^D(\theta), i = 1, \cdots, N_\theta$, are defined to be

$$\begin{aligned} \beta_1^D(\theta) &\equiv \beta_1(\theta) - \beta_0(\theta) \\ \beta_j^D(\theta) &\equiv \beta_j(\theta), \qquad j = 2, \cdots, N_\theta - 1 \\ \beta_{N_\theta}^D(\theta) &\equiv \beta_{N_\theta}(\theta) - \beta_{N_\theta+1}(\theta) \end{aligned}$$

3.2.3 Latitudinal Boundary Conditions — ϕ_Δ^{n+1}

Homogeneous Neumann boundary conditions are imposed on ϕ_Δ^{n+1} and ζ_Δ^{n+1} at the poles, since their θ-derivatives vanish there (see Section 2.1). The associated basis functions are adjusted to be

$$\begin{aligned}
\beta_1^N(\theta) &\equiv \beta_1(\theta) + \beta_0(\theta) \\
\beta_j^N(\theta) &\equiv \beta_j(\theta), \qquad\qquad j = 2, \cdots, N_\theta - 1 \\
\beta_{N_\theta}^N(\theta) &\equiv \beta_{N_\theta}(\theta) + \beta_{N_\theta+1}(\theta)
\end{aligned}$$

3.2.4 Latitudinal Boundary Conditions — V_Δ^{n+1}

The latitudinal homogeneous Dirichlet boundary conditions on V_Δ^{n+1} are imposed at the poles ($V_\Delta^{n+1}(\lambda, \pm\pi/2) = 0$), but the poles are *not* gridpoints of $\hat{\Delta}_\theta$, since $\hat{\theta}_i = -\pi/2 + (i + 1/2)\Delta\theta$ for $i = -1, \cdots, N_\theta$ due to staggering. Therefore, we cannot incorporate homogeneous Dirichlet boundary conditions for V_Δ^{n+1} in the same way we did for U_Δ^{n+1}. Instead, we first consider the $N_\theta + 3$ basis functions $\hat{\beta}_j(\theta)$ for $j = -1, \cdots, N_\theta + 1$, as shown in Figure 3.2. The basis functions are then adjusted to be

$$\begin{array}{ll}
\hat{\beta}_0^D(\theta) = \hat{\beta}_0(\theta) - 6\hat{\beta}_{-1}(\theta), & \hat{\beta}_1^D(\theta) = \hat{\beta}_1(\theta) - \hat{\beta}_{-1}(\theta) \\
\hat{\beta}_j^D(\theta) = \hat{\beta}_j(\theta), & j = 2, \cdots, N_\theta - 2 \\
\hat{\beta}_{N_\theta-1}^D(\theta) = \hat{\beta}_{N_\theta-1}(\theta) - \hat{\beta}_{N_\theta+1}(\theta), & \hat{\beta}_{N_\theta}^D(\theta) = \hat{\beta}_{N_\theta}(\theta) - 6\hat{\beta}_{N_\theta+1}(\theta)
\end{array}$$

3.3 Polar Values of the Upstream Functions

The latitudinal boundary conditions for the upstream functions need to be defined carefully. Recall that the upstream wind image component $\tilde{U}_\Delta^n$ is defined by

$$\tilde{U}_\Delta^n(\lambda, \theta) = U_\Delta^n(\lambda - \delta\lambda^{n+1}, \theta - \delta\theta^{n+1}) \tag{3.5}$$

for the displacement $(\delta\lambda^{n+1}, \delta\theta^{n+1})$ associated with the downstream gridpoint (λ, θ) for the time interval t_n to t_{n+1} (see Section 2.6).

What do we know about $\tilde{U}^n_\Delta(\lambda, \pm\pi/2)$? Even though U^{n+1}_Δ and U^n_Δ vanish at the poles, the upstream wind image $\tilde{U}^n_\Delta$ is not necessarily zero there. To better understand this, note from the definition (3.5) that

$$\begin{aligned} \tilde{U}^n_\Delta(\lambda, -\pi/2) &= U^n_\Delta(\lambda - \delta\lambda^{n+1}, -\pi/2 - \delta\theta^{n+1}_0) \qquad (3.6) \\ \tilde{U}^n_\Delta(\lambda, \pi/2) &= U^n_\Delta(\lambda - \delta\lambda^{n+1}, \pi/2 - \delta\theta^{n+1}_{N_\theta}) \qquad (3.7) \end{aligned}$$

By construction, U^n_Δ vanishes at the poles. However, $-\pi/2 - \delta\theta^{n+1}_0$ and $\pi/2 - \delta\theta^{n+1}_{N_\theta}$ do not necessarily coincide with the poles; hence, $U^n_\Delta(\lambda - \delta\lambda^{n+1}, -\pi/2 - \delta\theta^{n+1}_0)$ and $U^n_\Delta(\lambda-\delta\lambda^{n+1}, \pi/2-\delta\theta^{n+1}_{N_\theta})$, and consequently $\tilde{U}^n(\lambda, \pm\pi/2)$ are not necessarily zero, which means that the latitudinal boundary conditions for $\tilde{U}^n_\Delta$ are not necessarily homogeneous but general Dirichlet. Extrapolation is used to estimate $U^n_\Delta(\lambda - \delta\lambda^{n+1}, \pm\pi/2 - \delta\theta^{n+1}_j)$, where $j = 0$ or N_θ, when $-\pi/2 - \delta\theta^{n+1}_0 \notin [-\pi/2, \pi/2]$ or $\pi/2 - \delta\theta^{n+1}_{N_\theta} \notin [-\pi/2, \pi/2]$.

Following similar procedures, recall that the upstream wind image component $\tilde{V}^n_\Delta$ is defined by

$$\begin{aligned} \tilde{V}^n_\Delta(\lambda, -\pi/2) &= V^n_\Delta(\lambda - \delta\lambda^{n+1}, -\pi/2 - \delta\hat{\theta}^{n+1}_0) \qquad (3.8) \\ \tilde{V}^n_\Delta(\lambda, \pi/2) &= V^n_\Delta(\lambda - \delta\lambda^{n+1}, \pi/2 - \delta\hat{\theta}^{n+1}_{N_\theta}) \qquad (3.9) \end{aligned}$$

This results in general Dirichlet latitudinal boundary conditions being imposed on $\tilde{V}^n_\Delta$.

Since ϕ, unlike the wind images, takes on multiple values at the poles, we impose the general Neumann latitudinal boundary conditions on $\tilde{\phi}^n_\Delta$:

$$\begin{aligned} (\tilde{\phi}^n_\Delta)_\theta(\lambda, -\pi/2) &= (\phi^n_\Delta)_\theta(\lambda - \delta\lambda^{n+1}, -\pi/2 - \delta\theta^{n+1}_0) \qquad (3.10) \\ (\tilde{\phi}^n_\Delta)_\theta(\lambda, \pi/2) &= (\phi^n_\Delta)_\theta(\lambda - \delta\lambda^{n+1}, \pi/2 - \delta\theta^{n+1}_{N_\theta}) \qquad (3.11) \end{aligned}$$

Similar boundary conditions are also imposed on $\tilde{\zeta}^n_\Delta$.

The modified latitudinal functions introduced in Section 3.2 satisfy homogeneous boundary conditions by construction. Consequently, the target approximations, U^{n+1}_Δ,

V_Δ^{n+1}, ϕ_Δ^{n+1} and ζ_Δ^{n+1}, which indeed satisfy homogeneous boundary conditions, can be expressed as linear combinations of the appropriate modified basis functions:

$$\begin{aligned}
U_\Delta^{n+1}(\lambda,\theta) &= \sum_{i,j=1}^{N_\lambda,N_\theta} \mathsf{U}_{i,j}^{n+1}\hat{\beta}_i^P(\lambda)\beta_j^D(\theta) \\
V_\Delta^{n+1}(\lambda,\theta) &= \sum_{i=1,j=0}^{N_\lambda,N_\theta} \mathsf{V}_{i,j}^{n+1}\beta_i^P(\lambda)\hat{\beta}_j^D(\theta) \\
\phi_\Delta^{n+1}(\lambda,\theta) &= \sum_{i,j=1}^{N_\lambda,N_\theta} \Phi_{i,j}^{n+1}\beta_i^P(\lambda)\beta_j^N(\theta) \\
\zeta_\Delta^{n+1}(\lambda,\theta) &= \sum_{i,j=1}^{N_\lambda,N_\theta} \Gamma_{i,j}^{n+1}\beta_i^P(\lambda)\beta_j^N(\theta)
\end{aligned} \tag{3.12}$$

However, the upstream functions, $\tilde{U}_\Delta^n$, $\tilde{V}_\Delta^n$ $\tilde{\phi}_\Delta^n$ and $\tilde{\zeta}_\Delta^n$, satisfy general latitudinal boundary conditions. Therefore, these functions can be expressed as linear combinations of the standard basis functions as in (3.1) to (3.4), but not of the modified ones in the latitudinal dimension. Instead, they satisfy the following relations:

$$\tilde{U}_\Delta^n(\lambda,\theta) = \sum_{i,j=1}^{N_\lambda,N_\theta} \tilde{\mathsf{U}}_{i,j}^n\hat{\beta}_i^P(\lambda)\beta_j^D(\theta) + \eta_u^n(\lambda,\theta) \tag{3.13}$$

$$\tilde{V}_\Delta^n(\lambda,\theta) = \sum_{i=1,j=0}^{N_\lambda,N_\theta} \tilde{\mathsf{V}}_{i,j}^n\beta_i^P(\lambda)\hat{\beta}_j^D(\theta) + \eta_v^n(\lambda,\theta) \tag{3.14}$$

$$\tilde{\phi}_\Delta^n(\lambda,\theta) = \sum_{i,j=1}^{N_\lambda,N_\theta} \tilde{\Phi}_{i,j}^n\beta_i^P(\lambda)\beta_j^N(\theta) + \eta_\phi^n(\lambda,\theta) \tag{3.15}$$

$$\tilde{\zeta}_\Delta^n(\lambda,\theta) = \sum_{i,j=1}^{N_\lambda,N_\theta} \tilde{\Gamma}_{i,j}^n\beta_i^P(\lambda)\beta_j^N(\theta) + \eta_\zeta^n(\lambda,\theta) \tag{3.16}$$

Since (3.13) to (3.16) are useful in both our implementation and analysis, we will derive the expressions for η_u^n, η_v^n, η_ϕ^n and η_ζ^n. We first consider η_u^n. From the definition of the modified latitudinal basis functions for $\tilde{U}_\Delta^n$ in Section 3.2.2, $\beta_j(\theta) = \beta_j^D(\theta)$ for $j = 2,\cdots,N_\theta - 1$. Rewriting the quadratic spline expansion for $\tilde{U}_\Delta^n$ (3.1) in terms of $\{\hat{\beta}_i^P(\lambda)\}_{i=1}^{N_\lambda}$ and $\{\beta_j^D(\theta)\}_{j=2}^{N_\theta-1}$ yields

$$\tilde{U}_\Delta^n(\lambda,\theta) = \sum_{i=1,j=2}^{N_\lambda,N_\theta-1} \tilde{\mathsf{U}}_{i,j}^n\hat{\beta}_i^P(\lambda)\beta_j^D(\theta)$$

$$+\sum_{i=1}^{N_\lambda}\hat{\beta}_i^P(\lambda)\left[\tilde{\mathsf{U}}^n_{i,0}\beta_0(\theta)+\tilde{\mathsf{U}}^n_{i,1}\beta_1(\theta)+\tilde{\mathsf{U}}^n_{i,N_\theta}\beta_{N_\theta}(\theta)+\tilde{\mathsf{U}}^n_{i,N_\theta+1}\beta_{N_\theta+1}(\theta)\right] \tag{3.17}$$

From the definition of β_1^D and $\beta_{N_\theta}^D$, we have $\beta_1=\beta_1^D+\beta_0$ and $\beta_{N_\theta}=\beta_{N_\theta}^D+\beta_{N_\theta+1}$, which can then be used to express the second summation in the right side of (3.17) as

$$\sum_{i=1}^{N_\lambda}\hat{\beta}_i^P(\lambda)\left[\left(\tilde{\mathsf{U}}^n_{i,0}+\tilde{\mathsf{U}}^n_{i,1}\right)\beta_0(\theta)+\tilde{\mathsf{U}}^n_{i,1}\beta_1^D(\theta)+\tilde{\mathsf{U}}^n_{i,N_\theta}\beta_{N_\theta}^D(\theta)+\left(\tilde{\mathsf{U}}^n_{i,N_\theta}+\tilde{\mathsf{U}}^n_{i,N_\theta+1}\right)\beta_{N_\theta+1}(\theta)\right]$$

Substituting the above expression into (3.17) and rearranging yields

$$\begin{aligned}\tilde{U}^n_\Delta(\lambda,\theta) &= \sum_{i,j=1}^{N_\lambda,N_\theta}\tilde{\mathsf{U}}^n_{i,j}\hat{\beta}_i^P(\lambda)\beta_j^D(\theta)\\ &+\sum_{i=1}^{N_\lambda}\hat{\beta}_i^P(\lambda)\left[\left(\tilde{\mathsf{U}}^n_{i,0}+\tilde{\mathsf{U}}^n_{i,1}\right)\beta_0(\theta)+\left(\tilde{\mathsf{U}}^n_{i,N_\theta}+\tilde{\mathsf{U}}^n_{i,N_\theta+1}\right)\beta_{N_\theta+1}(\theta)\right]\end{aligned} \tag{3.18}$$

Comparing (3.18) with (3.13), we obtain the following expression for η_u^n:

$$\eta_u^n(\lambda,\theta) = \sum_{i=1}^{N_\lambda}\hat{\beta}_i^P(\lambda)\left[\left(\tilde{\mathsf{U}}^n_{i,0}+\tilde{\mathsf{U}}^n_{i,1}\right)\beta_0(\theta)+\left(\tilde{\mathsf{U}}^n_{i,N_\theta}+\tilde{\mathsf{U}}^n_{i,N_\theta+1}\right)\beta_{N_\theta+1}(\theta)\right]$$

To compute η_u^n, the coefficients $\{\tilde{\mathsf{U}}^n_{i,j}\}_{i=1,j=0}^{N_\lambda,N_\theta+1}$ are first computed by applying quadratic spline interpolation to

$$\tilde{U}^n_\Delta(\lambda,\theta)=\sum_{i=1,j=0}^{N_\lambda,N_\theta+1}\tilde{\mathsf{U}}^n_{i,j}\hat{\beta}_i^P(\lambda)\beta_j(\theta)$$

using the known values of $\tilde{U}^n_\Delta$ at $\{(\hat{\tau}_{\lambda_i},\tau_{\theta_j})\}_{i=1,j=0}^{N_\lambda,N_\theta+1}$. Then η_u^n is computed using these coefficients. Similar procedures are used to compute η_v^n, η_ϕ^n and η_ζ^n.

From the definition of the modified basis functions for V_Δ^{n+1} in Section 3.2.4, we have $\hat{\beta}_0=\hat{\beta}_0^D+6\hat{\beta}_{-1}$, $\hat{\beta}_1=\hat{\beta}_1^D+\hat{\beta}_{-1}$, $\hat{\beta}_j=\hat{\beta}_j^D$ for $j=2,\cdots,N_\theta-2$, $\hat{\beta}_{N_\theta-1}=\hat{\beta}_{N_\theta-1}^D+\hat{\beta}_{N_\theta+1}$, and $\hat{\beta}_{N_\theta}=\hat{\beta}_{N_\theta}^D+6\hat{\beta}_{N_\theta+1}$. Following similar procedures, the quadratic spline expansion for $\tilde{V}^n_\Delta$ (3.2) can be rewritten in terms of $\{\beta_i^P(\lambda)\}_{i=1}^{N_\lambda}$ and $\{\hat{\beta}_j^D(\theta)\}_{j=0}^{N_\theta}$ to yield

$$\tilde{V}^n_\Delta(\lambda,\theta) = \sum_{i=1,j=0}^{N_\lambda,N_\theta}\tilde{\mathsf{V}}^n_{i,j}\beta_i^P(\lambda)\hat{\beta}_j^D(\theta)$$

$$
\begin{aligned}
&+\sum_{i=1}^{N_\lambda}\beta_i^P(\lambda)\left[\left(\tilde{\mathsf{V}}^n_{i,-1}+6\tilde{\mathsf{V}}^n_{i,0}+\tilde{\mathsf{V}}^n_{i,1}\right)\beta_{-1}(\theta)\right.\\
&\qquad\left.+\left(\tilde{\mathsf{V}}^n_{i,N_\theta-1}+6\tilde{\mathsf{V}}^n_{i,N_\theta}+\tilde{\mathsf{V}}^n_{i,N_\theta+1}\right)\beta_{N_\theta+1}(\theta)\right]\\
\Rightarrow \eta_v^n(\lambda,\theta) \;=\; &\sum_{i=1}^{N_\lambda}\beta_i^P(\lambda)\left[\left(\tilde{\mathsf{V}}^n_{i,-1}+6\tilde{\mathsf{V}}^n_{i,0}+\tilde{\mathsf{V}}^n_{i,1}\right)\beta_{-1}(\theta)\right.\\
&\qquad\left.+\left(\tilde{\mathsf{V}}^n_{i,N_\theta-1}+6\tilde{\mathsf{V}}^n_{i,N_\theta}+\tilde{\mathsf{V}}^n_{i,N_\theta+1}\right)\beta_{N_\theta+1}(\theta)\right]
\end{aligned}
$$

Similarly, from the definition of the modified basis functions for $\tilde{\phi}^n_\Delta$ in Section 3.2.3, we obtain that $\beta_1=\beta_1^N-\beta_0$, $\beta_j=\beta_j^N$ for $j=2,\cdots,N_\theta-1$, and $\beta_{N_\theta}=\beta^N_{N_\theta}-\beta_{N_\theta+1}$. Following similar procedures, the quadratic spline expansion for $\tilde{\phi}^n_\Delta$ (3.3) can be rewritten in terms of $\{\beta_i^P(\lambda)\}_{i=1}^{N_\lambda}$ and $\{\beta_j^N(\theta)\}_{j=1}^{N_\theta}$ to yield

$$
\begin{aligned}
\tilde{\phi}^n_\Delta(\lambda,\theta) \;=\; &\sum_{i,j=1}^{N_\lambda,N_\theta}\tilde{\Phi}^n_{i,j}\beta_i^P(\lambda)\beta_j^N(\theta)\\
&+\sum_{i=1}^{N_\lambda}\beta_i^P(\lambda)\left[\left(\tilde{\Phi}^n_{i,1}-\tilde{\Phi}^n_{i,0}\right)\beta_0(\theta)+\left(\tilde{\Phi}^n_{i,N_\theta}-\tilde{\Phi}^n_{i,N_\theta+1}\right)\beta_{N_\theta+1}(\theta)\right]\\
\Rightarrow \eta_\phi^n(\lambda,\theta) \;=\; &\sum_{i=1}^{N_\lambda}\beta_i^P(\lambda)\left[\left(\tilde{\Phi}^n_{i,1}-\tilde{\Phi}^n_{i,0}\right)\beta_0(\theta)+\left(\tilde{\Phi}^n_{i,N_\theta}-\tilde{\Phi}^n_{i,N_\theta+1}\right)\beta_{N_\theta+1}(\theta)\right] \qquad (3.19)
\end{aligned}
$$

A similar expression can also be derived for η^n_ζ:

$$
\eta_\zeta^n(\lambda,\theta)=\sum_{i=1}^{N_\lambda}\beta_i^P(\lambda)\left[\left(\tilde{\Gamma}^n_{i,1}-\tilde{\Gamma}^n_{i,0}\right)\beta_0(\theta)+\left(\tilde{\Gamma}^n_{i,N_\theta}-\tilde{\Gamma}^n_{i,N_\theta+1}\right)\beta_{N_\theta+1}(\theta)\right]
$$

3.4 The Weighted Residual Formulation

In the weighted residual method, the discrete equations are obtained by incorporating boundary conditions as described in Section 3.2, and imposing conditions on the residuals. Three sets of two-dimensional test functions are chosen in the following manner. Let $\{\varphi_i^P(\lambda)\}_{i=1}^{N_\lambda}$ and $\{\hat{\varphi}_i^P(\lambda)\}_{i=1}^{N_\lambda}$ be the sets of test functions for the one-dimensional spaces corresponding to partitions Δ_λ and $\hat{\Delta}_\lambda$, respectively. Let $\{\varphi_j^S(\theta)\}_{j=1}^{N_\theta}$ and $\{\hat{\varphi}_j^D(\theta)\}_{j=0}^{N_\theta}$ be the corresponding test functions for partitions Δ_θ and $\hat{\Delta}_\theta$, respectively, where $S=D$ for Dirichlet boundary conditions and $S=N$ for Neumann boundary conditions. The sets of two-dimensional test functions for the tensor product grids Δ_1, Δ_2 and Δ_3 are defined to be $\{\hat{\varphi}_i^P(\lambda)\varphi_j^D(\theta)\}_{i=1,j=1}^{N_\lambda,N_\theta}$, $\{\varphi_i^P(\lambda)\hat{\varphi}_j^D(\theta)\}_{i=1,j=0}^{N_\lambda,N_\theta}$, and $\{\varphi_i^P(\lambda)\varphi_j^N(\theta)\}_{i=1,j=1}^{N_\lambda,N_\theta}$, respectively. The approximate solutions (3.1) to (3.4) are rewritten in terms of the adjusted basis functions defined in Section 3.2, and then substituted into equations (2.58) and (2.60). We then set the inner products of the residuals of the resulting equations with each of the two-dimensional test functions, computed on the partitions associated with the test functions, to zero. Imposing the above condition on the residuals yields

$$\begin{aligned}
&\int_{\theta_0}^{\theta_{N_\theta}}\int_{\lambda_0}^{\lambda_{N_\lambda}}\sum_{i=1}^{N_\lambda}\sum_{j=1}^{N_\theta}\Big\{\mathsf{U}_{i,j}^{n+1}\hat{\beta}_i^P(\lambda)\beta_j^D(\theta)\\
&\quad+\left(\frac{\Delta t}{2R^2}\right)\left[c(\theta)\Phi_{i,j}^{n+1}\beta_i^{P'}(\lambda)\beta_j^N(\theta)+d(\theta)\cos\tilde{\theta}\Phi_{i,j}^{n+1}\beta_i^P(\lambda)\beta_j^{N'}(\theta)\right]\Big\}\,\hat{\varphi}_k^P(\lambda)\varphi_l^D(\theta)d\lambda d\theta\\
&\quad=\int_{\theta_0}^{\theta_{N_\theta}}\int_{\lambda_0}^{\lambda_{N_\lambda}}\Bigg\{\sum_{i=1}^{N_\lambda}\sum_{j=1}^{N_\theta}a(\theta)\tilde{\mathsf{U}}_{i,j}^n\hat{\beta}_i^P(\lambda)\beta_j^D(\theta)+\sum_{i=1}^{N_\lambda}\sum_{\hat{j}=0}^{N_\theta}b(\theta)\tilde{\mathsf{V}}_{i,\hat{j}}^n\beta_i^P(\lambda)\hat{\beta}_{\hat{j}}^D(\theta)\\
&\quad-\left(\frac{\Delta t}{2R^2}\right)\sum_{i=1}^{N_\lambda}\sum_{j=1}^{N_\theta}\left[c(\theta)\tilde{\Phi}_{i,j}^n\beta_i^{P'}(\lambda)\beta_j^N(\theta)+d(\theta)\cos\tilde{\theta}\tilde{\Phi}_{i,j}^n\beta_i^P(\lambda)\beta_j^{N'}(\theta)\right]\\
&\quad-\Delta t d(\theta)\tilde{\delta}^{n+\frac{1}{2}}(\lambda,\theta)+r_u^n(\lambda,\theta)\Bigg\}\,\hat{\varphi}_k^P(\lambda)\varphi_l^D(\theta)d\lambda d\theta
\end{aligned}\tag{3.20}$$

for $k=1,\cdots,N_\lambda$, $l=1,\cdots,N_\theta$,

$$\begin{aligned}
&\int_{\theta_0}^{\theta_{N_\theta}}\int_{\lambda_0}^{\lambda_{N_\lambda}}\Bigg\{\sum_{i=1}^{N_\lambda}\sum_{\hat{j}=0}^{N_\theta}\mathsf{V}_{i,\hat{j}}^{n+1}\beta_i^P(\lambda)\hat{\beta}_{\hat{j}}^D(\theta)\\
&\quad+\left(\frac{\Delta t}{2R^2}\right)\sum_{i=1}^{N_\lambda}\sum_{j=1}^{N_\theta}\left[-d(\theta)\Phi_{i,j}^{n+1}\beta_i^{P'}(\lambda)\beta_j^N(\theta)+c(\theta)\cos\tilde{\theta}\Phi_{i,j}^{n+1}\beta_i^P(\lambda)\beta_j^{N'}(\theta)\right]\Bigg\}\\
&\quad\varphi_k^P(\lambda)\hat{\varphi}_{\hat{l}}^D(\theta)d\lambda d\theta\\
&\quad=\int_{\theta_0}^{\theta_{N_\theta}}\int_{\lambda_0}^{\lambda_{N_\lambda}}\Bigg\{-\sum_{i=1}^{N_\lambda}\sum_{j=1}^{N_\theta}b(\theta)\tilde{\mathsf{U}}_{i,j}^n\hat{\beta}_i^P(\lambda)\beta_j^D(\theta)+\sum_{i=1}^{N_\lambda}\sum_{\hat{j}=0}^{N_\theta}a(\theta)\tilde{\mathsf{V}}_{i,\hat{j}}^n\beta_i^P(\lambda)\hat{\beta}_{\hat{j}}^D(\theta)\\
&\quad-\left(\frac{\Delta t}{2R^2}\right)\sum_{i=1}^{N_\lambda}\sum_{j=1}^{N_\theta}\left[-d(\theta)\tilde{\Phi}_{i,j}^n\beta_i^{P'}(\lambda)\beta_j^N(\theta)+c(\theta)\cos\tilde{\theta}\tilde{\Phi}_{i,j}^n\beta_i^P(\lambda)\beta_j^{N'}(\theta)\right]\\
&\quad-\Delta t c(\theta)\tilde{\delta}^{n+\frac{1}{2}}(\lambda,\theta)+r_v^n(\lambda,\theta)\Bigg\}\,\varphi_k^P(\lambda)\hat{\varphi}_{\hat{l}}^D(\theta)d\lambda d\theta
\end{aligned}\tag{3.21}$$

for $k = 1, \cdots, N_\lambda$, $\hat{l} = 0, \cdots, N_\theta$, and

$$\int_{\theta_0}^{\theta_{N_\theta}} \int_{\lambda_0}^{\lambda_{N_\lambda}} \left\{ \sum_{i=1}^{N_\lambda} \sum_{j=1}^{N_\theta} \cos\tilde{\theta}\Gamma_{i,j}^{n+1} \beta_i^P(\lambda)\beta_j^N(\theta) \right.$$
$$\left. + \left(\frac{\Delta t}{2}\right) \left[\sum_{i=1}^{N_\lambda} \sum_{j=1}^{N_\theta} \frac{1}{\cos\tilde{\theta}} \mathsf{U}_{i,j}^{n+1} \hat{\beta}_i^{P'}(\lambda)\beta_j^D(\theta) + \sum_{i=1}^{N_\lambda} \sum_{\hat{j}=0}^{N_\theta} \mathsf{V}_{i,\hat{j}}^{n+1} \beta_i^P(\lambda)\hat{\beta}_{\hat{j}}^{D'}(\theta) \right] \right\}$$
$$\varphi_k^P(\lambda)\varphi_l^N(\theta) d\lambda d\theta$$
$$= \int_{\theta_0}^{\theta_{N_\theta}} \int_{\lambda_0}^{\lambda_{N_\lambda}} \left\{ \sum_{i=1}^{N_\lambda} \sum_{j=1}^{N_\theta} \cos\tilde{\theta}\tilde{\Gamma}_{i,j}^{n} \beta_i^P(\lambda)\beta_j^N(\theta) \right.$$
$$- \left(\frac{\Delta t}{2}\right) \left[\frac{1}{\cos\tilde{\theta}} \sum_{i=1}^{N_\lambda} \sum_{j=1}^{N_\theta} \tilde{\mathsf{U}}_{i,j}^{n} \hat{\beta}_i^{P'}(\lambda)\beta_j^D(\theta) + \sum_{i=1}^{N_\lambda} \sum_{\hat{j}=0}^{N_\theta} \tilde{\mathsf{V}}_{i,\hat{j}}^{n} \beta_i^P(\lambda)\hat{\beta}_{\hat{j}}^{\prime D}(\theta) \right]$$
$$\left. + r_\phi^n(\lambda,\theta) \right\} \varphi_k^P(\lambda)\varphi_l^N(\theta) d\lambda d\theta \tag{3.22}$$

for $k = 1, \cdots, N_\lambda$, $l = 1, \cdots, N_\theta$. The residual terms r_u^n, r_v^n and r_ϕ^n arise from non-homogeneous boundary conditions imposed on the upstream functions, and are defined by

$$\begin{aligned}
r_u^n(\lambda,\theta) &= a(\theta)\eta_u^n(\lambda,\theta) + b(\theta)\eta_v^n(\lambda,\theta) \\
&\quad - \left(\frac{\Delta t}{2R^2}\right) \left[c(\theta)(\eta_\phi^n)_\lambda(\lambda,\theta) + d(\theta)\cos\tilde{\theta}(\eta_\phi^n)_\theta(\lambda,\theta) \right] \\
r_v^n(\lambda,\theta) &= -b(\theta)\eta_u^n(\lambda,\theta) + a(\theta)\eta_v^n(\lambda,\theta) \\
&\quad - \left(\frac{\Delta t}{2R^2}\right) \left[-d(\theta)(\eta_\phi^n)_\lambda(\lambda,\theta) + c(\theta)\cos\tilde{\theta}(\eta_\phi^n)_\theta(\lambda,\theta) \right] \\
r_\phi^n(\lambda,\theta) &= \cos\tilde{\theta}\eta_\zeta^n(\lambda,\theta) - \left(\frac{\Delta t}{2}\right) \left[\frac{1}{\cos\tilde{\theta}} (\eta_u^n)_\lambda(\lambda,\theta) + (\eta_v^n)_\theta(\lambda,\theta) \right]
\end{aligned}$$

Equations (3.20) to (3.22) can be expressed in matrix form using the mass and first derivative matrices defined below.

3.4.1 Matrices in the Longitudinal Dimension

The mass and first derivative matrices in the longitudinal dimension, where functions are assumed to be periodic, may be written in terms of the adjusted basis functions as

$$
\begin{aligned}
P_{i,j} &= \tfrac{1}{\omega_\lambda}\int_{\lambda_0}^{\lambda_{N_\lambda}} \beta_j^P(\lambda)\varphi_i^P(\lambda)d\lambda, & P_{\lambda i,j} &= \tfrac{1}{\omega_\lambda}\int_{\lambda_0}^{\lambda_{N_\lambda}} \beta_j^{P'}(\lambda)\varphi_i^P(\lambda)d\lambda,\\
\hat{P}_{i,j} &= \tfrac{1}{\omega_\lambda}\int_{\lambda_0}^{\lambda_{N_\lambda}} \hat{\beta}_j^P(\lambda)\hat{\varphi}_i^P(\lambda)d\lambda, & \hat{P}_{\lambda_{i,j}} &= \tfrac{1}{\omega_\lambda}\int_{\lambda_0}^{\lambda_{N_\lambda}} \hat{\beta}_j^{P'}(\lambda)\hat{\varphi}_i^P(\lambda)d\lambda,\\
P_{i,j}^{\Delta\to\hat{\Delta}} &= \tfrac{1}{\omega_\lambda}\int_{\lambda_0}^{\lambda_{N_\lambda}} \beta_j^P(\lambda)\hat{\varphi}_i^P(\lambda)d\lambda, & P_{\lambda i,j}^{\Delta\to\hat{\Delta}} &= \tfrac{1}{\omega_\lambda}\int_{\lambda_0}^{\lambda_{N_\lambda}} \beta_j^{P'}(\lambda)\hat{\varphi}_i^P(\lambda)d\lambda,\\
P_{i,j}^{\hat{\Delta}\to\Delta} &= \tfrac{1}{\omega_\lambda}\int_{\lambda_0}^{\lambda_{N_\lambda}} \hat{\beta}_j^P(\lambda)\varphi_i^P(\lambda)d\lambda, & P_{\lambda i,j}^{\hat{\Delta}\to\Delta} &= \tfrac{1}{\omega_\lambda}\int_{\lambda_0}^{\lambda_{N_\lambda}} \hat{\beta}_j^{P'}(\lambda)\varphi_i^P(\lambda)d\lambda
\end{aligned}
$$

for $i,\ j = 1, \cdots, N_\lambda$, where ω_λ is a scaling factor independent of λ and θ. Since both the basis functions and test functions are periodic in the longitudinal dimension, and $\hat{\beta}_j(\lambda) = \beta_j(\lambda - \Delta\lambda/2)$, if $\hat{\varphi}_j^P(\lambda) = \varphi_j^P(\lambda - \Delta\lambda/2)$, which holds for the test functions for Galerkin and collocation, then $\hat{P}_{i,j} = P_{i,j}$ and $\hat{P}_{\lambda_{i,j}} = P_{\lambda_{i,j}}$. Therefore, throughout this thesis, we will drop $\hat{P}_{i,j}$ and $\hat{P}_{\lambda_{i,j}}$ and use $P_{i,j}$ and $P_{\lambda_{i,j}}$ instead.

In our mathematical analysis, we use periodic boundary conditions in the latitudinal dimension as well. When periodic boundary conditions are applied in the latitudinal dimension, the mass and first derivative matrices in the latitudinal dimension are defined similarly as the corresponding matrices in the longitudinal dimension, and are written without a superscript.

In our implementation, as mentioned before, we use homogeneous Dirichlet boundary conditions for U_Δ^{n+1} and V_Δ^{n+1}, and Neumann ones for ϕ_Δ^{n+1}. Next we describe the mass and first derivative matrices corresponding to the latitudinal dimension and arising in our implementation.

3.4.2 Matrices in the Latitudinal Dimension — U_Δ^{n+1}

In the θ-direction, the integrals may involve functions other than the basis or test functions, such as $a(\theta)$, $b(\theta)$, $c(\theta)$ or $d(\theta)$ defined in (2.61). We first define in terms of β_j^D the matrices

$$Q^D_{i,j} = \frac{1}{\omega_\theta}\int_{\theta_0}^{\theta_{N_\theta}} \beta^D_j(\theta)\varphi^D_i(\theta)d\theta, \qquad Q^D_{\theta\ i,j} = \frac{1}{\omega_\theta}\int_{\theta_0}^{\theta_{N_\theta}} \beta^{D'}_j(\theta)\varphi^D_i(\theta)d\theta,$$
$$Q^{D,\Delta\to\hat{\Delta}}_{k,j} = \frac{1}{\omega_\theta}\int_{\theta_0}^{\theta_{N_\theta}} \beta^D_j(\theta)\hat{\varphi}^D_k(\theta)d\theta, \quad Q_\theta{}^{D,\Delta\to\hat{\Delta}}_{k,j} = \frac{1}{\omega_\theta}\int_{\theta_0}^{\theta_{N_\theta}} \beta^{D'}_j(\theta)\hat{\varphi}^D_k(\theta)d\theta$$

for $i,\ j = 1,\cdots,N_\theta$, and $k = 0,\cdots,N_\theta$, The scaling factor ω_θ is independent of λ and θ. Note that Q^D and Q^D_θ are $N_\theta \times N_\theta$ matrices whereas $Q^{D,\Delta\to\hat{\Delta}}$ and $Q^{D,\Delta\to\hat{\Delta}}_\theta$ are $(N_\theta+1)\times N_\theta$. We then consider an arbitrary function $g(\theta)$ and use the following notation to define the associated mass and first derivative matrices

$$\{Q^D \circ g\}_{i,j} = \frac{1}{\omega_\theta}\int_{\theta_0}^{\theta_{N_\theta}} g(\theta)\beta^D_j(\theta)\varphi^D_i(\theta)d\theta,$$
$$\{Q^D_\theta \circ g\}_{i,j} = \frac{1}{\omega_\theta}\int_{\theta_0}^{\theta_{N_\theta}} g(\theta)\beta^{D'}_j(\theta)\varphi^D_i(\theta)d\theta,$$
$$\{Q^{D,\Delta\to\hat{\Delta}} \circ g\}_{k,j} = \frac{1}{\omega_\theta}\int_{\theta_0}^{\theta_{N_\theta}} g(\theta)\beta^D_j(\theta)\hat{\varphi}^D_k(\theta)d\theta,$$
$$\{Q^{D,\Delta\to\hat{\Delta}}_\theta \circ g\}_{k,j} = \frac{1}{\omega_\theta}\int_{\theta_0}^{\theta_{N_\theta}} g(\theta)\beta^{D'}_j(\theta)\hat{\varphi}^D_k(\theta)d\theta$$

for $i,\ j = 1,\cdots,N_\theta$, and $k = 0,\cdots,N_\theta$. Note that in the above definition the symbol $\circ$ does not mean function composition.

3.4.3 Matrices in the Latitudinal Dimension — ϕ^{n+1}_Δ

The mass and first derivative matrices for ϕ^{n+1}_Δ in the latitudinal dimension are identified by the superscript N, and expressed in terms of β^N_j. We first define the matrices

$$Q^N_{i,j} = \frac{1}{\omega_\theta}\int_{\theta_0}^{\theta_{N_\theta}} \beta^N_j(\theta)\varphi^N_i(\theta)d\theta, \qquad Q^N_{\theta\ i,j} = \frac{1}{\omega_\theta}\int_{\theta_0}^{\theta_{N_\theta}} \beta^{N'}_j(\theta)\varphi^N_i(\theta)d\theta,$$
$$Q^{N,\Delta\to\hat{\Delta}}_{k,j} = \frac{1}{\omega_\theta}\int_{\theta_0}^{\theta_{N_\theta}} \beta^N_j(\theta)\hat{\varphi}^D_k(\theta)d\theta, \quad Q_\theta{}^{N,\Delta\to\hat{\Delta}}_{k,j} = \frac{1}{\omega_\theta}\int_{\theta_0}^{\theta_{N_\theta}} \beta^{N'}_j(\theta)\hat{\varphi}^D_k(\theta)d\theta$$

for $i,\ j = 1,\cdots,N_\theta$, and $k = 0,\cdots,N_\theta$. Note that Q^N and $Q^N_\theta \in R^{N_\theta\times N_\theta}$ whereas $Q^{N,\Delta\to\hat{\Delta}}$ and $Q^{N,\Delta\to\hat{\Delta}}_\theta \in R^{(N_\theta+1)\times N_\theta}$. The associated mass and first derivative matrices for ϕ^{n+1}_Δ in the latitudinal dimension are defined by

$$\{Q^N \circ g\}_{i,j} = \frac{1}{\omega_\theta}\int_{\theta_0}^{\theta_{N_\theta}} g(\theta)\beta^N_j(\theta)\varphi^N_i(\theta)d\theta,$$
$$\{Q^N_\theta \circ g\}_{i,j} = \frac{1}{\omega_\theta}\int_{\theta_0}^{\theta_{N_\theta}} g(\theta)\beta^{N'}_j(\theta)\varphi^N_i(\theta)d\theta,$$
$$\{Q^{N,\Delta\to\hat{\Delta}} \circ g\}_{k,j} = \frac{1}{\omega_\theta}\int_{\theta_0}^{\theta_{N_\theta}} g(\theta)\beta^N_j(\theta)\hat{\varphi}^D_k(\theta)d\theta,$$
$$\{Q^{N,\Delta\to\hat{\Delta}}_\theta \circ g\}_{k,j} = \frac{1}{\omega_\theta}\int_{\theta_0}^{\theta_{N_\theta}} g(\theta)\beta^{N'}_j(\theta)\hat{\varphi}^D_k(\theta)d\theta$$

for $i,\ j = 1,\cdots,N_\theta$, and $k = 0,\cdots,N_\theta$.

3.4.4 Matrices in the Latitudinal Dimension — V_Δ^{n+1}

The mass and first derivative matrices for V_Δ^{n+1} in the latitudinal dimension are identified by the superscript D and the hat symbol, or the superscript $\hat{\Delta} \to \Delta$. We first define the matrices

$$\{\hat{Q}^D\}_{i,j} = \frac{1}{\omega_\theta}\int_{\theta_0}^{\theta_{N_\theta}} \hat{\beta}_j^D(\theta)\hat{\varphi}_i^D(\theta)d\theta, \qquad \{\hat{Q}_\theta^D\}_{i,j} = \frac{1}{\omega_\theta}\int_{\theta_0}^{\theta_{N_\theta}} g(\theta)\hat{\beta}_j^{D\prime}(\theta)\hat{\varphi}_i^D(\theta)d\theta,$$
$$\{Q^{D,\hat{\Delta}\to\Delta}\}_{k,j} = \frac{1}{\omega_\theta}\int_{\theta_0}^{\theta_{N_\theta}} \hat{\beta}_j^D(\theta)\varphi_k^D(\theta)d\theta, \quad \{Q_\theta^{D,\hat{\Delta}\to\Delta}\}_{k,j} = \frac{1}{\omega_\theta}\int_{\theta_0}^{\theta_{N_\theta}} \hat{\beta}_j^{\prime D}(\theta)\varphi_k^N(\theta)d\theta$$

for $i,\ j = 0,\cdots,N_\theta$, and $k = 1,\cdots,N_\theta$. The matrices $\hat{Q}^D$ and $\hat{Q}_\theta^D \in R^{(N_\theta+1)\times(N_\theta+1)}$ whereas $Q^{D,\hat{\Delta}\to\Delta}$ and $Q_\theta^{D,\hat{\Delta}\to\Delta} \in R^{N_\theta\times(N_\theta+1)}$. The associated mass and first derivative matrices are then defined by

$$\begin{aligned}
\{\hat{Q}^D \circ g\}_{i,j} &= \frac{1}{\omega_\theta}\int_{\theta_0}^{\theta_{N_\theta}} g(\theta)\hat{\beta}_j^D(\theta)\hat{\varphi}_i^D(\theta)d\theta,\\
\{\hat{Q}_\theta^D \circ g\}_{i,j} &= \frac{1}{\omega_\theta}\int_{\theta_0}^{\theta_{N_\theta}} g(\theta)\hat{\beta}_j^{D\prime}(\theta)\hat{\varphi}_i^D(\theta)d\theta,\\
\{Q^{D,\hat{\Delta}\to\Delta} \circ g\}_{k,j} &= \frac{1}{\omega_\theta}\int_{\theta_0}^{\theta_{N_\theta}} g(\theta)\hat{\beta}_j^D(\theta)\varphi_k^D(\theta)d\theta,\\
\{Q_\theta^{D,\hat{\Delta}\to\Delta} \circ g\}_{k,j} &= \frac{1}{\omega_\theta}\int_{\theta_0}^{\theta_{N_\theta}} g(\theta)\hat{\beta}_j^{\prime D}(\theta)\varphi_k^N(\theta)d\theta
\end{aligned}$$

for $i,\ j = 0,\cdots,N_\theta$, and $k = 1,\cdots,N_\theta$.

3.5 Upstream Function Representation

The values of a function can be related to the coefficients in its spline representation as follows. Let $\mathbf{U}^{n+1}$, $\mathbf{\Gamma}^{n+1}$, $\mathbf{\Phi}^{n+1} \in R^{N_\lambda\cdot N_\theta}$ and $\mathbf{V}^{n+1} \in R^{N_\lambda\cdot(N_\theta+1)}$ be the coefficient vectors for U_Δ^{n+1}, ζ_Δ^{n+1}, ϕ_Δ^{n+1} and V_Δ^{n+1}, respectively, in the natural ordering beginning with the λ-dimension. That is, $\mathbf{U}_{i+(j-1)N_\lambda}^{n+1} = \mathsf{U}_{i,j}^{n+1}$, for example.

Consider the biquadratic spline approximation for the geopotential ϕ_Δ^{n+1} evaluated at a midpoint $(\tau_{\lambda_i}, \tau_{\theta_j})$:

$$\phi_\Delta^{n+1}(\tau_{\lambda_i}, \tau_{\theta_j}) = \sum_{k,l} \Phi_{k,l}^{n+1}\beta_k^P(\tau_{\lambda_i})\beta_l^N(\tau_{\theta_j})$$

Let

$$E_{\lambda_{i,k}} = \beta_k^P(\tau_{\lambda_i}), \qquad E^N_{\theta_{j,l}} = \beta_l^N(\tau_{\theta_j})$$

and $E_\lambda = (E_{\lambda_{i,k}})_{i,k=1}^{N_\lambda}$ and $E_\theta^N = (E^N_{\theta_{j,l}})_{j,l=1}^{N_\theta}$ be the associated matrices. Let $\boldsymbol{\phi}_{\boldsymbol{\Delta}}^{\boldsymbol{n+1}} \in R^{N_\lambda \cdot N_\theta}$ be the vector of function values $\phi_\Delta^{n+1}(\tau_{\lambda_i}, \tau_{\theta_j})$ in the natural ordering beginning with the λ-dimension. Then

$$(E_\lambda \otimes E_\theta^N)\mathbf{\Phi}^{n+1} = \boldsymbol{\phi}_{\boldsymbol{\Delta}}^{\boldsymbol{n+1}} \tag{3.23}$$

Similar relations hold for the other functions and the associated vectors of coefficients and values of functions. The matrices associated with U_Δ^{n+1} and V_Δ^{n+1} are $(E_\lambda \otimes E_\theta^D)$ and $(E_\lambda \otimes \hat{E}_\theta^D)$, respectively, where

$$E^D_{\theta_{i,k}} = \beta_k^D(\tau_{\theta_i}), \qquad \hat{E}^D_{\theta_{j,l}} = \hat{\beta}_l^D(\tau_{\theta_j})$$

and $E_\theta^D = (E^D_{\theta_{i,k}})_{i,k=1}^{N_\theta}$ and $\hat{E}_\theta^D = (\hat{E}^D_{\theta_{j,l}})_{j,l=0}^{N_\theta}$. Note that, if linear splines are used, the coefficients are the same as the function values at gridpoints, and so each of the above matrices reduces to the identity matrix.

The inverses of $(E_\lambda \otimes E_\theta^N)$, $(E_\lambda \otimes E_\theta^D)$ and $(E_\lambda \otimes \hat{E}_\theta^D)$ can be used to compute spline coefficients from function values. Suppose we want to compute the spline representation for ϕ^{n+1} given its values at midpoints. Then it follows from (3.23) that the spline coefficient vector $\mathbf{\Phi}^{n+1}$ can be computed as

$$\mathbf{\Phi}^{n+1} = (E_\lambda \otimes E_\theta^N)^{-1}\boldsymbol{\phi}_{\boldsymbol{\Delta}}^{\boldsymbol{n+1}} \tag{3.24}$$

Now suppose we want to expand the function $\tilde{\phi}_\Delta^n$ in terms of the splines. The spline coefficient vector $\tilde{\mathbf{\Phi}}^n$ can be computed from the values of ϕ_Δ^n at the midpoints as follows. First, the values of ϕ_Δ^n at departure points $(\tau_{\lambda_i} - \delta\tau_{\lambda_i}^{n+1}, \tau_{\theta_j} - \delta\tau_{\theta_j}^{n+1})$ are estimated from midpoint values using cubic Lagrange interpolation. Cubic Lagrange interpolation is used instead of quadratic spline interpolation because the latter gives third-order errors at points that are neither gridpoints nor midpoints. Second, recall the definition of $\tilde{\phi}_\Delta^n$

$$\tilde{\phi}_\Delta^n(\tau_{\lambda_i}, \tau_{\theta_j}) \equiv \phi_\Delta^n(\tau_{\lambda_i} - \delta\tau_{\lambda_i}^{n+1}, \tau_{\theta_j} - \delta\tau_{\theta_j}^{n+1}) \tag{3.25}$$

where $\delta\tau_{\lambda_i}^{n+1}$ and $\delta\tau_{\theta_j}^{n+1}$ denote the particle displacements in the λ- and θ-coordinates, respectively, in the time interval t_n to t_{n+1}.[1] Third, as described in Section 3.3, $\tilde{\mathbf{\Phi}}^n$ is computed by applying quadratic interpolation to

$$\tilde{\phi}_\Delta^n(\lambda,\theta) = \sum_{i=1,j=0}^{N_\lambda,N_\theta+1} \tilde{\Phi}_{i,j}^n \beta_i^P(\lambda)\beta_j^N(\theta)$$

using the known values of $\tilde{\phi}_\Delta^n$ at $\{(\tau_{\lambda_i},\tau_{\theta_j})\}_{i=1,j=0}^{N_\lambda,N_\theta}$. The spline coefficient vector satisfies the following relation:

$$(E_\lambda \otimes E_\theta^N)\tilde{\mathbf{\Phi}}^n = (\tilde{\boldsymbol{\phi}}_{\boldsymbol{\Delta}}^{\boldsymbol{n}} - \boldsymbol{\eta}_\phi^n) \tag{3.26}$$

where η_ϕ^n arises from the general boundary conditions imposed on $\tilde{\phi}_\Delta$ (see Section 3.3), and $(\boldsymbol{\eta}_\phi^n)_{i+(j-1)N_\lambda} \equiv \eta_\phi^n(\tau_{\lambda_i},\tau_{\theta_j})$ for $i = 1,\cdots,N_\lambda$ and $j = 1,\cdots,N_\theta$. Similarly, $\tilde{\mathsf{U}}_\Delta^n$ and $\tilde{\mathsf{V}}_\Delta^n$ can be computed from the midpoint values of U_Δ^n and V_Δ^n.

3.6 Derivation of the Helmholtz Equation

Equations (3.20) to (3.22) are expressed in matrix form using the mass and first derivative matrices defined in Section 3.4, and then solved by using (3.20) and (3.21) to eliminate the U^{n+1} and V^{n+1} dependence in (3.22), and then using the relationship between Γ and Φ (see Section 3.1.1). The result is a discretized Helmholtz equation for ϕ_Δ^{n+1}, which is nonlinear due to the presence of a logarithmic term. The discretized Helmholtz equation is linearized and solved using fixed-point iteration. Once ϕ_Δ^{n+1} is computed, U_Δ^{n+1} and V_Δ^{n+1} are updated using the discretized motion equations (3.20) and (3.21). The details of this procedure are described below.

Let $\tilde{\boldsymbol{\delta}}_u^{n+\frac{1}{2}}$ and $\tilde{\boldsymbol{\delta}}_v^{n+\frac{1}{2}}$ denote the vectors of values of the integrals $\frac{1}{\omega_\lambda\omega_\theta}\int\int d(\theta)\tilde{\delta}^{n+\frac{1}{2}}(\lambda,\theta)\hat{\varphi}_i^P(\lambda)\varphi_j^D(\theta)d\lambda d\theta$ and $\frac{1}{\omega_\lambda\omega_\theta}\int\int c(\theta)\tilde{\delta}^{n+\frac{1}{2}}(\lambda,\theta)\varphi_i^P(\lambda)\hat{\varphi}_j^D(\theta)d\lambda d\theta$, re-

[1]Note that with quadratic splines, function values at midpoints of the spline grid partitions are needed to compute the approximate solution. Therefore, in this context, we modify the definition of $\delta\lambda_l^{n+1}$ and $\delta\theta_m^{n+1}$ given in Section 2.6 to be the distance traveled by a fluid particle in the time interval t_n to t_{n+1} whose trajectory ends at the (l,m)-th *midpoint* (instead of gridpoint) at time-level t_{n+1}.

spectively, and $\boldsymbol{r}_u^n$, $\boldsymbol{r}_v^n$ and $\boldsymbol{r}_\phi^n$ denote the vectors of values of $\frac{1}{\omega_\lambda\omega_\theta}\int\int r_u^n(\lambda,\theta)\hat{\varphi}_i^P(\lambda)\varphi_j^D(\theta)d\lambda d\theta$, $\frac{1}{\omega_\lambda\omega_\theta}\int\int r_v^n(\lambda,\theta)\varphi_i^P(\lambda)\hat{\varphi}_j^D(\theta)d\lambda d\theta$ and $\frac{1}{\omega_\lambda\omega_\theta}\int\int r_\phi^n(\lambda,\theta)\varphi_i^P(\lambda)\varphi_j^D(\theta)d\lambda d\theta$, respectively, arranged in the natural ordering. Equations (3.20) to (3.22) can be expressed in tensor product form and rearranged as

$$\begin{aligned}(P\otimes Q^D)\mathbf{U}^{n+1} &+ \left(\frac{\Delta t}{2R^2}\right)\left[(P_\lambda^{\Delta\to\hat{\Delta}}\otimes Q^N\circ c)+(P^{\Delta\to\hat{\Delta}}\otimes Q_\theta^N\circ(d\cos\tilde{\theta}))\right]\mathbf{\Phi}^{n+1}\\ &= (P\otimes Q^D\circ a)\tilde{\mathbf{U}}^n+(P^{\Delta\to\hat{\Delta}}\otimes Q^{D,\hat{\Delta}\to\Delta}\circ b)\tilde{\mathbf{V}}^n\\ &-\left(\frac{\Delta t}{2R^2}\right)\left[\left(P_\lambda^{\Delta\to\hat{\Delta}}\otimes Q^N\circ c\right)+(P^{\Delta\to\hat{\Delta}}\otimes Q_\theta^N\circ(d\cos\tilde{\theta}))\right]\tilde{\mathbf{\Phi}}^n-\Delta t\tilde{\boldsymbol{\delta}}_u^{n+\frac{1}{2}}+\boldsymbol{r}_u^n\end{aligned}\tag{3.27}$$

$$\begin{aligned}(P\otimes\hat{Q}^D)\mathbf{V}^{n+1} &+ \left(\frac{\Delta t}{2R^2}\right)\left[-(P_\lambda\otimes Q^{N,\Delta\to\hat{\Delta}}\circ d)+(P\otimes Q_\theta^{N,\Delta\to\hat{\Delta}}\circ(c\cos\tilde{\theta}))\right]\mathbf{\Phi}^{n+1}\\ &= -(P^{\hat{\Delta}\to\Delta}\otimes Q^{D,\Delta\to\hat{\Delta}}\circ b)\tilde{\mathbf{U}}^n+(P\otimes\hat{Q}^D\circ a)\tilde{\mathbf{V}}^n\\ &-\left(\frac{\Delta t}{2R^2}\right)\left[-(P_\lambda\otimes Q^{N,\Delta\to\hat{\Delta}}\circ d)+(P\otimes Q_\theta^{N,\Delta\to\hat{\Delta}}\circ(c\cos\tilde{\theta}))\right]\tilde{\mathbf{\Phi}}^n-\Delta t\tilde{\boldsymbol{\delta}}_v^{n+\frac{1}{2}}+\boldsymbol{r}_v^n\end{aligned}\tag{3.28}$$

$$\begin{aligned}(P\otimes Q^N\circ\cos\tilde{\theta})\mathbf{\Gamma}^{n+1} &+ \left(\frac{\Delta t}{2}\right)\left[\left(P_\lambda^{\hat{\Delta}\to\Delta}\otimes Q^D\circ\left(\frac{1}{\cos\tilde{\theta}}\right)\right)\mathbf{U}^{n+1}+\left(P\otimes Q_\theta^{D,\hat{\Delta}\to\Delta}\right)\mathbf{V}^{n+1}\right]\\ &= (P\otimes Q^N\circ\cos\tilde{\theta})\tilde{\mathbf{\Gamma}}^n-\left(\frac{\Delta t}{2}\right)\left[\left(P_\lambda^{\hat{\Delta}\to\Delta}\otimes Q^D\circ\left(\frac{1}{\cos\tilde{\theta}}\right)\right)\tilde{\mathbf{U}}^n\right.\\ &\qquad\left.+\left(P\otimes Q_\theta^{D,\hat{\Delta}\to\Delta}\right)\tilde{\mathbf{V}}^n\right]+\boldsymbol{r}_\phi^n\end{aligned}\tag{3.29}$$

The next step involves eliminating the $\mathbf{U}^{n+1}$ and $\mathbf{V}^{n+1}$ dependence from the discretized continuity equation (3.29) using (3.27) and (3.28). By pre-multiplying (3.27) and (3.28) by the inverses of $(P\otimes Q^D)$ and $(P\otimes\hat{Q}^D)$, respectively, and rearranging, $\mathbf{U}^{n+1}$ and $\mathbf{V}^{n+1}$ can be expressed in terms of $\mathbf{\Phi}^{n+1}$ and other quantities that are known. Then by pre-multiplying the resulting equations by $(P_\lambda^{\hat{\Delta}\to\Delta}\otimes Q^D\circ(\frac{1}{\cos\tilde{\theta}}))$ and $(P\otimes Q_\theta^{D,\hat{\Delta}\to\Delta})$ respectively, we obtain

$$\begin{aligned}\left(P_\lambda^{\hat{\Delta}\to\Delta}\otimes Q^D\circ\left(\frac{1}{\cos\tilde{\theta}}\right)\right)\mathbf{U}^{n+1} &= \left(P_\lambda^{\hat{\Delta}\to\Delta}\otimes Q^D\circ\left(\frac{1}{\cos\tilde{\theta}}\right)\right)(P\otimes Q^D)^{-1}\times\\ &\left\{-\left(\frac{\Delta t}{2R^2}\right)\left[\left(P_\lambda^{\Delta\to\hat{\Delta}}\otimes Q^N\circ c\right)+(P^{\Delta\to\hat{\Delta}}\otimes Q_\theta^N\circ(d\cos\tilde{\theta}))\right](\mathbf{\Phi}^{n+1}+\tilde{\mathbf{\Phi}}^n)\right.\end{aligned}$$

$$+ (P \otimes Q^D \circ a)\tilde{\mathbf{U}}^n + (P^{\Delta\to\hat{\Delta}} \otimes Q^{D,\hat{\Delta}\to\Delta} \circ b)\tilde{\mathbf{V}}^n - \Delta t \tilde{\boldsymbol{\delta}}_u^{n+\frac{1}{2}} + \boldsymbol{r}_u^n \Big\} \tag{3.30}$$

$$\begin{aligned}(P \otimes Q_\theta^{D,\hat{\Delta}\to\Delta})\mathbf{V}^{n+1} = {}& (P \otimes Q_\theta^{D,\hat{\Delta}\to\Delta})(P \otimes \hat{Q}^D)^{-1} \times \\ & \Big\{ -\left(\frac{\Delta t}{2R^2}\right) \left[-(P_\lambda \otimes Q^{N,\Delta\to\hat{\Delta}} \circ d) + (P \otimes Q_\theta^{N,\Delta\to\hat{\Delta}} \circ (c\cos\tilde{\theta}))\right] (\boldsymbol{\Phi}^{n+1} + \tilde{\boldsymbol{\Phi}}^n) \\ & - (P^{\hat{\Delta}\to\Delta} \otimes Q^{D,\Delta\to\hat{\Delta}} \circ b)\tilde{\mathbf{U}}^n + (P \otimes \hat{Q}^D \circ a)\tilde{\mathbf{V}}^n - \Delta t \tilde{\boldsymbol{\delta}}_v^{n+\frac{1}{2}} + \boldsymbol{r}_v^n \Big\}\end{aligned} \tag{3.31}$$

which can then be substituted into (3.29) to eliminate the divergence term and yield the equation

$$\begin{aligned}(P \otimes Q^N \circ \cos\tilde{\theta})\boldsymbol{\Gamma}^{n+1} &+ \left(\frac{\Delta t}{2}\right) \left(P_\lambda^{\hat{\Delta}\to\Delta} \otimes Q^D \circ \left(\frac{1}{\cos\tilde{\theta}}\right)\right) (P \otimes Q^D)^{-1} \times \\ & \Big\{ (P \otimes Q^D \circ a)\tilde{\mathbf{U}}^n + (P^{\Delta\to\hat{\Delta}} \otimes Q^{D,\hat{\Delta}\to\Delta} \circ b)\tilde{\mathbf{V}}^n - \Delta t \tilde{\boldsymbol{\delta}}_u^{n+\frac{1}{2}} + \boldsymbol{r}_u^n \\ & - \left(\frac{\Delta t}{2R^2}\right) \left[(P_\lambda^{\Delta\to\hat{\Delta}} \otimes Q^N \circ c) + (P^{\Delta\to\hat{\Delta}} \otimes Q_\theta^N \circ (d\cos\tilde{\theta}))\right] (\boldsymbol{\Phi}^{n+1} + \tilde{\boldsymbol{\Phi}}^n) \Big\} \\ & + \left(\frac{\Delta t}{2}\right) \left(P \otimes Q_\theta^{D,\hat{\Delta}\to\Delta}\right) (P \otimes \hat{Q}^D)^{-1} \times \\ & \Big\{ -(P^{\hat{\Delta}\to\Delta} \otimes Q^{D,\Delta\to\hat{\Delta}} \circ b)\tilde{\mathbf{U}}^n + (P \otimes \hat{Q}^D \circ a)\tilde{\mathbf{V}}^n - \Delta t \tilde{\boldsymbol{\delta}}_v^{n+\frac{1}{2}} + \boldsymbol{r}_v^n \\ & - \left(\frac{\Delta t}{2R^2}\right) \left[-(P_\lambda \otimes Q^{N,\Delta\to\hat{\Delta}} \circ d) + (P \otimes Q_\theta^{N,\Delta\to\hat{\Delta}} \circ (c\cos\tilde{\theta}))\right] (\boldsymbol{\Phi}^{n+1} + \tilde{\boldsymbol{\Phi}}^n) \Big\} \\ = {}& (P \otimes Q^N \circ \cos\tilde{\theta})\tilde{\boldsymbol{\Gamma}}^n - \left(\frac{\Delta t}{2}\right) \left[\left(P_\lambda^{\hat{\Delta}\to\Delta} \otimes Q^D \circ \left(\frac{1}{\cos\tilde{\theta}}\right)\right) \tilde{\mathbf{U}}^n \right. \\ & \left. + \left(P \otimes Q_\theta^{D,\hat{\Delta}\to\Delta}\right) \tilde{\mathbf{V}}^n \right] + \boldsymbol{r}_\phi^n\end{aligned} \tag{3.32}$$

which is an approximation to a Helmholtz equation, with

$$\left(P_\lambda^{\hat{\Delta}\to\Delta} \otimes Q^D \circ \left(\frac{1}{\cos\tilde{\theta}}\right)\right) (P \otimes Q^D)^{-1} \left(P_\lambda^{\Delta\to\hat{\Delta}} \otimes Q^N \circ c\right) \boldsymbol{\Phi}^{n+1}, \text{ and}$$
$$\left(P \otimes Q_\theta^{D,\hat{\Delta}\to\Delta}\right) (P \otimes \hat{Q}^D)^{-1} \left(P \otimes Q_\theta^{N,\Delta\to\hat{\Delta}} \circ (c\cos\tilde{\theta})\right) \boldsymbol{\Phi}^{n+1}$$

approximating the second derivative terms $(\frac{c}{\cos\tilde{\theta}})\phi_{\lambda\lambda}^{n+1}$ and $(c\cos\tilde{\theta})\phi_{\theta\theta}^{n+1}$, respectively, at the midpoints of Δ_3. Note that the two terms

$$\left(P_\lambda^{\hat{\Delta}\to\Delta} \otimes Q^D \circ \left(\frac{1}{\cos\tilde{\theta}}\right)\right) (P \otimes Q^D)^{-1} \left(P^{\Delta\to\hat{\Delta}} \otimes Q_\theta^N \circ (d\cos\tilde{\theta})\right) \boldsymbol{\Phi}^{n+1} \text{ and}$$
$$-\left(P \otimes Q_\theta^{D,\hat{\Delta}\to\Delta}\right) (P \otimes \hat{Q}^D)^{-1} \left(P_\lambda \otimes Q^{N,\Delta\to\hat{\Delta}} \circ d\right) \boldsymbol{\Phi}^{n+1}$$

almost cancel out.[2] Throughout this thesis, equation (3.32) is referred to as a *discrete Helmholtz equation* even though, technically speaking, it is not. Equation (3.32) is nonlinear because of the nonlinear relationship between $\mathbf{\Gamma}^{n+1}$ and $\mathbf{\Phi}^{n+1}$ (see Section 3.1.1). Hence, (3.32) is solved using fixed-point iteration. Following the approach of [34], we first linearize (3.32) by moving the nonlinear term $(P \otimes Q^N \circ \cos\tilde{\theta})\mathbf{\Gamma}^{n+1}$ and the known terms to the right side. Then a fixed-point relation is obtained by adding $(P \otimes Q^N)\mathbf{\Phi}^{n+1}$ to both sides. Therefore, at the k-th iteration, we solve for $\mathbf{\Phi}^{n+1,[k]}$ in the following equation, which will be referred to as the *linearized Helmholtz equation* throughout this thesis:

$$
\begin{aligned}
\Bigg\{&(P \otimes Q^N) - \left(\frac{\Delta t}{2R}\right)^2 \left(P_\lambda^{\hat{\Delta}\to\Delta} \otimes Q^D \circ \left(\frac{1}{\cos\tilde{\theta}}\right)\right)(P \otimes Q^D)^{-1} \times \\
&\qquad\qquad \left[\left(P_\lambda^{\Delta\to\hat{\Delta}} \otimes Q^N \circ c\right) + (P^{\Delta\to\hat{\Delta}} \otimes Q_\theta^N \circ (d\cos\tilde{\theta}))\right] \\
&- \left(\frac{\Delta t}{2R}\right)^2 \left(P \otimes Q_\theta^{D,\hat{\Delta}\to\Delta}\right)(P \otimes \hat{Q}^D)^{-1} \times \\
&\qquad\qquad \left[-(P_\lambda \otimes Q^{N,\Delta\to\hat{\Delta}} \circ d) + (P \otimes Q_\theta^{N,\Delta\to\hat{\Delta}} \circ (c\cos\tilde{\theta}))\right]\Bigg\}\, \mathbf{\Phi}^{n+1,[k]} \\
=&(P \otimes Q^N)\mathbf{\Phi}^{n+1,[k-1]} - (P \otimes Q^N \circ \cos\tilde{\theta})\mathbf{\Gamma}^{n+1,[k-1]} + (P \otimes Q^N \circ \cos\tilde{\theta})\tilde{\mathbf{\Gamma}}^n \\
&- \left(\frac{\Delta t}{2}\right)\left(P_\lambda^{\hat{\Delta}\to\Delta} \otimes Q^D \circ \left(\frac{1}{\cos\tilde{\theta}}\right)\right)(P \otimes Q^D)^{-1} \times \\
&\qquad \Bigg\{(P \otimes Q^D \circ a)\tilde{\mathbf{U}}^n + (P^{\Delta\to\hat{\Delta}} \otimes Q^{D,\hat{\Delta}\to\Delta} \circ b)\tilde{\mathbf{V}}^n - \Delta t\tilde{\boldsymbol{\delta}}_u^{n+\frac{1}{2}} + \boldsymbol{r}_u^n \\
&\qquad - \left(\frac{\Delta t}{2R^2}\right)\left[\left(P_\lambda^{\Delta\to\hat{\Delta}} \otimes Q^N \circ c\right) + (P^{\Delta\to\hat{\Delta}} \otimes Q_\theta^N \circ (d\cos\tilde{\theta}))\right]\tilde{\mathbf{\Phi}}^n\Bigg\} \\
&- \left(\frac{\Delta t}{2}\right)\left(P \otimes Q_\theta^{D,\hat{\Delta}\to\Delta}\right)(P \otimes \hat{Q}^D)^{-1} \times \\
&\qquad \Bigg\{-(P^{\hat{\Delta}\to\Delta} \otimes Q^{D,\Delta\to\hat{\Delta}} \circ b)\tilde{\mathbf{U}}^n + (P \otimes Q^D \circ a)\tilde{\mathbf{V}}^n - \Delta t\tilde{\boldsymbol{\delta}}_v^{n+\frac{1}{2}} + \boldsymbol{r}_v^n \\
&\qquad - \left(\frac{\Delta t}{2R^2}\right)\left[-\left(P_\lambda \otimes Q^{N,\Delta\to\hat{\Delta}} \circ d\right) + (P \otimes Q_\theta^{N,\Delta\to\hat{\Delta}} \circ (c\cos\tilde{\theta}))\right]\tilde{\mathbf{\Phi}}^n\Bigg\}
\end{aligned}
$$

[2] In fact, the cancellation would be exact if (a) an unstaggered grid were used, (b) the boundary conditions were biperiodic, and (c) the functions $(\frac{1}{\cos\theta})$ and d were constants, or, as in the case of collocation methods, could be pulled out of the inner products associated with the Q-matrices. This is because, under these conditions, the operators commute.

$$- \left(\frac{\Delta t}{2}\right) \left[\left(P_\lambda^{\hat{\Delta}\to\Delta} \otimes Q^D \circ \left(\frac{1}{\cos\tilde{\theta}}\right)\right) \tilde{\mathbf{U}}^n + \left(P \otimes Q_\theta^{D,\hat{\Delta}\to\Delta}\right) \tilde{\mathbf{V}}^n \right] + \boldsymbol{r}_\phi^n \tag{3.33}$$

Note that some variables in equation (3.33) can be computed directly from others. According to (3.1), (3.4) and the relation between ζ^{n+1} and ϕ^{n+1}, the coefficients vectors $\tilde{\mathbf{\Phi}}^n$ and $\mathbf{\Phi}^{n+1}$ are related to $\tilde{\mathbf{\Gamma}}^n$ and $\mathbf{\Gamma}^{n+1}$ by the equations

$$\tilde{\mathbf{\Gamma}}^n = (E_\lambda \otimes E_\theta^N)^{-1} \left\{ \log[(E_\lambda \otimes E_\theta^N)\tilde{\mathbf{\Phi}}^n + \boldsymbol{\eta}_\phi^n] - \boldsymbol{\eta}_\zeta^n \right\} \tag{3.34}$$

$$\mathbf{\Gamma}^{n+1} = (E_\lambda \otimes E_\theta^N)^{-1} \log[(E_\lambda \otimes E_\theta^N)\mathbf{\Phi}^{n+1}] \tag{3.35}$$

where $(\boldsymbol{\eta}_\zeta^n)_{i+(j-1)N_\lambda} \equiv \eta_\zeta^n(\tau_{\lambda_i}, \tau_{\theta_j})$ for $i = 1, \cdots, N_\lambda$ and $j = 1, \cdots, N_\theta$. At the k-th iteration, new values for $\mathbf{\Phi}^{n+1,[k]}$ are computed, which can then be used to update $\mathbf{\Gamma}^{n+1,[k]}$ using (3.35).

When applying the fixed-point iteration (3.33) with an initial guess formed by linear extrapolation

$$\mathbf{\Phi}^{n+1,[0]} = 2\mathbf{\Phi}^n - \mathbf{\Phi}^{n-1} \tag{3.36}$$

two fixed-point iterations usually suffice. The solution $\mathbf{\Phi}^{n+1}$ is used to compute $\mathbf{U}^{n+1}$ and $\mathbf{V}^{n+1}$ using the discretized motion equations (3.27) and (3.28).

Chapter 4

The Quadratic Spline Galerkin Method

The quadratic spline Galerkin (QSG) method is discussed in this chapter. We present the steps with which QSG, originally derived for systems discretized on unstaggered grids, can be modified to be applicable to the shallow water equations, which are discretized on a C-grid. In particular, we discuss the implications staggering has on the evaluation of the inner products, and show mathematically in Section 4.3 that a unique solution exists when QSG is used to solve a simplified version of the shallow water equations.

4.1 Background

The Galerkin method is among the class of weighted residual methods in which the test functions are chosen to be the basis functions. That is,

$$\begin{aligned}
&\varphi_i^P(\lambda) = \beta_i^P(\lambda), \qquad \hat{\varphi}_i^P(\lambda) = \hat{\beta}_i^P(\lambda) \\
&\varphi_j^D(\theta) = \beta_j^D(\theta), \qquad \varphi_j^N(\theta) = \beta_j^N(\theta), \qquad \hat{\varphi}_{\hat{j}}^D(\theta) = \hat{\beta}_{\hat{j}}^D(\theta)
\end{aligned}$$

where $i = 1, \cdots, N_\lambda$, $j = 1, \cdots, N_\theta$, and $\hat{j} = 0, \cdots, N_\theta$. With this choice of test functions, the residual is orthogonal to the approximation space. The scaling factors ω_λ and ω_θ in the definitions of the mass and derivative matrices are chosen to be $\Delta\lambda$ and $\Delta\theta$, respectively. That is, the linearized Helmholtz equation (3.33) is solved with the following mass and derivative matrices

$$
\begin{aligned}
P_{i,j} &= \frac{1}{\Delta\lambda}\int_{\lambda_0}^{\lambda_{N_\lambda}} \beta_j^P(\lambda)\beta_i^P(\lambda)d\lambda = \frac{1}{\Delta\lambda}\int_{\lambda_0}^{\lambda_{N_\lambda}} \hat{\beta}_j^P(\lambda)\hat{\beta}_i^P(\lambda)d\lambda,\\
P_{\lambda i,j} &= \frac{1}{\Delta\lambda}\int_{\lambda_0}^{\lambda_{N_\lambda}} \beta_j^{P'}(\lambda)\beta_i^P(\lambda)d\lambda = \frac{1}{\Delta\lambda}\int_{\lambda_0}^{\lambda_{N_\lambda}} \hat{\beta}_j^{P'}(\lambda)\hat{\beta}_i^P(\lambda)d\lambda,\\
P_{i,j}^{\Delta\to\hat{\Delta}} &= \frac{1}{\Delta\lambda}\int_{\lambda_0}^{\lambda_{N_\lambda}} \beta_j^P(\lambda)\hat{\beta}_i^P(\lambda)d\lambda, \quad P_{\lambda i,j}^{\Delta\to\hat{\Delta}} = \frac{1}{\Delta\lambda}\int_{\lambda_0}^{\lambda_{N_\lambda}} \beta_j^{P'}(\lambda)\hat{\beta}_i^P(\lambda)d\lambda,\\
P_{i,j}^{\hat{\Delta}\to\Delta} &= \frac{1}{\Delta\lambda}\int_{\lambda_0}^{\lambda_{N_\lambda}} \hat{\beta}_j^P(\lambda)\beta_i^P(\lambda)d\lambda, \quad P_{\lambda i,j}^{\hat{\Delta}\to\Delta} = \frac{1}{\Delta\lambda}\int_{\lambda_0}^{\lambda_{N_\lambda}} \hat{\beta}_j^{P'}(\lambda)\beta_i^P(\lambda)d\lambda
\end{aligned}
$$

in the λ-direction for $i, j = 1, \cdots, N_\lambda$, and

$$
\begin{aligned}
\{Q^S \circ g\}_{i,j} &= \frac{1}{\Delta\theta}\int_{\theta_0}^{\theta_{N_\theta}} g(\theta)\beta_j^S(\theta)\beta_i^S(\theta)d\theta, && \text{for } i,j = 1,\cdots,N_\theta\\
\{Q_\theta^S \circ g\}_{i,j} &= \frac{1}{\Delta\theta}\int_{\theta_0}^{\theta_{N_\theta}} g(\theta)\beta_j^{S'}(\theta)\beta_i^S(\theta)d\theta, && \text{for } i,j = 1,\cdots,N_\theta\\
\{\hat{Q}^D \circ g\}_{i,j} &= \frac{1}{\Delta\theta}\int_{\theta_0}^{\theta_{N_\theta}} g(\theta)\hat{\beta}_j^D(\theta)\hat{\beta}_i^D(\theta)d\theta, && \text{for } i,j = 0,\cdots,N_\theta\\
\{\hat{Q}_\theta^D \circ g\}_{i,j} &= \frac{1}{\Delta\theta}\int_{\theta_0}^{\theta_{N_\theta}} g(\theta)\hat{\beta}_j^{D'}(\theta)\hat{\beta}_i^D(\theta)d\theta, && \text{for } i,j = 0,\cdots,N_\theta\\
\{Q^{S,\Delta\to\hat{\Delta}} \circ g\}_{i,j} &= \frac{1}{\Delta\theta}\int_{\theta_0}^{\theta_{N_\theta}} g(\theta)\beta_j^S(\theta)\hat{\beta}_i^D(\theta)d\theta, && \text{for } i = 0,\cdots,N_\theta,\ j = 1,\cdots,N_\theta\\
\{Q_\theta^{S,\Delta\to\hat{\Delta}} \circ g\}_{i,j} &= \frac{1}{\Delta\theta}\int_{\theta_0}^{\theta_{N_\theta}} g(\theta)\beta_j^{S'}(\theta)\hat{\beta}_i^D(\theta)d\theta, && \text{for } i = 0,\cdots,N_\theta,\ j = 1,\cdots,N_\theta\\
\{Q^{D,\hat{\Delta}\to\Delta} \circ g\}_{i,j} &= \frac{1}{\Delta\theta}\int_{\theta_0}^{\theta_{N_\theta}} g(\theta)\hat{\beta}_j^D(\theta)\beta_i^D(\theta)d\theta, && \text{for } i = 1,\cdots,N_\theta,\ j = 0,\cdots,N_\theta\\
\{Q_\theta^{D,\hat{\Delta}\to\Delta} \circ g\}_{i,j} &= \frac{1}{\Delta\theta}\int_{\theta_0}^{\theta_{N_\theta}} g(\theta)\hat{\beta}_j^{D'}(\theta)\beta_i^N(\theta)d\theta, && \text{for } i = 1,\cdots,N_\theta,\ j = 0,\cdots,N_\theta
\end{aligned}
$$

in the θ-direction, where g denotes an arbitrary function of θ and $S = D$ or N. On a uniform spatial grid, the error of the resulting numerical solution is fourth-order locally at nodes and midpoints of the grid and third-order globally, as will be shown numerically in Chapter 6.

4.2 Quadrature Rule

The entries of the P-matrices are simply inner products of the basis functions or their derivatives, and are therefore time-independent and need only be computed once analytically at the initialization stage. The entries of the Q-matrices, on the other hand, involve functions that may be time-dependent. For instance, $(Q^D \circ a)$, which appears in the linearized Helmholtz equation (3.33), varies with time since $a = (1 - (\frac{\Delta t \tilde{f}}{2})^2)/(1 + (\frac{\Delta t \tilde{f}}{2})^2)$, which depends on the departure points. Therefore, $(Q^D \circ a)$, together with other Q-matrices that involve time-dependent functions, are numerically computed at every timestep.

In order to preserve the locally fourth-order convergence, the two-point Gauss quadrature rule is used. Care must be taken in defining the grid partition on which the quadrature rule is computed, since the quadratic spline basis functions, being piecewise polynomials, have discontinuous second derivatives at gridpoints. Therefore, unless the integration grid partition is chosen properly, the assumption associated with the two-point Gauss rule that the integrand has a continuous fourth-derivative within each interval of the integration grid partition may be violated, and, consequently, fourth-order convergence cannot be guaranteed. In order to satisfy the smoothness requirement of the two-point Gauss rule, the integration grid is defined to be twice as refined as the spline grid in each space dimension. That is, the integration grids are $\Delta_\lambda^I \equiv (\Delta_\lambda \bigcup \hat{\Delta}_\lambda) \bigcap [0, 2\pi]$ and $\Delta_\theta^I \equiv (\Delta_\theta \bigcup \hat{\Delta}_\theta) \bigcap [-\pi/2, \pi/2]$ in the λ- and θ-directions, respectively. Consequently, the points of discontinuity of the spline basis and test functions do not fall within the integration grid intervals (see Figure 4.1). This complication would not arise if an unstaggered grid were used because in that case all points of discontinuity of the basis and test functions would coincide with the spline grid, and consequently, the spline grid could be used as the integration grid for computing the integral.

When the QSG method is applied to the linearized Helmholtz equation (3.33), the inner products in the θ-dimension are first computed using the two-point Gauss rule as

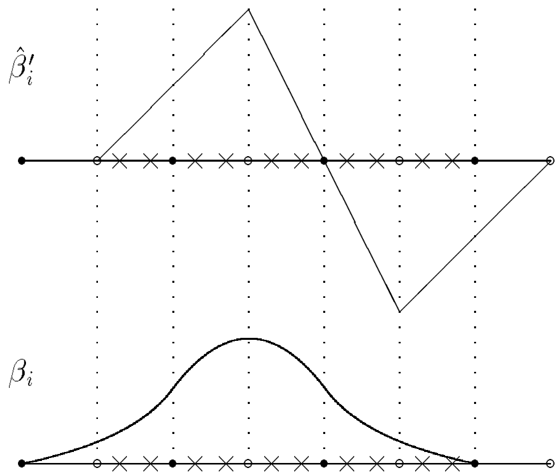

Figure 4.1: This diagram show the integration partition for the two-point Gauss-rule used to approximate the inner product of $\hat{\beta}_i'$ and β_i. The solid and open circles mark the gridpoints of the Δ- and $\hat{\Delta}$-partitions, respectively. (Note that they are staggered with respect to each other.) The solid and open circles together form the gridpoints of the integration partition, which is also indicated by the dotted lines. The crosses indicate the positions of the Gauss points.

described above before the iteration (3.33) is begun. Then at each iteration of (3.33), the linear system is solved with the conjugate gradient iterative method to yield $\mathbf{\Phi}^{n+1,[k]}$. The convergence behaviour of the solution, together with the accuracy and efficiency of the method, is discussed in Chapter 6.

4.3 Existence and Uniqueness

In this section, we prove that the solution of a simplified version of the linearized Helmholtz equation (3.33), obtained with the QSG method, exists and is unique. To be more specific, the analysis is done on the linearized shallow water equations with constant coefficients, equations (2.12) to (2.14), with the additional assumption that the boundary conditions are biperiodic. Since these equations are linear and do not contain the logarithmic term, the associated Helmholtz equation (3.32) and its linearized form

(3.33) are essentially the same. Therefore, by showing the existence of a solution for (3.33), we also show that the Helmholtz equation (3.32) associated with the simplified shallow water equations is solvable.

The linearized Helmholtz equation (3.33) of the simplified system, derived by first discretizing the equations and then eliminating the divergence terms from the discretized continuity equation corresponding to equation (2.14), takes the form

$$K\mathbf{\Phi}^{n+1} = R_H \tag{4.1}$$

where R_H is known. We will prove that a unique solution exists for the above equation when the discretization is done on an unstaggered grid, and also on the C-grid.

4.3.1 The Unstaggered Case

On an unstaggered grid, the linear operator K is defined as follows:

$$\begin{aligned} K \equiv\ & (P \otimes Q) - \left(\frac{\Delta t}{2R}\right)^2 \Phi^* \Big[\frac{c}{\cos\Theta^*}(P_\lambda \otimes Q)(P \otimes Q)^{-1}(P_\lambda \otimes Q) \\ & + d(P_\lambda \otimes Q)(P \otimes Q)^{-1}(P \otimes Q_\theta) - d(P \otimes Q_\theta)(P \otimes Q)^{-1}(P_\lambda \otimes Q) \\ & + c\cos\Theta^*(P \otimes Q_\theta)(P \otimes Q)^{-1}(P \otimes Q_\theta)\Big] \end{aligned} \tag{4.2}$$

Note that K differs from the operator associated with the left side of (3.33) in that the latter operates on a staggered grid and allows variable coefficients, and that biperiodic boundary conditions are assumed in K.

A unique solution exists for equation (4.1) if and only if K is nonsingular. We will prove that K is nonsingular by showing that all eigenvalues of K are nonzero. Since constant values are assumed for the coefficients in the linearized shallow water equations, the integrals associated with the mass and derivative matrices involve only the products of the basis functions or their derivatives, and can be computed analytically. These matrices are defined in Appendix A. An important property of these matrices is that P and P_λ have the same eigenvectors. Similarly, Q and Q_θ have the same eigenvectors.

Let p_k and p_{λ_k} be the eigenvalues associated with the k-th eigenvector of P and P_λ, respectively, and q_l and q_{θ_l} be those corresponding to the l-th eigenvector of Q and Q_θ, respectively. In Appendix A we show that

$$\begin{aligned}
p_k &= \frac{1}{15}\left[15 - 15\sin^2\left(\frac{k\Delta\lambda}{2}\right) + 2\sin^4\left(\frac{k\Delta\lambda}{2}\right)\right] \\
p_{\lambda_k} &= \imath\frac{2}{3\Delta\lambda}\sin\left(\frac{k\Delta\lambda}{2}\right)\cos\left(\frac{k\Delta\lambda}{2}\right)\left[3 - \sin^2\left(\frac{k\Delta\lambda}{2}\right)\right] \\
q_l &= \frac{1}{15}\left[15 - 15\sin^2\left(\frac{l\Delta\theta}{2}\right) + 2\sin^4\left(\frac{l\Delta\theta}{2}\right)\right] \\
q_{\theta_l} &= \imath\frac{2}{3\Delta\theta}\sin\left(\frac{l\Delta\theta}{2}\right)\cos\left(\frac{l\Delta\theta}{2}\right)\left[3 - \sin^2\left(\frac{l\Delta\theta}{2}\right)\right]
\end{aligned}$$

where $\imath \equiv \sqrt{-1}$, $k = 1, \cdots, N_\lambda$ and $l = 1, \cdots, N_\theta$.

Let

$$\alpha_k = \sin^2\left(\frac{k\Delta\lambda}{2}\right), \qquad \alpha'_l = \sin^2\left(\frac{l\Delta\theta}{2}\right)$$

With biperiodic boundary conditions, the second and third terms inside the square brackets in (4.2) cancel out, and the eigenvalues of K, denoted by $\sigma_{k,l}$, can be expressed in terms of the eigenvalues of P, P_λ, Q and Q_θ as follows:

$$\begin{aligned}
\sigma_{k,l} &= p_k q_l - \left(\frac{\Delta t}{2R}\right)^2 \Phi^* c\left[\frac{1}{\cos\Theta^*}\frac{p_{\lambda_k}^2 q_l}{p_k} + \cos\Theta^* \frac{p_k q_{\theta_l}^2}{q_l}\right] \\
&= \left[\frac{1}{15}(15 - 15\alpha_k + 2\alpha_k^2)\right]\left[\frac{1}{15}(15 - 15\alpha'_l + 2\alpha_l'^2)\right] \\
&\quad + \left(\frac{\Delta t}{2R}\right)^2 \Phi^* c\left\{\frac{\left[\frac{4}{9\Delta\lambda^2\cos\Theta^*}\alpha_k(1-\alpha_k)(3-\alpha_k)^2\right]\left[\frac{1}{15}(15 - 15\alpha'_l + 2\alpha_l'^2)\right]}{\frac{1}{15}(15 - 15\alpha_k + 2\alpha_k^2)}\right. \\
&\qquad \left. + \frac{\left[\frac{\cos\Theta^*}{15}(15 - 15\alpha_k + 2\alpha_k^2)\right]\left[\frac{4}{9\Delta\theta^2}\alpha'_l(1-\alpha'_l)(3-\alpha'_l)^2\right]}{\frac{1}{15}(15 - 15\alpha'_l + 2\alpha_l'^2)}\right\} \\
&= \frac{1}{15^2}(15 - 15\alpha_k + 2\alpha_k^2)(15 - 15\alpha'_l + 2\alpha_l'^2) \\
&\quad + \left(\frac{\Delta t}{2R}\right)^2 \Phi^* c\left\{\frac{4}{9\Delta\lambda^2\cos\Theta^*}\frac{\alpha_k(1-\alpha_k)(3-\alpha_k)^2(15 - 15\alpha'_l + 2\alpha_l'^2)}{(15 - 15\alpha_k + 2\alpha_k^2)}\right. \\
&\qquad \left. + \frac{4\cos\Theta^*}{9\Delta\theta^2}\frac{\alpha'_l(1-\alpha'_l)(3-\alpha'_l)^2(15 - 15\alpha_k + 2\alpha_k^2)}{(15 - 15\alpha'_l + 2\alpha_l'^2)}\right\}
\end{aligned} \tag{4.3}$$

Note that for all values of k and l

$$0 \le \alpha_k,\ \alpha'_l \le 1,$$

$$\Rightarrow \quad \alpha_k(1-\alpha_k)(3-\alpha_k)^2 \geq 0, \quad \alpha_l'(1-\alpha_l')(3-\alpha_l')^2 \geq 0,$$
$$\text{and} \quad (15-15\alpha_k+2\alpha_k^2), \geq 2, \quad (15-15\alpha_l'+2\alpha_l'^2) \geq 2$$

Since $\Phi^* \geq 0$, $c \geq 0$ and $\cos\Theta^* > 0$ for $\Theta^* \in (-\pi/2, \pi/2)$, we conclude that $\sigma_{k,l} \geq (\frac{2}{15})^2 > 0$. This implies that K^{-1} exists. Consequently, a unique solution exists for the Helmholtz equation (4.1).

As mentioned before, K is not, strictly speaking, a Helmholtz operator when the "Helmholtz" equation is derived algebraically, i.e. the elimination of the divergence terms is done after spatial discretization. A true Helmholtz equation may be derived analytically by eliminating U^{n+1} and V^{n+1} from the space continuous equation (2.58). If we follow this approach, the Helmholtz operator K^H becomes

$$K^H \equiv (P\otimes Q) - \left(\frac{\Delta t}{2R}\right)^2 \Phi^* c \left[\frac{1}{\cos\Theta^*}(P_{\lambda\lambda}\otimes Q) + \cos\Theta^*(P\otimes Q_{\theta\theta})\right] \tag{4.4}$$

where $P_{\lambda\lambda}$ and $Q_{\theta\theta}$ are the second derivative operators in the λ and θ-directions, respectively, and are defined in Appendix A. These matrices have the same eigenvectors as P and Q, respectively. The associated eigenvalues are

$$\begin{aligned}
p_{\lambda\lambda_k} &= \frac{4}{3\Delta\lambda^2}\sin^2\left(\frac{k\Delta\lambda}{2}\right)\left[-3+2\sin^2\left(\frac{k\Delta\lambda}{2}\right)\right] \\
q_{\theta\theta_l} &= \frac{4}{3\Delta\theta^2}\sin^2\left(\frac{l\Delta\theta}{2}\right)\left[-3+2\sin^2\left(\frac{l\Delta\theta}{2}\right)\right]
\end{aligned}$$

The eigenvalues $\sigma_{k,l}^H$ of K^H satisfy

$$\begin{aligned}
\sigma_{k,l}^H &= p_k q_l - \left(\frac{\Delta t}{2R}\right)^2 \Phi^* c\left[\frac{1}{\cos\Theta^*}p_{\lambda\lambda k}q_l + \cos\Theta^* p_k q_{\theta\theta l}\right] \\
&= \left[\frac{1}{15}(15-15\alpha_k+2\alpha_k^2)\right]\left[\frac{1}{15}(15-15\alpha_l'+2\alpha_l'^2)\right] \\
&\quad + \left(\frac{\Delta t}{2R}\right)^2 \Phi^* c\left\{\frac{4}{3\Delta\lambda^2\cos\Theta^*}\alpha_k(3-2\alpha_k)\left[\frac{1}{15}(15-15\alpha_l'+2\alpha_l'^2)\right]\right. \\
&\qquad \left. + \frac{4\cos\Theta^*}{3\Delta\theta^2}\alpha_l'(3-2\alpha_l')\left[\frac{1}{15}(15-15\alpha_k+2\alpha_k^2)\right]\right\}
\end{aligned} \tag{4.5}$$

Comparing (4.3) and (4.5), we note that $\frac{4}{9}(1-\alpha_k)(3-\alpha_k)^2/(15-15\alpha_k+2\alpha_k^2) \leq \frac{4}{3\cdot 15}(3-2\alpha_k)$ and $\frac{4}{9}(1-\alpha_l')(3-\alpha_l')^2/(15-15\alpha_l'+2\alpha_l'^2) \leq \frac{4}{3\cdot 15}(3-2\alpha_l')$. Thus, we conclude that $0 < \sigma_{k,l} \leq \sigma^H_{k,l}$, implying that (4.4) is uniquely solvable too. However, as will be explained in Chapter 7, this approach of analytically deriving the Helmholtz equation is not recommended as it tends to damp the Rossby waves.

4.3.2 The C-grid

When the simplified shallow water equations (2.12) to (2.14) are discretized on a C-grid, the linear operator K becomes:

$$\begin{aligned} K \equiv (P \otimes Q) - \left(\frac{\Delta t}{2R}\right)^2 \Phi^* \Big[& \frac{c}{\cos\Theta^*}(P_\lambda^{\hat{\Delta}\to\Delta} \otimes Q)(P \otimes Q)^{-1}(P_\lambda^{\Delta\to\hat{\Delta}} \otimes Q) \\ & + d(P_\lambda^{\hat{\Delta}\to\Delta} \otimes Q)(P \otimes Q)^{-1}(P^{\Delta\to\hat{\Delta}} \otimes Q_\theta) \\ & - d(P \otimes Q_\theta^{\hat{\Delta}\to\Delta})(P \otimes Q)^{-1}(P_\lambda \otimes Q^{\Delta\to\hat{\Delta}}) \\ & + c\cos\Theta^*(P \otimes Q_\theta^{\hat{\Delta}\to\Delta})(P \otimes Q)^{-1}(P \otimes Q_\theta^{\Delta\to\hat{\Delta}})\Big] \end{aligned} \tag{4.6}$$

The staggering operators $P^{\Delta\to\hat{\Delta}}$ and $P_\lambda^{\Delta\to\hat{\Delta}}$ share the same eigenvectors as P and P_λ, as do $P^{\hat{\Delta}\to\Delta}$ and $P_\lambda^{\hat{\Delta}\to\Delta}$. The eigenvalues associated with the k-th eigenvectors of $P^{\Delta\to\hat{\Delta}}$ and $P^{\hat{\Delta}\to\Delta}$ are $e^{\imath k\frac{\Delta\lambda}{2}}p_k^{\rightarrow}$ and $e^{-\imath k\frac{\Delta\lambda}{2}}p_k^{\rightarrow}$, respectively, where

$$p_k^{\rightarrow} = \frac{1}{120}\cos\left(\frac{k\Delta\lambda}{2}\right)\left[120 - 60\sin^2\left(\frac{k\Delta\lambda}{2}\right) + \sin^4\left(\frac{k\Delta\lambda}{2}\right)\right]$$

Similarly, the eigenvalues associated with the k-th eigenvectors of $P_\lambda^{\Delta\to\hat{\Delta}}$ and $P_\lambda^{\hat{\Delta}\to\Delta}$ are $e^{\imath k\frac{\Delta\lambda}{2}}p_{\lambda_k}^{\rightarrow}$ and $e^{-\imath k\frac{\Delta\lambda}{2}}p_{\lambda_k}^{\rightarrow}$, respectively, where

$$p_{\lambda_k}^{\rightarrow} = \imath\frac{32}{\Delta\lambda}\sin\left(\frac{k\Delta\lambda}{2}\right)\left[24 - 20\sin^2\left(\frac{k\Delta\lambda}{2}\right) + \sin^4\left(\frac{k\Delta\lambda}{2}\right)\right]$$

In the latitudinal dimension, $Q^{\Delta\to\hat{\Delta}}$ and $Q_\theta^{\hat{\Delta}\to\Delta}$ share the same eigenvectors as Q and Q_θ, as do $Q^{\hat{\Delta}\to\Delta}$ and $Q_\theta^{\hat{\Delta}\to\Delta}$. The eigenvalues associated with the l-th eigenvectors of $Q^{\Delta\to\hat{\Delta}}$ and $Q^{\hat{\Delta}\to\Delta}$ are $e^{\imath l\frac{\Delta\theta}{2}}q_l^{\rightarrow}$ and $e^{-\imath l\frac{\Delta\theta}{2}}q_l^{\rightarrow}$, respectively, where

$$q_l^{\rightarrow} = \frac{1}{120}\cos\left(\frac{l\Delta\theta}{2}\right)\left[120 - 60\sin^2\left(\frac{l\Delta\theta}{2}\right) + \sin^4\left(\frac{l\Delta\theta}{2}\right)\right]$$

Similarly, the eigenvalues associated with the l-eigenvectors of $Q_\theta^{\Delta\to\hat\Delta}$ and $Q_\theta^{\hat\Delta\to\Delta}$ are $e^{\imath l\frac{\Delta\theta}{2}} q_{\theta_l}^{\rightarrow}$ and $e^{-\imath l\frac{\Delta\theta}{2}} q_{\theta_l}^{\rightarrow}$, respectively, where

$$q_{\theta_l}^{\rightarrow} = \imath\frac{32}{\Delta\theta}\sin\left(\frac{l\Delta\theta}{2}\right)\left[24 - 20\sin^2\left(\frac{l\Delta\theta}{2}\right) + \sin^4\left(\frac{l\Delta\theta}{2}\right)\right]$$

The derivation of the above expressions can be found in Appendix A. The eigenvalues of K are

$$\begin{aligned}\sigma_{k,l} &= p_k q_l - \left(\frac{\Delta t}{2R}\right)^2 \Phi^* \left\{ c\left[\frac{1}{\cos\Theta^*}\frac{p_{\lambda_k}^{\rightarrow 2} q_l}{p_k} + \cos\Theta^* \frac{p_k q_{\theta_l}^{\rightarrow 2}}{q_l}\right]\right.\\ &\qquad\left. + d\left[\frac{p_k^{\rightarrow} p_{\lambda_k}^{\rightarrow} q_{\theta_l}}{p_k} - \frac{p_{\lambda_k} q_l^{\rightarrow} q_{\theta_l}^{\rightarrow}}{q_l}\right]\right\} &(4.7)\\ &= \left[\frac{1}{15}(15 - 15\alpha_k + 2\alpha_k^2)\right]\left[\frac{1}{15}(15 - 15\alpha_l' + 2\alpha_l'^2)\right] + A_1 + A_2 &(4.8)\end{aligned}$$

where

$$\begin{aligned}A_1 &= -\left(\frac{\Delta t}{2R}\right)^2 \Phi^* \frac{p_{\lambda_k}^{\rightarrow}}{p_k}\left(\frac{c}{\cos\Theta^*} p_{\lambda_k}^{\rightarrow} q_l + d p_k^{\rightarrow} q_{\theta_l}\right) &(4.9)\\ &= \left(\frac{\Delta t}{2R}\right)^2 \Phi^* \frac{\frac{32}{\Delta\lambda}\sin\left(\frac{k\Delta\lambda}{2}\right)(24 - 20\alpha_k + \alpha_k^2)}{\frac{1}{15}(15 - 15\alpha_k + 2\alpha_k^2)}\\ &\quad\left[\frac{c}{\cos\Theta^*}\frac{32}{\Delta\lambda}\sin\left(\frac{k\Delta\lambda}{2}\right)(24 - 20\alpha_k + \alpha_k^2)\frac{1}{15}(15 - 15\alpha_l' + 2\alpha_l'^2)\right.\\ &\quad\left. + \frac{d}{120}\cos\left(\frac{k\Delta\lambda}{2}\right)(120 - 60\alpha_k + \alpha_k^2)\frac{2}{3\Delta\theta}\sin\left(\frac{l\Delta\theta}{2}\right)\cos\left(\frac{l\Delta\theta}{2}\right)(3 - \alpha_l')\right]\\ &= \left(\frac{\Delta t}{2R}\right)^2 \Phi^* \frac{32\cdot 15(24 - 20\alpha_k + \alpha_k^2)}{\Delta\lambda(15 - 15\alpha_k + 2\alpha_k^2)}\\ &\quad\left[\frac{32c}{15\cos\Theta^*\Delta\lambda}\alpha_k(24 - 20\alpha_k + \alpha_k^2)(15 - 15\alpha_l' + 2\alpha_l'^2)\right.\\ &\quad\left. + \frac{2d\sin(k\Delta\lambda)\sin(l\Delta\theta)}{4\cdot 120\cdot 3\Delta\theta}(120 - 60\alpha_k + \alpha_k^2)(3 - \alpha_l')\right] &(4.10)\\ A_2 &= -\left(\frac{\Delta t}{2R}\right)^2 \Phi^* \frac{q_{\theta_l}^{\rightarrow}}{q_l}\left(c\cos\Theta^* p_k q_{\theta_l}^{\rightarrow} - d p_{\lambda_k} q_l^{\rightarrow}\right)\\ &= \left(\frac{\Delta t}{2R}\right)^2 \Phi^* \frac{\frac{32}{\Delta\theta}\sin\left(\frac{l\Delta\theta}{2}\right)(24 - 20\alpha_l' + \alpha_l'^2)}{\frac{1}{15}(15 - 15\alpha_l' + 2\alpha_l'^2)}\\ &\quad\left[\frac{c\cos\Theta^*}{15}(15 - 15\alpha_k + 2\alpha_k^2)\frac{32}{\Delta\theta}\sin\left(\frac{l\Delta\theta}{2}\right)(24 - 20\alpha_l' + \alpha_l'^2)\right.\\ &\quad\left. - \frac{2d}{3\Delta\lambda}\sin\left(\frac{k\Delta\lambda}{2}\right)\cos\left(\frac{k\Delta\lambda}{2}\right)(3 - \alpha_k)\frac{1}{120}\cos\left(\frac{l\Delta\theta}{2}\right)(120 - 60\alpha_l' + \alpha_l'^2)\right]\end{aligned}$$

$$
\begin{aligned}
= & \left(\frac{\Delta t}{2R}\right)^2 \Phi^* \frac{32\cdot 15(24-20\alpha_l'+\alpha_l'^2)}{\Delta\theta(15-15\alpha_l'+2\alpha_l'^2)} \\
& \left[\frac{32c\cos\Theta^*}{15\Delta\theta}\alpha_l'(15-15\alpha_k+2\alpha_k^2)(24-20\alpha_l'+\alpha_l'^2)\right. \\
& \left. -\frac{2d\sin(k\Delta\lambda)\sin(l\Delta\theta)}{4\cdot 120\cdot 3\Delta\lambda}(3-\alpha_k)(120-60\alpha_l'+\alpha_l'^2)\right] \qquad (4.11)
\end{aligned}
$$

We study the behaviour of $\sigma_{k,l}$ for typical parameter values. Since it has been shown in the previous section that $\left[\frac{1}{15}(15-15\alpha_k+2\alpha_k^2)\right]\left[\frac{1}{15}(15-15\alpha_l'+2\alpha_l'^2)\right] \geq \frac{4}{225}$, in order for $\sigma_{k,l}>0$, it is sufficient to show that $A_1 > -\frac{2}{225}$ and $A_2 > -\frac{2}{225}$. For simplicity, assume that $\Delta t = \Delta\lambda = \Delta\theta \equiv h$. We first consider A_1. Since $c>0$ and $\cos\Theta^*>0$, the first term inside the square brackets in (4.10) is always nonnegative. Since $d=\frac{\Delta t\tilde{f}}{2}c$, the second term is much smaller than the first for sufficiently large α_k and sufficiently small h. When $\alpha_k \approx 0$, the first term approaches zero. Nonetheless, at $\alpha_k = 0$,

$$
\sin^2\left(\frac{k\Delta\lambda}{2}\right) = 0 \Rightarrow k\Delta\lambda = 0 \text{ or } 2\pi \Rightarrow \sin(k\Delta\lambda) = 0
$$

which means that the second term also vanishes. Hence, $A_1 = 0$. Also, for small positive k's, we have $\alpha_k = \sin^2(kh/2) \approx (kh/2)^2$. Substituting this approximation into the expression for A_1, and writing d as $\frac{h\tilde{f}}{2}c$ yields

$$
\begin{aligned}
A_1 = & \left(\frac{h}{2R}\right)^2 \Phi^* c \frac{32\cdot 15\left[24-20\left(\frac{kh}{2}\right)^2+\left(\frac{kh}{2}\right)^4\right]}{h\left[15-15\left(\frac{kh}{2}\right)^2+2\left(\frac{kh}{2}\right)^4\right]} \times \\
& \left\{\frac{32}{15\cos\Theta^* h}\left(\frac{kh}{2}\right)^2\left[24-20\left(\frac{kh}{2}\right)^2+\left(\frac{kh}{2}\right)^4\right]\left(15-15\alpha_l'+2\alpha_l'^2\right)\right. \\
& \left. + \frac{2\frac{h\tilde{f}}{2}\cdot kh\sin(l\Delta\theta)}{4\cdot 120\cdot 3h}\left[120-60\left(\frac{kh}{2}\right)^2+\left(\frac{kh}{2}\right)^4\right](3-\alpha_l')\right\}
\end{aligned}
$$

Since the first term inside the curly brackets is positive, we have

$$
\begin{aligned}
A_1 \geq & -\left(\frac{h}{2R}\right)^2 \Phi^* c \frac{32\cdot 15\left[24-20\left(\frac{kh}{2}\right)^2+\left(\frac{kh}{2}\right)^4\right]}{h\left[15-15\left(\frac{kh}{2}\right)^2+2\left(\frac{kh}{2}\right)^4\right]} \times \\
& \left\{\frac{2\frac{h\tilde{f}}{2}\cdot kh}{4\cdot 120\cdot 3h}\left[120-60\left(\frac{kh}{2}\right)^2+\left(\frac{kh}{2}\right)^4\right]\cdot 3\right\}
\end{aligned}
$$

by noting that $\sin(l\Delta\theta) \geq -1$ and $3 - \sin^2(\frac{l\Delta\theta}{2}) \leq 3$. Since $\tilde{f} \ll 1$, $h \ll 1$, $R \gg \Phi^*$ and $c \approx 1$, we have $A_1 = \mathcal{O}(h^2)$. Hence, when $\alpha_k \approx (kh/2)^2$ for a small positive integer k, $A_1 > -\frac{2}{225}$ for h sufficiently small.

Similar reasoning may be applied to A_2 to show that $A_2 > -\frac{2}{225}$ for small $l \geq 0$ and sufficiently small h. Hence, $\sigma_{k,l} > 0$, in the cases that we have considered. Unfortunately, this does not cover all possible cases, so we have not actually proved that $\sigma_{k,l} > 0$ for all k and l. However, our numerical results in Section 6 indicate that the matrix K associated with (4.1) is nonsingular when the simplified problem (2.12) to (2.14) is discretized on the C-grid.

Chapter 5

The Optimal Quadratic Spline Collocation Methods

In this chapter, we present details on the optimal quadratic spline collocation (OQSC) methods. The quadratic spline collocation (QSC) method, when applied in its standard form, leads to suboptimal solution approximations, in the sense that the order of convergence of the spline collocation approximation is lower than that of the spline interpolant in the same approximation space. To obtain optimal solution approximations, the OQSC methods can be used [6, 20]. In Section 5.1, we summarize previous work done in OQSC and outline how the methods yield optimal solutions for an elliptic partial different equation. In the rest of this chapter, we will explain how the two OQSC methods, originally derived for a single elliptic partial differential equation and later generalized to systems on unstaggered grids [25], can be modified to be applicable to the shallow water equations, which are discretized on the staggered C-grid.

5.1 Background

A collocation method can be interpreted as a special case of the weighted residual method where the test functions are chosen to be delta functions associated with the collocation points, which, for quadratic splines, are usually chosen to be the midpoints of the partition. The scaling factors in the definitions of the mass and derivative matrices are set to be one: $\omega_\lambda = \omega_\theta = 1$. With collocation, the mass matrix P maps coefficients to function values at collocation points in the same partition, whereas $P^{\Delta\to\hat{\Delta}}$ maps coefficients defined with respect to partition Δ_λ to the corresponding function values at collocation points of $\hat{\Delta}_\lambda$, and similarly for $P^{\hat{\Delta}\to\Delta}$. The first derivative matrix P_λ maps coefficients to first derivative values at collocation points within the same partition, while $P_\lambda^{\Delta\to\hat{\Delta}}$ maps coefficients defined with respect to Δ_λ to first derivative values at collocation points in $\hat{\Delta}_\lambda$, and similarly for $P_\lambda^{\hat{\Delta}\to\Delta}$. More specifically, we have

$$
\begin{aligned}
P_{i,j} &= \beta_j^P(\tau_{\lambda_i}) = \hat{\beta}_j^P(\hat{\tau}_{\lambda_i}), & P_{\lambda_{i,j}} &= \beta_j^{P'}(\tau_{\lambda_i}) = \hat{\beta}_j^{P'}(\hat{\tau}_{\lambda_i}),\\
P_{i,j}^{\Delta\to\hat{\Delta}} &= \beta_j^P(\hat{\tau}_{\lambda_i}), & P_{\lambda_{i,j}}^{\Delta\to\hat{\Delta}} &= \beta_j^{P'}(\hat{\tau}_{\lambda_i}),\\
P_{i,j}^{\hat{\Delta}\to\Delta} &= \hat{\beta}_j^P(\tau_{\lambda_i}), & P_{\lambda_{i,j}}^{\hat{\Delta}\to\Delta} &= \hat{\beta}_j^{P'}(\tau_{\lambda_i})
\end{aligned}
$$

for $i, j = 1, \cdots, N_\lambda$. Note that $P_{i,j} = E_{\lambda i,j}$, where E_λ was defined in Section 3.5.

Similarly, the mass and first derivative matrices in the θ-direction are defined by

$$
\begin{aligned}
Q_{i,j}^S &= \beta_j^S(\tau_{\theta_i}), & Q_{\theta_{i,j}}^S &= \beta_j^{S'}(\tau_{\theta_i}), & & i,j = 1,\cdots,N_\theta\\
\hat{Q}_{i,j}^D &= \hat{\beta}_j^D(\hat{\tau}_{\theta_i}), & \hat{Q}_{\theta_{i,j}}^D &= \hat{\beta}_j^{D'}(\hat{\tau}_{\theta_i}), & & i,j = 0,\cdots,N_\theta\\
Q_{i,j}^{S,\Delta\to\hat{\Delta}} &= \beta_j^S(\hat{\tau}_{\theta_i}), & Q_{\theta_{i,j}}^{S,\Delta\to\hat{\Delta}} &= \beta_j^{S'}(\hat{\tau}_{\theta_i}), & & i = 0,\cdots,N_\theta,\ j = 1,\cdots,N_\theta\\
Q_{i,j}^{D,\hat{\Delta}\to\Delta} &= \hat{\beta}_j^D(\tau_{\theta_i}), & Q_{\theta_{i,j}}^{D,\hat{\Delta}\to\Delta} &= \hat{\beta}_j^{D'}(\tau_{\theta_i}), & & i = 1,\cdots,N_\theta,\ j = 0,\cdots,N_\theta
\end{aligned}
$$

where $S = D$ or N. For the Galerkin method, evaluating the finite element matrices may require evaluating integrals involving functions other than the basis functions. For the collocation method, however, it is a lot simpler to compute the Q-matrices since the test functions are chosen to be the delta functions. For an arbitrary function $g(\theta)$, we have the following

$$
\begin{array}{ll}
\{Q^S \circ g\}_{i,j} = g(\tau_{\theta_i}) Q^S_{i,j}, & \{Q^S_\theta \circ g\}_{i,j} = g(\tau_{\theta_i}) Q^S_{\theta_{i,j}}, \\
 & i,j = 1,\cdots,N_\theta \\
\{\hat{Q}^D \circ g\}_{i,j} = g(\hat{\tau}_{\theta_i}) \hat{Q}^D_{i,j}, & \{\hat{Q}^D_\theta \circ g\}_{i,j} = g(\hat{\tau}_{\theta_i}), \hat{Q}^D_{\theta_{i,j}} \\
 & i,j = 0,\cdots,N_\theta \\
\{Q^{S,\Delta\to\hat{\Delta}} \circ g\}_{i,j} = g(\hat{\tau}_{\theta_i}) Q^{S,\Delta\to\hat{\Delta}}_{i,j}, & \{Q^{S,\Delta\to\hat{\Delta}}_\theta \circ g\}_{i,j} = g(\hat{\tau}_{\theta_i}) Q^{S,\Delta\to\hat{\Delta}}_{\theta_{i,j}}, \\
 & i = 0,\cdots,N_\theta,\ j = 1,\cdots,N_\theta \\
\{Q^{D,\hat{\Delta}\to\Delta} \circ g\}_{i,j} = g(\tau_{\theta_i}) Q^{D,\hat{\Delta}\to\Delta}_{i,j}, & \{Q^{D,\hat{\Delta}\to\Delta}_\theta \circ g\}_{i,j} = g(\tau_{\theta_i}) Q^{D,\hat{\Delta}\to\Delta}_{\theta_{i,j}}, \\
 & i = 1,\cdots,N_\theta,\ j = 0,\cdots,N_\theta
\end{array}
$$

where $S = D$ or N.

The standard QSC method gives only second-order convergence, which is suboptimal. To obtain optimal solution approximations, the one-step or two-step correction method can be used [6, 20]. In the one-step method, the differential operators are perturbed to eliminate the low-order residual terms, and optimal solutions are computed using the perturbed operators. In the two-step method, a second-order approximation is generated first, using the standard formulation, and then a higher order solution is computed in a second step by perturbing the right sides of the equations appropriately.

5.1.1 The Elliptic Problem

The OQSC methods were motivated by the second-order linear elliptic partial differential equation

$$\mathcal{L}u \equiv au_{\lambda\lambda} + bu_{\lambda\theta} + cu_{\theta\theta} + du_\lambda + eu_\theta + fu = g \tag{5.1}$$

on $\Omega \equiv (a_1, b_1) \times (a_2, b_2)$, subject to mixed boundary conditions

$$\mathcal{B}u \equiv \alpha u + \beta u_n = \gamma \tag{5.2}$$

on $\partial\Omega \equiv$ boundary of Ω, where u, a, b, c, d, e, f, g, α, β, and γ are functions of λ and θ and u_n denotes the normal derivatives of u. We will briefly describe the formulation of the OQSC methods for the above problem. Further details can be found in [6].

Consider the rectangle $\bar{\Omega} \equiv \Omega \bigcup \partial\Omega = [a_1, b_1] \times [a_2, b_2]$, and let Δ_λ and Δ_θ be uniform partitions of the intervals $[a_1, b_1]$ and $[a_2, b_2]$, respectively. That is, $\Delta_\lambda \equiv \{\lambda_0 = a_1, \lambda_i = a_1 + i(b_1 - a_1)/N_\lambda\}_{i=1}^{N_\lambda}$ and $\Delta_\theta \equiv \{\theta_0 = a_2, \theta_j = a_2 + j(b_2 - a_2)/N_\theta\}_{j=1}^{N_\theta}$, as are defined in Section 3.1. Let $\{\tau_{\lambda_i} = (\lambda_{i-1} + \lambda_i)/2\}_{i=1}^{N_\lambda}$ and $\{\tau_{\theta_j} = (\theta_{j-1} + \theta_j)/2\}_{j=1}^{N_\theta}$ be the midpoints of Δ_λ and Δ_θ, respectively. For an arbitrary function $\psi(\lambda, \theta)$, let $\psi_{i,j} \equiv \psi(\tau_{\lambda_i}, \tau_{\theta_j})$, for $i = 0, \cdots, N_\lambda + 1$ and $j = 0, \cdots, N_\theta + 1$, where $\tau_{\lambda_0} = \lambda_0 = a_1$, $\tau_{\lambda_{N_\lambda+1}} = \lambda_{N_\lambda} = b_1$, $\tau_{\theta_0} = \theta_0 = a_2$ and $\tau_{\theta_{N_\theta+1}} = \theta_{N_\theta} = b_2$. Let u_I, defined on the induced grid partition $\Delta_\lambda \times \Delta_\theta$, be the biquadratic spline interpolant of a function $u \in C^6$ such that

$$u_{I_{i,j}} = u_{i,j} \tag{5.3}$$

for $i = 1, \cdots, N_\lambda$ and $j = 1, \cdots, N_\theta$,

$$u_{I_{i,j}} = u_{i,j} - \frac{\Delta\lambda^4}{128}(D_\lambda^4 u)_{i,j} \tag{5.4}$$

for $i = 0$ or $N_\lambda + 1$ and $j = 1, \cdots, N_\theta$, and

$$u_{I_{i,j}} = u_{i,j} - \frac{\Delta\theta^4}{128}(D_\theta^4 u)_{i,j} \tag{5.5}$$

for $i = 1, \cdots, N_\lambda$ and $j = 0$ or $N_\theta + 1$. At each of the four corners of Ω where $i = 0$ or $N_\lambda + 1$ and $j = 0$ or $N_\theta + 1$, u_I satisfies one of the interpolation relations (5.4) or (5.5).

5.1.2 Previous Results

The following results in Christara [6] are useful in deriving the OQSC methods for the elliptic problem (5.1) and (5.2) and also for the modified methods on staggered grids.

Theorem 1 *Let u_I be the biquadratic spline interpolant of a function $u \in C^6$ as defined by (5.3), (5.4) and (5.5). Then the following relations hold at the midpoints*

$\{\tau_{\lambda_i}, \tau_{\theta_j}\}_{i=1,j=1}^{N_\lambda,N_\theta}$:

$$(D_\lambda u_I)_{i,j} = (D_\lambda u)_{i,j} + \frac{\Delta\lambda^2}{24}(D_\lambda^3 u)_{i,j} + \mathcal{O}(\Delta\lambda^4) \tag{5.6}$$

$$(D_\theta u_I)_{i,j} = (D_\theta u)_{i,j} + \frac{\Delta\theta^2}{24}(D_\theta^3 u)_{i,j} + \mathcal{O}(\Delta\theta^4) \tag{5.7}$$

$$(D_{\lambda\theta} u_I)_{i,j} = (D_{\lambda\theta} u)_{i,j} + \frac{\Delta\lambda^2}{24}(D_\lambda^3 D_\theta u)_{i,j} + \frac{\Delta\theta^2}{24}(D_\lambda D_\theta^3 u)_{i,j} + \mathcal{O}(h^4) \tag{5.8}$$

$$(D_\lambda^2 u_I)_{i,j} = (D_\lambda^2 u)_{i,j} - \frac{\Delta\lambda^2}{24}(D_\lambda^4 u)_{i,j} + \mathcal{O}(\Delta\lambda^4) \tag{5.9}$$

$$(D_\theta^2 u_I)_{i,j} = (D_\theta^2 u)_{i,j} - \frac{\Delta\theta^2}{24}(D_\theta^4 u)_{i,j} + \mathcal{O}(\Delta\theta^4) \tag{5.10}$$

where D_s^k denotes the k-th derivative operator with respect to the variable s, $D_{\lambda\theta}$ denotes the cross-derivative operator with respect to λ and θ, and $h \equiv \max(\Delta\lambda, \Delta\theta)$.

At the points $\{\lambda_i, \tau_{\theta_j}\}_{i=0,j=1}^{N_\lambda,N_\theta}$ and $\{\tau_{\lambda_i}, \theta_j\}_{i=1,j=0}^{N_\lambda,N_\theta}$ of a uniform partition Δ the following relations hold:

$$D_\lambda u_I(\lambda_i, \tau_{\theta_j}) = D_\lambda u(\lambda_i, \tau_{\theta_j}) - \frac{\Delta\lambda^2}{12} D_\lambda^3 u(\lambda_i, \tau_{\theta_j}) + \mathcal{O}(\Delta\lambda^4) \tag{5.11}$$

$$D_\theta u_I(\tau_{\lambda_i}, \theta_j) = D_\theta u(\tau_{\lambda_i}, \theta_j) - \frac{\Delta\theta^2}{12} D_\theta^3 u(\tau_{\lambda_i}, \theta_j) + \mathcal{O}(\Delta\theta^4) \tag{5.12}$$

Theorem 2 *Define the difference operator Λ_λ by*

$$(\Lambda_\lambda u)_{i,j} \equiv \frac{u_{i-1,j} - 2u_{i,j} + u_{i+1,j}}{\Delta\lambda^2} \tag{5.13}$$

for $i = 2, \cdots, N_\lambda - 1$ and $j = 1, \cdots, N_\theta$, and Λ_θ by

$$(\Lambda_\theta u)_{i,j} \equiv \frac{u_{i,j-1} - 2u_{i,j} + u_{i,j+1}}{\Delta\theta^2} \tag{5.14}$$

for $i = 1, \cdots, N_\lambda$ and $j = 2, \cdots, N_\theta - 1$. If u_I is the biquadratic spline interpolant of $u \in C^6$ defined by (5.3), (5.4) and (5.5), then

$$(D_\lambda^4 u)_{i,j} = \Lambda_\lambda (D_\lambda^2 u_I)_{i,j} + \mathcal{O}(\Delta\lambda^2), \qquad (D_\lambda^3 u)_{i,j} = \Lambda_\lambda (D_\lambda u_I)_{i,j} + \mathcal{O}(\Delta\lambda^2) \tag{5.15}$$

for $i = 2, \cdots, N_\lambda - 1$ and $j = 1, \cdots, N_\theta$, and

$$(D_\theta^4 u)_{i,j} = \Lambda_\theta (D_\theta^2 u_I)_{i,j} + \mathcal{O}(\Delta\theta^2), \qquad (D_\theta^3 u)_{i,j} = \Lambda_\theta (D_\theta u_I)_{i,j} + \mathcal{O}(\Delta\theta^2) \tag{5.16}$$

for $i = 1, \cdots, N_\lambda$ *and* $j = 2, \cdots, N_\theta - 1$. *At the collocation points close to the boundaries, the higher derivatives in the* θ*-direction are approximated by*

$$
\begin{aligned}
(D_\theta^k u)_{i,0} &= \frac{1}{2}\Big(5\Lambda_\theta(D_\theta^{(k-2)} u_I)_{i,2} - 3\Lambda_\theta(D_\theta^{(k-2)} u_I)_{i,3}\Big) + \mathcal{O}(\Delta\theta^2) && (5.17)\\
(D_\theta^k u)_{i,1} &= 2\Lambda_\theta(D_\theta^{(k-2)} u_I)_{i,2} - \Lambda_\theta(D_\theta^{(k-2)} u_I)_{i,3} + \mathcal{O}(\Delta\theta^2) && (5.18)\\
(D_\theta^k u)_{i,N_\theta} &= 2\Lambda_\theta(D_\theta^{(k-2)} u_I)_{i,N_\theta-1} - \Lambda_\theta(D_\theta^{(k-2)} u_I)_{i,N_\theta-2} + \mathcal{O}(\Delta\theta^2) && (5.19)\\
(D_\theta^k u)_{i,N_\theta+1} &= \frac{1}{2}\Big(5\Lambda_\theta(D_\theta^{(k-2)} u_I)_{i,N_\theta-1} - 3\Lambda_\theta(D_\theta^{(k-2)} u_I)_{i,N_\theta-2}\Big) + \mathcal{O}(\Delta\theta^2) && (5.20)
\end{aligned}
$$

for $k = 3$ *or 4 and* $i = 1, \cdots, N_\lambda$. *Similarly, approximations for the derivatives with respect to* λ *are obtained.*

5.1.3 The OQSC Methods for the Elliptic Problem

From the relations in Theorem 1, the differential equation (5.1) and the boundary conditions (5.2), we observe that the interpolant u_I of the true solution u of (5.1) and (5.2), defined by (5.3), (5.4) and (5.5), satisfies the relations

$$
\begin{aligned}
(\mathcal{L}u_I)_{i,j} = \; & g_{i,j} - a_{i,j}\frac{\Delta\lambda^2}{24}(D_\lambda^4 u)_{i,j} - c_{i,j}\frac{\Delta\theta^2}{24}(D_\theta^4 u)_{i,j} \\
& + b_{i,j}\frac{\Delta\lambda^2}{24}(D_\lambda^3 D_\theta u)_{i,j} + b_{i,j}\frac{\Delta\theta^2}{24}(D_\theta^3 D_\lambda u)_{i,j} \\
& + d_{i,j}\frac{\Delta\lambda^2}{24}(D_\lambda^3 u)_{i,j} + e_{i,j}\frac{\Delta\theta^2}{24}(D_\theta^3 u)_{i,j} + \mathcal{O}(h^4) \qquad (5.21)
\end{aligned}
$$

at the points $\{\tau_{\lambda_i}, \tau_{\theta_j}\}_{i=1,j=1}^{N_\lambda,N_\theta}$, and

$$(\mathcal{B}u_I)_{i,j} = \gamma_{i,j} - \beta_{i,j}\frac{\Delta\lambda^2}{12}(D_\lambda^3 u)_{i,j} + \mathcal{O}(h^4) \qquad (5.22)$$

at the points $(\tau_{\lambda_i}, \tau_{\theta_j})$ for $i = 0$ or $N_\lambda + 1$ and $j = 1, \cdots, N_\theta$, and

$$(\mathcal{B}u_I)_{i,j} = \gamma_{i,j} - \beta_{i,j}\frac{\Delta\theta^2}{12}(D_\theta^3 u)_{i,j} + \mathcal{O}(h^4) \qquad (5.23)$$

at the points $(\tau_{\lambda_i}, \tau_{\theta_j})$ for $i = 1, \cdots, N_\lambda$ and $j = 0$ or $N_\theta + 1$. At the four corners $(\tau_{\lambda_i}, \tau_{\theta_j})$ where $i = 0$ or $N_\lambda + 1$ and $j = 0$ or $N_\theta + 1$, $u_{I_{i,j}}$ satisfies either (5.22) or (5.23).

Fourth-order approximations to the residual terms can be obtained by approximating the higher derivatives of u on the right sides of the above equations using u_I and the difference operators. Using results in Theorem 2, equation (5.21) can be rewritten as

$$\begin{aligned}(\mathcal{L}u_I)_{i,j} &= g_{i,j} - a_{i,j}\frac{\Delta\lambda^2}{24}\Lambda_\lambda(D_\lambda^2 u_I)_{i,j} - c_{i,j}\frac{\Delta\theta^2}{24}\Lambda_\theta(D_\theta^2 u_I)_{i,j} \\ &\quad + b_{i,j}\frac{\Delta\lambda^2}{24}\Lambda_\lambda(D_\lambda D_\theta u_I)_{i,j} + b_{i,j}\frac{\Delta\theta^2}{24}\Lambda_\theta(D_\theta D_\lambda u_I)_{i,j} \\ &\quad + d_{i,j}\frac{\Delta\lambda^2}{24}\Lambda_\lambda(D_\lambda u_I)_{i,j} + e_{i,j}\frac{\Delta\theta^2}{24}\Lambda_\theta(D_\theta u_I)_{i,j} + \mathcal{O}(h^4) \\ &\equiv g_{i,j} - (\delta\mathcal{L}u_I)_{i,j} + \mathcal{O}(h^4) \end{aligned} \tag{5.24}$$

for $i = 2, \cdots, N_\lambda - 1$ and $j = 2, \cdots, N_\theta - 1$, where $\delta\mathcal{L}$ is an $\mathcal{O}(h^2)$ perturbation operator. At points close to the boundaries, the higher derivatives are obtained by applying (5.18) and (5.19). In this way, the definition of $\delta\mathcal{L}$ is extended to all interior collocation points. More details can be found in Section 5.2, where we present similar procedures for the OQSC methods on staggered grids.

The boundary operator residual equations (5.22) and (5.23) at boundary collocation points $\{(\lambda_0, \tau_{\lambda_j}), (\lambda_{N_\lambda}, \tau_{\lambda_j})\}_{j=0}^{N_\theta+1}$ take the form

$$\begin{aligned}(\mathcal{B}u_I)_{k,j} &= \gamma_{k,j} - \beta_{k,j}\frac{\Delta\lambda^2}{24}\left[5\Lambda_\lambda(D_\lambda u_I)_{l,j} - 3\Lambda_\lambda(D_\lambda u_I)_{m,j}\right] + \mathcal{O}(h^4) \\ &\equiv \gamma_{k,j} - (\delta\mathcal{B}u_I)_{k,j} + \mathcal{O}(h^4)\end{aligned} \tag{5.25}$$

where $(k, l, m) = (0, 2, 3)$ or $(N_\lambda + 1, N_\lambda - 1, N_\lambda - 2)$, and $\delta\mathcal{B}$ is an $\mathcal{O}(h^2)$ perturbation operator. At the points $\{(\tau_{\lambda_i}, \theta_0), (\tau_{\lambda_i}, \theta_{N_\theta})\}_{i=0}^{N_\lambda+1}$, a similar relation can be derived.

The one-step OQSC method can be derived by moving the perturbation terms in (5.24) and (5.25) to the left and determining a biquadratic spline u_Δ that satisfies

$$(\mathcal{L} + \delta\mathcal{L})u_\Delta = g \tag{5.26}$$

at the midpoints of $\Delta_\lambda \times \Delta_\theta$, and

$$(\mathcal{B} + \delta\mathcal{B})u_\Delta = \gamma \tag{5.27}$$

at the boundary collocation points including corners. It has been shown in [6] that u_Δ is fourth-order locally at gridpoints and midpoints, and third-order globally. Superconvergence is also exhibited by its derivatives at special points [6].

In the two-step OQSC method, a second-order biquadratic spline approximation $\breve{u}_\Delta$ is generated first by forcing it to satisfy

$$\mathcal{L}\breve{u}_\Delta = g \tag{5.28}$$

at the midpoints of $\Delta_\lambda \times \Delta_\theta$, and

$$\mathcal{B}\breve{u}_\Delta = \gamma \tag{5.29}$$

at the boundary collocation points. The second-order approximation $\breve{u}_\Delta$ is then used to perturb the right sides of the differential equation and boundary conditions, thereby eliminating the second-order residual terms. By determining a biquadratic spline u_Δ that satisfies

$$\mathcal{L}u_\Delta = g - \delta\mathcal{L}\breve{u}_\Delta \tag{5.30}$$

at the midpoints of $\Delta_\lambda \times \Delta_\theta$, and

$$\mathcal{B}u_\Delta = \gamma - \delta\mathcal{B}\breve{u}_\Delta \tag{5.31}$$

at the boundary collocation points and corners, we obtain an approximate solution to (5.1) and (5.2) that is, as in the case of the one-step method, locally fourth-order at gridpoints and midpoints of the uniform partition, and globally third-order.

5.2 Derivation of OQSC Methods on Staggered Grids

We will extend the methods described above to staggered grids and demonstrate through numerical experiments that the locally fourth-order accuracy is preserved when the OQSC methods are applied to the coupled shallow water equations, which are discretized spatially on the staggered C-grid. The collocation points for $\Delta_1 = \hat{\Delta}_\lambda \times \Delta_\theta$, $\Delta_2 = \Delta_\lambda \times \hat{\Delta}_\theta$

and $\Delta_3 = \Delta_\lambda \times \Delta_\theta$ are chosen to be $\{\hat{\tau}_{\lambda_i}, \tau_{\theta_j}\}_{i=1,j=1}^{N_\lambda,N_\theta}$, $\{\tau_{\lambda_i}, \hat{\tau}_{\theta_j}\}_{i=1,j=0}^{N_\lambda,N_\theta}$, and $\{\tau_{\lambda_i}, \tau_{\theta_j}\}_{i=1,j=1}^{N_\lambda,N_\theta}$, respectively. Note that the collocation points $\hat{\tau}_{\theta_0} = \hat{\theta}_0$ and $\hat{\tau}_{\theta_{N_\theta}} = \hat{\theta}_{N_\theta-1}$ are gridpoints of $\hat{\Delta}_\theta$ (see Section 3.1.1).

Let U_I^{n+1} and $\tilde{U}_I^n$ be the biquadratic spline interpolants of U^{n+1} and $\tilde{U}^n$, which are the true solution and its upstream function for the time-discretized shallow water equations (2.58) and (2.60), respectively, defined on the partition Δ_1 (see Section 3.1.1), such that the relations

$$U_I^{n+1}(\hat{\tau}_{\lambda_i}, \tau_{\theta_j}) = U^{n+1}(\hat{\tau}_{\lambda_i}, \tau_{\theta_j}), \qquad \tilde{U}_I^n(\hat{\tau}_{\lambda_i}, \tau_{\theta_j}) = \tilde{U}^n(\hat{\tau}_{\lambda_i}, \tau_{\theta_j}) \tag{5.32}$$

are satisfied for $i = 1, \cdots, N_\lambda$ and $j = 1, \cdots, N_\theta$, and

$$U_I^{n+1}(\hat{\tau}_{\lambda_i}, \tau_{\theta_j}) = U^{n+1}(\hat{\tau}_{\lambda_i}, \tau_{\theta_j}) - \frac{\Delta\theta^4}{128} D_\theta^4 U^{n+1}(\hat{\tau}_{\lambda_i}, \tau_{\theta_j}) \tag{5.33}$$

$$\tilde{U}_I^n(\hat{\tau}_{\lambda_i}, \tau_{\theta_j}) = \tilde{U}^n(\hat{\tau}_{\lambda_i}, \tau_{\theta_j}) - \frac{\Delta\theta^4}{128} D_\theta^4 \tilde{U}^n(\hat{\tau}_{\lambda_i}, \tau_{\theta_j}) \tag{5.34}$$

for $i = 1, \cdots, N_\lambda$ and $j = 0$ or $N_\theta + 1$. No perturbed boundary relation is required in the longitudinal dimension where functions are assumed to be periodic. Similarly, let V_I^{n+1} and $\tilde{V}_I^n$ be the biquadratic spline interpolants of V^{n+1} and $\tilde{V}^n$, respectively, defined on Δ_2, and ϕ_I^{n+1}, ζ_I^{n+1}, $\tilde{\phi}_I^n$ and $\tilde{\zeta}_I^n$, be the interpolants of ϕ^{n+1}, $\log\phi^{n+1}$, $\tilde{\phi}^n$ and $\log\tilde{\phi}^n$, respectively, defined on Δ_3.

From Theorem 1, the above spline interpolants satisfy the time-discretized equations (2.58) and (2.60) at $\{\hat{\tau}_{\lambda_i}, \tau_{\theta_j}\}_{i=1,j=1}^{N_\lambda,N_\theta}$, $\{\tau_{\lambda_i}, \hat{\tau}_{\theta_j}\}_{i=1,j=0}^{N_\lambda,N_\theta}$ and $\{\tau_{\lambda_i}, \tau_{\theta_j}\}_{i=1,j=1}^{N_\lambda,N_\theta}$, respectively,

$$U_I^{n+1} + \left(\frac{\Delta t}{2R^2}\right)(cD_\lambda\phi_I^{n+1} + d\cos\tilde{\theta} D_\theta\phi_I^{n+1}) = R_u^{n+1} + \varepsilon_u^{n+1} \tag{5.35}$$

$$V_I^{n+1} + \left(\frac{\Delta t}{2R^2}\right)(-dD_\lambda\phi_I^{n+1} + c\cos\tilde{\theta} D_\theta\phi_I^{n+1}) = R_v^{n+1} + \varepsilon_v^{n+1} \tag{5.36}$$

$$\cos\tilde{\theta}\zeta_I^{n+1} + \left(\frac{\Delta t}{2}\right)\left[\left(\frac{1}{\cos\tilde{\theta}}\right) D_\lambda U_I^{n+1} + D_\theta V_I^{n+1}\right] = R_\phi^{n+1} + \varepsilon_\phi^{n+1} \tag{5.37}$$

where

$$R_u^{n+1} = a\tilde{U}_I^n + b\tilde{V}_I^n - \left(\frac{\Delta t}{2R^2}\right)(cD_\lambda\tilde{\phi}_I^n + d\cos\tilde{\theta} D_\theta\tilde{\phi}_I^n) - \Delta t\tilde{\delta}_u^{n+\frac{1}{2}}$$

$$R_v^{n+1} = -b\tilde{U}_I^n + a\tilde{V}_I^n - \left(\frac{\Delta t}{2R^2}\right)(-dD_\lambda\tilde{\phi}_I^n + c\cos\tilde{\theta}D_\theta\tilde{\phi}_I^n) - \Delta t\tilde{\delta}_v^{n+\frac{1}{2}}$$
$$R_\phi^{n+1} = \cos\tilde{\theta}\tilde{\zeta}_I^n - \left(\frac{\Delta t}{2}\right)\left[\left(\frac{1}{\cos\tilde{\theta}}\right)D_\lambda\tilde{U}_I^n + D_\theta\tilde{V}_I^n\right]$$

To derive an expression for ε_u^{n+1} at $\{\hat{\tau}_{\lambda_i}, \tau_{\theta_j}\}_{i=1,j=1}^{N_\lambda,N_\theta}$, we note that the second-order residual terms in ε_u^{n+1} arise from terms associated with the derivatives of the interpolant ϕ_I^{n+1}, namely, $(\frac{\Delta t}{2R^2})cD_\lambda\phi_I^{n+1}$ and $(\frac{\Delta t}{2R^2})d\cos\tilde{\theta}D_\theta\phi_I^{n+1}$. We first consider the former. Since equation (5.35) is collocated at $\{\hat{\tau}_{\lambda_i}, \tau_{\theta_j}\}_{i=1,j=1}^{N_\lambda,N_\theta}$, which align in the λ-dimension with the gridpoints of Δ_3, the partition on which ϕ_I^{n+1} is defined, the second-order residual term associated with $(\frac{\Delta t}{2R^2})cD_\lambda\phi_I^{n+1}$ is given by (5.11) as $-\left(\frac{\Delta t}{2R^2}\right)\frac{\Delta\lambda^2}{12}cD_\lambda^3\phi^{n+1}$. On the other hand, the collocation points $\{\hat{\tau}_{\lambda_i}, \tau_{\theta_j}\}_{i=1,j=1}^{N_\lambda,N_\theta}$ align with the midpoints of Δ_3 in the θ-dimension. Therefore, the second-order residual term associated with $(\frac{\Delta t}{2R^2})d\cos\tilde{\theta}D_\theta\phi_I^{n+1}$ is given by (5.6) as $\left(\frac{\Delta t}{2R^2}\right)\frac{\Delta\theta^2}{24}d\cos\tilde{\theta}D_\theta^3\phi^{n+1}$. Combining these results, we obtain that at $\{\hat{\tau}_{\lambda_i}, \tau_{\theta_j}\}_{i=1,j=1}^{N_\lambda,N_\theta}$

$$\varepsilon_u^{n+1} = -\left(\frac{\Delta t}{2R^2}\right)\left[\frac{\Delta\lambda^2}{12}c\left(D_\lambda^3\phi^{n+1} + D_\lambda^3\tilde{\phi}^n\right) - \frac{\Delta\theta^2}{24}d\cos\tilde{\theta}\left(D_\theta^3\phi^{n+1} + D_\theta^3\tilde{\phi}^n\right)\right] + \mathcal{O}(h^4) \tag{5.38}$$

Similarly, the residuals ε_v^{n+1} and ε_ϕ^{n+1} at $\{\tau_{\lambda_i}, \hat{\tau}_{\theta_j}\}_{i=1,j=1}^{N_\lambda,N_\theta-1}$ and $\{\tau_{\lambda_i}, \tau_{\theta_j}\}_{i=1,j=1}^{N_\lambda,N_\theta}$, respectively, are

$$\varepsilon_v^{n+1} = -\left(\frac{\Delta t}{2R^2}\right)\left[-\frac{\Delta\lambda^2}{24}d\left(-D_\lambda^3\phi^{n+1} - D_\lambda^3\tilde{\phi}^n\right) + \frac{\Delta\theta^2}{12}c\cos\tilde{\theta}\left(D_\theta^3\phi^{n+1} + D_\theta^3\tilde{\phi}^n\right)\right] + \mathcal{O}(h^4) \tag{5.39}$$

$$\varepsilon_\phi^{n+1} = -\left(\frac{\Delta t}{2}\right)\left[\frac{\Delta\lambda^2}{12}\frac{1}{\cos\tilde{\theta}}\left(D_\lambda^3U^{n+1} + D_\lambda^3\tilde{U}^n\right) + \frac{\Delta\theta^2}{12}\left(D_\theta^3V^{n+1} + D_\theta^3\tilde{V}^n\right)\right] + \mathcal{O}(h^4) \tag{5.40}$$

At $\{(\tau_{\lambda_i}, \hat{\tau}_{\theta_0}), (\tau_{\lambda_i}, \hat{\tau}_{\theta_{N_\theta}})\}_{i=1}^{N_\theta}$, the residual ε_v^{n+1} takes on a slightly different form

$$\varepsilon_v^{n+1} = -\left(\frac{\Delta t}{2R^2}\right)\left[-\frac{\Delta\lambda^2}{24}d\left(-D_\lambda^3\phi^{n+1} - D_\lambda^3\tilde{\phi}^n\right) - \frac{\Delta\theta^2}{24}c\cos\tilde{\theta}\left(D_\theta^3\phi^{n+1} + D_\theta^3\tilde{\phi}^n\right)\right] + \mathcal{O}(h^4) \tag{5.41}$$

because $\hat{\tau}_{\theta_0}$ and $\hat{\tau}_{\theta_{N_\theta}}$ are gridpoints of $\hat{\Delta}_\theta$ (midpoints of Δ_θ) while $\{\hat{\tau}_{\theta_j}\}_{j=1}^{N_\theta-1}$ are midpoints of $\hat{\Delta}_\theta$ (gridpoints of Δ_θ). According to Theorem 1, this implies that the coefficients of the perturbation terms associated with $D_\theta(\phi_I^{n+1} + \tilde{\phi}_I^n)$ are different in the two cases.

The derivatives of the interpolants of the geopotential ϕ^{n+1} and its logarithm satisfy

$$D_\theta \phi_I^{n+1}\left(\tau_{\lambda_i}, \pm\frac{\pi}{2}\right) = -\frac{\Delta\theta^2}{12} D_\theta^3 \phi^{n+1}\left(\tau_{\lambda_i}, \pm\frac{\pi}{2}\right) + \mathcal{O}(h^4) \tag{5.42}$$

$$D_\theta \zeta_I^{n+1}\left(\tau_{\lambda_i}, \pm\frac{\pi}{2}\right) = -\frac{\Delta\theta^2}{12} D_\theta^3 \zeta^{n+1}\left(\tau_{\lambda_i}, \pm\frac{\pi}{2}\right) + \mathcal{O}(h^4) \tag{5.43}$$

at the poles, for $i = 1, \cdots, N_\lambda$, since $D_\theta \phi^{n+1}(\tau_{\lambda_i}, \pm\pi/2) = 0$ and $D_\theta \zeta^{n+1}(\tau_{\lambda_i}, \pm\pi/2) = 0$.

In order to derive a method with optimal convergence, the second-order terms in the residuals of (5.38) to (5.41) and the boundary residuals (5.42) and (5.43) need to be eliminated. The idea is to approximate the third derivatives to second-order accuracy with the spline interpolants, and then use these approximations to eliminate the second-order terms. To this end, we extend the definitions of the difference operators Λ_θ to handle collocation points near the boundaries. Along the longitude, where the boundary conditions are periodic, the centered difference operator Λ_λ can be redefined to be Λ'_λ given by

$$\begin{aligned}
(\Lambda'_\lambda u)_{1,j} &\equiv \frac{u_{N_\lambda,j} - 2u_{1,j} + u_{2,j}}{\Delta\lambda^2} \\
(\Lambda'_\lambda u)_{i,j} &\equiv (\Lambda_\lambda u)_{i,j}, \qquad\qquad i = 2, \cdots, N_\lambda - 2 \\
(\Lambda'_\lambda u)_{N_\lambda,j} &\equiv \frac{u_{N_\lambda-1,j} - 2u_{N_\lambda,j} + u_{1,j}}{\Delta\lambda^2}
\end{aligned}$$

for $j = 1, \cdots, N_\theta$, while in the latitudinal direction, we combine relations (5.16) to (5.20) to get

$$\begin{aligned}
(\Lambda'_\theta u)_{i,1} &\equiv \frac{2u_{i,1} - 5u_{i,2} + 4u_{i.3} - u_{i,4}}{\Delta\theta^2} \\
(\Lambda'_\theta u)_{i,j} &\equiv (\Lambda_\theta u)_{i,j}, \qquad\qquad j = 2, \cdots, N_\theta - 1 \\
(\Lambda'_\theta u)_{i,N_\theta} &\equiv \frac{2u_{i,N_\theta} - 5u_{i,N_\theta-1} + 4u_{i,N_\theta-2} - u_{i,N_\theta-3}}{\Delta\theta^2}
\end{aligned}$$

for $i = 1, \cdots, N_\lambda$. The operator Λ'_θ is useful for approximating the residuals on Δ_θ, where the collocation points are midpoints. We define another difference operator $\hat{\Lambda}'_\theta$ for $\hat{\Delta}_\theta$, where the first and last collocation points are gridpoints

$$\begin{aligned}
(\hat{\Lambda}'_\theta u)_{i,0} &\equiv \frac{5u_{i,1} - 13u_{i,2} + 11u_{i.3} - 3u_{i,4}}{2\Delta\theta^2} \\
(\hat{\Lambda}'_\theta u)_{i,1} &\equiv \frac{2u_{i,1} - 5u_{i,2} + 4u_{i.3} - u_{i,4}}{\Delta\theta^2} \\
(\hat{\Lambda}'_\theta u)_{i,j} &\equiv (\Lambda_\theta u)_{i,j}, \qquad\qquad j = 2, \cdots, N_\theta - 2 \\
(\hat{\Lambda}'_\theta u)_{i,N_\theta-1} &\equiv \frac{2u_{i,N_\theta-1} - 5u_{i,N_\theta-2} + 4u_{i,N_\theta-3} - u_{i,N_\theta-4}}{\Delta\theta^2} \\
(\hat{\Lambda}'_\theta u)_{i,N_\theta} &\equiv \frac{5u_{i,N_\theta-1} - 13u_{i,N_\theta-2} + 11u_{i,N_\theta-3} - 3u_{i,N_\theta-4}}{2\Delta\theta^2}
\end{aligned}$$

for $i = 1, \cdots, N_\lambda$.

From the results in Theorem 2, the third derivatives of U^{n+1}, for instance, can be approximated to second order using the first derivative of its interpolant U_I^{n+1} and the above difference operators. More specifically, $D_\lambda^3 U^{n+1}$ and $D_\lambda^3 U^{n+1}$ can be approximated at the collocation points of Δ_1 using $D_\lambda U_I^{n+1}$ and $D_\theta U_I^{n+1}$, respectively, by

$$\begin{aligned}
(D_\lambda^3 U^{n+1})(\hat{\tau}_{\lambda_i}, \tau_{\theta_j}) &= (\Lambda'_\lambda(D_\lambda U_I^{n+1}))(\hat{\tau}_{\lambda_i}, \tau_{\theta_j}) + \mathcal{O}(\Delta\lambda^2) \\
(D_\theta^3 U^{n+1})(\hat{\tau}_{\lambda_i}, \tau_{\theta_j}) &= (\Lambda'_\theta(D_\theta U_I^{n+1}))(\hat{\tau}_{\lambda_i}, \tau_{\theta_j}) + \mathcal{O}(\Delta\theta^2)
\end{aligned}$$

for $i = 1, \cdots, N_\lambda$ and $j = 1, \cdots, N_\theta$. On the other hand, the difference operator $\hat{\Lambda}'_\theta$ and the interpolant V_I^{n+1} can be used to approximate $D_\theta^3 V^{n+1}$ at the collocation points of Δ_2 by

$$(D_\theta^3 V^{n+1})(\tau_{\lambda_i}, \hat{\tau}_{\theta_j}) = (\hat{\Lambda}_\theta(D_\theta V_I^{n+1}))(\tau_{\lambda_i}, \hat{\tau}_{\theta_j}) + \mathcal{O}(\Delta\theta^2)$$

for $i = 1, \cdots, N_\lambda$ and $j = 0, \cdots, N_\theta$. Similar relations hold for the other functions, leading to the following fourth-order approximations for the residuals of (5.38) to (5.40) at the collocation points of Δ_1, Δ_2 and Δ_3, respectively:

$$\begin{aligned}
\varepsilon_u^{n+1}(\hat{\tau}_{\lambda_i}, \tau_{\theta_j}) = -\left(\frac{\Delta t}{2R^2}\right) \Bigg[&\frac{\Delta\lambda^2}{12} c(\tau_{\theta_j}) \left(\Lambda'_\lambda(D_\lambda \phi_I^{n+1} + D_\lambda \tilde{\phi}_I^n)\right)(\hat{\tau}_{\lambda_i}, \tau_{\theta_j}) \\
&- \frac{\Delta\theta^2}{24} d(\tau_{\theta_j}) \cos\tilde{\tau}_{\theta_j} \left(\Lambda'_\theta(D_\theta \phi_I^{n+1} + D_\theta \tilde{\phi}_I^n)\right)(\hat{\tau}_{\lambda_i}, \tau_{\theta_j}) \Bigg] + \mathcal{O}(h^4)
\end{aligned}$$

$$\text{for } i = 1, \cdots, N_\lambda,\ j = 1, \cdots, N_\theta \tag{5.44}$$

$$\varepsilon_v^{n+1}(\tau_{\lambda_i}, \hat{\tau}_{\theta_j}) = -\left(\frac{\Delta t}{2R^2}\right)\left[-\frac{\Delta\lambda^2}{24}d(\hat{\tau}_{\theta_j})\left(\Lambda'_\lambda(-D_\lambda\phi_I^{n+1} - D_\lambda\tilde{\phi}_I^n)\right)(\tau_{\lambda_i}, \hat{\tau}_{\theta_j}) + \frac{\Delta\theta^2}{12}c(\hat{\tau}_{\theta_j})\cos\tilde{\hat{\tau}}_{\theta_j}\left(\hat{\Lambda}'_\theta(D_\theta\phi_I^{n+1} + D_\theta\tilde{\hat{\phi}}_I^n)\right)(\tau_{\lambda_i}, \hat{\tau}_{\theta_j})\right] + \mathcal{O}(h^4)$$

$$\text{for } i = 1, \cdots, N_\lambda,\ j = 1, \cdots, N_\theta - 1 \tag{5.45}$$

$$\varepsilon_v^{n+1}(\tau_{\lambda_i}, \hat{\tau}_{\theta_j}) = -\left(\frac{\Delta t}{2R^2}\right)\left[-\frac{\Delta\lambda^2}{24}d(\hat{\tau}_{\theta_j})\left(\Lambda'_\lambda(-D_\lambda\phi_I^{n+1} - D_\lambda\tilde{\phi}_I^n)\right)(\tau_{\lambda_i}, \hat{\tau}_{\theta_j}) - \frac{\Delta\theta^2}{24}c(\hat{\tau}_{\theta_j})\cos\tilde{\hat{\tau}}_{\theta_j}\left(\hat{\Lambda}'_\theta(D_\theta\phi_I^{n+1} + D_\theta\tilde{\hat{\phi}}_I^n)\right)(\tau_{\lambda_i}, \hat{\tau}_{\theta_j})\right] + \mathcal{O}(h^4)$$

$$\text{for } i = 1, \cdots, N_\lambda,\ j = 0, N_\theta \tag{5.46}$$

$$\varepsilon_\phi^{n+1}(\tau_{\lambda_i}, \tau_{\theta_j}) = -\left(\frac{\Delta t}{2}\right)\left[\frac{\Delta\lambda^2}{12}\frac{1}{\cos\tilde{\tau}_{\theta_j}}\left(\Lambda'_\lambda(D_\lambda U_I^{n+1} + D_\lambda\tilde{U}_I^n)\right)(\tau_{\lambda_i}, \tau_{\theta_j}) + \frac{\Delta\theta^2}{12}\left(\Lambda'_\theta(D_\theta V_I^{n+1} + D_\theta\tilde{V}_I^n)\right)(\tau_{\lambda_i}, \tau_{\theta_j})\right] + \mathcal{O}(h^4)$$

$$\text{for } i = 1, \cdots, N_\lambda,\ j = 1, \cdots, N_\theta \tag{5.47}$$

The points $\tilde{\tau}_{\theta_j}$ and $\tilde{\hat{\tau}}_{\theta_j}$ are defined as the latitudinal positions at t_n of fluid particles whose trajectories have latitudinal positions of τ_{θ_j} and $\hat{\tau}_{\theta_j}$, respectively, at t_{n+1}. The above equations allow us to eliminate the second-order terms of the residuals in (5.35) to (5.37) and to obtain higher-order solutions, as will be explained in the sections to follow.

5.2.1 The One-Step Optimal Quadratic Spline Collocation Method

In the one-step method, the second-order perturbation terms inside the square brackets in (5.44) to (5.47) are combined with the associated derivative operators to form *perturbed operators*, which are then incorporated into the system to yield a higher-order approximation. For example, the first perturbation term inside the square brackets of (5.44), $(\frac{\Delta\lambda^2}{12})c\Lambda'_\lambda(D_\lambda\phi_I^{n+1})$, comes from the second term on the left side of (5.35), $cD_\lambda\phi_I^{n+1}$. These two terms can therefore be combined to form

$$c\left(I + \frac{\Delta\lambda^2}{12}\Lambda'_\lambda\right)D_\lambda\phi_I^{n+1}$$

where I denotes the identity operator. This motivates us to define the perturbed operator

$$D_\lambda^{\prime\Delta\to\hat{\Delta}} = \left(I + \frac{\Delta\lambda^2}{12}\Lambda_\lambda'\right) D_\lambda$$

Similarly, the first perturbation term inside the square brackets of (5.47), $(\frac{\Delta\lambda^2}{12})\frac{1}{\cos\tilde{\theta}}\Lambda_\lambda'(D_\lambda U_I^{n+1})$, comes from the second term on the left side of (5.37), $\frac{1}{\cos\tilde{\theta}}D_\lambda U_I^{n+1}$. Combining these two terms gives

$$\frac{1}{\cos\tilde{\theta}}\left(I + \frac{\Delta\lambda^2}{12}\Lambda_\lambda'\right) D_\lambda U_I^{n+1} \equiv \frac{1}{\cos\tilde{\theta}} D_\lambda^{\prime\hat{\Delta}\to\Delta} U_I^{n+1}$$

Since $D_\lambda^{\prime\Delta\to\hat{\Delta}} = D_\lambda^{\prime\hat{\Delta}\to\Delta} = (I + \frac{\Delta\lambda^2}{12}\Lambda_\lambda')D_\lambda$, we define

$$D_\lambda^{\prime\to} \equiv \left(I + \frac{\Delta\lambda^2}{12}\Lambda_\lambda'\right) D_\lambda = D_\lambda^{\prime\Delta\to\hat{\Delta}} = D_\lambda^{\prime\hat{\Delta}\to\Delta}$$

The arrow indicates that $D_\lambda^{\prime\to}$ computes the perturbed derivative values at collocation points in $\hat{\Delta}_\lambda$ from spline coefficients defined in Δ_λ, or vice versa. Furthermore, combining the term $-\frac{\Delta\theta^2}{24}d\cos\tilde{\theta}\Lambda_\theta'(D_\theta\phi_I^{n+1})$ of (5.44) with $d\cos\tilde{\theta}D_\theta\phi_I^{n+1}$ of (5.35), the term $-\frac{\Delta\lambda^2}{24}d\Lambda_\lambda'(D_\lambda\phi_I^{n+1})$ of (5.45) with $dD_\lambda\phi_I^{n+1}$ of (5.36), and the term $\frac{\Delta\theta^2}{12}\Lambda_\theta'(D_\theta V_I^{n+1})$ of (5.47) with $D_\theta V_I^{n+1}$ of (5.37), we obtain

$$d\cos\tilde{\theta}\left(I - \frac{\Delta\theta^2}{24}\Lambda_\theta'\right) D_\theta\phi_I^{n+1}, \quad d\left(I - \frac{\Delta\lambda^2}{24}\Lambda_\lambda'\right) D_\lambda\phi_I^{n+1}, \quad \left(I + \frac{\Delta\theta^2}{12}\Lambda_\theta'\right) D_\theta V_I^{n+1}$$

Thus, we define the following perturbed operators:

$$D_\lambda' = \left(I - \frac{\Delta\lambda^2}{24}\Lambda_\lambda'\right) D_\lambda, \quad D_\theta' = \left(I - \frac{\Delta\theta^2}{24}\Lambda_\theta'\right) D_\theta, \quad D_\theta^{\prime\hat{\Delta}\to\Delta} = \left(I + \frac{\Delta\theta^2}{12}\Lambda_\theta'\right) D_\theta$$

The perturbed operator $D_\theta^{\prime\Delta\to\hat{\Delta}}$, which computes first derivative values in the θ direction and the associated residual terms on the $\hat{\Delta}_\theta$-grid, needs to be defined carefully because, as noted before, the residual terms for the collocation points $\{(\tau_{\lambda_i}, \hat{\tau}_{\theta_0}), (\tau_{\lambda_i}, \hat{\tau}_{\theta_{N_\theta}})\}_{i=1}^{N_\lambda}$ are slightly different from the rest. At $\{\tau_{\lambda_i}, \hat{\tau}_{\theta_j}\}_{i=1,j=1}^{N_\lambda,N_\theta-1}$, the residual term associated with $c\cos\tilde{\theta}D_\theta\phi_I^{n+1}$ is $\frac{\Delta\theta^2}{12}c\cos\tilde{\theta}\hat{\Lambda}_\theta\phi_I^{n+1}$ in (5.45), whereas at $\{(\tau_{\lambda_i}, \hat{\tau}_{\theta_0}), (\tau_{\lambda_i}, \hat{\tau}_{\theta_{N_\theta}})\}_{i=1}^{N_\lambda}$ the residual term takes the form $-\frac{\Delta\theta^2}{24} c\cos\tilde{\theta}\hat{\Lambda}_\theta \phi_I^{n+1}$ in (5.46). Therefore, we define $D_\theta'^{\Delta\to\hat{\Delta}}$ at $\{\tau_{\lambda_i}, \hat{\tau}_{\theta_j}\}_{i=1,j=1}^{N_\lambda, N_\theta-1}$ as

$$(D_\theta'^{\Delta\to\hat{\Delta}} u)(\tau_{\lambda_i}, \hat{\tau}_{\theta_j}) = \left[\left(I + \frac{\Delta\theta^2}{12}\hat{\Lambda}_\theta'\right)(D_\theta u)\right](\tau_{\lambda_i}, \hat{\tau}_{\theta_j})$$

and at $\{(\tau_{\lambda_i}, \hat{\tau}_{\theta_0}), (\tau_{\lambda_i}, \hat{\tau}_{\theta_{N_\theta}})\}_{i=1}^{N_\lambda}$ as

$$(D_\theta'^{\Delta\to\hat{\Delta}} u)(\tau_{\lambda_i}, \hat{\tau}_{\theta_j}) = \left[\left(I - \frac{\Delta\theta^2}{24}\hat{\Lambda}_\theta'\right)(D_\theta u)\right](\tau_{\lambda_i}, \hat{\tau}_{\theta_j})$$

for $j = 0,\ N_\theta$.

Having defined the perturbed operators, we can derive the one-step OQSC method. In the one-step method, we determine the approximations U_Δ^{n+1}, V_Δ^{n+1} and ϕ_Δ^{n+1} such that they satisfy the equations

$$\begin{aligned}
U_\Delta^{n+1} &+ \left(\frac{\Delta t}{2R^2}\right)(cD_\lambda'^{\to}\phi_\Delta^{n+1} + d\cos\tilde{\theta}D_\theta'\phi_\Delta^{n+1}) \\
&= a\tilde{U}_\Delta^n + b\tilde{V}_\Delta^n - \left(\frac{\Delta t}{2R^2}\right)(cD_\lambda'^{\to}\tilde{\phi}_\Delta^n + d\cos\tilde{\theta}D_\theta'\tilde{\phi}_\Delta^n) - \Delta t\tilde{\delta}_u^{n+\frac{1}{2}} \qquad (5.48)\\
V_\Delta^{n+1} &+ \left(\frac{\Delta t}{2R^2}\right)(-dD_\lambda'\phi_\Delta^{n+1} + c\cos\tilde{\theta}D_\theta'^{\Delta\to\hat{\Delta}}\phi_\Delta^{n+1}) \\
&= -b\tilde{U}_\Delta^n + a\tilde{V}_\Delta^n - \left(\frac{\Delta t}{2R^2}\right)(-dD_\lambda'\tilde{\phi}_\Delta^n + c\cos\tilde{\theta}D_\theta'^{\Delta\to\hat{\Delta}}\tilde{\phi}_\Delta^n) - \Delta t\tilde{\delta}_v^{n+\frac{1}{2}} \qquad (5.49)\\
\cos\tilde{\theta}\zeta_\Delta^{n+1} &+ \left(\frac{\Delta t}{2}\right)\left[\left(\frac{1}{\cos\tilde{\theta}}\right)D_\lambda'^{\to}U^{n+1} + D_\theta'^{\hat{\Delta}\to\Delta}V^{n+1}\right] \\
&= \cos\tilde{\theta}\tilde{\zeta}_\Delta^n - \left(\frac{\Delta t}{2}\right)\left[\left(\frac{1}{\cos\tilde{\theta}}\right)D_\lambda'^{\to}\tilde{U}_\Delta^n + D_\theta'^{\hat{\Delta}\to\Delta}\tilde{V}_\Delta^n\right] \qquad (5.50)
\end{aligned}$$

at $\{\hat{\tau}_{\lambda_i}, \tau_{\theta_j}\}_{i=1,j=1}^{N_\lambda,N_\theta}$, $\{\tau_{\lambda_i}, \hat{\tau}_{\theta_j}\}_{i=1,j=0}^{N_\lambda,N_\theta}$ and $\{\tau_{\lambda_i}, \tau_{\theta_j}\}_{i=1,j=1}^{N_\lambda,N_\theta}$, respectively. The approximate solutions are assumed to be periodic in the longitudinal dimension and subject to the following boundary conditions in the latitudinal dimension:

$$\begin{aligned}
&U_\Delta^{n+1}(\hat{\tau}_{\lambda_i}, \pm\tfrac{\pi}{2}) = 0, && V_\Delta^{n+1}(\tau_{\lambda_i}, \pm\tfrac{\pi}{2}) = 0,\\
&D_\theta'^{\hat{\Delta}\to\Delta}\phi_\Delta^{n+1}(\tau_{\lambda_i}, \pm\tfrac{\pi}{2}) = 0, && D_\theta'^{\hat{\Delta}\to\Delta}\zeta_\Delta^{n+1}(\tau_{\lambda_i}, \pm\tfrac{\pi}{2}) = 0
\end{aligned}$$

for $i = 1, \cdots, N_\lambda$.

Following the procedures outlined in Section 3.6, a Helmholtz equation is derived by eliminating the divergence terms from (5.50) using (5.48) and (5.49), and is then linearized and solved using fixed-point iteration.

In Chapter 6, we report results of numerical experiments that show that the solutions of the resulting Helmholtz equation have fourth-order errors at midpoints, which is optimal for quadratic splines.

5.2.2 The Two-Step Optimal Quadratic Spline Collocation Method

Alternatively, the two-step optimal collocation method can be used. First, the approximate solution, denoted by $\breve{U}_\Delta^{n+1}$, $\breve{V}_\Delta^{n+1}$, and $\breve{\phi}_\Delta^{n+1}$, that satisfies the equations

$$\breve{U}_\Delta^{n+1} + \left(\frac{\Delta t}{2R^2}\right)(cD_\lambda \breve{\phi}_\Delta^{n+1} + d\cos\tilde{\theta} D_\theta \breve{\phi}_\Delta^{n+1}) = R_u^{n+1} \tag{5.51}$$

$$\breve{V}_\Delta^{n+1} + \left(\frac{\Delta t}{2R^2}\right)(-dD_\lambda \breve{\phi}_\Delta^{n+1} + c\cos\tilde{\theta} D_\theta \breve{\phi}_\Delta^{n+1}) = R_v^{n+1} \tag{5.52}$$

$$\cos\tilde{\theta}\breve{\zeta}_\Delta^{n+1} + \left(\frac{\Delta t}{2}\right)\left[\left(\frac{1}{\cos\tilde{\theta}}\right)D_\lambda \breve{U}_\Delta^{n+1} + D_\theta \breve{V}_\Delta^{n+1}\right] = R_\phi^{n+1} \tag{5.53}$$

at $\{\hat{\tau}_{\lambda_i}, \tau_{\theta_j}\}_{i=1,j=1}^{N_\lambda,N_\theta}$, $\{\tau_{\lambda_i}, \hat{\tau}_{\theta_j}\}_{i=1,j=0}^{N_\lambda,N_\theta}$ and $\{\tau_{\lambda_i}, \tau_{\theta_j}\}_{i=1,j=1}^{N_\lambda,N_\theta}$, respectively, is determined. The right sides are defined to be

$$R_u^{n+1} = a\tilde{U}_\Delta^n + b\tilde{V}_\Delta^n - \left(\frac{\Delta t}{2R^2}\right)(cD_\lambda \tilde{\phi}_\Delta^n + d\cos\tilde{\theta} D_\theta \tilde{\phi}_\Delta^n) - \Delta t \tilde{\delta}_u^{n+\frac{1}{2}} \tag{5.54}$$

$$R_v^{n+1} = -b\tilde{U}_\Delta^n + a\tilde{V}_\Delta^n - \left(\frac{\Delta t}{2R^2}\right)(-dD_\lambda \tilde{\phi}_\Delta^n + c\cos\tilde{\theta} D_\theta \tilde{\phi}_\Delta^n) - \Delta t \tilde{\delta}_v^{n+\frac{1}{2}} \tag{5.55}$$

$$R_\phi^{n+1} = \cos\tilde{\theta}\tilde{\zeta}_\Delta^n - \left(\frac{\Delta t}{2}\right)\left[\left(\frac{1}{\cos\tilde{\theta}}\right)D_\lambda \tilde{U}_\Delta^n + D_\theta \tilde{V}_\Delta^n\right] \tag{5.56}$$

The approximate functions are assumed to be periodic in the longitudinal dimension, and subject to the following boundary conditions in the latitudinal dimension:

$$\breve{U}_\Delta^{n+1}(\hat{\tau}_{\lambda_i}, \pm\tfrac{\pi}{2}) = 0, \qquad \breve{V}_\Delta^{n+1}(\tau_{\lambda_i}, \pm\tfrac{\pi}{2}) = 0,$$
$$D_\theta\breve{\phi}_\Delta^{n+1}(\tau_{\lambda_i}, \pm\tfrac{\pi}{2}) = 0, \quad D_\theta\breve{\zeta}_\Delta^{n+1}(\tau_{\lambda_i}, \pm\tfrac{\pi}{2}) = 0$$

for $i = 1, \cdots, N_\lambda$. These low-order solutions are then used to approximate the residual terms to fourth-order. To this end, we define $\varepsilon_u'^{n+1}$, $\varepsilon_v'^{n+1}$ and $\varepsilon_\phi'^{n+1}$ at the associated collocation points as

$$\varepsilon_u'^{n+1}(\hat{\tau}_{\lambda_i}, \tau_{\theta_j}) = -\left(\frac{\Delta t}{2R^2}\right)\left[\frac{\Delta\lambda^2}{12}c(\tau_{\theta_j})\left(\Lambda_\lambda'(D_\lambda\breve{\phi}_\Delta^{n+1} + D_\lambda\tilde{\phi}_\Delta^n)\right)(\hat{\tau}_{\lambda_i}, \tau_{\theta_j})\right.$$

$$-\frac{\Delta\theta^2}{24}d(\tau_{\theta_j})\cos\tilde{\tau}_\theta\left(\Lambda'_\theta(D_\theta\breve{\phi}_\Delta^{n+1}+D_\theta\tilde{\phi}_\Delta^n)\right)(\hat{\tau}_{\lambda_i},\tau_{\theta_j})\Big] \quad (5.57)$$

for $i = 1,\cdots,N_\lambda,\ j = 1,\cdots,N_\theta$

$$\varepsilon_v'^{n+1}(\tau_{\lambda_i},\hat{\tau}_{\theta_j}) = -\left(\frac{\Delta t}{2R^2}\right)\Big[-\frac{\Delta\lambda^2}{24}d(\hat{\tau}_{\theta_j})\left(\Lambda'_\lambda(-D_\lambda\breve{\phi}_\Delta^{n+1}-D_\lambda\tilde{\phi}_\Delta^n)\right)(\tau_{\lambda_i},\hat{\tau}_{\theta_j})$$
$$+\frac{\Delta\theta^2}{12}c(\hat{\tau}_{\theta_j})\cos\tilde{\hat{\tau}}_\theta\left(\hat{\Lambda}'_\theta(D_\theta\breve{\phi}_\Delta^{n+1}+D_\theta\tilde{\phi}_\Delta^n)\right)(\tau_{\lambda_i},\hat{\tau}_{\theta_j})\Big] \quad (5.58)$$

for $i = 1,\cdots,N_\lambda,\ j = 1,\cdots,N_\theta-1$

$$\varepsilon_v'^{n+1}(\tau_{\lambda_i},\hat{\tau}_{\theta_j}) = -\left(\frac{\Delta t}{2R^2}\right)\Big[-\frac{\Delta\lambda^2}{24}d(\hat{\tau}_{\theta_j})\left(\Lambda'_\lambda(-D_\lambda\breve{\phi}_\Delta^{n+1}-D_\lambda\tilde{\phi}_\Delta^n)\right)(\tau_{\lambda_i},\hat{\tau}_{\theta_j})$$
$$-\frac{\Delta\theta^2}{24}c(\hat{\tau}_{\theta_j})\cos\tilde{\hat{\tau}}_\theta\left(\hat{\Lambda}'_\theta(D_\theta\breve{\phi}_\Delta^{n+1}+D_\theta\tilde{\phi}_\Delta^n)\right)(\tau_{\lambda_i},\hat{\tau}_{\theta_j})\Big] \quad (5.59)$$

for $i = 1,\cdots,N_\lambda,\ j = 0, N_\theta$

$$\varepsilon_\phi'^{n+1}(\tau_{\lambda_i},\tau_{\theta_j}) = -\left(\frac{\Delta t}{2}\right)\Big[\frac{\Delta\lambda^2}{12}\frac{1}{\cos\tilde{\tau}_{\theta_j}}\left(\Lambda'_\lambda(D_\lambda\breve{U}_\Delta^{n+1}+D_\lambda\tilde{U}_\Delta^n)\right)(\tau_{\lambda_i},\tau_{\theta_j})$$
$$+\frac{\Delta\theta^2}{12}\left(\Lambda'_\theta(D_\theta\breve{V}_\Delta^{n+1}+D_\theta\tilde{V}_\Delta^n)\right)(\tau_{\lambda_i},\tau_{\theta_j})\Big] \quad (5.60)$$

for $i = 1,\cdots,N_\lambda,\ j = 1,\cdots,N_\theta$

Similarly, the boundary residuals can also be estimated to fourth-order accuracy using the second-order solution. To this end, we define

$$\gamma_\phi^{n+1}(\tau_{\lambda_i},\tau_{\theta_q}) = -\frac{\Delta\theta^2}{24}\left[5\Lambda_\theta D_\theta\breve{\phi}_\Delta^{n+1}(\tau_{\lambda_i},\tau_{\theta_l})-3\Lambda_\theta D_\theta\breve{\phi}_\Delta^{n+1}(\tau_{\lambda_i},\tau_{\theta_m})\right] \quad (5.61)$$
$$\gamma_\zeta^{n+1}(\tau_{\lambda_i},\tau_{\theta_q}) = -\frac{\Delta\theta^2}{24}\left[5\Lambda_\theta D_\theta\breve{\zeta}_\Delta^{n+1}(\tau_{\lambda_i},\tau_{\theta_l})-3\Lambda_\theta D_\theta\breve{\zeta}_\Delta^{n+1}(\tau_{\lambda_i},\tau_{\theta_m})\right] \quad (5.62)$$

where $(q,l,m) = (0,2,3)$ or $(N_\theta+1, N_\theta-1, N_\theta-2)$, and $i = 1,\cdots,N_\lambda$.

The terms $\varepsilon_u'^{n+1}$, $\varepsilon_v'^{n+1}$, and $\varepsilon_\phi'^{n+1}$ are added to the right sides of (5.51) to (5.53), and the equations (5.63) to (5.65) are solved:

$$U_\Delta^{n+1}+\left(\frac{\Delta t}{2R^2}\right)(cD_\lambda\phi_\Delta^{n+1}+d\cos\tilde{\theta}D_\theta\phi_\Delta^{n+1}) = R_u^{n+1}+\varepsilon_u'^{n+1} \quad (5.63)$$
$$V_\Delta^{n+1}+\left(\frac{\Delta t}{2R^2}\right)(-dD_\lambda\phi_\Delta^{n+1}+c\cos\tilde{\theta}D_\theta\phi_\Delta^{n+1}) = R_v^{n+1}+\varepsilon_v'^{n+1} \quad (5.64)$$
$$\cos\tilde{\theta}\zeta_\Delta^{n+1}+\left(\frac{\Delta t}{2}\right)\left[\left(\frac{1}{\cos\tilde{\theta}}\right)D_\lambda U_\Delta^{n+1}+D_\theta V_\Delta^{n+1}\right] = R_\phi^{n+1}+\varepsilon_\phi'^{n+1} \quad (5.65)$$

at $\{\hat{\tau}_{\lambda_i}, \tau_{\theta_j}\}_{i=1,j=1}^{N_\lambda,N_\theta}$, $\{\tau_{\lambda_i}, \hat{\tau}_{\theta_j}\}_{i=1,j=0}^{N_\lambda,N_\theta}$ and $\{\tau_{\lambda_i}, \tau_{\theta_j}\}_{i=1,j=1}^{N_\lambda,N_\theta}$, respectively, with periodic conditions in the longitudinal dimension and the following boundary conditions in the θ-dimension:

$$\begin{array}{ll} U_\Delta^{n+1}(\hat{\tau}_{\lambda_i}, \pm\frac{\pi}{2}) = 0, & V_\Delta^{n+1}(\tau_{\lambda_i}, \pm\frac{\pi}{2}) = 0, \\ D_\theta \phi_\Delta^{n+1}(\tau_{\lambda_i}, \pm\frac{\pi}{2}) = \gamma_\phi^{n+1}(\tau_{\lambda_i}, \pm\frac{\pi}{2}), & D_\theta \zeta_\Delta^{n+1}(\tau_{\lambda_i}, \pm\frac{\pi}{2}) = \gamma_\zeta^{n+1}(\tau_{\lambda_i}, \pm\frac{\pi}{2}) \end{array}$$

for $i = 1, \cdots, N_\lambda$, to yield solution that is, as in the case of one-step OQSC, locally fourth-order at gridpoints and midpoints and globally third-order.

5.3 Existence and Uniqueness

In this section, we show that the biquadratic spline collocation approximation for a simplified version of the linearized Helmholtz equation (3.33) exists and is unique. As in Section 4.3, the analysis is done on the linearized shallow water equations with constant coefficients, (2.12) to (2.14), subject to biperiodic boundary conditions.

5.3.1 The Unstaggered Case

We first demonstrate the existence of a unique solution for the two-step OQSC method for the simplified shallow water equations (2.12) to (2.14) on an unstaggered grid. The linearized Helmholtz equation (3.33), derived by first discretizing the shallow water equations, and then eliminating the divergence terms from the discretized continuity equation corresponding to (2.14), takes the form

$$K\mathbf{\Phi}^{n+1} = R_H \tag{5.66}$$

where R_H is known. The linear operator K satisfies

$$K \equiv (P \otimes Q) - \left(\frac{\Delta t}{2R}\right)^2 \Phi^* \left[\frac{c}{\cos\Theta^*}(P_\lambda \otimes Q)(P \otimes Q)^{-1}(P_\lambda \otimes Q)\right.$$
$$+ d(P_\lambda \otimes Q)(P \otimes Q)^{-1}(P \otimes Q_\theta) - d(P \otimes Q_\theta)(P \otimes Q)^{-1}(P_\lambda \otimes Q)$$

$$+ c\cos\Theta^*(P\otimes Q_\theta)(P\otimes Q)^{-1}(P\otimes Q_\theta)\big] \tag{5.67}$$

which is the same as the operator in (4.2). Again, we prove the existence of a unique solution for (5.66) by showing that all eigenvalues of K are positive. The matrices in (5.67) are defined in Appendix A. An important property of these matrices is that P and P_λ share the same eigenvectors, as do Q and Q_θ. The eigenvalues associated with the k-th eigenvector of P and P_λ are

$$p_k = 1-\frac{1}{2}\sin^2\left(\frac{k\Delta\lambda}{2}\right), \qquad p_{\lambda_k} = \imath\frac{2}{\Delta\lambda}\sin\left(\frac{k\Delta\lambda}{2}\right)\cos\left(\frac{k\Delta\lambda}{2}\right)$$

for $k=0,\cdots,N_\lambda-1$, where $\imath\equiv\sqrt{-1}$. The derivation can be found in Appendix A. The eigenvalues associated with the l-th eigenvector of Q and Q_θ are

$$q_l = 1-\frac{1}{2}\sin^2\left(\frac{l\Delta\theta}{2}\right), \qquad q_{\theta_l} = \imath\frac{2}{\Delta\theta}\sin\left(\frac{l\Delta\theta}{2}\right)\cos\left(\frac{l\Delta\theta}{2}\right)$$

for $l=0,\cdots,N_\theta-1$.

With biperiodic boundary conditions, the second and third terms inside the square brackets in (5.67) cancel out. Therefore, the eigenvalues of K, denoted by $\sigma_{k,l}$, can be expressed in terms of the eigenvalues of P, P_λ, Q and Q_θ as follows:

$$\begin{aligned}
\sigma_{k,l} &= p_k q_l - \left(\frac{\Delta t}{2R}\right)^2\Phi^* c\left[\frac{1}{\cos\Theta^*}\frac{p_{\lambda_k}^2 q_l}{p_k} + \cos\Theta^*\frac{p_k q_{\theta_l}^2}{q_l}\right]\\
&= \left[1-\frac{1}{2}\sin^2\left(\frac{k\Delta\lambda}{2}\right)\right]\left[1-\frac{1}{2}\sin^2\left(\frac{l\Delta\theta}{2}\right)\right]\\
&\quad -\left(\frac{\Delta t}{2R}\right)^2\Phi^* c\left[\frac{1}{\cos\Theta^*\Delta\lambda^2}\frac{\left(\imath 2\sin\left(\frac{k\Delta\lambda}{2}\right)\cos\left(\frac{k\Delta\lambda}{2}\right)\right)^2\left[1-\frac{1}{2}\sin^2\left(\frac{l\Delta\theta}{2}\right)\right]}{1-\frac{1}{2}\sin^2\left(\frac{k\Delta\lambda}{2}\right)}\right.\\
&\qquad\left.+\frac{\cos\Theta^*}{\Delta\theta^2}\frac{\left(\imath 2\sin\left(\frac{l\Delta\theta}{2}\right)\cos\left(\frac{l\Delta\theta}{2}\right)\right)^2\left[1-\frac{1}{2}\sin^2\left(\frac{k\Delta\lambda}{2}\right)\right]}{1-\frac{1}{2}\sin^2\left(\frac{l\Delta\theta}{2}\right)}\right]
\end{aligned} \tag{5.68}$$

If we let

$$\alpha_k = \sin^2\left(\frac{k\Delta\lambda}{2}\right), \quad \alpha_l' = \sin^2\left(\frac{l\Delta\theta}{2}\right)$$

then the above relation can be rewritten as

$$\sigma_{k,l} = \left(1-\frac{\alpha_k}{2}\right)\left(1-\frac{\alpha_l'}{2}\right)$$

$$+\left(\frac{\Delta t}{R}\right)^2 \Phi^* c \left[\frac{1}{\cos\Theta^*\Delta\lambda^2}\frac{\alpha_k(1-\alpha_k)\left(1-\frac{\alpha_l'}{2}\right)}{1-\frac{\alpha_k}{2}} + \frac{\cos\Theta^*}{\Delta\theta^2}\frac{\alpha_l'(1-\alpha_l')\left(1-\frac{\alpha_k}{2}\right)}{1-\frac{\alpha_l'}{2}}\right] \tag{5.69}$$

Note that for all values of k and l,

$$0 \le \alpha_k,\ \alpha_l' \le 1 \Rightarrow \frac{1}{2} \le 1-\frac{\alpha_k}{2} \le 1 \quad \text{and} \quad \frac{1}{2} \le 1-\frac{\alpha_l'}{2} \le 1$$

Since $\Phi^* > 0$, $c > 0$ and $\cos\Theta^* > 0$ for $\Theta^* \in (-\pi/2, \pi/2)$, we conclude that $\sigma_{k,l} \ge \frac{1}{4}$, whence K^{-1} exists. Consequently, a unique solution exists for the discrete Helmholtz equation (5.66).

If the Helmholtz equation is derived analytically, the second derivatives matrices $P_{\lambda\lambda}$ and $Q_{\theta\theta}$ appear in the Helmholtz operator K^H, defined in (4.4). The eigenvalues associated with the k-th and l-th eigenvectors of $P_{\lambda\lambda}$ and $Q_{\theta\theta}$ are

$$p_{\lambda\lambda k} = -\frac{4}{\Delta\lambda^2}\sin^2\left(\frac{k\Delta\lambda}{2}\right), \qquad q_{\theta\theta l} = -\frac{4}{\Delta\theta^2}\sin^2\left(\frac{l\Delta\theta}{2}\right)$$

respectively. The eigenvalues $\sigma^H_{k,l}$ of K^H satisfy

$$\begin{aligned}\sigma^H_{k,l} &= p_k q_l - \left(\frac{\Delta t}{2R}\right)^2 \Phi^* c\left[\frac{1}{\cos\Theta^*}p_{\lambda\lambda k}q_l + \cos\Theta^* p_k q_{\theta\theta l}\right] \\ &= \left(1-\frac{\alpha_k}{2}\right)\left(1-\frac{\alpha_l'}{2}\right) + \left(\frac{\Delta t}{R}\right)^2 \Phi^* c\left[\frac{1}{\cos\Theta^*\Delta\lambda^2}\alpha_k\left(1-\frac{\alpha_l'}{2}\right) + \frac{\cos\Theta^*}{\Delta\theta^2}\left(1-\frac{\alpha_k}{2}\right)\alpha_l'\right]\end{aligned} \tag{5.70}$$

Following similar reasoning as for $\sigma_{k,l}$, it can be shown that $\sigma^H_{k,l} \ge \frac{1}{4}$. Moreover, since $\Phi^* > 0$, $c > 0$, $(1-\alpha_k)/(1-\frac{\alpha_k}{2}) \le 1$ and $(1-\alpha_l')/(1-\frac{\alpha_l'}{2}) \le 1$, we have $\sigma_{k,l} \le \sigma^H_{k,l}$. However, as will be shown in Chapter 7, this alternative approach is not recommended as it tends to damp the Rossby waves.

For the one-step method, we define the following perturbed operators:

$$P_\lambda' = \left(I - \frac{\Delta\lambda^2}{24}\Lambda_\lambda'\right)P_\lambda \qquad Q_\theta' = \left(I - \frac{\Delta\theta^2}{24}\Lambda_\theta'\right)Q_\theta$$

where Λ'_θ is redefined to be similar to Λ'_λ because of the biperiodic boundary conditions. The operator K becomes

$$\begin{aligned} K' \equiv (P\otimes Q) - \left(\frac{\Delta t}{2R}\right)^2 \Phi^* \Big[& \frac{c}{\cos\Theta^*}(P'_\lambda \otimes Q)(P\otimes Q)^{-1}(P'_\lambda\otimes Q) \\ & + d(P'_\lambda\otimes Q)(P\otimes Q)^{-1}(P\otimes Q'_\theta) \\ & - d(P\otimes Q'_\theta)(P\otimes Q)^{-1}(P'_\lambda\otimes Q) \\ & + c\cos\Theta^*(P\otimes Q'_\theta)(P\otimes Q)^{-1}(P\otimes Q'_\theta)\Big] \end{aligned} \tag{5.71}$$

Again, with biperiodic boundary conditions, the second and third terms inside the square brackets of in the above expression cancel out. The matrix P'_λ shares the same eigenvectors as P, with the eigenvalue associated with the k-th eigenvector for P'_λ being

$$p'_{\lambda_k} = \imath\frac{2}{\Delta\lambda}\sin\left(\frac{k\Delta\lambda}{2}\right)\cos\left(\frac{k\Delta\lambda}{2}\right)\left[1+\frac{1}{6}\sin^2\left(\frac{k\Delta\lambda}{2}\right)\right]$$

respectively. Similarly, the eigenvalue associated with the l-th eigenvector of Q'_θ is

$$q'_{\theta_l} = \imath\frac{2}{\Delta\theta}\sin\left(\frac{l\Delta\theta}{2}\right)\cos\left(\frac{l\Delta\theta}{2}\right)\left[1+\frac{1}{6}\sin^2\left(\frac{l\Delta\theta}{2}\right)\right]$$

respectively. Expressed in terms of the above eigenvalues, the eigenvalues for K' take the following form:

$$\begin{aligned} \sigma'_{k,l} &= p_k q_l - \left(\frac{\Delta t}{2R}\right)^2 \Phi^* c\left[\frac{1}{\cos\Theta^*} p_{\lambda_k}'^2 q_l + \cos\Theta^* p_k q_{\theta_l}'^2\right] \\ &= \left(1-\frac{\alpha_k}{2}\right)\left(1-\frac{\alpha'_l}{2}\right) \\ &\quad + \left(\frac{\Delta t}{R}\right)^2 \Phi^* c\left[\frac{1}{\cos\Theta^*\Delta\lambda^2}\frac{\alpha_k(1-\alpha_k)\left(1+\frac{\alpha_k}{6}\right)^2\left(1-\frac{\alpha'_l}{2}\right)}{1-\frac{\alpha_k}{2}}\right. \\ &\qquad \left. + \frac{\cos\Theta^*}{\Delta\theta^2}\frac{\alpha'_l(1-\alpha'_l)\left(1+\frac{\alpha'_l}{6}\right)^2\left(1-\frac{\alpha_k}{2}\right)}{1-\frac{\alpha'_l}{2}}\right] \end{aligned} \tag{5.72}$$

Following the same logic as we did for the two-step method, we conclude that $\sigma'_{k,l} \geq \frac{1}{4}$, and consequently that K'^{-1} exists.

5.3.2 The C-grid

When the shallow water equations are discretized on the C-grid, the linear operator K appearing in (5.66) satisfies

$$\begin{aligned} K \equiv (P \otimes Q) - \left(\frac{\Delta t}{2R}\right)^2 \Phi^* \Big[& \frac{c}{\cos\Theta^*}(P_\lambda^{\hat\Delta\to\Delta} \otimes Q)(P \otimes Q)^{-1}(P_\lambda^{\Delta\to\hat\Delta} \otimes Q) \\ & + d(P_\lambda^{\hat\Delta\to\Delta} \otimes Q)(P \otimes Q)^{-1}(P^{\Delta\to\hat\Delta} \otimes Q_\theta) \\ & - d(P \otimes Q_\theta^{\hat\Delta\to\Delta})(P \otimes Q)^{-1}(P_\lambda \otimes Q^{\Delta\to\hat\Delta}) \\ & + c\cos\Theta^*(P \otimes Q_\theta^{\hat\Delta\to\Delta})(P \otimes Q)^{-1}(P \otimes Q_\theta^{\Delta\to\hat\Delta})\Big] \end{aligned} \tag{5.73}$$

involves the staggering operators $P^{\Delta\to\hat\Delta}$, $P_\lambda^{\Delta\to\hat\Delta}$ etc.

The staggering operators $P^{\Delta\to\hat\Delta}$ and $P_\lambda^{\Delta\to\hat\Delta}$ share the same eigenvectors as P and P_λ, as do $P^{\hat\Delta\to\Delta}$ and $P_\lambda^{\hat\Delta\to\Delta}$. The eigenvalues associated with the k-th eigenvectors of $P^{\Delta\to\hat\Delta}$ and $P^{\hat\Delta\to\Delta}$ are $e^{\imath k\frac{\Delta\lambda}{2}} p_k^{\rightarrow}$ and $e^{-\imath k\frac{\Delta\lambda}{2}} p_k^{\rightarrow}$, respectively, where

$$p_k^{\rightarrow} = \cos\left(\frac{k\Delta\lambda}{2}\right)$$

Similarly, the eigenvalues associated with the k-th eigenvectors of $P_\lambda^{\Delta\to\hat\Delta}$ and $P_\lambda^{\hat\Delta\to\Delta}$ are $e^{\imath k\frac{\Delta\lambda}{2}} p_{\lambda_k}^{\rightarrow}$ and $e^{-\imath k\frac{\Delta\lambda}{2}} p_{\lambda_k}^{\rightarrow}$, respectively, where

$$p_{\lambda_k}^{\rightarrow} = \imath\frac{2}{\Delta\lambda}\sin\left(\frac{k\Delta\lambda}{2}\right)$$

In the latitudinal dimension, $Q^{\Delta\to\hat\Delta}$ and $Q_\theta^{\Delta\to\hat\Delta}$ share the same eigenvectors as Q and Q_θ, as do $Q^{\hat\Delta\to\Delta}$ and $Q_\theta^{\hat\Delta\to\Delta}$. The eigenvalues associated with the l-th eigenvectors of $Q^{\Delta\to\hat\Delta}$ and $Q^{\hat\Delta\to\Delta}$ are $e^{\imath l\frac{\Delta\theta}{2}} q_l^{\rightarrow}$ and $e^{-\imath l\frac{\Delta\theta}{2}} q_l^{\rightarrow}$, respectively, where

$$q_l^{\rightarrow} = \cos\left(\frac{l\Delta\theta}{2}\right)$$

Similarly, the eigenvalues associated with the l-eigenvectors of $Q_\theta^{\Delta\to\hat\Delta}$ and $Q_\theta^{\hat\Delta\to\Delta}$ are $e^{\imath l\frac{\Delta\theta}{2}} q_{\theta_l}^{\rightarrow}$ and $e^{-\imath l\frac{\Delta\theta}{2}} q_{\theta_l}^{\rightarrow}$, respectively, where

$$q_{\theta_l}^{\rightarrow} = \imath\frac{2}{\Delta\theta}\sin\left(\frac{l\Delta\theta}{2}\right)$$

The derivation of the above expressions can be found in Appendix A. The eigenvalues of K are

$$\begin{aligned}
\sigma_{k,l} &= p_k q_l - \left(\frac{\Delta t}{2R}\right)^2 \Phi^* \left\{ c \left[\frac{1}{\cos\Theta^*} \frac{\overrightarrow{p_{\lambda_k}}^2 q_l}{p_k} + \cos\Theta^* \frac{p_k \overrightarrow{q_{\theta_l}}^2}{q_l} \right] \right. \\
&\qquad \left. + d \left[\frac{\overrightarrow{p_k}\,\overrightarrow{p_{\lambda_k}}\, q_{\theta_l}}{p_k} - \frac{p_{\lambda_k} \overrightarrow{q_l}\,\overrightarrow{q_{\theta_l}}}{q_l} \right] \right\} &(5.74)\\
&= \left(1 - \frac{\alpha_k}{2}\right)\left(1 - \frac{\alpha_l'}{2}\right) \\
&\quad + \left(\frac{\Delta t}{2R}\right)^2 \Phi^* \left\{ c \left[\frac{1}{\cos\Theta^*} \frac{\frac{4}{\Delta\lambda^2}\alpha_k \left(1 - \frac{\alpha_l'}{2}\right)}{\left(1 - \frac{\alpha_k}{2}\right)} + \cos\Theta^* \frac{\left(1 - \frac{\alpha_k}{2}\right)\frac{4}{\Delta\theta^2}\alpha_l'}{\left(1 - \frac{\alpha_l'}{2}\right)} \right] \right. \\
&\qquad + d \left[\frac{\cos\left(\frac{k\Delta\lambda}{2}\right)\frac{2}{\Delta\lambda}\sin\left(\frac{k\Delta\lambda}{2}\right)\frac{2}{\Delta\theta}\sin\left(\frac{l\Delta\theta}{2}\right)\cos\left(\frac{l\Delta\theta}{2}\right)}{\left(1 - \frac{\alpha_k}{2}\right)} \right. \\
&\qquad \left.\left. - \frac{\frac{2}{\Delta\lambda}\sin\left(\frac{k\Delta\lambda}{2}\right)\cos\left(\frac{k\Delta\lambda}{2}\right)\cos\left(\frac{l\Delta\theta}{2}\right)\frac{2}{\Delta\theta}\sin\left(\frac{l\Delta\theta}{2}\right)}{\left(1 - \frac{\alpha_l'}{2}\right)} \right] \right\} &(5.75)\\
&= \left(1 - \frac{\alpha_k}{2}\right)\left(1 - \frac{\alpha_l'}{2}\right) \\
&\quad + \left(\frac{\Delta t}{2R}\right)^2 \Phi^* \left\{ 4c \left[\frac{1}{\cos\Theta^* \Delta\lambda^2} \frac{\alpha_k \left(1 - \frac{\alpha_l'}{2}\right)}{\left(1 - \frac{\alpha_k}{2}\right)} + \frac{\cos\Theta^*}{\Delta\theta^2} \frac{\left(1 - \frac{\alpha_k}{2}\right)\alpha_l'}{\left(1 - \frac{\alpha_l'}{2}\right)} \right] \right. \\
&\qquad \left. + \frac{d\sin(k\Delta\lambda)\sin(l\Delta\theta)}{\Delta\lambda\Delta\theta} \left[\frac{1}{1 - \frac{\alpha_k}{2}} - \frac{1}{1 - \frac{\alpha_l'}{2}} \right] \right\} &(5.76)\\
&= \left(1 - \frac{\alpha_k}{2}\right)\left(1 - \frac{\alpha_l'}{2}\right) + A_1 + A_2 &(5.77)
\end{aligned}$$

where

$$\begin{aligned}
A_1 &\equiv \left(\frac{\Delta t}{2R}\right)^2 \frac{\Phi^*}{1 - \frac{\alpha_k}{2}} \left[\frac{4c}{\cos\Theta^*\Delta\lambda^2}\alpha_k \left(1 - \frac{\alpha_l'}{2}\right) + \frac{d\sin(k\Delta\lambda)\sin(l\Delta\theta)}{\Delta\lambda\Delta\theta} \right] &(5.78)\\
A_2 &\equiv \left(\frac{\Delta t}{2R}\right)^2 \frac{\Phi^*}{1 - \frac{\alpha_l'}{2}} \left[\frac{4c\cos\Theta^*}{\Delta\theta^2} \left(1 - \frac{\alpha_k}{2}\right)\alpha_l' - \frac{d\sin(k\Delta\lambda)\sin(l\Delta\theta)}{\Delta\lambda\Delta\theta} \right] &(5.79)
\end{aligned}$$

We study the behaviour of $\sigma_{k,l}$ for typical parameter values. Since $0 \le \alpha_k,\ \alpha_l' \le 1$, the first term in (5.77), $(1 - \frac{\alpha_k}{2})(1 - \frac{\alpha_l'}{2})$, is always greater than or equal to $\frac{1}{4}$. Therefore, $\sigma_{k,l}$ is positive if $A_1,\ A_2 > -\frac{1}{8}$. Assume that $\Delta t = \Delta\lambda = \Delta\theta \equiv h$. We first consider A_1. Note that the first term inside the square brackets of (5.78) is always non-negative.

Since $d = \frac{\Delta t \tilde{f}}{2} c$, the second term is much smaller than the first for sufficiently large α_k and sufficiently small h. When $\alpha_k \approx 0$, the first term approaches zero. Nonetheless, at $\alpha_k = 0$,

$$\sin^2\left(\frac{k\Delta\lambda}{2}\right) = 0 \Rightarrow k\Delta\lambda = 0 \text{ or } 2\pi \Rightarrow \sin(k\Delta\lambda) = 0$$

so the second term also vanishes. Hence, $A_1 = 0$. Also, for small positive k's, we have $\alpha_k = \sin^2(k\Delta\lambda/2) \approx (kh/2)^2$. Substituting this approximation into the expression for A_1, and letting $d = \frac{h\tilde{f}}{2} c$ yields

$$A_1 = \left(\frac{h}{2R}\right)^2 \frac{\Phi^* c}{1 - \frac{1}{2}\left(\frac{kh}{2}\right)^2} \left\{ \frac{4}{\cos\Theta^* h^2} \left(\frac{kh}{2}\right)^2 \left[1 - \frac{1}{2}\sin^2\left(\frac{l\Delta\theta}{2}\right)\right] + \left(\frac{h\tilde{f}}{2}\right) \frac{k}{h} \sin(l\Delta\theta) \right\}$$

Since $\cos\Theta^* > 0$, the first term in the curly brackets is always positive, and since $\sin(l\Delta\theta) \geq -1$, we have

$$A_1 \geq -\left(\frac{h}{2R}\right)^2 \frac{\Phi^* c}{1 - \frac{1}{2}\left(\frac{kh}{2}\right)^2} \left[\left(\frac{\tilde{f}}{2}\right) k\right]$$

Since $\tilde{f} \ll 1$, $h \ll 1$, $R \gg \Phi^*$ and $c \approx 1$, we have $A_1 = \mathcal{O}(h^2)$. Hence, when $\alpha_k \approx (kh/2)^2$ for a small positive integer k, $A_1 > -\frac{1}{8}$ for all sufficiently small h.

Similar reasoning may be applied to A_2 to show that $A_2 > -\frac{1}{8}$ for small $l \geq 0$ and all sufficiently small h. Hence $\sigma_{k,l} > 0$ in the cases that we have considered. Unfortunately, as in Section 4.3.2, this does not cover all possible cases, so we have not actually proved $\sigma_{k,l} > 0$ for all k and l. However, our numerical results in Section 6 indicate that (5.66) has a unique solution when the simplified problem (2.12) to (2.14) is discretized on the C-grid.

Chapter 6

Numerical Results

Since no analytical solution is known for the general form of the two dimensional shallow water equations (2.9) to (2.11), we introduce into the equations forcing terms constructed in such a way that an analytical solution is known a priori. Our modified shallow water equations are

$$\frac{dU}{dt} - fV + \frac{\phi_\lambda}{R^2} = F_u \tag{6.1}$$

$$\frac{dV}{dt} + fU + \frac{\cos\theta}{R^2}\phi_\theta + \frac{\sin\theta}{\cos^2\theta}\frac{U^2+V^2}{R^2} = F_v \tag{6.2}$$

$$\cos\theta\frac{d}{dt}\log\phi + \left[\frac{U_\lambda}{\cos\theta} + V_\theta\right] = F_\phi \tag{6.3}$$

where F_u, F_v and F_ϕ are known functions of λ, θ and t, defined to yield the following solution to equations (6.1) to (6.3):

$$\begin{aligned}
\phi(\lambda,\theta,t) &= \phi_0 \left\{\exp\left[-a_1(\lambda-\lambda_0)^2 - a_1(\theta-\theta_0)^2\right]\right. \\
&\quad \left. - \log_e\left(1+\frac{t}{T_0}\right)\exp\left[-a_2(\lambda-\lambda_0)^2 - a_2(\theta-\theta_0)^2\right]\right\} && (6.4) \\
U(\lambda,\theta,t) &= \frac{u_0}{R}\left[1-\exp\left(-\frac{t}{T_0}\right)\right]\cos\theta \times \\
&\quad \left\{\exp\left[-a_3(\lambda-\lambda_0-d_0)^2 - a_3(\theta-\theta_0)^2\right]\right. \\
&\quad \left. - \exp\left[-a_3(\lambda-\lambda_0+d_0)^2 - a_3(\theta-\theta_0)^2\right]\right\} && (6.5) \\
V(\lambda,\theta,t) &= \frac{v_0}{R}\left[1-\exp\left(-\frac{t}{T_0}\right)\right]\cos\theta \times
\end{aligned}$$

$$\Big\{\exp\left[-a_3(\lambda-\lambda_0)^2 - a_3(\theta-\theta_0-d_0)^2\right]$$
$$-\exp\left[-a_3(\lambda-\lambda_0)^2 - a_3(\theta-\theta_0+d_0)^2\right]\Big\} \tag{6.6}$$

These functions are designed to resemble the true solutions of the original shallow water equations (2.9) to (2.11). In our experiments, we chose the following values for the constants

$$\begin{array}{lll} \phi_0 = 50\ g, & u_0 = v_0 = 3/2, & T_0 = 12000\ \text{s}, \\ a_1 = 10, & a_2 = 60, & a_3 = 25, \\ \lambda_0 = \pi, & \theta_0 = 0, & d_0 = \pi/10 \end{array}$$

where $g = 9.80616\ \text{ms}^{-2}$ is the gravitational constant.

The system was integrated on the sphere $\{(\lambda, \theta) \in [0, 2\pi] \times [-\pi/2, \pi/2]\}$, with timesteps of 60 seconds (i.e. $\Delta t = 60$ s). The solution for ϕ was computed at $T = 16\frac{2}{3}$ hours and compared to the reference solution (6.4), illustrated in Figure 6.1.

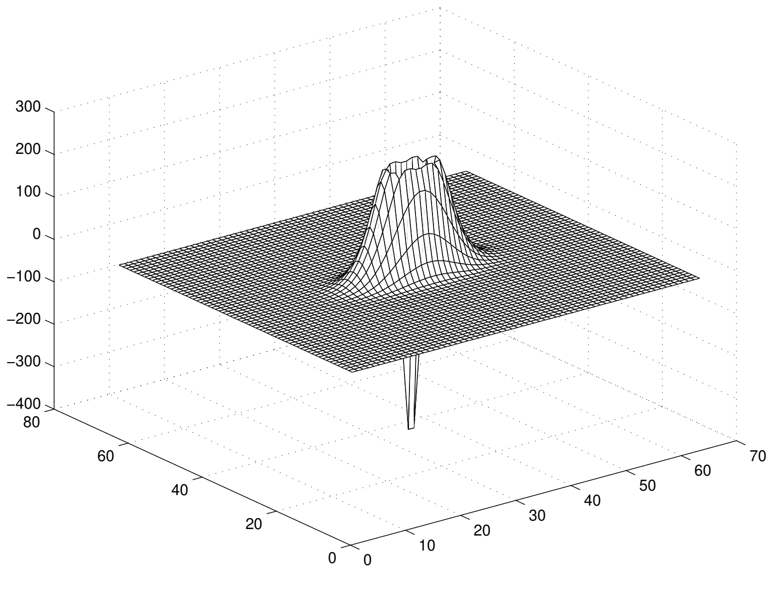

Figure 6.1: Reference solution for the pressure field ϕ at $t = 16\frac{2}{3}$ hours.

We solved the system using the linear Galerkin (LSG) method, the QSG method, the standard QSC method, and the one-step and two-step OQSC methods with grid sizes

32×32, 64×64, 128×128 and 256×256. The Arakawa C-grid was used in our discretization. The convergence results are shown in Tables 6.1 to 6.3 and Figure 6.2, where N is the number of subintervals in one dimension. The error is computed as the 2-norm of the difference between the numerical solution and the reference solution at gridpoints, divided by the 2-norm of the reference solution at gridpoints. The errors reflect the local truncation error of each method, which, in our experiments, is found to be roughly second-order for LSG and QSC, and roughly fourth-order for QSG and OQSC, as expected. We estimate the convergence order of the errors by

$$p = -\frac{\log\left(\frac{e_1}{e_2}\right)}{\log\left(\frac{N_1}{N_2}\right)}$$

where e_1 and e_2 are errors corresponding to grid sizes N_1 and N_2, respectively. The computed values for p are listed in the columns labelled "order p" in Tables 6.1 to 6.3.

N	QSG				LSG			
	error	order p	flops	order k	error	order p	flops	order k
32	1.836e-1	N/A	3.952e11	N/A	2.485e-1	N/A	4.947e10	N/A
64	1.868e-2	3.297	1.506e12	1.930	1.351e-1	1.840	1.892e11	1.935
128	1.471e-3	3.667	5.745e12	1.932	7.474e-2	1.807	7.263e11	1.941
256	1.068e-4	3.783	2.171e13	1.918	3.849e-2	1.942	2.765e12	1.929

Table 6.1: The convergence results and computational costs for QSG and LSG with different grid sizes.

We measured the number of floating-point operations (flops) for the five spatial discretization methods using MATLAB; the results are shown in Tables 6.1 to 6.3. We estimate the order with which the number of flops increases by

$$k = -\frac{\log\left(\frac{f_1}{f_2}\right)}{\log\left(\frac{N_1}{N_2}\right)}$$

N	one-step OQSC				two-step OQSC			
	error	order p	flops	order k	error	order p	flops	order k
32	1.468e-1	N/A	3.719e11	N/A	1.651e-1	N/A	3.234e11	N/A
64	1.625e-2	3.175	1.418e12	1.931	1.359e-2	3.603	1.250e12	1.951
128	1.138e-3	3.836	5.402e12	1.930	1.003e-3	3.760	4.821e12	1.947
256	8.637e-5	3.720	2.049e13	1.923	7.217e-5	3.797	1.842e13	1.934

Table 6.2: The convergence results and computational costs for one-step and two-step OQSC with different grid sizes.

N	standard QSC			
	error	order p	flops	order k
32	2.103e-1	N/A	1.988e11	N/A
64	1.197e-1	1.761	7.627e11	1.939
128	6.338e-2	1.888	2.913e12	1.933
256	3.284e-2	1.930	1.107e13	1.927

Table 6.3: The convergence results and computational costs for standard QSC with different grid sizes.

where f_1 and f_2 are the number of flops corresponding to grid sizes N_1 and N_2, respectively. The computed values for k are listed in the columns labelled "order k" in Tables 6.1 to 6.3. The conjugate gradient (CG) iterative method was used to solve the linear Helmholtz equation (3.33), and the matrices are stored in sparse format. Thus, the computational cost per CG iteration should increase by a factor of four when N, the number of subintervals in one dimension, is doubled. Therefore, if the number of CG iterations were to stay about the same as N increases, the total work in the method should increase by about a factor of four. In our experiments, however, the flop counts showed sub-quadratic increase, as slightly fewer CG iterations were required as N increased. This, we believe, is caused by a small decrease in the condition number of the

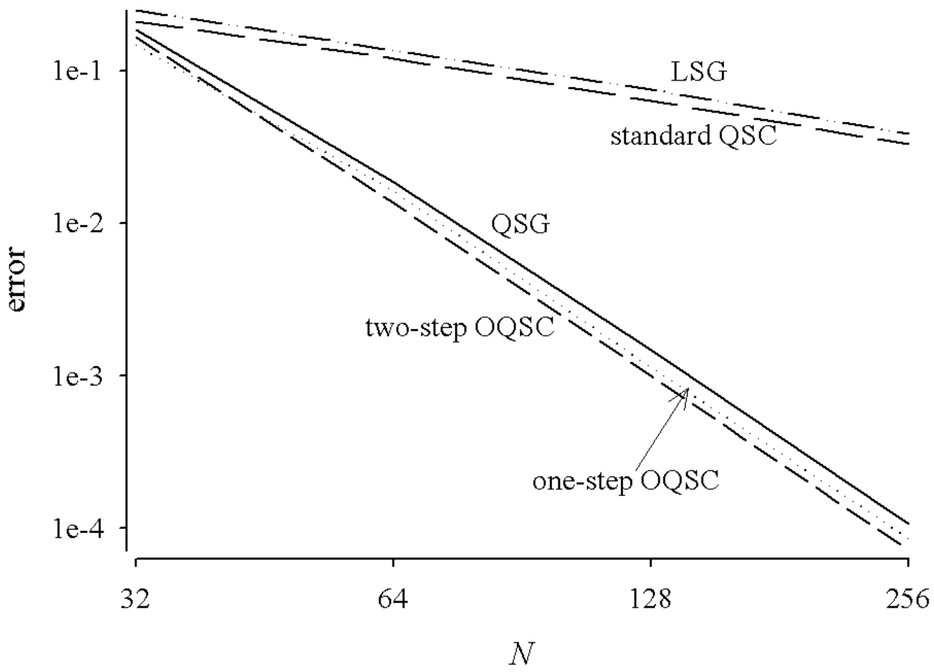

Figure 6.2: A log-log scale plot of the errors versus N (the number of sub-intervals in each dimension) for different methods.

matrix associated with the linear Helmholtz equation when the grid size increases. A detailed analysis of the behaviour of the eigenvalues of the system is beyond the scope of this thesis. The QSG method is more expensive than the OQSC methods because the former involves computing inner products using quadrature rules, an expense not required by the collocation methods.

Figure 6.3 compares the efficiencies of the methods. Although the fourth-order methods require more work than the second-order methods for a given grid size, they are more efficient for large systems ($N > 50$ in our problem). This is because the cost for all methods considered increases at about the same rate, but the accuracy for the fourth-order methods increases much more rapidly than for the second-order methods. Among the fourth-order methods, the two-step OQSC method is the most efficient for our problem.

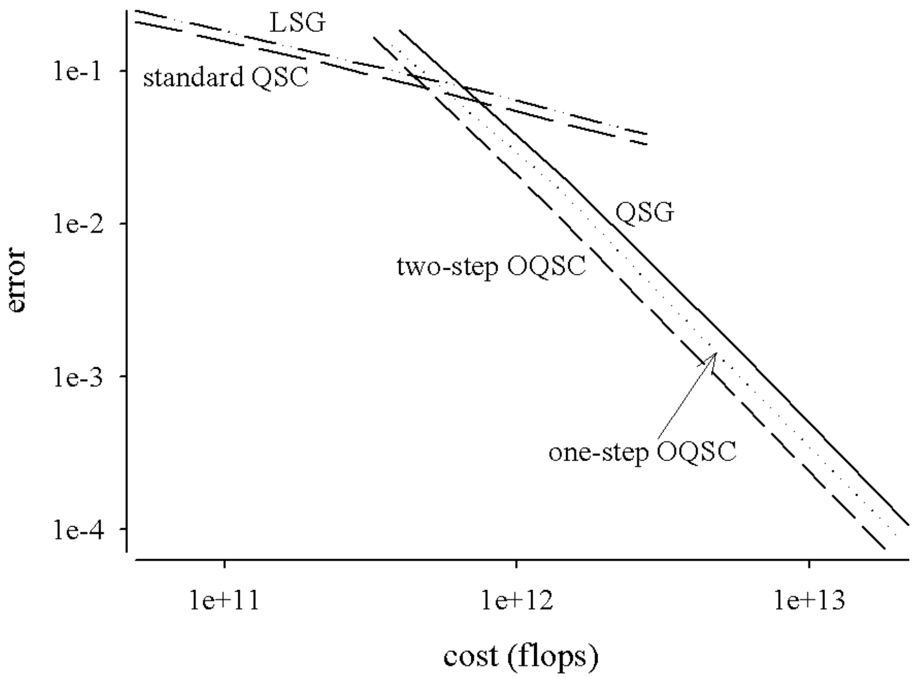

Figure 6.3: A log-log scale plot of the errors versus computational costs, measured as the total number of flops, for different methods.

Chapter 7

Rossby Wave Stability

7.1 Linear Stability Analysis

In this section, we perform a stability analysis for the quadratic spline Galerkin and collocation methods applied to the simplified shallow water equations (2.12) to (2.14). We examine the conditions under which the discretized solutions are stable. We assume, for simplicity, an unstaggered grid and biperiodic boundary conditions. Staniforth and Mitchell [30] showed that if Cartesian coordinates are used, $f = 0$ is assumed and biperiodic boundary conditions are applied, then the Helmholtz equation should be derived algebraically rather than analytically in order for the standard spatial discretization methods to be neutrally stable for the Rossby waves. We extend their study and demonstrate similar results in spherical coordinates with a Coriolis parameter f that is not necessarily zero.

7.1.1 The Continuous Case

We first examine the continuous problem. Assume that the solution to (2.12) to (2.14) is of the form

$$\begin{pmatrix} u(\lambda,\theta,t) \\ v(\lambda,\theta,t) \\ \phi(\lambda,\theta,t) \end{pmatrix} = \begin{pmatrix} u_0 \\ v_0 \\ \phi_0 \end{pmatrix} e^{\imath(k\lambda+l\theta+\omega t)} \tag{7.1}$$

where k and l are the longitudinal and latitudinal wave numbers, respectively, and ω denotes the *wave frequency.* The *Lagrangian frequency* ν is defined by

$$\nu \equiv \frac{u^*}{R\cos\Theta^*} + \frac{v^*}{R} + \omega \tag{7.2}$$

To compute the Lagrangian frequency of the true solution, (7.1) is substituted into the simplified shallow water equations (2.12) to (2.14). This results in a 3×3 system of equations for u_0, v_0 and ϕ_0. Then, by setting the determinant of the system to zero and applying (7.2), an expression for the Lagrangian frequency ν can be obtained. This expression can then be solved to yield the solutions

$$\nu = 0, \pm\sqrt{\Phi^*\left[\left(\frac{k}{R\cos\Theta^*}\right)^2 + \left(\frac{l}{R}\right)^2\right] + f^{*2}} \tag{7.3}$$

The first solution, $\nu = 0$ or $\omega = -u^*/(R\cos\Theta^*) - v^*/R$, corresponds to the solution of interest — the Rossby waves. The other two frequencies are associated with the gravity waves.

7.1.2 Algebraic Derivation of the Helmholtz Equation

We now solve the simplified shallow water equations (2.12) to (2.14) using the two-level semi-Lagrangian semi-implicit time integration method with a finite-element spatial discretization scheme. We analyze the stability of the solution when the Helmholtz equation is derived algebraically; in other words, we compare (7.3) to the Lagrangian frequency of the discretized solution when the divergence terms are eliminated *after* spatial discretization. We assume that the longitudinal mass matrix P and the first derivative matrix P_λ associated with the finite-element scheme have common eigenvectors $\vartheta_k = \{e^{\imath kj\Delta\lambda}\}_{j=0}^{N_\lambda-1}$ for $k = 0, \cdots, N_\lambda - 1$. Let the associated eigenvalues be p_k and $p_{\lambda k}$, respectively. Thus we have

$$P\vartheta_k = p_k\vartheta_k, \quad P_\lambda\vartheta_k = p_{\lambda k}\vartheta_k \tag{7.4}$$

Similarly, we assume that both the latitudinal mass matrix Q and the first derivative matrix Q_θ have common eigenvectors denoted by $\vartheta'_l = \{e^{\imath lj\Delta\theta}\}_{j=0}^{N_\theta-1}$ for $l = 0, \cdots, N_\theta - 1$, with the associated eigenvalues denoted by q_l and $q_{\theta l}$, respectively. Thus we have

$$Q\vartheta'_l = q_l\vartheta'_l, \quad Q_\theta\vartheta'_l = q_{\theta l}\vartheta'_l \tag{7.5}$$

The discretized solution at time-level t_{n+1} is assumed to be of the following wave form:

$$\begin{pmatrix} u_\Delta^{n+1}(\lambda,\theta) \\ v_\Delta^{n+1}(\lambda,\theta) \\ \phi_\Delta^{n+1}(\lambda,\theta) \end{pmatrix} = \begin{pmatrix} u_0 \\ v_0 \\ \phi_0 \end{pmatrix} e^{\imath(k\lambda+l\theta+\omega(n+1)\Delta t)} \tag{7.6}$$

QSG, QSC and One-Step OQSC Methods

The mass and first derivative matrices arising from the quadratic spline Galerkin (QSG), the quadratic spline collocation (QSC), and the optimal quadratic spline collocation (OQSC) methods with biperiodic boundary conditions satisfy relations (7.4) and (7.5), with the eigenvalues for each method as indicated in Appendix A. In this subsection, we study the stability of the Rossby solutions obtained with the QSG, the QSC and the one-step OQSC methods. Analysis for the two-step OQSC method follows in the next subsection.

For an arbitrary function $\psi(\lambda,\theta,t)$, let $\tilde{\psi}^n(\lambda,\theta) \equiv \psi(\lambda - u^*\Delta t/(R\cos\Theta^*), \theta - v^*\Delta t/R, t_n)$. Discretizing the simplified shallow water equations (2.12) to (2.14) in time using the semi-

Lagrangian semi-implicit (SLSI) method yields

$$\frac{u^{n+1}-\tilde{u}^n}{\Delta t} - f^*\left(\frac{v^{n+1}+\tilde{v}^n}{2}\right) + \frac{1}{R\cos\Theta^*}\left(\frac{\phi_\lambda^{n+1}+\tilde{\phi}_\lambda^n}{2}\right) = 0 \tag{7.7}$$

$$\frac{v^{n+1}-\tilde{v}^n}{\Delta t} + f^*\left(\frac{u^{n+1}+\tilde{u}^n}{2}\right) + \frac{1}{R}\left(\frac{\phi_\theta^{n+1}+\tilde{\phi}_\theta^n}{2}\right) = 0 \tag{7.8}$$

$$\frac{\phi^{n+1}-\tilde{\phi}^n}{\Delta t} + \frac{\Phi^*}{R\cos\Theta^*}\left(\frac{u_\lambda^{n+1}+\tilde{u}_\lambda^n}{2}\right) + \frac{\Phi^*}{R}\left(\frac{v_\theta^{n+1}+\tilde{v}_\theta^n}{2}\right) = 0 \tag{7.9}$$

Following the notation introduced in Chapter 3, the spatially discretized form of equation (7.7) is

$$\begin{aligned}(P\otimes Q)\left(\frac{\mathsf{U}^{n+1}-\tilde{\mathsf{U}}^n}{\Delta t}\right) - f^*(P\otimes Q)\left(\frac{\mathsf{V}^{n+1}+\tilde{\mathsf{V}}^n}{2}\right)&\\ + \frac{1}{R\cos\Theta^*}(P_\lambda\otimes Q)\left(\frac{\mathbf{\Phi}^{n+1}+\tilde{\mathbf{\Phi}}^n}{2}\right) &= 0\end{aligned} \tag{7.10}$$

In order to facilitate the eigenvalue analysis, we rewrite equation (7.10) in terms of the target solution u_Δ, v_Δ and ϕ_Δ, instead of the spline coefficients U^{n+1}, V^{n+1} and Φ^{n+1}, since the target solution is assumed to be of the wave form (7.6):

$$\begin{aligned}(P\otimes Q)(E_\lambda\otimes E_\theta)^{-1}\left(\frac{\boldsymbol{u}_\Delta^{n+1}-\tilde{\boldsymbol{u}}_\Delta^n}{\Delta t}\right) - f^*(P\otimes Q)(E_\lambda\otimes E_\theta)^{-1}\left(\frac{\boldsymbol{v}_\Delta^{n+1}+\tilde{\boldsymbol{v}}_\Delta^n}{2}\right)&\\ + \frac{1}{R\cos\Theta^*}(P_\lambda\otimes Q)(E_\lambda\otimes E_\theta)^{-1}\left(\frac{\boldsymbol{\phi}_\Delta^{n+1}+\tilde{\boldsymbol{\phi}}_\Delta^n}{2}\right) &= 0\end{aligned} \tag{7.11}$$

With biperiodic boundary conditions, all matrices in parentheses in (7.11) commute. By pre-multiplying (7.11) through by $(E_\lambda\otimes E_\theta)$ and simplifying we obtain

$$\begin{aligned}(P\otimes Q)\left(\frac{\boldsymbol{u}_\Delta^{n+1}-\tilde{\boldsymbol{u}}_\Delta^n}{\Delta t}\right) - f^*(P\otimes Q)\left(\frac{\boldsymbol{v}_\Delta^{n+1}+\tilde{\boldsymbol{v}}_\Delta^n}{2}\right)&\\ + \frac{1}{R\cos\Theta^*}(P_\lambda\otimes Q)\left(\frac{\boldsymbol{\phi}_\Delta^{n+1}+\tilde{\boldsymbol{\phi}}_\Delta^n}{2}\right) &= 0\end{aligned} \tag{7.12}$$

Following a similar procedure, we obtain the following discretized form of (7.8) and (7.9):

$$(P\otimes Q)\left(\frac{\boldsymbol{v}_\Delta^{n+1}-\tilde{\boldsymbol{v}}_\Delta^n}{\Delta t}\right) + f^*(P\otimes Q)\left(\frac{\boldsymbol{u}_\Delta^{n+1}+\tilde{\boldsymbol{u}}_\Delta^n}{2}\right)$$

$$+\frac{1}{R}(P\otimes Q_\theta)\left(\frac{\boldsymbol{\phi}_\Delta^{n+1}+\tilde{\boldsymbol{\phi}}_\Delta^n}{2}\right)=0 \qquad (7.13)$$

$$(P\otimes Q)\left(\frac{\boldsymbol{\phi}_\Delta^{n+1}-\tilde{\boldsymbol{\phi}}_\Delta^n}{\Delta t}\right)+\frac{\Phi^*}{R\cos\Theta^*}(P_\lambda\otimes Q)\left(\frac{\boldsymbol{u}_\Delta^{n+1}+\tilde{\boldsymbol{u}}_\Delta^n}{2}\right)$$
$$+\frac{\Phi^*}{R}(P\otimes Q_\theta)\left(\frac{\boldsymbol{v}_\Delta^{n+1}+\tilde{\boldsymbol{v}}_\Delta^n}{2}\right)=0 \qquad (7.14)$$

When the discrete solution (7.6) is evaluated at the midpoints of the partitions, the resulting set of values equals a scalar multiple of an eigenvector of the discretized operators. To illustrate this, let $\vartheta_{k,l}\equiv\vartheta_k\otimes\vartheta_l'=\left(e^{\imath(ki\Delta\lambda+lj\Delta\theta)}\right)_{i=0,j=0}^{N_\lambda-1,N_\theta-1}$, for $k=0,\cdots,N_\lambda-1$ and $l=0,\cdots,N_\theta-1$, be an eigenvector of the discretized operators. When evaluated at midpoints, the geopotential solution ϕ_Δ^{n+1} takes the form

$$\phi_\Delta^{n+1}\left((i+\frac{1}{2})\Delta\lambda,(j+\frac{1}{2})\Delta\theta\right)=\phi_0e^{\imath\left[k(i+\frac{1}{2})\Delta\lambda+l(j+\frac{1}{2})\Delta\theta+\omega(n+1)\Delta t\right]}$$
$$=\phi_0e^{\imath(k\frac{\Delta\lambda}{2}+l\frac{\Delta\theta}{2}+\omega(n+1)\Delta t)}(\vartheta_{k,l})_{i,j}$$

for $i=0,\cdots,N_\lambda-1$ and $j=0,\cdots,N_\theta-1$. Thus, if we let
$\boldsymbol{\phi}_{\boldsymbol{\Delta}}^{\boldsymbol{n+1}}=\phi_\Delta^{n+1}\left((i+\frac{1}{2})\Delta\lambda,(j+\frac{1}{2})\Delta\theta\right)_{i=0,j=0}^{N_\lambda-1,N_\theta-1}$ and
$\tilde{\boldsymbol{\phi}}_{\boldsymbol{\Delta}}^{\boldsymbol{n}}=\phi_\Delta^n\left((i+\frac{1}{2})\Delta\lambda-\frac{u^*\Delta t}{R\cos\Theta^*},(j+\frac{1}{2})\Delta\theta-\frac{v^*\Delta t}{R}\right)_{i=0,j=0}^{N_\lambda-1,N_\theta-1}$, then
$\boldsymbol{\phi}_{\boldsymbol{\Delta}}^{\boldsymbol{n+1}}=\phi_0e^{\imath(k\frac{\Delta\lambda}{2}+l\frac{\Delta\theta}{2}+\omega(n+1)\Delta t)}\boldsymbol{\vartheta}_{k,l}$ and $\tilde{\boldsymbol{\phi}}_{\boldsymbol{\Delta}}^{\boldsymbol{n}}=\phi_0e^{\imath(k\frac{\Delta\lambda}{2}-\frac{u^*\Delta t}{R\cos\Theta^*},+l\frac{\Delta\theta}{2}-\frac{v^*\Delta t}{R}+\omega n\Delta t)}\boldsymbol{\vartheta}_{k,l}$. Similarly, $\boldsymbol{u}_\Delta^{n+1}$, $\tilde{\boldsymbol{u}}_\Delta^n$, $\boldsymbol{v}_\Delta^{n+1}$ and $\tilde{\boldsymbol{v}}_\Delta^n$ are equal to scalar multiples of an eigenvector of the discrete operators. These eigenvectors are then substituted into equations (7.12) to (7.14). Note also that

$$\begin{aligned}\boldsymbol{\phi}_{\boldsymbol{\Delta}}^{\boldsymbol{n+1}} &= \phi_0e^{\imath(k\frac{\Delta\lambda}{2}+l\frac{\Delta\theta}{2}+\omega(n+1)\Delta t)}\boldsymbol{\vartheta}_{k,l}\\ &= e^{\imath\left(\frac{u^*}{R\cos\Theta^*}+\frac{v^*}{R}+\omega\right)\Delta t}\phi_0e^{\imath\left[\left(k\frac{\Delta\lambda}{2}-\frac{u^*\Delta t}{R\cos\Theta^*}\right)+\left(l\frac{\Delta\theta}{2}-\frac{v^*\Delta t}{R}\right)+\omega n\Delta t\right]}\boldsymbol{\vartheta}_{k,l}\\ &= e^{\imath\nu\Delta t}\tilde{\boldsymbol{\phi}}_{\boldsymbol{\Delta}}^{\boldsymbol{n}}\end{aligned}$$

and that similar relations hold for $\boldsymbol{u}_\Delta^{n+1}$ and $\boldsymbol{v}_\Delta^{n+1}$. Using relations (7.4) and (7.5), we obtain

$$pq\left(\frac{e^{\imath\nu\Delta t}-1}{\Delta t}\right)u_0-f^*pq\left(\frac{e^{\imath\nu\Delta t}+1}{2}\right)v_0+\frac{p_\lambda q}{R\cos\Theta^*}\left(\frac{e^{\imath\nu\Delta t}+1}{2}\right)\phi_0=0 \qquad (7.15)$$

$$pq\left(\frac{e^{\imath\nu\Delta t}-1}{\Delta t}\right)v_0+f^*pq\left(\frac{e^{\imath\nu\Delta t}+1}{2}\right)u_0+\frac{pq_\theta}{R}\left(\frac{e^{\imath\nu\Delta t}+1}{2}\right)\phi_0=0 \quad (7.16)$$
$$pq\left(\frac{e^{\imath\nu\Delta t}-1}{\Delta t}\right)\phi_0+\Phi^*\left[\frac{p_\lambda q}{R\cos\Theta^*}\left(\frac{e^{\imath\nu\Delta t}+1}{2}\right)u_0+\frac{pq_\theta}{R}\left(\frac{e^{\imath\nu\Delta t}+1}{2}\right)v_0\right]=0 \quad (7.17)$$

To simplify notation, we have dropped the subscripts k and l in the eigenvalues p_k, $p_{\lambda k}$, q_l and $q_{\theta l}$. The above equations hold for $k=0,\cdots,N_\lambda-1$ and $l=0,\cdots,N_\theta-1$.

Equations (7.15) to (7.17) form a 3×3 system for u_0, v_0 and ϕ_0. By setting the determinant of the resulting system to zero to find a nontrivial solution to (7.15) to (7.17), an equation for $e^{\imath\nu\Delta t}$ can be obtained. The roots are found to be

$$e^{\imath\nu\Delta t}=1,\ \frac{4A-B\pm\imath4\sqrt{AB}}{4A+B} \quad (7.18)$$

where

$$\begin{aligned} A &= (pqR\cos\Theta^*)^2 \\ B &= (\Delta t f^* R\cos\Theta^* pq)^2-\Delta t^2\Phi^*(p_\lambda^2q^2+\cos^2\Theta^*p^2q_\theta^2) \end{aligned}$$

Since $e^{\imath\nu\Delta t}=1$, or $\nu=0$, is one of the solutions, the numerical scheme is neutrally stable for the Rossby waves. The solutions for the gravity waves are also bounded since

$$|e^{\imath\nu\Delta t}|=\left|\frac{4A-B\pm\imath4\sqrt{AB}}{4A+B}\right|=1$$

Therefore, the numerical scheme is also stable for the gravitational modes. The accuracy of the gravity waves will be considered in Chapter 8.

Two-Step OQSC Method

In the two-step OQSC method, a second-order intermediate solution is computed first, and is then used to perturb the equations appropriately. The perturbed equations are then solved to yield a locally fourth-order solution (see Section 5.2.2 for details). The mass and first derivative matrices for the two-step OQSC method are the same as those for the QSC method. In fact, the solution obtained from the first step of the two-step method, when the unperturbed equations are solved, *is* that of the QSC method. We denote this intermediate solution by

$$\begin{pmatrix} \breve{u}_\Delta^{n+1} \\ \breve{v}_\Delta^{n+1} \\ \breve{\phi}_\Delta^{n+1} \end{pmatrix} = \begin{pmatrix} u_0 \\ v_0 \\ \phi_0 \end{pmatrix} e^{\imath(k\lambda + l\theta + \breve{\omega}(n+1)\Delta t)} \tag{7.19}$$

The Lagrangian frequency $\breve{\nu}$ of the intermediate solution can be computed following the steps described in the previous section, and is given by (7.18), with the eigenvalues p, q, p_λ and q_θ given in Section A.2. In the second step, because of these perturbation terms, the associated 3×3 system for u_0, v_0 and ϕ_0 is different from that derived in the previous subsection. We assume that the solution of the second step satisfies (7.6). Note that the Lagrangian frequency $\breve{\nu}$ of the intermediate solution may be different from the Lagrangian frequency ν of the solution of the second step. Since the equations solved in the second step of the two-step collocation method are perturbed, the eigenvalue analysis for this method needs to be done differently. Using relations (5.6) and (5.7), and following procedures similar to those outlined in Section 5.2, we obtain the following discretized perturbed equations for the A-grid:

$$\begin{aligned} &(P \otimes Q)\left(\frac{\boldsymbol{u}_\Delta^{n+1} - \tilde{\boldsymbol{u}}_\Delta^n}{\Delta t}\right) - f^*(P \otimes Q)\left(\frac{\boldsymbol{v}_\Delta^{n+1} + \tilde{\boldsymbol{v}}_\Delta^n}{2}\right) + \frac{1}{R\cos\Theta^*}(P_\lambda \otimes Q)\left(\frac{\boldsymbol{\phi}_\Delta^{n+1} + \tilde{\boldsymbol{\phi}}_\Delta^n}{2}\right) \\ &\qquad = -\frac{1}{R\cos\Theta^*}\frac{\Delta\lambda^2}{24}(\Lambda_\lambda \otimes I)(P_\lambda \otimes Q)\left(\frac{\breve{\boldsymbol{\phi}}_\Delta^{n+1} + \tilde{\boldsymbol{\phi}}_\Delta^n}{2}\right) \end{aligned} \tag{7.20}$$

$$\begin{aligned} &(P \otimes Q)\left(\frac{\boldsymbol{v}_\Delta^{n+1} - \tilde{\boldsymbol{v}}_\Delta^n}{\Delta t}\right) + f^*(P \otimes Q)\left(\frac{\boldsymbol{u}_\Delta^{n+1} + \tilde{\boldsymbol{u}}_\Delta^n}{2}\right) + \frac{1}{R}(P \otimes Q_\theta)\left(\frac{\boldsymbol{\phi}_\Delta^{n+1} + \tilde{\boldsymbol{\phi}}_\Delta^n}{2}\right) \\ &\qquad = -\frac{1}{R}\frac{\Delta\theta^2}{24}(I \otimes \Lambda_\theta)(P \otimes Q_\theta)\left(\frac{\breve{\boldsymbol{\phi}}_\Delta^{n+1} + \tilde{\boldsymbol{\phi}}_\Delta^n}{2}\right) \end{aligned} \tag{7.21}$$

$$\begin{aligned} &(P \otimes Q)\left(\frac{\boldsymbol{\phi}_\Delta^{n+1} - \tilde{\boldsymbol{\phi}}_\Delta^n}{\Delta t}\right) + \frac{\Phi^*}{R\cos\Theta^*}(P_\lambda \otimes Q)\left(\frac{\boldsymbol{u}_\Delta^{n+1} + \tilde{\boldsymbol{u}}_\Delta^n}{2}\right) + \frac{\Phi^*}{R}(P \otimes Q_\theta)\left(\frac{\boldsymbol{v}_\Delta^{n+1} + \tilde{\boldsymbol{v}}_\Delta^n}{2}\right) \\ &\qquad = -\frac{\Phi^*}{R\cos\Theta^*}\frac{\Delta\lambda^2}{24}(\Lambda_\lambda \otimes I)(P_\lambda \otimes Q)\left(\frac{\breve{\boldsymbol{u}}_\Delta^{n+1} + \tilde{\boldsymbol{u}}_\Delta^n}{2}\right) \\ &\qquad\quad - \frac{\Phi^*}{R}\frac{\Delta\theta^2}{24}(I \otimes \Lambda_\theta)(P \otimes Q_\theta)\left(\frac{\breve{\boldsymbol{v}}_\Delta^{n+1} + \tilde{\boldsymbol{v}}_\Delta^n}{2}\right) \end{aligned} \tag{7.22}$$

For the two-step OQSC method, the centered difference operators Λ_λ and Λ_θ are the same as the stiffness matrices $P_{\lambda\lambda}$ and $Q_{\theta\theta}$, respectively, and thus they have the same eigenvalues $p_{\lambda\lambda}$ and $q_{\theta\theta}$, respectively, which can be found in Appendix A. Rewriting equations (7.20) to (7.22) in terms of the eigenvalues and simplifying, we obtain

$$\begin{aligned} pq\left(\frac{e^{\imath\nu\Delta t}-1}{\Delta t}\right)u_0 - f^* pq\left(\frac{e^{\imath\nu\Delta t}+1}{2}\right)v_0 + \frac{p_\lambda q}{R\cos\Theta^*}\left(\frac{e^{\imath\nu\Delta t}+1}{2}\right)\phi_0 & \\ = -\frac{1}{R\cos\Theta^*}\frac{\Delta\lambda^2}{24}p_{\lambda\lambda}p_\lambda q\left(\frac{e^{\imath\breve{\nu}\Delta t}+1}{2}\right)\phi_0 & \quad (7.23) \\ pq\left(\frac{e^{\imath\nu\Delta t}-1}{\Delta t}\right)v_0 + f^* pq\left(\frac{e^{\imath\nu\Delta t}+1}{2}\right)u_0 + \frac{pq_\theta}{R}\left(\frac{e^{\imath\nu\Delta t}+1}{2}\right)\phi_0 & \\ = -\frac{1}{R}\frac{\Delta\theta^2}{24}pq_{\theta\theta}q_\theta\left(\frac{e^{\imath\breve{\nu}\Delta t}+1}{2}\right)\phi_0 & \quad (7.24) \\ pq\left(\frac{e^{\imath\nu\Delta t}-1}{\Delta t}\right)\phi_0 + \Phi^*\left[\frac{p_\lambda q}{\cos\Theta^*}\left(\frac{e^{\imath\nu\Delta t}+1}{2}\right)u_0 + \frac{pq_\theta}{R}\left(\frac{e^{\imath\nu\Delta t}+1}{2}\right)v_0\right] & \\ = -\Phi^*\left[\frac{\Delta\lambda^2}{24}\frac{p_{\lambda\lambda}p_\lambda q}{R\cos\Theta^*}\left(\frac{e^{\imath\breve{\nu}\Delta t}+1}{2}\right)u_0 + \frac{\Delta\theta^2}{24}\frac{pq_{\theta\theta}q_\theta}{R}\left(\frac{e^{\imath\breve{\nu}\Delta t}+1}{2}\right)v_0\right] & \\ & \quad (7.25) \end{aligned}$$

By setting the determinant of the above system to zero, and solving for $e^{\imath\nu\Delta t}$, we find

$$e^{\imath\nu\Delta t} = 1,\ \frac{4A - B + C \pm \imath 2\sqrt{4A(B-C) - \Delta t^2\Phi^*(4+\Delta t^2 f^{*2})(\delta\lambda^2 + \cos\Theta^{*2}\delta\theta^2)A + D}}{4A+B} \quad (7.26)$$

where

$$\begin{aligned} A &= (R\cos\Theta^* pq)^2 \\ B &= (\Delta t f^* R\cos\Theta^* pq)^2 - \Delta t^2\Phi^*(p_\lambda^2 q^2 + \cos^2\Theta^* p^2 q_\theta^2) \\ C &= 2\Delta t^2\Phi^*(p_\lambda q\delta\lambda + \cos^2\Theta^* pq_\theta\delta\theta) \\ D &= \Delta t^4\Phi^{*2}\cos^2\Theta^*(pq_\theta\delta\lambda - p_\lambda q\delta\theta)^2 \\ \delta\lambda &= \frac{\Delta\lambda^2}{24}p_{\lambda\lambda}p_\lambda q\left(\frac{e^{\imath\breve{\nu}\Delta t}+1}{2}\right) \\ \delta\theta &= \frac{\Delta\theta^2}{24}pq_{\theta\theta}q_\theta\left(\frac{e^{\imath\breve{\nu}\Delta t}+1}{2}\right) \end{aligned}$$

Since $e^{\imath\nu\Delta t} = 1$, or $\nu = 0$, is one of the roots, the numerical solution for the two-step OQSC method is neutrally stable for the Rossby waves. We have also verified using

MAPLE that the gravity solutions are bounded.

7.1.3 Analytic Derivation of the Helmholtz Equation

A genuine Helmholtz equation may be derived by eliminating the wind velocity dependence from the continuity equation (2.14) *before* spatial discretization. The simplified shallow water equations (2.12) to (2.14) are first discretized in time to yield

$$\frac{u^{n+1}-\tilde{u}^n}{\Delta t} - f^*\left(\frac{v^{n+1}+\tilde{v}^n}{2}\right) + \frac{1}{R\cos\Theta^*}\left(\frac{\phi_\lambda^{n+1}+\tilde{\phi}_\lambda^n}{2}\right) = 0 \tag{7.27}$$

$$\frac{v^{n+1}-\tilde{v}^n}{\Delta t} + f^*\left(\frac{u^{n+1}+\tilde{u}^n}{2}\right) + \frac{1}{R}\left(\frac{\phi_\theta^{n+1}+\tilde{\phi}_\theta^n}{2}\right) = 0 \tag{7.28}$$

$$\frac{\phi^{n+1}-\tilde{\phi}^n}{\Delta t} + \Phi^*\left[\left(\frac{u_\lambda^{n+1}+\tilde{u}_\lambda^n}{2R\cos\Theta^*}\right) + \left(\frac{v_\theta^{n+1}+\tilde{v}_\theta^n}{2R}\right)\right] = 0 \tag{7.29}$$

We solve (7.27) and (7.28) for u^{n+1} and v^{n+1} in terms of ϕ_λ^{n+1} and ϕ_θ^{n+1} as we did in Section 2.6. Then taking the λ- and θ-derivatives of the resulting equations, we get

$$u_\lambda^{n+1} = a\tilde{u}_\lambda^n + b\tilde{v}_\lambda^n - \frac{\Delta t}{R}\left[c\left(\frac{\phi_{\lambda\lambda}^{n+1}+\tilde{\phi}_{\lambda\lambda}^n}{2\cos\Theta^*}\right) + d\left(\frac{\phi_{\theta\lambda}^{n+1}+\tilde{\phi}_{\theta\lambda}^n}{2}\right)\right] \tag{7.30}$$

$$v_\theta^{n+1} = -b\tilde{u}_\theta^n + a\tilde{v}_\theta^n - \frac{\Delta t}{R}\left[-d\left(\frac{\phi_{\lambda\theta}^{n+1}+\tilde{\phi}_{\lambda\theta}^n}{2\cos\Theta^*}\right) + c\left(\frac{\phi_{\theta\theta}^{n+1}+\tilde{\phi}_{\theta\theta}^n}{2}\right)\right] \tag{7.31}$$

where

$$a = \frac{1-\left(\frac{\Delta t f^*}{2}\right)^2}{1+\left(\frac{\Delta t f^*}{2}\right)^2}, \qquad b = \frac{\Delta t f^*}{1+\left(\frac{\Delta t f^*}{2}\right)^2}$$

$$c = \frac{1}{1+\left(\frac{\Delta t f^*}{2}\right)^2}, \qquad d = \frac{\frac{\Delta t f^*}{2}}{1+\left(\frac{\Delta t f^*}{2}\right)^2}$$

which can be considered as a special case of (2.61) with constant Coriolis parameter. Equations (7.30) and (7.31) can then be used to eliminate the unknown divergence terms from the continuity equation (7.29) to yield

$$\begin{aligned}(\phi^{n+1}-\tilde{\phi}^n) - \Phi^*\left(\frac{\Delta t}{2R}\right)^2 c\left[\left(\frac{\phi_{\lambda\lambda}^{n+1}+\tilde{\phi}_{\lambda\lambda}^n}{\cos^2\Theta^*}\right) + (\phi_{\theta\theta}^{n+1}+\tilde{\phi}_{\theta\theta}^n)\right] \\ + \Phi^*\left(\frac{\Delta t}{2R}\right)\left[\left(\frac{1+a}{\cos\Theta^*}\right)\tilde{u}_\lambda^n - b\tilde{u}_\theta^n + \frac{b}{\cos\Theta^*}\tilde{v}_\lambda^n + (1+a)\tilde{v}_\theta^n\right] = 0\end{aligned}$$

$$(7.32)$$

Recall that $P_{\lambda\lambda}$ and $Q_{\theta\theta}$ denote the stiffness matrices in the λ- and θ-directions, respectively, and $p_{\lambda\lambda_k}$ and $q_{\theta\theta_l}$ are the eigenvalues associated with their eigenvectors ϑ_k and ϑ'_l, respectively, as defined in Section 7.1.2. The spatially discretized form of equation (7.32) is

$$\begin{aligned}
&(P \otimes Q)(E_\lambda \otimes E_\theta)^{-1}(\boldsymbol{\phi}_\Delta^{n+1} - \tilde{\boldsymbol{\phi}}_\Delta^n) \\
&\quad - \Phi^* \left(\frac{\Delta t}{2R}\right)^2 c \left[\frac{1}{\cos^2\Theta^*}(P_{\lambda\lambda} \otimes Q) + (P \otimes Q_{\theta\theta})\right](E_\lambda \otimes E_\theta)^{-1}(\boldsymbol{\phi}_\Delta^{n+1} + \tilde{\boldsymbol{\phi}}_\Delta^n) \\
&\quad + \Phi^* \left(\frac{\Delta t}{2R}\right)\left\{\left[\frac{1+a}{\cos\Theta^*}(P_\lambda \otimes Q) - b(P \otimes Q_\theta)\right](E_\lambda \otimes E_\theta)^{-1}\tilde{\boldsymbol{u}}_\Delta^n\right. \\
&\qquad \left. + \left[\frac{b}{\cos\Theta^*}(P_\lambda \otimes Q) + (1+a)(P \otimes Q_\theta)\right](E_\lambda \otimes E_\theta)^{-1}\tilde{\boldsymbol{v}}_\Delta^n\right\} = 0
\end{aligned} \tag{7.33}$$

where we have written (7.33) in terms of the solution values $\boldsymbol{\phi}_{\boldsymbol{\Delta}}^{\boldsymbol{n+1}}$ rather than the spline coefficients $\boldsymbol{\Phi}^{n+1}$, as we did earlier in transforming equation (7.10) to (7.11). Recall that the matrices in parentheses commute given biperiodic boundary conditions. By pre-multiplying (7.33) by $(E_\lambda \otimes E_\theta)$ and simplifying, we obtain

$$\begin{aligned}
&(P \otimes Q)(\boldsymbol{\phi}_\Delta^{n+1} - \tilde{\boldsymbol{\phi}}_\Delta^n) - \Phi^* \left(\frac{\Delta t}{2R}\right)^2 c \left[\frac{1}{\cos^2\Theta^*}(P_{\lambda\lambda} \otimes Q) + (P \otimes Q_{\theta\theta})\right](\boldsymbol{\phi}_\Delta^{n+1} + \tilde{\boldsymbol{\phi}}_\Delta^n) \\
&\quad + \Phi^* \left(\frac{\Delta t}{2R}\right)\left\{\left[\frac{1+a}{\cos\Theta^*}(P_\lambda \otimes Q) - b(P \otimes Q_\theta)\right]\tilde{\boldsymbol{u}}_\Delta^n\right. \\
&\qquad \left. + \left[\frac{b}{\cos\Theta^*}(P_\lambda \otimes Q) + (1+a)(P \otimes Q_\theta)\right]\tilde{\boldsymbol{v}}_\Delta^n\right\} = 0
\end{aligned} \tag{7.34}$$

Substituting the solution (7.6) into the above equation, rewriting the resulting equation in terms of the eigenvalues and simplifying, we obtain

$$\begin{aligned}
&pq(e^{\imath\nu\Delta t} - 1)\phi_0 - \Phi^* \left(\frac{\Delta t}{2R}\right)^2 c \left[\frac{p_{\lambda\lambda}q}{\cos^2\Theta^*} + pq_{\theta\theta}\right](e^{\imath\nu\Delta t} + 1)\phi_0 \\
&\quad + \Phi^* \left(\frac{\Delta t}{2R}\right)\left\{\left[\left(\frac{1+a}{\cos\Theta^*}\right)p_\lambda q - bpq_\theta\right]u_0 + \left[\left(\frac{b}{\cos\Theta^*}\right)p_\lambda q + (1+a)pq_\theta\right]v_0\right\} = 0
\end{aligned} \tag{7.35}$$

By setting the determinant of equations (7.15), (7.16) and (7.35) to zero, an equation for $e^{\imath\nu\Delta t}$ is obtained. It is found that $e^{\imath\nu\Delta t} = 1$ is no longer a solution to this frequency equation, which implies that an undesirable phase shift has been introduced into the Rossby mode. Therefore, in our formulation, the Helmholtz equation is derived algebraically to preserve the neutral stability of the Rossby waves.

7.2 The Equatorial Rossby Wave

The equatorial solitary wave described by Boyd [4] is frequently used to test the stability of a numerical method for the shallow water equations with respect to Rossby waves. To use this test problem on our model, we transform Boyd's formulation, originally written in Cartesian coordinates, to spherical coordinates. We adopt Boyd's notation and let ϕ' be the geopotential perturbation; that is, if we denote the reference geopotential by the constant ϕ^*, then $\phi = \phi^* + \phi'$. The equations are nondimensionalized using the length and time scales

$$L = \frac{R}{E^{\frac{1}{4}}}, \qquad T = \frac{E^{\frac{1}{4}}}{2\Omega}$$

where $E = 4\Omega^2 R^2 / g\phi^*$ is the Lamb parameter. In our implementation, R is nondimensionalized by L, whereas the longitude λ and latitude θ are left unchanged; i.e., $0 \le \lambda \le 2\pi$ and $-\pi/2 \le \theta \le \pi/2$. The resulting nondimensional nonlinear shallow water equations on the equatorial β-plane[1] are

$$\frac{du}{dt} - R\theta v + \frac{\phi'_\lambda}{R\cos\theta} = 0 \qquad (7.36)$$

$$\frac{dv}{dt} + R\theta u + \frac{\phi'_\theta}{R} = 0 \qquad (7.37)$$

$$\frac{d}{dt}\log(1+\phi') + \frac{1}{R\cos\theta}[u_\lambda + (v\cos\theta)_\theta] = 0 \qquad (7.38)$$

[1]The β-plane approximation, valid for fluid motions restricted to a small range of latitudes, assumes that the Coriolis force varies linearly in the north-south direction [1]. For motions in close proximity to the equator, the Coriolis parameter is approximated by $R\theta$.

The above equations are integrated with the following initial conditions

$$\phi'(\lambda,\theta,0) = \eta(\lambda)\frac{3+6(R\theta)^2}{4}e^{(R\theta)^2/2} \quad (7.39)$$

$$u(\lambda,\theta,0) = \eta(\lambda)\frac{-9+6(R\theta)^2}{4}e^{(R\theta)^2/2} \quad (7.40)$$

$$v(\lambda,\theta,0) = \frac{2}{R\cos\theta}\frac{\partial\eta(\lambda)}{\partial\lambda}R\theta e^{(R\theta)^2/2} \quad (7.41)$$

where

$$\eta(\lambda) = A\mathrm{sech}^2(B\lambda)$$

$$A = 0.12$$

$$B = 0.394$$

In our study, a timestep of 0.05 non-dimensional units ($\Delta t = 0.05$, approximately two hours) is used. Experiments are conducted with grids of sizes $N = 32\times 32$, 64×64 and 128×128. Variables are staggered using the C-grid.

The equations describe an equatorial soliton which slowly propagates westward, with no change in shape. Figure 7.1 shows the result of a long simulation, using the two-step OQSC method on a 128×128 grid for 24 non-dimensional time units, approximately 41 days. Similar results were also obtained using the QSG and one-step OQSC methods. In our experiments, the height fields lost about 5% of their initial amplitude which traveled eastward as equatorial Kelvin waves. We believe this is because the initial conditions (7.39) to (7.41) are inexact, as suggested by Iskandarani et al. [21] and Ma [22]. The soliton propagated westward, as predicted, with little change in amplitude or phase, thereby confirming our analysis that spatial discretization with quadratic spline collocation is neutrally stable for the Rossby modes. The small amount of dispersion present can be explained as follows. With semi-Lagrangian integration, variables are needed at departures points, which are usually off-mesh points. Cubic Lagrange interpolation is used to estimate function values at departure points. Spatial interpolation causes damping and phase shift. Compared to linear or quadratic interpolation, the effects introduced by cubic interpolation are less severe. The finer the mesh, the less prominent the damping and dispersive effects should be [2, 24]. This is confirmed in our experiments (compare Figure 7.1 with Figure 7.2).

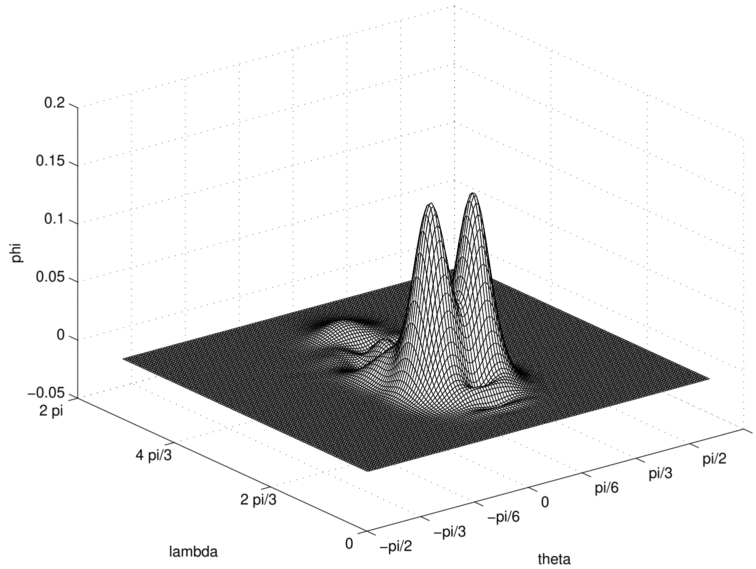

Figure 7.1: A simulation by the two-step OQSC method of a Rossby soliton traveling in the direction of decreasing λ values on a 128×128 grid for 24 time units (approximately 41 days).

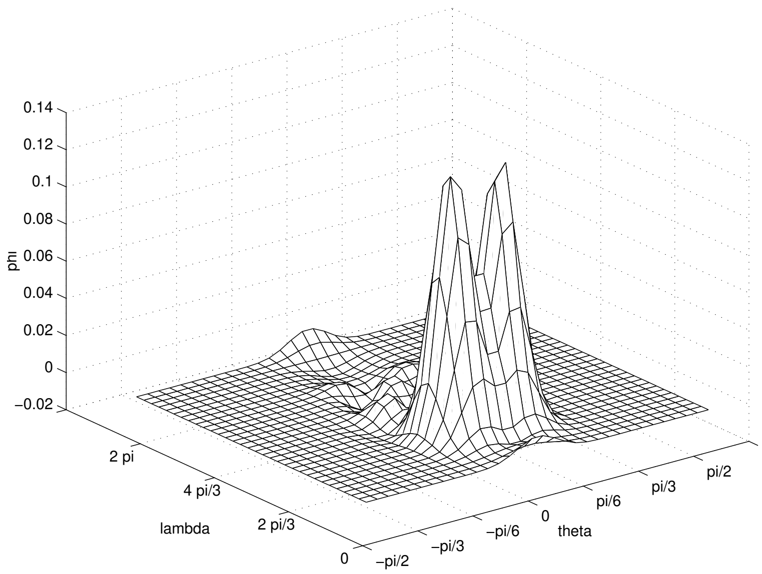

Figure 7.2: A simulation by the two-step OQSC method of a Rossby soliton traveling in the direction of decreasing λ values on a 32×32 grid for 24 time units. Substantial dispersion, caused by spatial interpolation, can be observed.

Chapter 8

Comparison of Staggering Schemes

In this section, we analyze the performance of three staggering schemes, namely the Arakawa A-grid, B-grid and C-grid, which are depicted in Figure 8.1. We concentrate on the group velocities of gravity waves, the accuracy of which is sensitive to the choice of discretization scheme. Our analysis of the simplified shallow water equations (2.12) to (2.14) with biperiodic boundary conditions shows that care must be taken in choosing an appropriate discretization scheme, otherwise energy associated with short gravity waves may propagate in the wrong direction. This conclusion is supported by numerical experiments involving equatorial Kelvin waves.

8.1 Linear Stability Analysis

A stability analysis is performed on the quadratic spline Galerkin and collocation methods applied to the simplified shallow water equations (2.12) to (2.14) with biperiodic boundary conditions. Our focus is on the group velocities of gravitational modes. Group velocity can be computed from wave frequency, as will be described in the next subsection.

Our analysis is done on a normalized system with $\Phi^* = 1$, $R = 1$, $\Theta^* = 0$ and $f^* = 0$, with the additional assumption that the mean wind speeds are zero; i.e. $u^* = v^* = 0$.

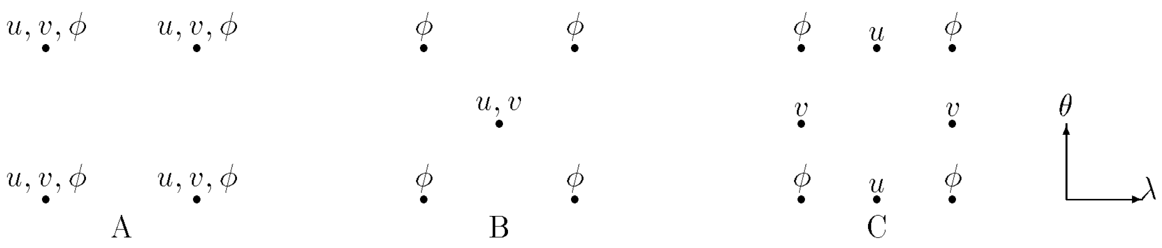

Figure 8.1: A schematic diagram of the Arakawa A-, B- and C-grids.

The discretized solutions are computed with $\Delta t = 0.1$, $\Delta\lambda = 0.25$ and $\Delta\theta = 0.25$.

8.1.1 The Continuous Case

The wave frequency of the gravity solution of the continuous problem can be derived from (7.2) and (7.3) as

$$\begin{aligned} \omega^{\pm} &= \nu - \frac{u^*}{R\cos\Theta^*} - \frac{v^*}{R} \\ &= -\frac{u^*}{R\cos\Theta^*} - \frac{v^*}{R} \pm \sqrt{\Phi^*\left[\left(\frac{k}{R\cos\Theta^*}\right)^2 + \left(\frac{l}{R}\right)^2\right] + f^{*2}} \end{aligned} \tag{8.1}$$

The group velocities of the gravity waves in the λ-dimension are given by

$$\begin{aligned} c_\lambda^{\pm} &\equiv \frac{d\omega^{\pm}}{dk} \\ &= \pm\frac{\Phi^*\frac{k}{(R\cos\Theta^*)^2}}{\sqrt{\Phi^*\left[\left(\frac{k}{R\cos\Theta^*}\right)^2 + \left(\frac{l}{R}\right)^2\right] + f^{*2}}} \end{aligned} \tag{8.2}$$

while in the θ-dimension the group velocities are given by

$$\begin{aligned} c_\theta^{\pm} &\equiv \frac{d\omega^{\pm}}{dl} \\ &= \pm\frac{\Phi^*\frac{l}{R^2}}{\sqrt{\Phi^*\left[\left(\frac{k}{R\cos\Theta^*}\right)^2 + \left(\frac{l}{R}\right)^2\right] + f^{*2}}} \end{aligned} \tag{8.3}$$

In this section, we will focus on the positive components of the group velocities c_λ^+ and c_θ^+. The group velocities for the continuous solution are shown in Figures 8.2 and 8.3. Note that $c_\lambda^+ \geq 0$, $c_\theta^+ \geq 0$ for all wavelengths.

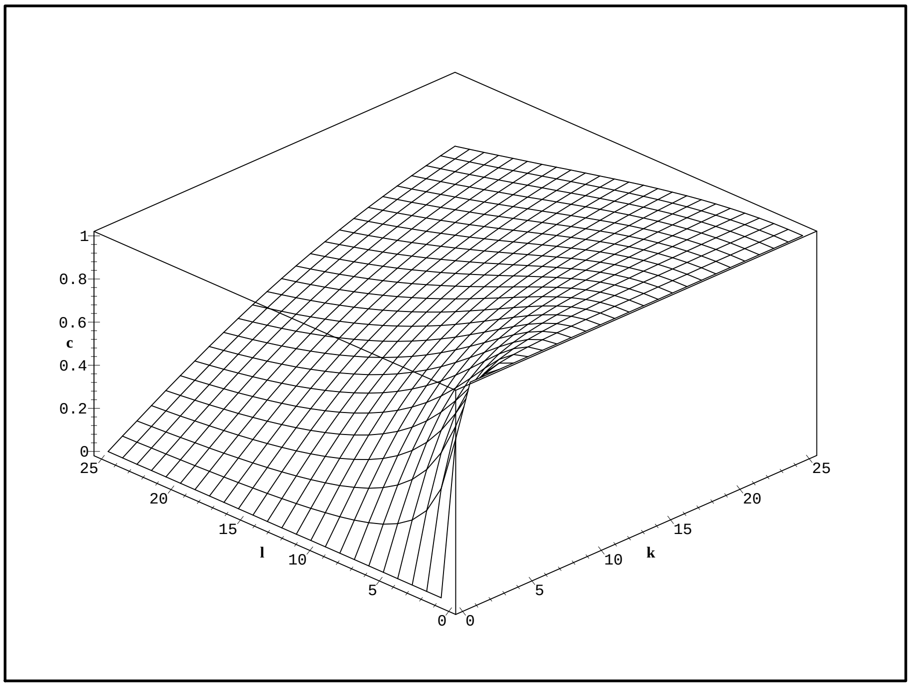

Figure 8.2: Group velocities of continuous gravity solution in the λ-direction. Note that all waves travel in the positive direction.

8.1.2 The A-grid

The A-grid is unstaggered, and the Lagrangian frequencies of its discrete solution computed with the quadratic spline Galerkin (QSG), the quadratic spline collocation (QSC), and the one-step optimal quadratic collocation (OQSC) methods can be derived from (7.18), since

$$e^{\imath\nu\Delta t} = \frac{4A - B \pm i4\sqrt{AB}}{4A + B} \Rightarrow \nu = \frac{1}{\Delta t}\mathrm{arctan}\left(\frac{\pm 4\sqrt{AB}}{4A - B}\right) \tag{8.4}$$

Then, using (7.2), we can compute the wave frequencies of the numerical solution as

$$\omega^{\pm} = -\frac{u^*}{R\cos\Theta^*} - \frac{v^*}{R} + \frac{1}{\Delta t}\mathrm{arctan}\left(\frac{\pm 4\sqrt{AB}}{4A - B}\right) \tag{8.5}$$

where A and B are defined in Section 7.1. Note both A and B vary with k or l since they are are functions of the eigenvalues p, p_λ, q and q_θ, which in turn depend on the wave numbers k and l. In addition, note that the expressions for p, p_λ, q and q_θ depend

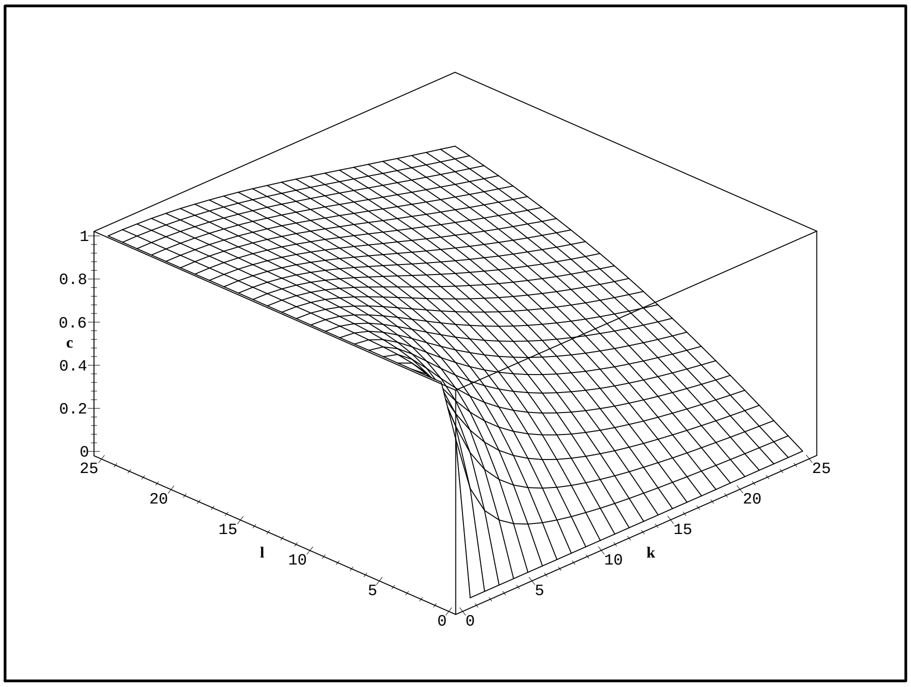

Figure 8.3: Group velocities of continuous gravity solution in the θ-direction. Note that all waves travel in the positive direction.

on the numerical method used. These values are given in Appendix A for the QSG, QSC and OQSC methods.

The wave frequencies of the gravity solution obtained with the two-step OQSC method can be obtained from (7.26) as

$$e^{\imath\nu\Delta t} = \frac{4A - B + C \pm \imath 2\sqrt{4A(B-C) + (4+f^{*2})(\delta\lambda^2 + \cos\Theta^{*2}\delta\theta^2)A + D}}{4A+B} \equiv \mathcal{F}_A^{\pm}$$

$$\Rightarrow \quad \omega^{\pm} = -\frac{u^*}{R\cos\Theta^*} - \frac{v^*}{R} + \frac{1}{\Delta t}\arctan\left[\frac{\mathcal{I}m(\mathcal{F}_A^{\pm})}{\mathcal{R}e(\mathcal{F}_A^{\pm})}\right] \tag{8.6}$$

where A, B, C, D, $\delta\lambda$ and $\delta\theta$ are defined in Section 7.1.2. Note that C, D, $\delta\lambda$ and $\delta\theta$ have imaginary parts.

The group velocities of gravity waves for different wave numbers corresponding to the QSG, QSC and OQSC methods on unstaggered grids are shown in Figures 8.4 to 8.11. Note that the group velocities of short waves (large wave numbers) are negative, even though, according to our analysis of the continuous solutions, all gravity waves should

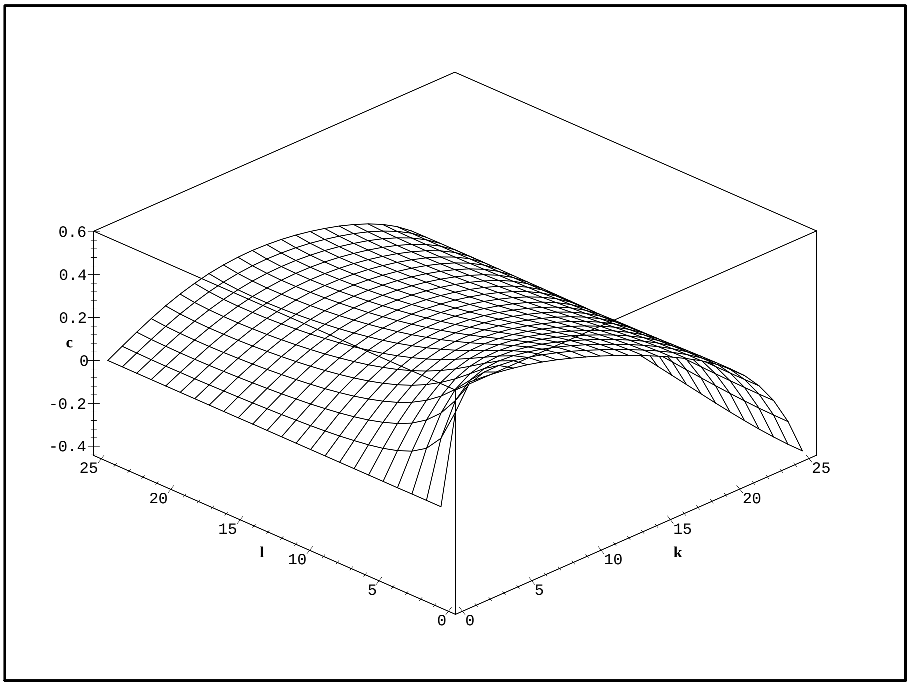

Figure 8.4: Group velocities of gravity waves in the λ-direction for the QSG method on an A-grid. Note that some waves travel with negative velocities.

travel in the positive direction. It can, therefore, be concluded that the (unstaggered) A-grid is inaccurate in capturing the group velocities of short gravity waves.

8.1.3 The B-grid

On the B-grid, the wind speed components u and v are computed at the same locations, while the geopotential ϕ is evaluated at points that are staggered with respect to the u, v-grid in both λ and θ-directions. Let $\hat{\boldsymbol{u}}_{\Delta}^{n+1}$ and $\hat{\boldsymbol{v}}_{\Delta}^{n+1}$ denote the vectors of values of u_{Δ}^{n+1} and v_{Δ}^{n+1} at the midpoints of the u, v-grid, and $\boldsymbol{\phi}_{\Delta}^{n+1}$ denote the vector of values of ϕ_{Δ}^{n+1} at the midpoints of the ϕ-grid.

Recall that $\vartheta_k = \left(e^{\imath kj\Delta\lambda}\right)_{j=0}^{N_\lambda-1}$. Let $\hat{\vartheta}_k = \left(e^{\imath k(j+\frac{1}{2})\Delta\lambda}\right)_{j=0}^{N_\lambda-1}$ for $k = 0, \cdots, N_\lambda - 1$ and observe that the staggering operators satisfy conditions similar to (7.4):

$$P^{\Delta\to\hat{\Delta}}\vartheta_k = p_k^{\to}\hat{\vartheta}_k, \qquad P^{\hat{\Delta}\to\Delta}\hat{\vartheta}_k = p_k^{\to}\vartheta_k$$

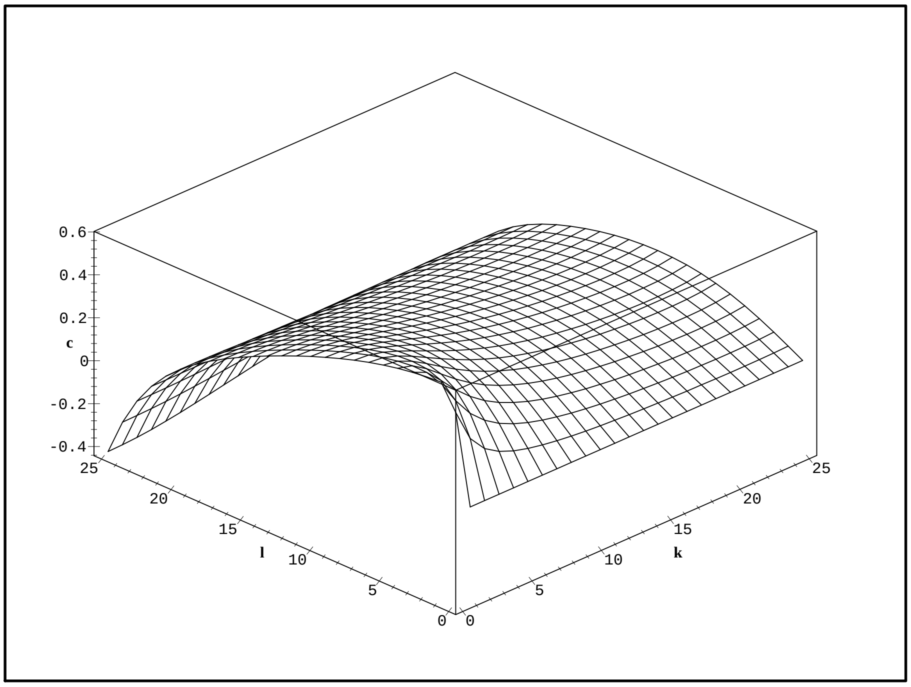

Figure 8.5: Group velocities of gravity waves in the θ-direction for the QSG method on an A-grid. Some waves travel with negative velocities.

$$P_\lambda^{\Delta\to\hat{\Delta}}\vartheta_k = p_{\lambda_k}^{\rightarrow}\hat{\vartheta}_k \qquad P_\lambda^{\hat{\Delta}\to\Delta}\hat{\vartheta}_k = p_{\lambda_k}^{\rightarrow}\vartheta_k$$

Since $\hat{\vartheta}_k = e^{i\frac{k}{2}\Delta\lambda}\vartheta_k$, we see that ϑ_k is an eigenvector of $P^{\Delta\to\hat{\Delta}}$ and $P_\lambda^{\Delta\to\hat{\Delta}}$, with $p_k^{\rightarrow}e^{i\frac{k}{2}\Delta\lambda}$ and $p_{\lambda_k}^{\rightarrow}e^{i\frac{k}{2}\Delta\lambda}$ being the associated eigenvalues, respectively. Similarly, $\hat{\vartheta}_k$ is an eigenvector of $P^{\hat{\Delta}\to\Delta}$ and $P_\lambda^{\hat{\Delta}\to\Delta}$, with $p_k^{\rightarrow}e^{-i\frac{k}{2}\Delta\lambda}$ and $p_{\lambda_k}^{\rightarrow}e^{-i\frac{k}{2}\Delta\lambda}$ being the associated eigenvalues, respectively. The arrows in $p_k^{\rightarrow}$ and $p_{\lambda_k}^{\rightarrow}$ indicate the fact that these scalars are associated with staggering operators. The scalars $p_k^{\rightarrow}$ and $p_{\lambda_k}^{\rightarrow}$ take on different values depending on the choice of spatial discretization methods (see Appendix A). Similar relations hold for the corresponding staggering operators in the θ-direction.

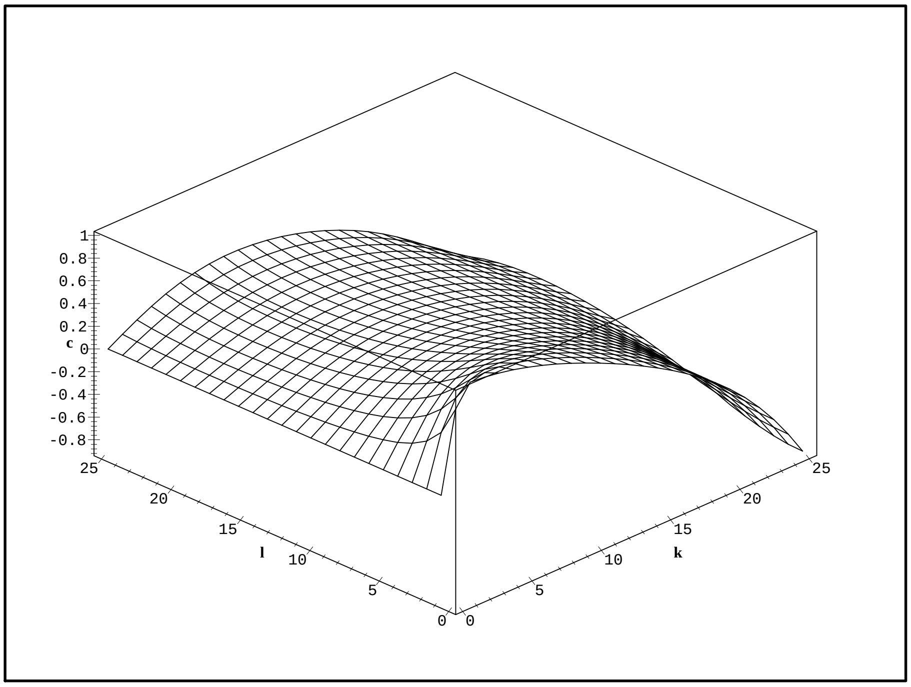

Figure 8.6: Group velocities of gravity waves in the λ-direction for the QSC method on an A-grid. Some waves travel with negative velocities.

QSG, QSC and One-Step OQSC Methods

With the B-grid, the discretized equations (7.12), (7.13) and (7.14) become:

$$
\begin{aligned}
(P \otimes Q)\left(\frac{\hat{\boldsymbol{u}}_{\Delta}^{n+1} - \tilde{\hat{\boldsymbol{u}}}_{\Delta}^{n}}{\Delta t}\right) &- f^*(P \otimes Q)\left(\frac{\hat{\boldsymbol{v}}_{\Delta}^{n+1} + \tilde{\hat{\boldsymbol{v}}}_{\Delta}^{n}}{2}\right) \\
&+ \frac{1}{R\cos\Theta^*}(P_{\lambda}^{\Delta\to\hat{\Delta}} \otimes Q^{\Delta\to\hat{\Delta}})\left(\frac{\boldsymbol{\phi}_{\Delta}^{n+1} + \tilde{\boldsymbol{\phi}}_{\Delta}^{n}}{2}\right) = 0 \qquad (8.7) \\
(P \otimes Q)\left(\frac{\hat{\boldsymbol{v}}_{\Delta}^{n+1} - \tilde{\hat{\boldsymbol{v}}}_{\Delta}^{n}}{\Delta t}\right) &+ f^*(P \otimes Q)\left(\frac{\hat{\boldsymbol{u}}_{\Delta}^{n+1} + \tilde{\hat{\boldsymbol{u}}}_{\Delta}^{n}}{2}\right) \\
&+ \frac{1}{R}(P^{\Delta\to\hat{\Delta}} \otimes Q_{\theta}^{\Delta\to\hat{\Delta}})\left(\frac{\boldsymbol{\phi}_{\Delta}^{n+1} + \tilde{\boldsymbol{\phi}}^{\boldsymbol{n}}{}_{\Delta}}{2}\right) = 0 \qquad (8.8) \\
(P \otimes Q)\left(\frac{\boldsymbol{\phi}_{\Delta}^{n+1} - \tilde{\boldsymbol{\phi}}_{\Delta}^{n}}{\Delta t}\right) &+ \frac{\Phi^*}{R\cos\Theta^*}(P_{\lambda}^{\hat{\Delta}\to\Delta} \otimes Q^{\hat{\Delta}\to\Delta})\left(\frac{\hat{\boldsymbol{u}}_{\Delta}^{n+1} + \tilde{\hat{\boldsymbol{u}}}_{\Delta}^{n}}{2}\right) \\
&+ \frac{\Phi^*}{R}(P^{\hat{\Delta}\to\Delta} \otimes Q_{\theta}^{\hat{\Delta}\to\Delta})\left(\frac{\hat{\boldsymbol{v}}_{\Delta}^{n+1} + \tilde{\hat{\boldsymbol{v}}}_{\Delta}^{n}}{2}\right) = 0 \qquad (8.9)
\end{aligned}
$$

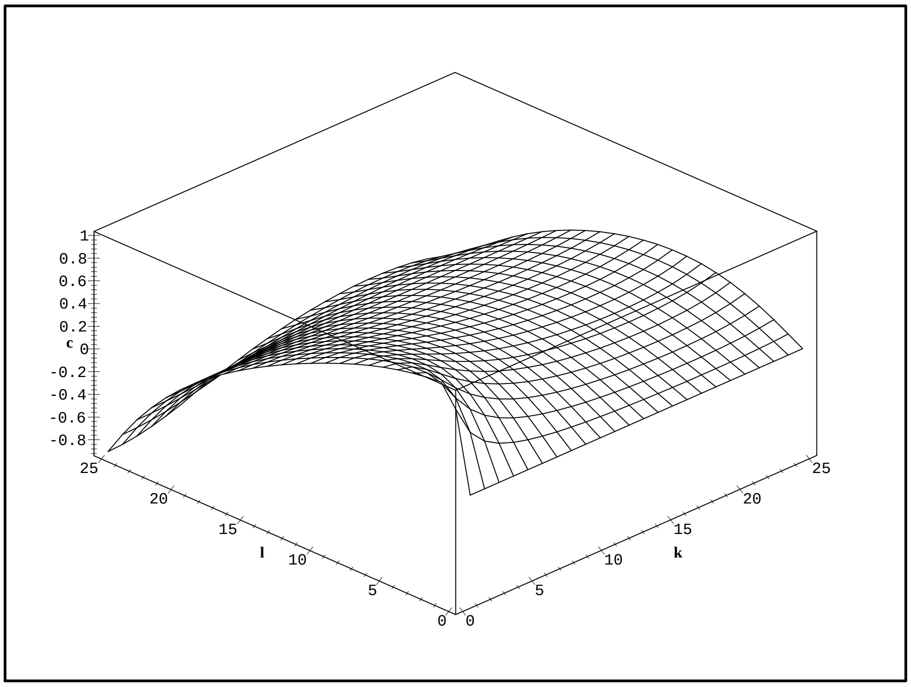

Figure 8.7: Group velocities of gravity waves in the θ-direction for the QSC method on an A-grid. Some waves travel with negative velocities.

Following the procedures described in Section 7.1.2, we rewrite equations (8.7) to (8.9) in terms of the eigenvalues of P and Q, and obtain the following after some simplifications:

$$pq\left(\frac{e^{\imath\nu\Delta t}-1}{\Delta t}\right)u_0 - f^*pq\left(\frac{e^{\imath\nu\Delta t}+1}{2}\right)v_0 + \frac{p_\lambda^{\rightarrow}q^{\rightarrow}}{R\cos\Theta^*}\left(\frac{e^{\imath\nu\Delta t}+1}{2}\right)\phi_0 = 0 \quad (8.10)$$

$$pq\left(\frac{e^{\imath\nu\Delta t}-1}{\Delta t}\right)v_0 + f^*pq\left(\frac{e^{\imath\nu\Delta t}+1}{2}\right)u_0 + \frac{p^{\rightarrow}q_\theta^{\rightarrow}}{R}\left(\frac{e^{\imath\nu\Delta t}+1}{2}\right)\phi_0 = 0 \quad (8.11)$$

$$pq\left(\frac{e^{\imath\nu\Delta t}-1}{\Delta t}\right)\phi_0 + \Phi^*\frac{p_\lambda^{\rightarrow}q^{\rightarrow}}{R\cos\Theta^*}\left(\frac{e^{\imath\nu\Delta t}+1}{2}\right)u_0 + \Phi^*\frac{p^{\rightarrow}q_\theta^{\rightarrow}}{R}\left(\frac{e^{\imath\nu\Delta t}+1}{2}\right)v_0 = 0 \quad (8.12)$$

The solution for the Lagrangian frequency for the B-grid is given by the relations

$$e^{\imath\nu\Delta t} = 1, \qquad \frac{4A - B \pm \imath 4\sqrt{AB}}{4A+B} \quad (8.13)$$

where

$$\begin{aligned} A &= (pqR\cos\Theta^*)^2 \\ B &= (\Delta t f^* R\cos\Theta pq)^2 - \Delta t^2\Phi^*(p_\lambda^{\rightarrow 2} q^{\rightarrow 2} + p^{\rightarrow 2} q_\theta^{\rightarrow 2}\cos^2\Theta^*) \end{aligned}$$

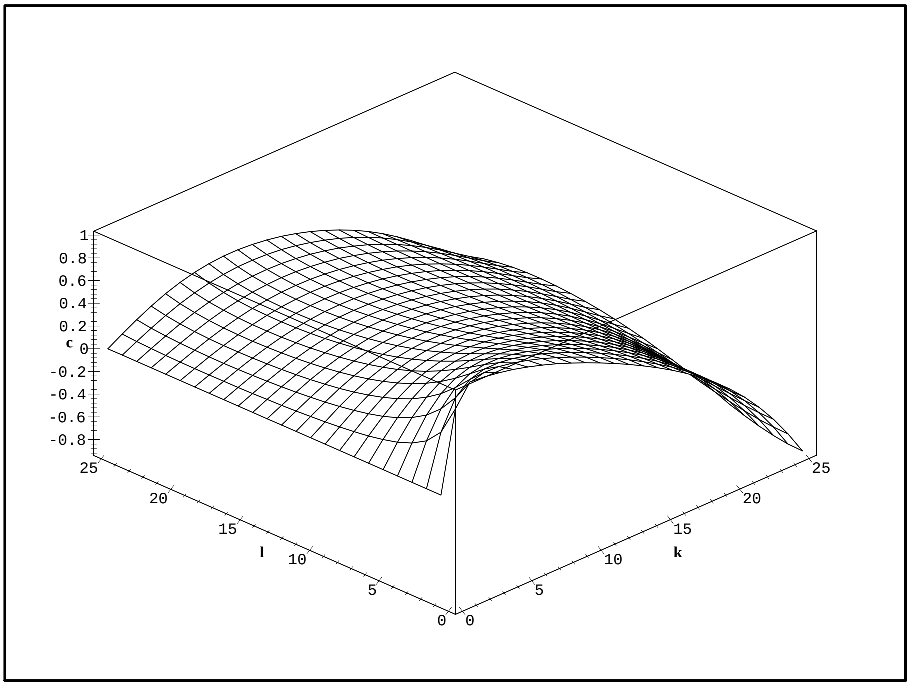

Figure 8.8: Group velocities of gravity waves in the λ-direction for the one-step OQSC method on an A-grid. Some waves travel with negative velocities.

The group velocities of gravity waves discretized by the QSG, QSC and one-step OQSC methods on a B-grid are shown in Figures 8.12 to 8.17. As with the A-grid, energy propagates in the wrong direction at small scales for all the methods considered, though the problem is less severe in this case.

Two-Step OQSC Method

For the two-step OQSC method, the discretized perturbed equations (7.20) to (7.22) for the B-grid take the following form:

$$(P \otimes Q)\left(\frac{\hat{\boldsymbol{u}}_{\Delta}^{n+1} - \hat{\tilde{\boldsymbol{u}}}_{\Delta}^{n}}{\Delta t}\right) - f^*(P \otimes Q)\left(\frac{\hat{\boldsymbol{v}}_{\Delta}^{n+1} + \hat{\tilde{\boldsymbol{v}}}_{\Delta}^{n}}{2}\right) \\ + \frac{1}{R\cos\Theta^*}(P_{\lambda}^{\Delta\to\hat{\Delta}} \otimes Q^{\Delta\to\hat{\Delta}})\left(\frac{\boldsymbol{\phi}_{\Delta}^{n+1} + \tilde{\boldsymbol{\phi}}_{\Delta}^{n}}{2}\right)$$

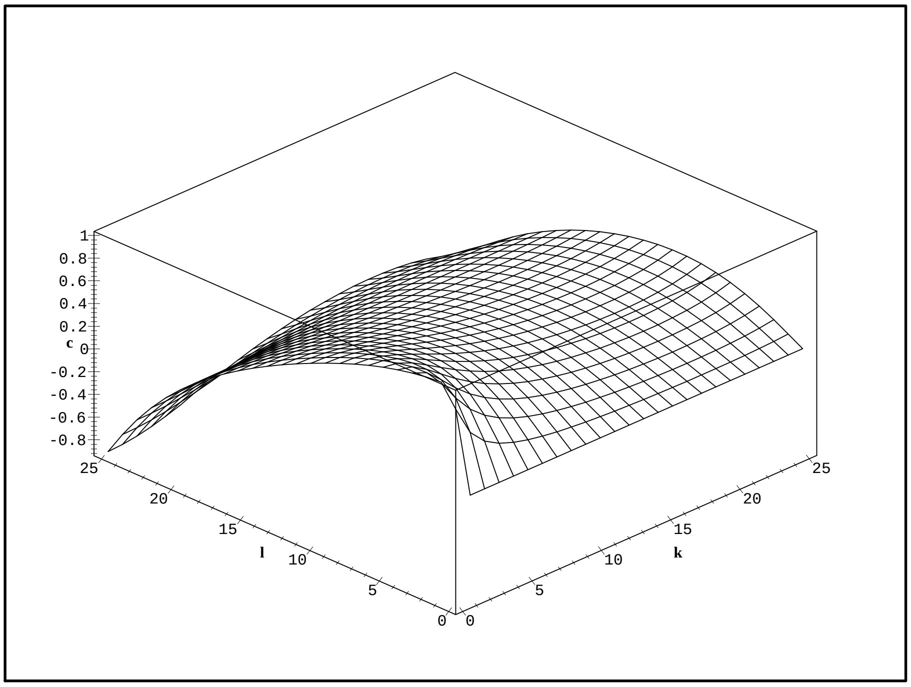

Figure 8.9: Group velocities of gravity waves in the θ-direction for the one-step OQSC method on an A-grid. Some waves travel with negative velocities.

$$= -\frac{1}{R\cos\Theta^*}\frac{\Delta\lambda^2}{24}(\Lambda_\lambda \otimes I)(P_\lambda^{\Delta\to\hat{\Delta}} \otimes Q^{\Delta\to\hat{\Delta}})\left(\frac{\breve{\boldsymbol{\phi}}_\Delta^{n+1} + \tilde{\boldsymbol{\phi}}_\Delta^{n}}{2}\right) \tag{8.14}$$

$$\begin{aligned}(P\otimes Q)\left(\frac{\hat{\boldsymbol{v}}_\Delta^{n+1} - \hat{\tilde{\boldsymbol{v}}}_\Delta^{n}}{\Delta t}\right) &+ f^*(P\otimes Q)\left(\frac{\hat{\boldsymbol{u}}_\Delta^{n+1} + \hat{\tilde{\boldsymbol{u}}}_\Delta^{n}}{2}\right) \\ &+ \frac{1}{R}(P^{\Delta\to\hat{\Delta}} \otimes Q_\theta^{\Delta\to\hat{\Delta}})\left(\frac{\boldsymbol{\phi}_\Delta^{n+1} + \tilde{\boldsymbol{\phi}}_\Delta^{n}}{2}\right) \\ &= -\frac{1}{R}\frac{\Delta\theta^2}{24}(I\otimes\Lambda_\theta)(P^{\Delta\to\hat{\Delta}} \otimes Q_\theta^{\Delta\to\hat{\Delta}})\left(\frac{\breve{\boldsymbol{\phi}}_\Delta^{n+1} + \tilde{\boldsymbol{\phi}}_\Delta^{n}}{2}\right)\end{aligned} \tag{8.15}$$

$$\begin{aligned}(P\otimes Q)\left(\frac{\boldsymbol{\phi}_\Delta^{n+1} - \tilde{\boldsymbol{\phi}}_\Delta^{n}}{\Delta t}\right) &+ \frac{\Phi^*}{R\cos\Theta^*}(P_\lambda^{\hat{\Delta}\to\Delta} \otimes Q^{\hat{\Delta}\to\Delta})\left(\frac{\hat{\boldsymbol{u}}_\Delta^{n+1} + \hat{\tilde{\boldsymbol{u}}}_\Delta^{n}}{2}\right) \\ &+ \frac{\Phi^*}{R}(P^{\hat{\Delta}\to\Delta} \otimes Q_\theta^{\hat{\Delta}\to\Delta})\left(\frac{\hat{\boldsymbol{v}}_\Delta^{n+1} + \hat{\tilde{\boldsymbol{v}}}_\Delta^{n}}{2}\right)\end{aligned}$$

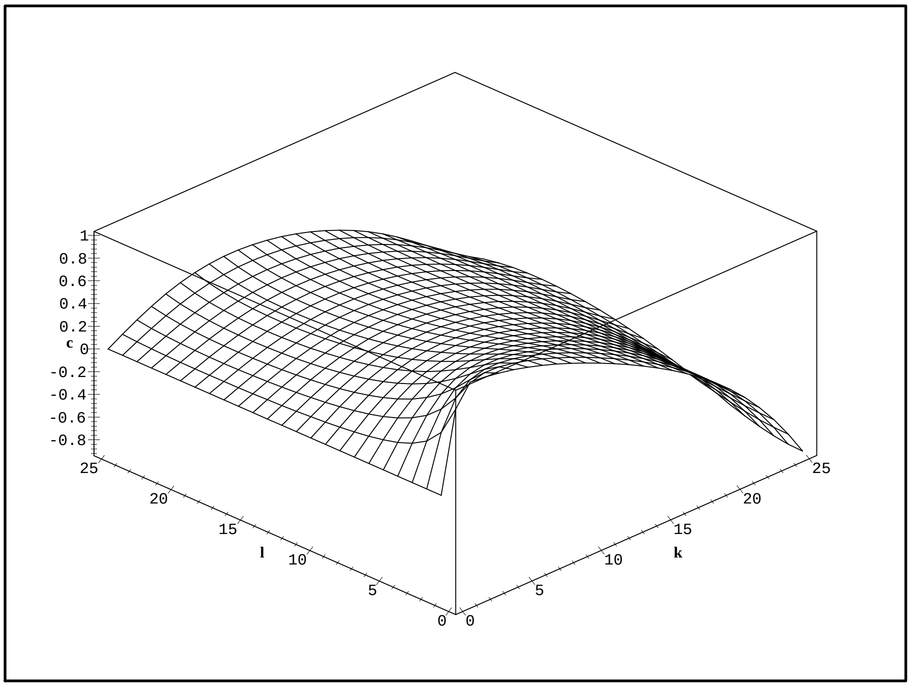

Figure 8.10: Group velocities of gravity waves in the λ-direction for the two-step OQSC method on an A-grid. Some waves travel with negative velocities.

$$
\begin{aligned}
&= -\frac{\Phi^*}{R\cos\Theta^*}\frac{\Delta\lambda^2}{24}(\Lambda_\lambda \otimes I)(P_\lambda^{\hat{\Delta}\to\Delta} \otimes Q^{\hat{\Delta}\to\Delta})\left(\frac{\check{\hat{\boldsymbol{u}}}_\Delta^{n+1} + \hat{\hat{\boldsymbol{u}}}_\Delta^{n}}{2}\right) \\
&\quad - \frac{\Phi^*}{R}\frac{\Delta\theta^2}{24}(I \otimes \Lambda_\theta)(P^{\hat{\Delta}\to\Delta} \otimes Q_\theta^{\hat{\Delta}\to\Delta})\left(\frac{\check{\hat{\boldsymbol{v}}}_\Delta^{n+1} + \hat{\hat{\boldsymbol{v}}}_\Delta^{n}}{2}\right) \qquad (8.16)
\end{aligned}
$$

Rewriting the above equations in terms of the eigenvalues and simplifying yields

$$
\begin{aligned}
&pq\left(\frac{e^{\imath\nu\Delta t}-1}{\Delta t}\right)u_0 - f^*pq\left(\frac{e^{\imath\nu\Delta t}+1}{2}\right)v_0 + \frac{p_\lambda^{\rightarrow}q^{\rightarrow}}{R\cos\Theta^*}\left(\frac{e^{\imath\nu\Delta t}+1}{2}\right)\phi_0 \\
&\qquad = -\frac{1}{R\cos\Theta^*}\frac{\Delta\lambda^2}{24}p_{\lambda\lambda}p_\lambda^{\rightarrow}q^{\rightarrow}\left(\frac{e^{\imath\check{\nu}\Delta t}+1}{2}\right)\phi_0 \qquad (8.17) \\
&pq\left(\frac{e^{\imath\nu\Delta t}-1}{\Delta t}\right)v_0 + f^*pq\left(\frac{e^{\imath\nu\Delta t}+1}{2}\right)u_0 + \frac{p^{\rightarrow}q_\theta^{\rightarrow}}{R}\left(\frac{e^{\imath\nu\Delta t}+1}{2}\right)\phi_0 \\
&\qquad = -\frac{1}{R}\frac{\Delta\theta^2}{24}p^{\rightarrow}q_{\theta\theta}q_\theta^{\rightarrow}\left(\frac{e^{\imath\check{\nu}\Delta t}+1}{2}\right)\phi_0 \qquad (8.18) \\
&pq\left(\frac{e^{\imath\nu\Delta t}-1}{\Delta t}\right)\phi_0 + \Phi^*\left[\frac{p_\lambda^{\rightarrow}q^{\rightarrow}}{R\cos\Theta^*}\left(\frac{e^{\imath\nu\Delta t}+1}{2}\right)u_0 + \frac{p^{\rightarrow}q_\theta^{\rightarrow}}{R}\left(\frac{e^{\imath\nu\Delta t}+1}{2}\right)v_0\right]
\end{aligned}
$$

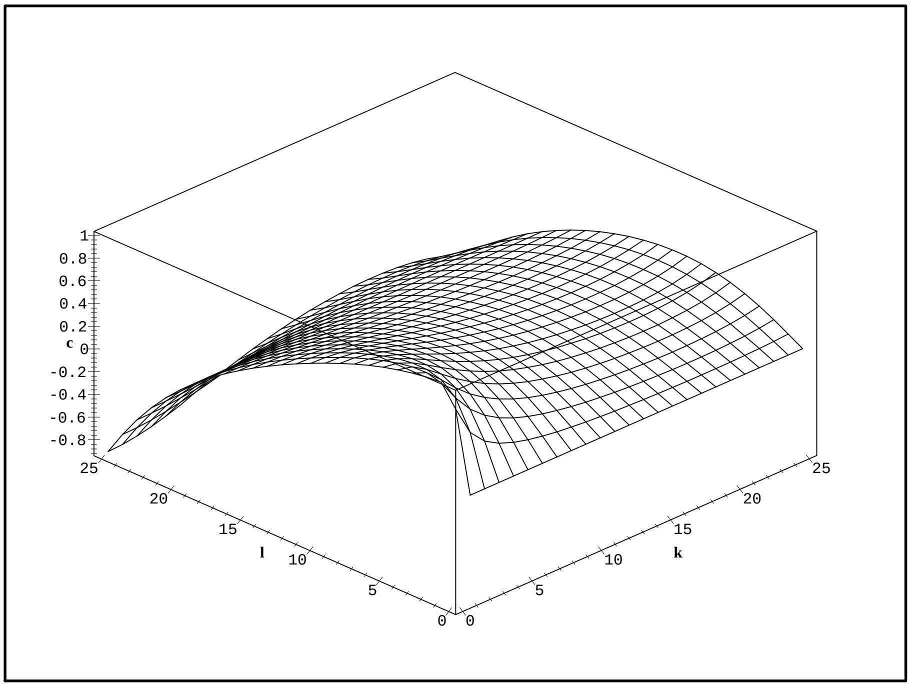

Figure 8.11: Group velocities of gravity waves in the θ-direction for the two-step OQSC method on an A-grid. Some waves travel with negative velocities.

$$= -\,\Phi^* \left[\frac{\Delta\lambda^2}{24} p_{\lambda\lambda} \frac{p_\lambda^{\rightarrow} q^{\rightarrow}}{R\cos\Theta^*}\left(\frac{e^{\imath\breve{\nu}\Delta t}+1}{2}\right) u_0 + \frac{\Delta\theta^2}{24}\frac{p^{\rightarrow} q_{\theta\theta} q_\theta^{\rightarrow}}{R}\left(\frac{e^{\imath\breve{\nu}\Delta t}+1}{2}\right) v_0\right] \tag{8.19}$$

By moving all terms to the left side, setting the determinant of the resulting system to zero, and solving for $e^{\imath\nu\Delta t}$, we find that

$$e^{\imath\nu\Delta t} = 1,\ \frac{4A - B + C \pm \imath 2\sqrt{4A(B-C) - \Delta t^2\Phi^*(4+\Delta t^2 f^{*2})(\delta\lambda^2 + \cos\Theta^{*2}\delta\theta^2)A + D}}{4A+B}$$
$$\equiv \mathcal{F}_B^{\pm} \tag{8.20}$$

where

$$A = (R\cos\Theta^* pq)^2$$
$$B = (\Delta t f^* R\cos\Theta^* pq)^2 - \Delta t^2\Phi^*(p_\lambda^{\rightarrow 2} q^{\rightarrow 2} + \cos^2\Theta^* p^{\rightarrow 2} q_\theta^{\rightarrow 2})$$
$$C = 2\Delta t^2\Phi^*(p_\lambda^{\rightarrow} q^{\rightarrow}\delta\lambda + \cos^2\Theta^* p^{\rightarrow} q_\theta^{\rightarrow}\delta\theta)$$

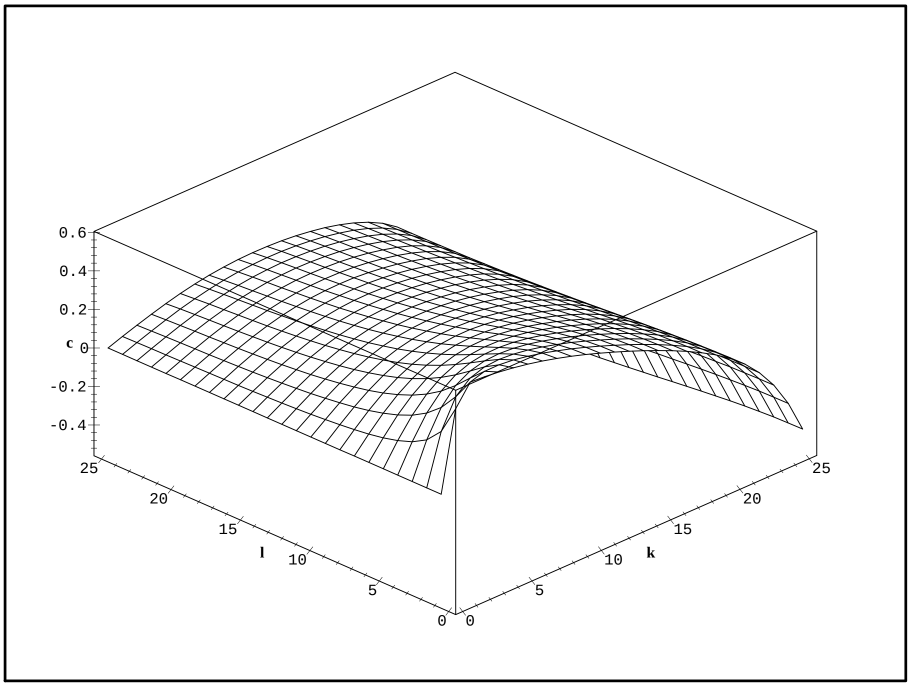

Figure 8.12: Group velocities of gravity waves in the λ-direction for the QSG method on a B-grid. Some short waves propagate with negative velocities.

$$\begin{aligned}
D &= \Delta t^4 \Phi^{*2} \cos^2 \Theta^* (p^{\rightarrow} q_\theta^{\rightarrow} \delta\lambda - p_\lambda^{\rightarrow} q^{\rightarrow} \delta\theta)^2 \\
\delta\lambda &= \frac{\Delta\lambda^2}{24} p_{\lambda\lambda} p_\lambda^{\rightarrow} q^{\rightarrow} \left(\frac{e^{\imath\breve{\nu}\Delta t} + 1}{2} \right) \\
\delta\theta &= \frac{\Delta\theta^2}{24} p^{\rightarrow} q_{\theta\theta} q_\theta^{\rightarrow} \left(\frac{e^{\imath\breve{\nu}\Delta t} + 1}{2} \right)
\end{aligned}$$

It has been verified using MAPLE that $|\mathcal{F}_B^{\pm}|$ is bounded by 1, so the gravity solution is bounded. The group velocities can be computed from the wave frequencies, which are given as

$$\omega^{\pm} = -\frac{u^*}{R\cos\Theta^*} - \frac{v^*}{R} + \frac{1}{\Delta t} \arctan \left[\frac{\mathcal{I}m(\mathcal{F}_B^{\pm})}{\mathcal{R}e(\mathcal{F}_B^{\pm})} \right] \tag{8.21}$$

and are shown in Figures 8.18 and 8.19. As with the QSG, QSC and one-step OQSC methods, some short gravity waves travel in the wrong direction.

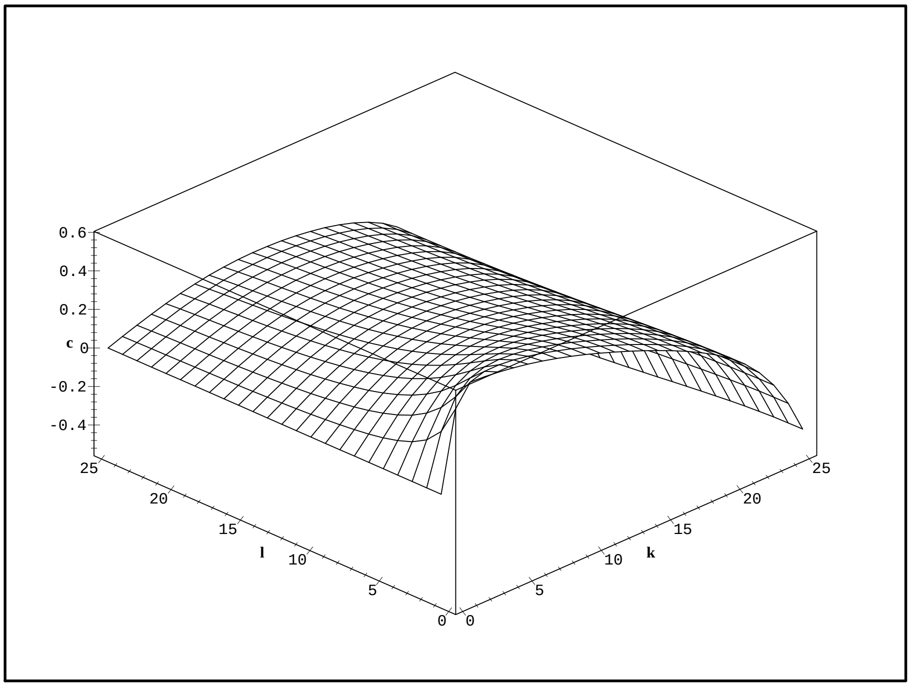

Figure 8.13: Group velocities of gravity waves in the θ-direction for the QSG method on a B-grid. Some short waves propagate with negative velocities.

8.1.4 The C-grid

The C-grid is used in our implementation of the shallow water equations; its structure has been described in Section 3.1 and depicted in Figure 8.1. In this case, the three target functions are evaluated at different locations, with the wind speed components u and v staggered with respect to the geopotential ϕ in the λ- and θ-directions, respectively. Let $\boldsymbol{u}_\Delta^{n+1}$, $\boldsymbol{v}_\Delta^{n+1}$ and $\boldsymbol{\phi}_\Delta^{n+1}$ be vectors of values of u_Δ^{n+1}, v_Δ^{n+1} and ϕ_Δ^{n+1} evaluated at the midpoints of the associated partitions, respectively.

QSG, QSC and One-Step OQSC Method

With the C-grid, the discretized equations corresponding to (7.12), (7.13) and (7.14) become

$$(P \otimes Q)\left(\frac{\boldsymbol{u}_\Delta^{n+1} - \tilde{\boldsymbol{u}}_\Delta^{n}}{\Delta t}\right) - f^*(P^{\Delta\to\hat{\Delta}} \otimes Q^{\hat{\Delta}\to\Delta})\left(\frac{\boldsymbol{v}_\Delta^{n+1} + \tilde{\boldsymbol{v}}_\Delta^{n}}{2}\right)$$

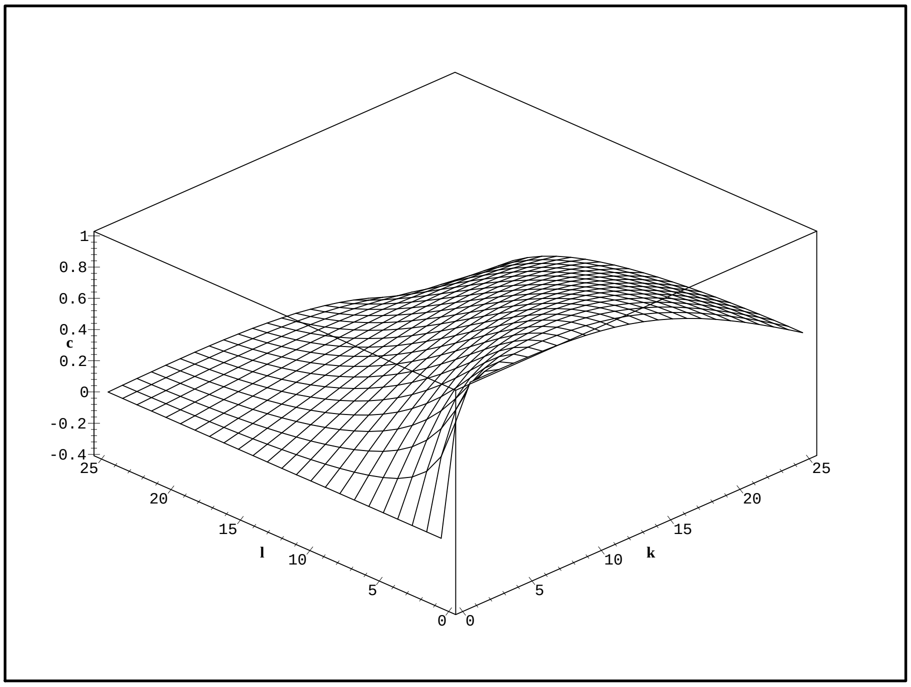

Figure 8.14: Group velocities of gravity waves in the λ-direction for the QSC method on a B-grid. Some short waves propagate with negative velocities.

$$+\frac{1}{R\cos\Theta^*}(P_\lambda^{\Delta\to\hat{\Delta}}\otimes Q)\left(\frac{\boldsymbol{\phi}_\Delta^{n+1}+\tilde{\boldsymbol{\phi}}^{\boldsymbol{n}}{}_\Delta}{2}\right)=0 \tag{8.22}$$

$$(P\otimes Q)\left(\frac{\boldsymbol{v}_\Delta^{n+1}-\tilde{\boldsymbol{v}}_\Delta^n}{\Delta t}\right)+f^*(P^{\hat{\Delta}\to\Delta}\otimes Q^{\Delta\to\hat{\Delta}})\left(\frac{\boldsymbol{u}_\Delta^{n+1}+\tilde{\boldsymbol{u}}_\Delta^n}{2}\right)$$

$$+\frac{1}{R}(P\otimes Q_\theta^{\Delta\to\hat{\Delta}})\left(\frac{\boldsymbol{\phi}_\Delta^{n+1}+\tilde{\boldsymbol{\phi}}^{\boldsymbol{n}}{}_\Delta}{2}\right)=0 \tag{8.23}$$

$$(P\otimes Q)\left(\frac{\boldsymbol{\phi}_\Delta^{n+1}-\tilde{\boldsymbol{\phi}}^{\boldsymbol{n}}{}_\Delta}{\Delta t}\right)+\frac{\Phi^*}{R\cos\Theta^*}(P_\lambda^{\hat{\Delta}\to\Delta}\otimes Q)\left(\frac{\boldsymbol{u}_\Delta^{n+1}+\tilde{\boldsymbol{u}}_\Delta^n}{2}\right)$$

$$+\frac{\Phi^*}{R}(P\otimes Q_\theta^{\hat{\Delta}\to\Delta})\left(\frac{\boldsymbol{v}_\Delta^{n+1}+\tilde{\boldsymbol{v}}_\Delta^n}{2}\right)=0 \tag{8.24}$$

The above equations, written in terms of the eigenvalues, take the form:

$$pq\left(\frac{e^{\imath\nu\Delta t}-1}{\Delta t}\right)u_0-f^*p^{\to}q^{\to}\left(\frac{e^{\imath\nu\Delta t}+1}{2}\right)v_0+\frac{p_\lambda^{\to}q}{R\cos\Theta^*}\left(\frac{e^{\imath\nu\Delta t}+1}{2}\right)\phi_0=0 \tag{8.25}$$

$$pq\left(\frac{e^{\imath\nu\Delta t}-1}{\Delta t}\right)v_0+f^*p^{\to}q^{\to}\left(\frac{e^{\imath\nu\Delta t}+1}{2}\right)u_0+\frac{pq_\theta^{\to}}{R}\left(\frac{e^{\imath\nu\Delta t}+1}{2}\right)\phi_0=0 \tag{8.26}$$

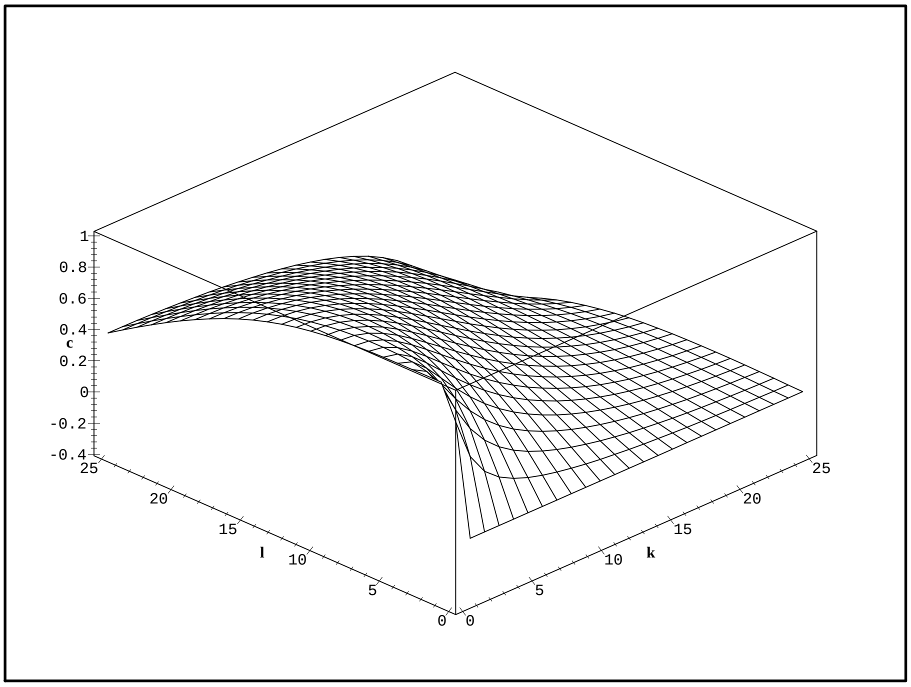

Figure 8.15: Group velocities of gravity waves in the θ-direction for the QSC method on a B-grid. Some short waves propagate with negative velocities.

$$pq\left(\frac{e^{\imath\nu\Delta t}-1}{\Delta t}\right)\phi_0+\Phi^*\frac{p_\lambda^{\rightarrow}q}{R\cos\Theta^*}\left(\frac{e^{\imath\nu\Delta t}+1}{2}\right)u_0+\Phi^*\frac{pq_\theta^{\rightarrow}}{R}\left(\frac{e^{\imath\nu\Delta t}+1}{2}\right)v_0=0 \quad (8.27)$$

The solution for the Lagrangian frequency for the C-grid is given by the relations

$$e^{\imath\nu\Delta t}=1, \quad \frac{4A-B\pm\imath4\sqrt{AB}}{4A+B} \quad (8.28)$$

where

$$\begin{aligned} A &= (R\cos\Theta^* pq)^2 \\ B &= (\Delta t f^* R\cos\Theta^* p^{\rightarrow} q^{\rightarrow})^2-\Delta t^2\Phi^*(p_\lambda^{\rightarrow 2}q^2+\cos^2\Theta^* p^2 q_\theta^{\rightarrow 2}) \end{aligned}$$

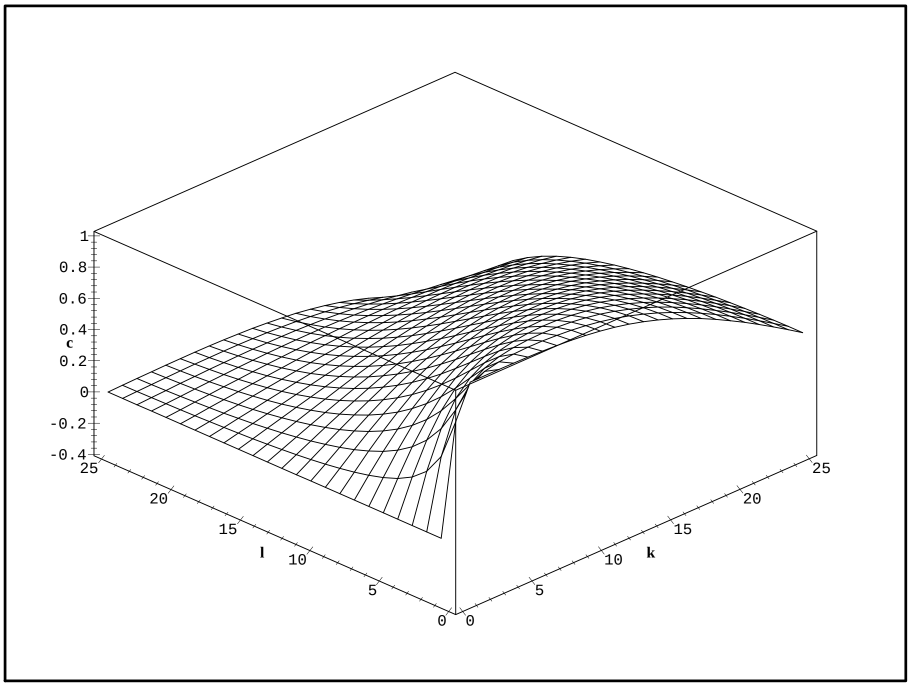

Figure 8.16: Group velocities of gravity waves in the λ-direction for the one-step OQSC method on a B-grid. Some short waves propagate with negative velocities.

Two-Step OQSC Method

For the two-step OQSC method, the discretized perturbed equations (7.20) to (7.22) for the C-grid take the following form:

$$\begin{aligned}
(P \otimes Q)\left(\frac{\boldsymbol{u}_\Delta^{n+1} - \tilde{\boldsymbol{u}}_\Delta^n}{\Delta t}\right) &- f^*(P^{\Delta\to\hat{\Delta}} \otimes Q^{\hat{\Delta}\to\Delta})\left(\frac{\boldsymbol{v}_\Delta^{n+1} + \tilde{\boldsymbol{v}}_\Delta^n}{2}\right) \\
&+ \frac{1}{R\cos\Theta^*}(P_\lambda^{\Delta\to\hat{\Delta}} \otimes Q)\left(\frac{\boldsymbol{\phi}_\Delta^{n+1} + \tilde{\boldsymbol{\phi}}_\Delta^n}{2}\right) \\
&= -\frac{1}{R\cos\Theta^*}\frac{\Delta\lambda^2}{24}(\Lambda_\lambda \otimes I)(P_\lambda^{\Delta\to\hat{\Delta}} \otimes Q)\left(\frac{\check{\boldsymbol{\phi}}_\Delta^{n+1} + \tilde{\boldsymbol{\phi}}_\Delta^n}{2}\right) \qquad (8.29) \\
(P \otimes Q)\left(\frac{\boldsymbol{v}_\Delta^{n+1} - \tilde{\boldsymbol{v}}_\Delta^n}{\Delta t}\right) &+ f^*(P^{\hat{\Delta}\to\Delta} \otimes Q^{\Delta\to\hat{\Delta}})\left(\frac{\boldsymbol{u}_\Delta^{n+1} + \tilde{\boldsymbol{u}}_\Delta^n}{2}\right) \\
&+ \frac{1}{R}(P \otimes Q_\theta^{\Delta\to\hat{\Delta}})\left(\frac{\boldsymbol{\phi}_\Delta^{n+1} + \tilde{\boldsymbol{\phi}}_\Delta^n}{2}\right)
\end{aligned}$$

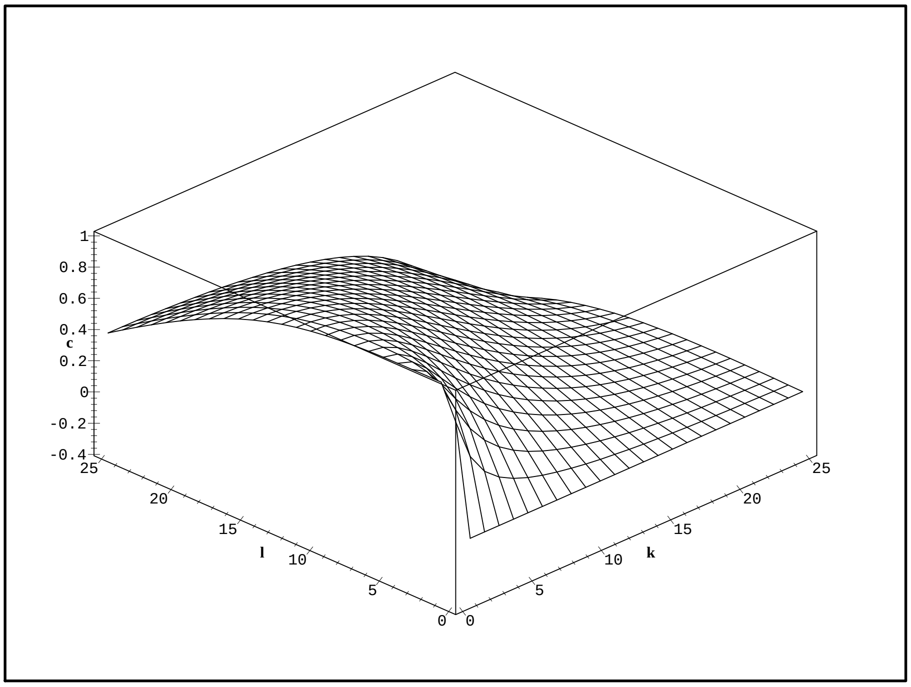

Figure 8.17: Group velocities of gravity waves in the θ-direction for the one-step OQSC method on a B-grid. Some short waves propagate with negative velocities.

$$= -\frac{1}{R}\frac{\Delta\theta^2}{24}(I\otimes\Lambda_\theta)(P\otimes Q_\theta^{\Delta\to\hat{\Delta}})\left(\frac{\breve{\boldsymbol{\phi}}_\Delta^{n+1}+\tilde{\boldsymbol{\phi}}_\Delta^{n}}{2}\right) \tag{8.30}$$

$$(P\otimes Q)\left(\frac{\boldsymbol{\phi}_\Delta^{n+1}-\tilde{\boldsymbol{\phi}}^n{}_\Delta}{\Delta t}\right)+\frac{\Phi^*}{R\cos\Theta^*}(P_\lambda^{\hat{\Delta}\to\Delta}\otimes Q)\left(\frac{\boldsymbol{u}_\Delta^{n+1}+\tilde{\boldsymbol{u}}_\Delta^{n}}{2}\right)$$
$$+\frac{\Phi^*}{R}(P\otimes Q_\theta^{\hat{\Delta}\to\Delta})\left(\frac{\boldsymbol{v}_\Delta^{n+1}+\tilde{\boldsymbol{v}}_\Delta^{n}}{2}\right)$$
$$= -\frac{\Phi^*}{R\cos\Theta^*}\frac{\Delta\lambda^2}{24}(\Lambda_\lambda\otimes I)(P_\lambda^{\hat{\Delta}\to\Delta}\otimes Q)\left(\frac{\breve{\boldsymbol{u}}_\Delta^{n+1}+\tilde{\boldsymbol{u}}_\Delta^{n}}{2}\right)$$
$$-\frac{\Phi^*}{R}\frac{\Delta\theta^2}{24}(I\otimes\Lambda_\theta)(P\otimes Q_\theta^{\hat{\Delta}\to\Delta})\left(\frac{\breve{\boldsymbol{v}}_\Delta^{n+1}+\tilde{\boldsymbol{v}}_\Delta^{n}}{2}\right) \tag{8.31}$$

Rewriting the above equations in terms of the eigenvalues and simplifying yields

$$pq\left(\frac{e^{\imath\nu\Delta t}-1}{\Delta t}\right)u_0 - f^*p^{\rightarrow}q^{\rightarrow}\left(\frac{e^{\imath\nu\Delta t}+1}{2}\right)v_0+\frac{p_\lambda^{\rightarrow}q}{R\cos\Theta^*}\left(\frac{e^{\imath\nu\Delta t}+1}{2}\right)\phi_0$$
$$= -\frac{1}{R\cos\Theta^*}\frac{\Delta\lambda^2}{24}p_{\lambda\lambda}p_\lambda^{\rightarrow}q\left(\frac{e^{\imath\breve{\nu}\Delta t}+1}{2}\right)\phi_0 \tag{8.32}$$

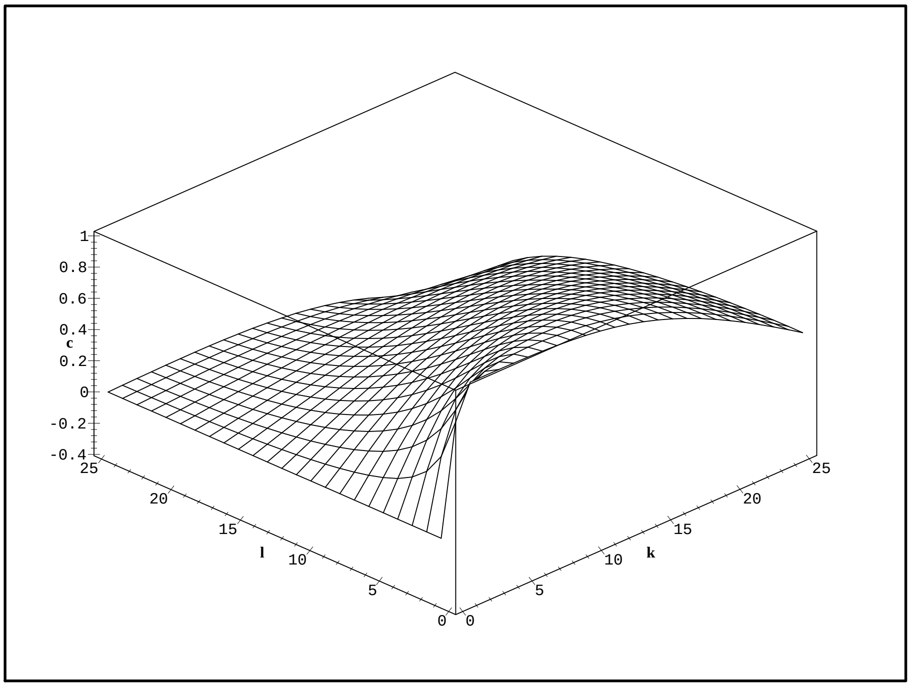

Figure 8.18: Group velocities of gravity waves in the λ-direction for the two-step OQSC method on a B-grid. Some short waves propagate with negative velocities.

$$
\begin{aligned}
pq\left(\frac{e^{\imath\nu\Delta t}-1}{\Delta t}\right)v_0 + f^* p^{\rightarrow} q^{\rightarrow}\left(\frac{e^{\imath\nu\Delta t}+1}{2}\right)u_0 + \frac{pq_\theta^{\rightarrow}}{R}\left(\frac{e^{\imath\nu\Delta t}+1}{2}\right)\phi_0 & \\
= -\frac{1}{R}\frac{\Delta\theta^2}{24}pq_{\theta\theta}q_\theta^{\rightarrow}\left(\frac{e^{\imath\breve{\nu}\Delta t}+1}{2}\right)\phi_0 & \qquad (8.33)
\end{aligned}
$$

$$
\begin{aligned}
pq\left(\frac{e^{\imath\nu\Delta t}-1}{\Delta t}\right)\phi_0 + \Phi^*\left[\frac{p_\lambda^{\rightarrow} q}{R\cos\Theta^*}\left(\frac{e^{\imath\nu\Delta t}+1}{2}\right)u_0 + \frac{pq_\theta^{\rightarrow}}{R}\left(\frac{e^{\imath\nu\Delta t}+1}{2}\right)v_0\right] & \\
= -\Phi^*\left[\frac{\Delta\lambda^2}{24}p_{\lambda\lambda}\frac{p_\lambda^{\rightarrow} q}{R\cos\Theta^*}\left(\frac{e^{\imath\breve{\nu}\Delta t}+1}{2\cos\Theta^*}\right)u_0 + \frac{\Delta\theta^2}{24}\frac{pq_{\theta\theta}q_\theta^{\rightarrow}}{R}\left(\frac{e^{\imath\breve{\nu}\Delta t}+1}{2}\right)v_0\right] & \\
& \qquad (8.34)
\end{aligned}
$$

By moving all terms to the left side, setting the determinant of the resulting system to zero, and solving for $e^{\imath\nu\Delta t}$, we find that

$$
\begin{aligned}
e^{\imath\nu\Delta t} = 1,\ & \frac{4A-B+C}{4A+B} \\
& \pm\frac{2\imath\sqrt{4A(B-C)-\Delta t^2\Phi^*[4A+(\Delta t f^* R\cos\Theta^* p^{\rightarrow}q^{\rightarrow})^2](\delta\lambda^2+\cos\Theta^{*2}\delta\theta^2)+D}}{4A+B} \\
& \equiv \mathcal{F}_C^{\pm} \qquad (8.35)
\end{aligned}
$$

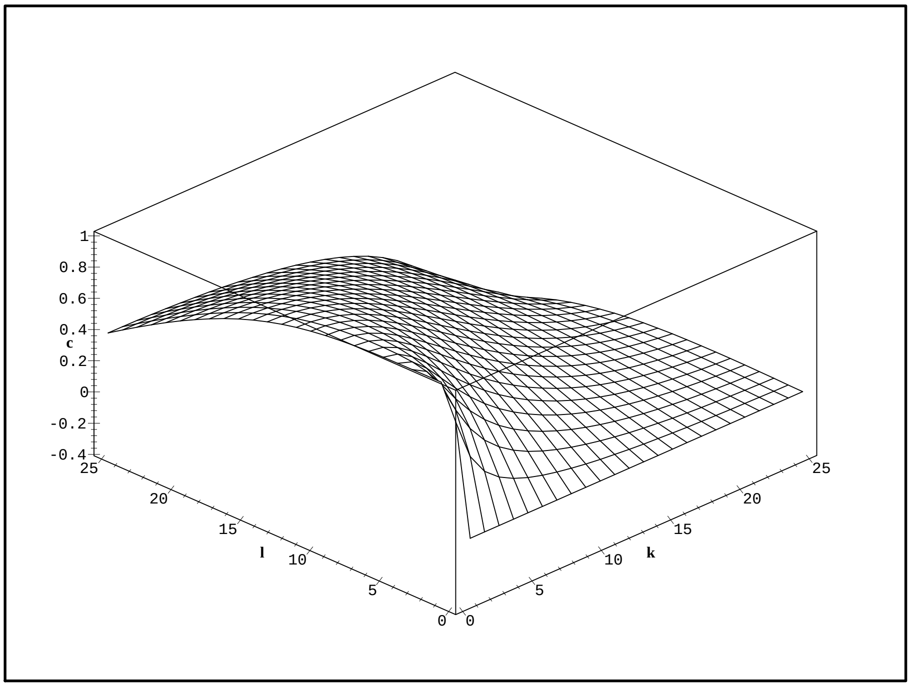

Figure 8.19: Group velocities of gravity waves in the θ-direction for the two-step OQSC method on a B-grid. Some short waves propagate with negative velocities.

where

$$
\begin{aligned}
A &= (R\cos\Theta^* pq)^2 \\
B &= (\Delta t f^* R\cos\Theta^* p^{\rightarrow} q^{\rightarrow})^2 - \Delta t^2 \Phi^* (p_\lambda^{\rightarrow 2} q^2 + \cos^2\Theta^* p^2 q_\theta^{\rightarrow 2}) \\
C &= 2\Delta t^2 \Phi^* (p_\lambda^{\rightarrow} q\delta\lambda + \cos^2\Theta^* p q_\theta^{\rightarrow}\delta\theta) \\
D &= \Delta t^4 \Phi^{*2} \cos^2\Theta^* (p q_\theta^{\rightarrow}\delta\lambda - p_\lambda^{\rightarrow} q\delta\theta)^2 \\
\delta\lambda &= \frac{\Delta\lambda^2}{24} p_{\lambda\lambda} p_\lambda^{\rightarrow} q \left(\frac{e^{\imath\breve{\nu}\Delta t}+1}{2}\right) \\
\delta\theta &= \frac{\Delta\theta^2}{24} p q_{\theta\theta} q_\theta^{\rightarrow} \left(\frac{e^{\imath\breve{\nu}\Delta t}+1}{2}\right)
\end{aligned}
$$

It has been verified using MAPLE that $|\mathcal{F}_C^{\pm}|$ is bounded by 1, so the the gravity solutions are bounded. The group velocities can be computed from the wave frequencies, which are given as

$$
\omega^{\pm} = -\frac{u^*}{R\cos\Theta^*} - \frac{v^*}{R} + \frac{1}{\Delta t}\arctan\left[\frac{\mathcal{I}m(\mathcal{F}_C^{\pm})}{\mathcal{R}e(\mathcal{F}_C^{\pm})}\right] \tag{8.36}
$$

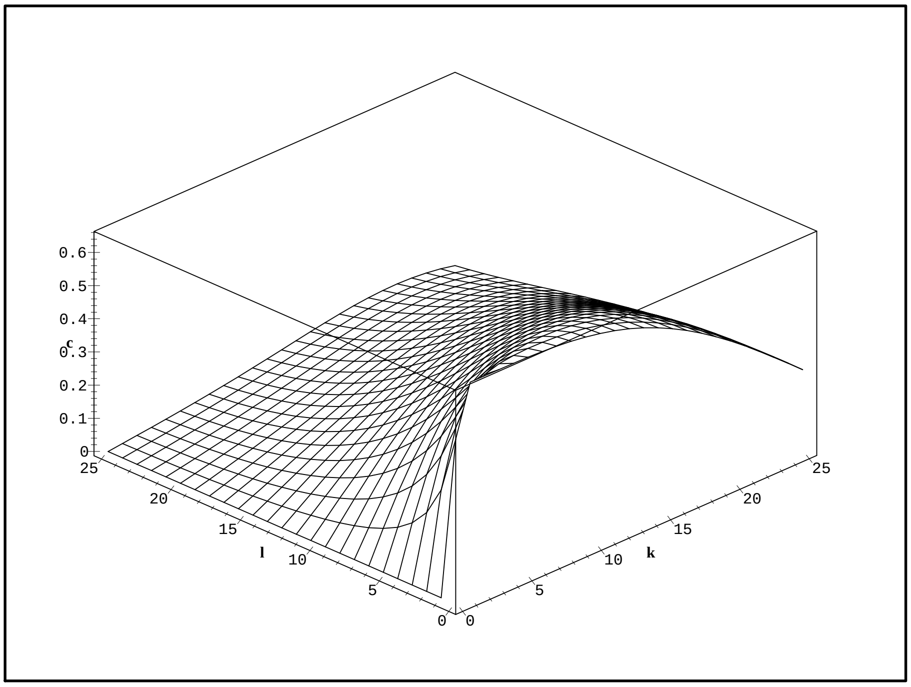

Figure 8.20: Group velocities of gravity waves in the λ-direction for the QSG method on a C-grid. The group velocities of all scales are positive.

Figures 8.20 to 8.27 show the group velocities of gravity waves for the QSG, QSC and OQSC methods, discretized on a C-grid, for different wave numbers. In this case, the group velocities are positive for all scales, which implies that energy propagates in the proper direction. Hence, we conclude that the Arakawa C-grid should outperform the other staggering systems in that it more accurately captures the group velocities of gravity waves of all wavelengths. It is also interesting to note that there is noticeable retardation in the group velocities of the gravity solution for the QSG method, but not for the QSC and OQSC methods. However, a detailed analysis of this phenomenon is beyond the scope of this thesis.

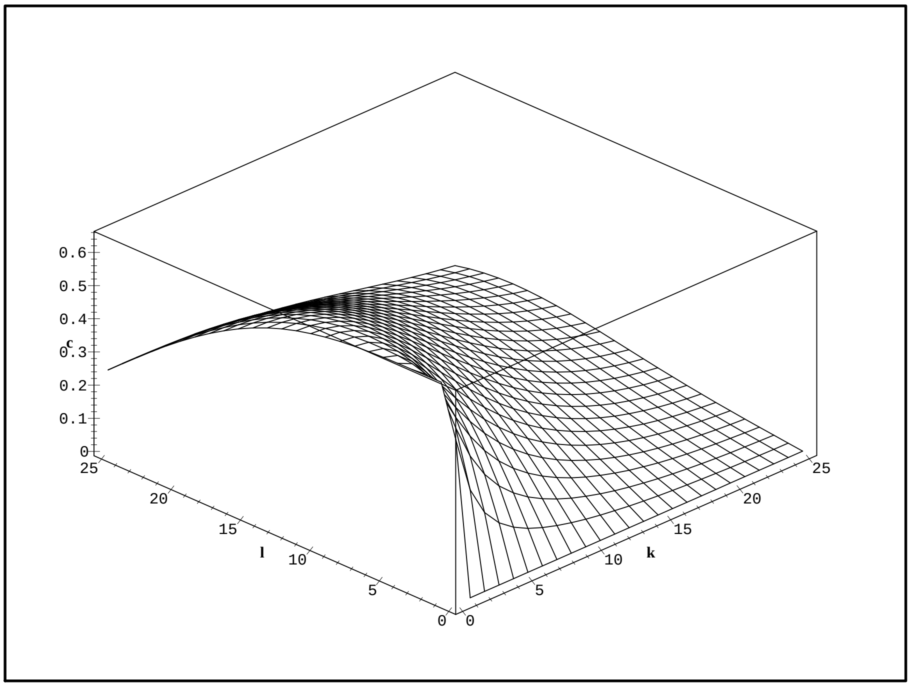

Figure 8.21: Group velocities of gravity waves in the θ-direction for the QSG method on a C-grid. As in the λ-direction, group velocities of all scales are positive.

8.2 The Equatorial Kelvin Wave

We now demonstrate numerically the effects staggering has on group velocities of short gravitational waves. The nonlinear equatorial Kelvin wave, investigated by Boyd [5], is used as the test case in our study. Equations (7.36) to (7.38) are integrated with a new set of initial conditions:

$$u(\lambda,\theta,0) = \frac{1}{3}e^{-(R\theta)^2/2-(R\lambda\cos\theta/\Delta\lambda)^2} \tag{8.37}$$

$$v(\lambda,\theta,0) = 0 \tag{8.38}$$

$$\phi'(\lambda,\theta,0) = \frac{1}{3}e^{-(R\theta)^2/2-(R\lambda\cos\theta/\Delta\lambda)^2} \tag{8.39}$$

The above initial conditions generate equatorially trapped gravity waves, traveling eastward, with wavelengths of the order of the longitudinal grid spacing. Results for the two-step OQSC method are shown in Figures 8.36, 8.37 and 8.38 on A, B and C-grids

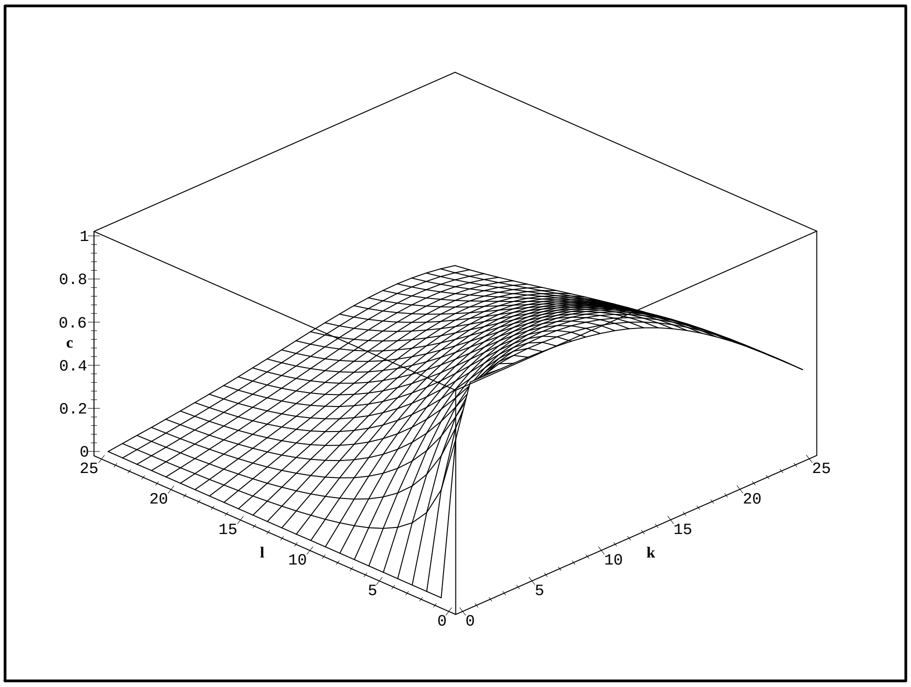

Figure 8.22: Group velocities of gravity waves in the λ-direction for the QSC method on a C-grid. Group velocities of all scales are positive.

respectively. The simulations were run for 8 non-dimensional time units on a 64×64 grid. Similar results are also obtained using the QSG and one-step OQSC methods.

When the A or B-grid is used, short gravity waves are observed to propagate westward, which is the wrong direction, thus demonstrating the failure of both the A and B-grids to faithfully capture the group velocity of short gravity waves. On the other hand, gravity waves of all scales propagate in the right direction when the C-grid is used.

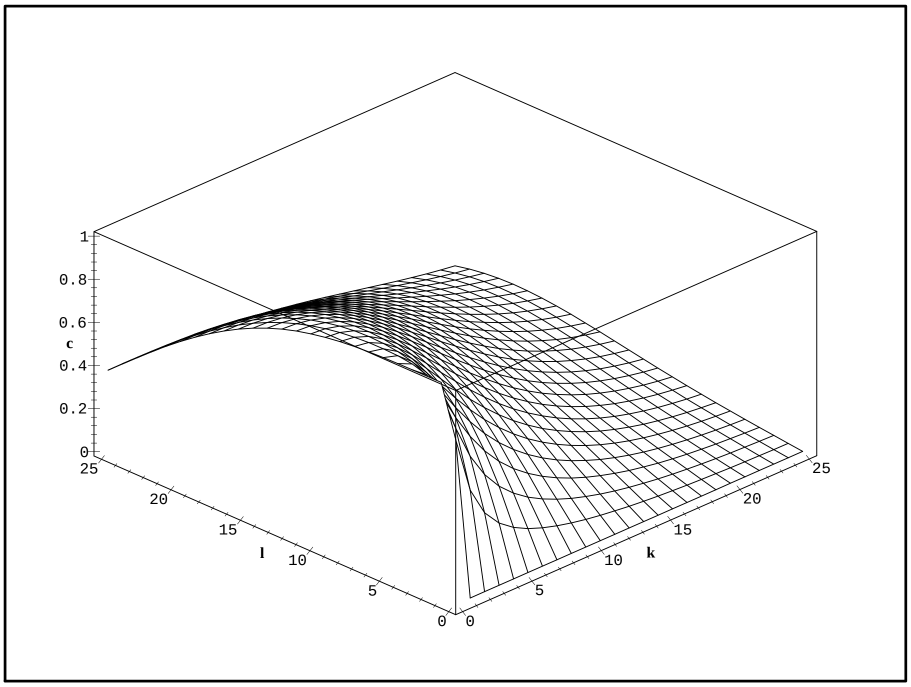

Figure 8.23: Group velocities of gravity waves in the θ-direction for the QSC method a C-grid. Group velocities of all scales are positive.

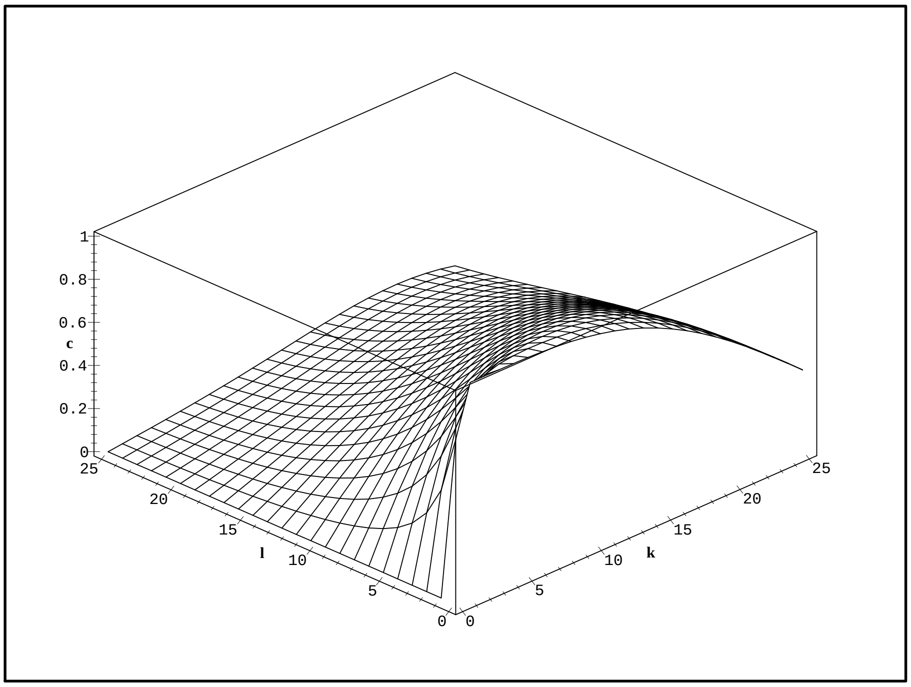

Figure 8.24: Group velocities of gravity waves in the λ-direction for the one-step OQSC method a C-grid. Group velocities of all scales are positive.

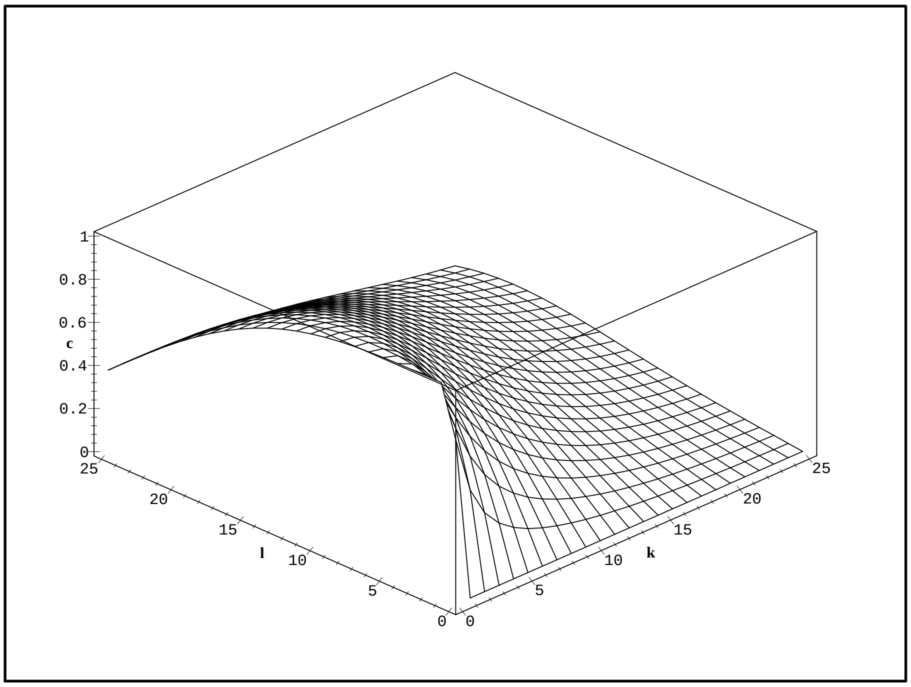

Figure 8.25: Group velocities of gravity waves in the θ-direction for the one-step OQSC method on a C-grid. Group velocities of all scales are positive.

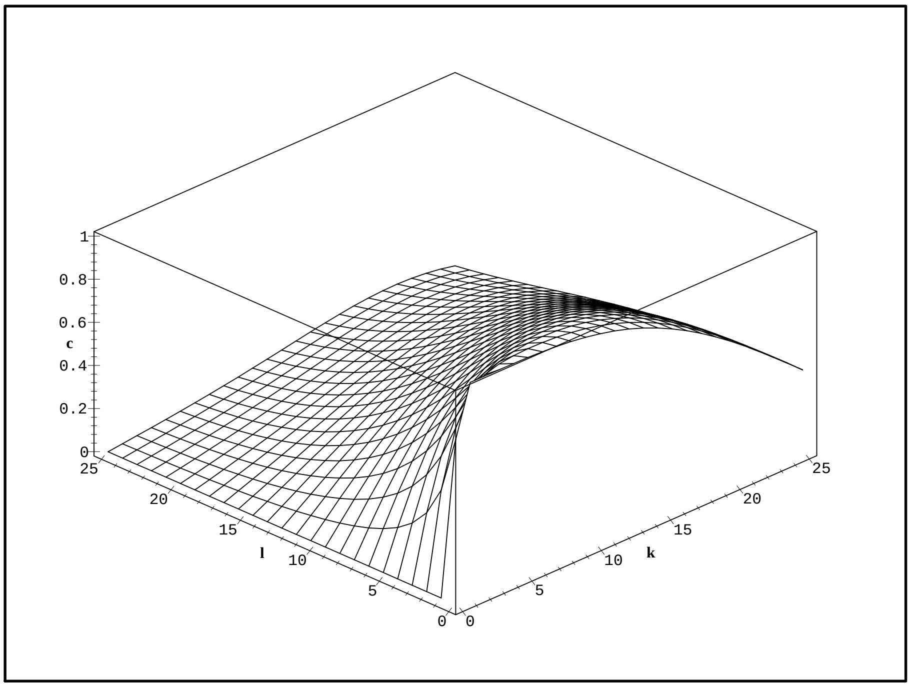

Figure 8.26: Group velocities of gravity waves in the λ-direction for the two-step OQSC method on a C-grid. Group velocities of all scales are positive.

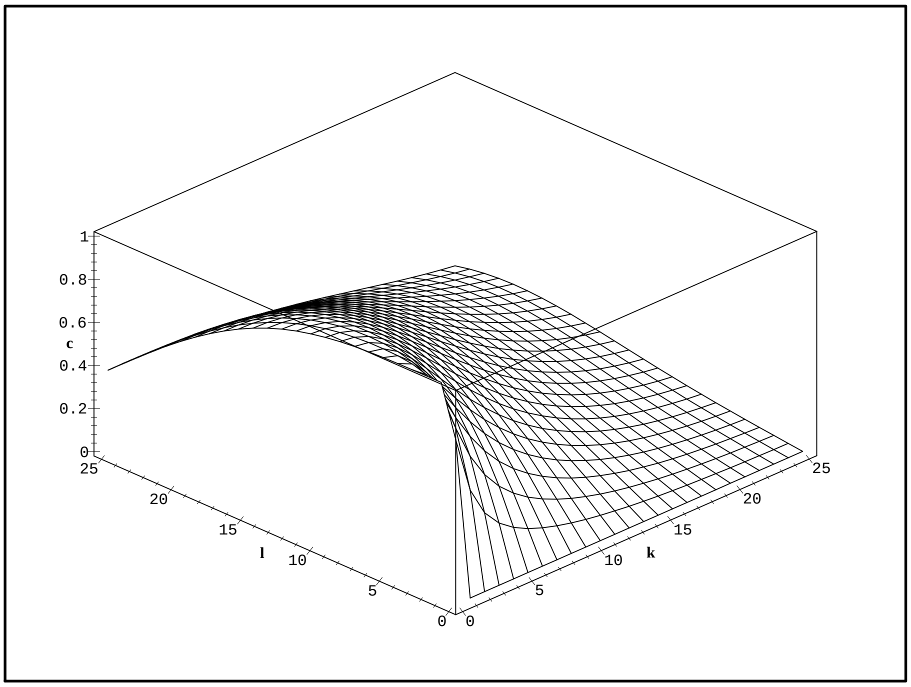

Figure 8.27: Group velocities of gravity waves in the θ-direction for the two-step OQSC method on a C-grid. Group velocities of all scales are positive.

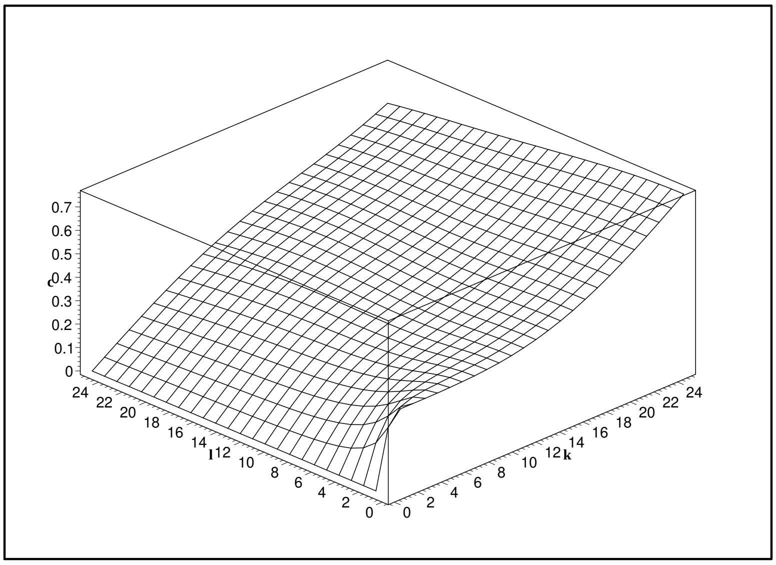

Figure 8.28: Group velocity errors of gravity waves in the λ-direction for the QSG method on a C-grid.

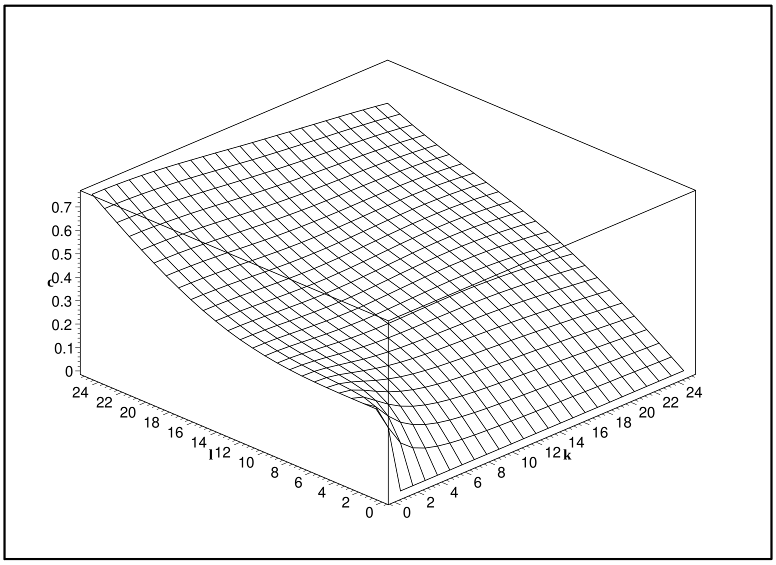

Figure 8.29: Group velocity errors of gravity waves in the θ-direction for the QSG method on a C-grid.

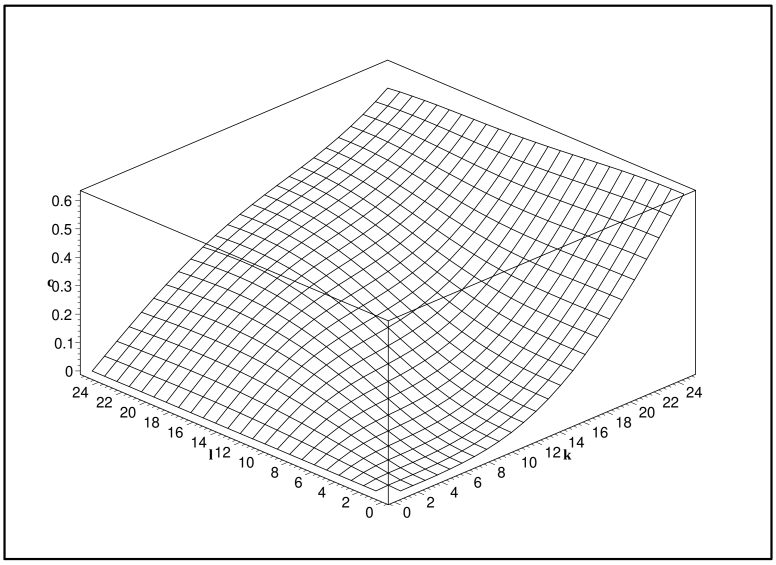

Figure 8.30: Group velocity errors of gravity waves in the λ-direction for the QSC method on a C-grid.

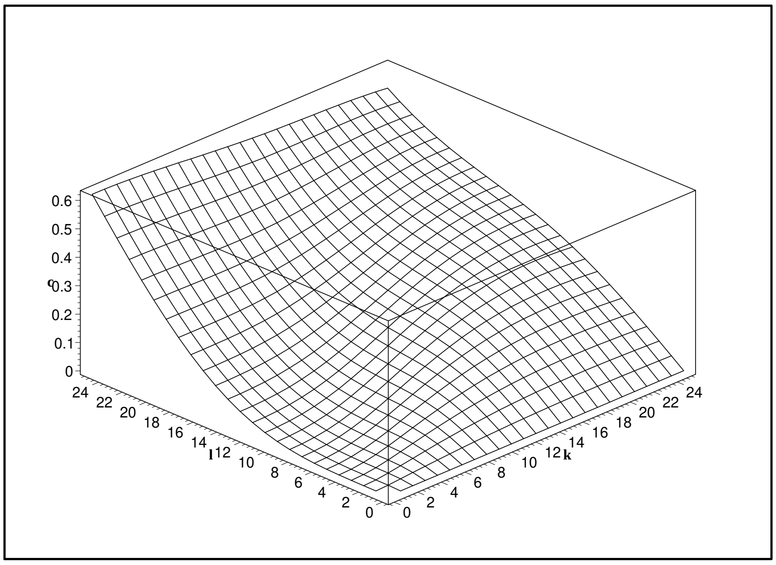

Figure 8.31: Group velocity errors of gravity waves in the θ-direction for the QSC method on a C-grid.

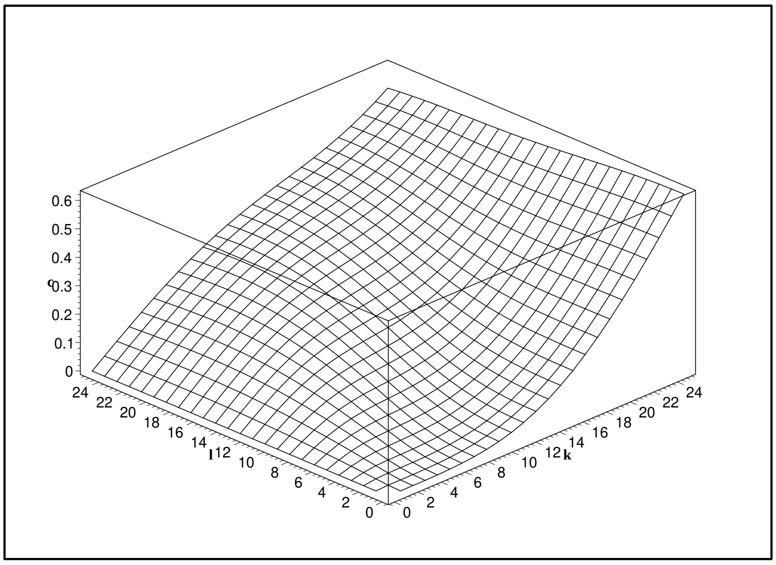

Figure 8.32: Group velocity errors of gravity waves in the λ-direction for the one-step OQSC method on a C-grid.

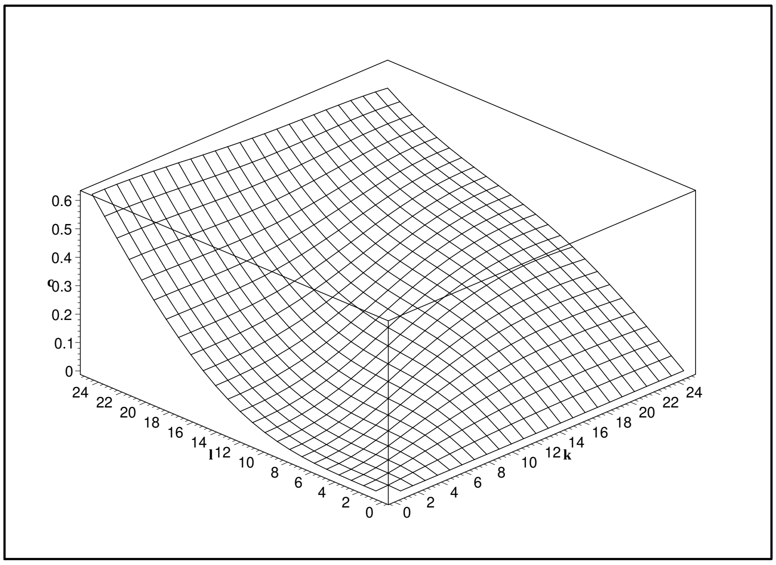

Figure 8.33: Group velocity errors of gravity waves in the θ-direction for the one-step QSC method on a C-grid.

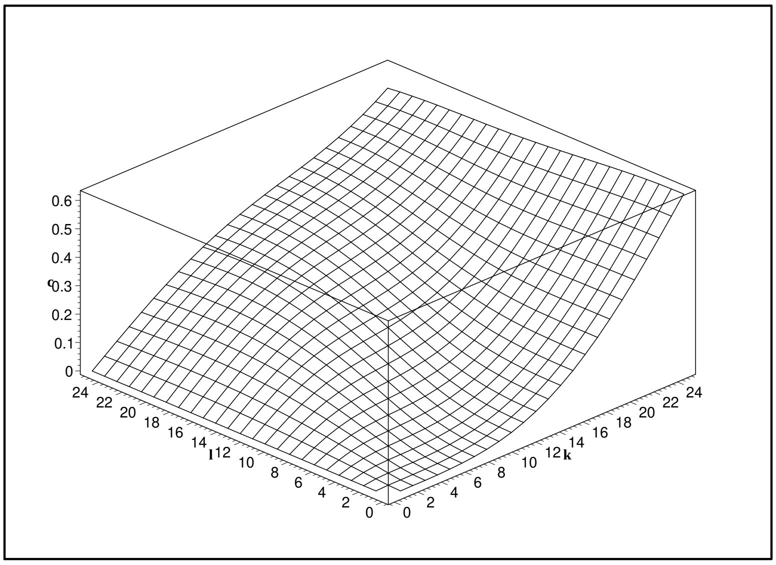

Figure 8.34: Group velocity errors of gravity waves in the λ-direction for the two-step OQSC method on a C-grid.

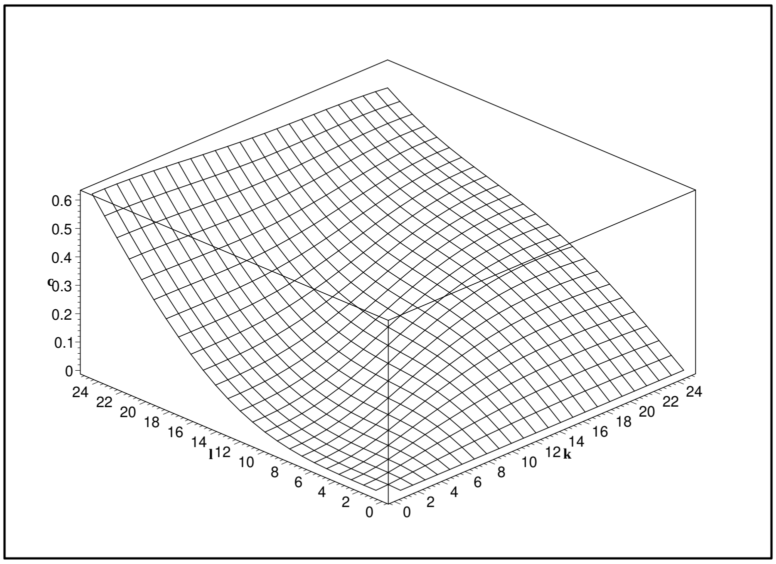

Figure 8.35: Group velocity errors of gravity waves in the θ-direction for the two-step QSC method on a C-grid.

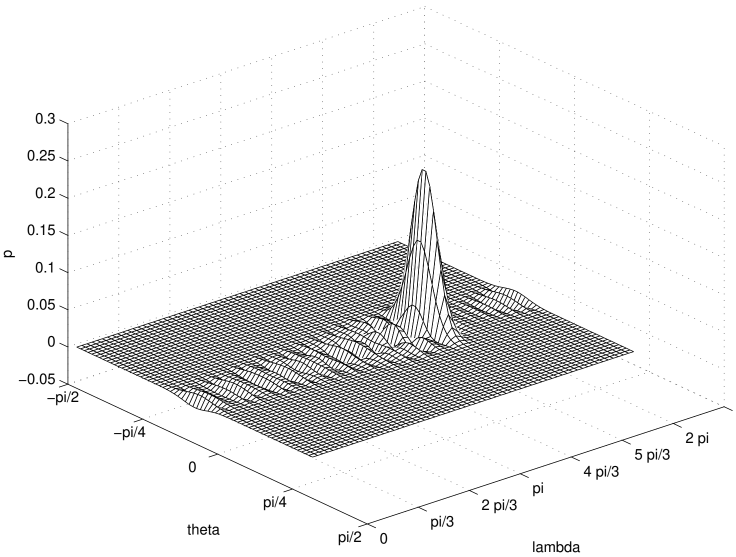

Figure 8.36: Simulation of gravity waves propagating eastward (in the increasing λ-direction) with the two-step OQSC method on an A-grid. Some gravity waves travel in the wrong direction.

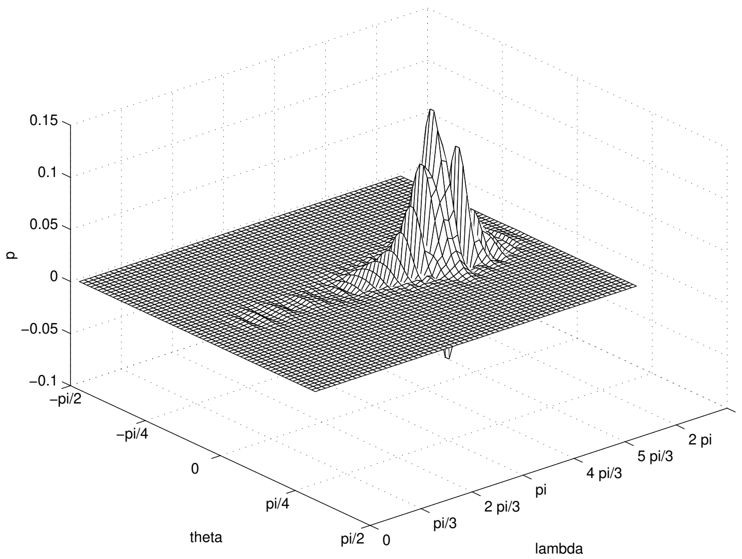

Figure 8.37: Simulation of gravity waves propagating eastward (in the increasing λ-direction) with the two-step OQSC method on a B-grid. Again, some gravity waves propagate in the wrong direction (in the decreasing λ-direction).

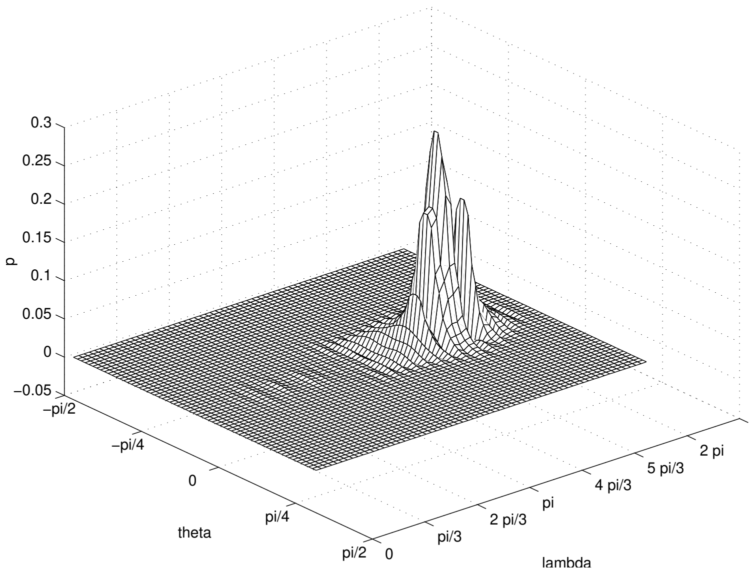

Figure 8.38: Simulation of gravity waves propagating eastward (in the increasing λ-direction) with the two-step OQSC method on a C-grid. The group velocities of waves of wavelengths have been captured correctly.

Chapter 9

Conclusions

9.1 Results

Spatial discretization schemes commonly used in meteorological applications are currently limited to spectral methods or low-order finite-difference/finite-element methods. In order to improve spatial accuracy, we present three algorithms that combine the semi-Lagrangian semi-implicit (SLSI) time integration method and high-order spatial discretization methods for solving the shallow water equations on the sphere. All three spatial discretization methods investigated in this thesis belong to the class of weighted residual methods and are based on quadratic splines. The following is a summary of the contributions of this thesis.

1. We point out that, when spatial discretization is done on staggered grids using quadratic splines, the boundary conditions at the poles may not be given at the end points for some partitions. In Section 3.2.4, we explain how the quadratic spline basis functions should be adjusted to satisfy the latitudinal boundary conditions associated with $\hat{\Delta}_\theta$ (see Section 3.1.1), where the poles are midpoints instead of gridpoints.

2. With the SLSI time discretization method, the functions are integrated or averaged along fluid trajectories. In the time-discretized equations, functions at time-level t_n are evaluated at *upstream points*. In Section 3.5, we explain how such upstream functions should be represented in the biquadratic spline approximation space, and how their nonhomogeneous boundary conditions should be handled.

3. We combine the quadratic spline Galerkin (QSG) method with the SLSI method to solve the shallow water equations, and discuss how the inner products should be evaluated when spatial discretization is done on staggered grids. We also demonstrate mathematically, on both the unstaggered grid and the C-grid, the existence and uniqueness of the numerical solution for the simplified shallow water equations (2.12) to (2.14) with biperiodic boundary conditions.

4. In Chapter 5, we describe how the shallow water equations can be solved using a combination of the SLSI method and the one-step and two-step optimal quadratic spline collocation (OQSC) methods. Previous work on OQSC methods is limited to unstaggered grids. We extend the OQSC methods to a system of first-order differential equations on staggered grids. As we have done for QSG, we demonstrate mathematically, on both the unstaggered grid and the C-grid, the existence of a unique solution for the OQSC methods for the simplified shallow water equations (2.12) to (2.14) with biperiodic boundary conditions.

5. In Chapter 6, we present some numerical results which support our conjecture that the QSG and OQSC methods have a fourth-order spatial convergence rate. We also compare these methods to the second-order linear spline Galerkin and the standard (non-optimal) quadratic spline collocation methods. We also compute the computational costs of the methods on our test problems, and conclude that, among the methods studied, the two-step OQSC method is the most efficient, in the sense that it achieves the smallest error for a given amount of computational

work.

6. With linear stability analysis, Staniforth and Mitchell [30] showed that if Cartesian coordinates are used, $f = 0$ is assumed and biperiodic boundary conditions are applied, then the Helmholtz equation should be derived algebraically rather than analytically in order for the standard spatial discretization methods to be neutrally stable for the Rossby waves. We extend their study and demonstrate similar results in spherical coordinates with a Coriolis parameter f that is not necessarily zero. We then verify, using Boyd's equatorial soliton test case, that the QSG and the OQSC methods, when applied in conjunction with the SLSI method, are indeed stable and non-dispersive for the Rossby waves.

7. Finally, we compare the performance of the QSG, QSC and OQSC methods on three different staggered grids, first mathematically through linear stability analysis, and then experimentally with the Kelvin wave test problem. We find that the C-grid offers the best accuracy for gravity waves for the new discretization methods studied in this thesis, confirming the general agreement that the C-grid is best for the standard discretization methods.

9.2 Future Work

It is our plan to theoretically prove the convergence behaviour, which have been shown numerically in this thesis, for the QSG and OQSC methods. Work is in progress for deriving the error bounds for, as well as the existence and uniqueness of, the solution for the OQSC method for a one-dimensional first-order system discretized on a staggered grid. Our next goal is to prove similar results for the two-dimensional case.

The spectral methods, which yield high-order solutions, give rise to dense matrices and are therefore non-scalable. On the other hand, finite-element methods are readily parallelizable. Therefore, high-order finite element methods seem to be a viable alternative to spectral methods. The techniques presented in this thesis for quadratic spline methods should be extendible to higher order spline methods, assuming the extra boundary conditions required by high order splines are set appropriately and the appropriate perturbation terms for collocation are derived. It would be an interesting project to compare the performance of spectral and high order finite element methods.

The spherical coordinate system suffers from many problems at the poles. For instance, the wind velocity components u and v take on multiple values at the poles. To avoid this difficulty, we compute, instead, the wind images U and V, which vanish at the poles by construction. Close to the poles, however, U and V tend to be small, which may generate large errors when the values of u and v are recovered to compute the fluid trajectories. Though this has not caused any noticeable problem in our experiments, how best to cope with the "pole problem" should nonetheless be investigated further.

The boundary conditions on U and V at the poles are naturally homogeneous Dirichlet, and those for the geopotential ϕ are designed to mimic the behaviour of its spherical harmonic expansion, for which the normal derivative vanishes at the poles. Though these boundary conditions have been adopted in the literature, it is conceivable that the geopotential may be changing along the latitude at the poles (i.e. have a nonzero normal derivative). A consistent and realistic set of boundary conditions, or a novel spatial discretization may prove to be interesting research projects.

The NCAR shallow water equations test set, developed by Williamson et. al. [36], which is composed of seven test cases with different levels of complexity, is designed to evaluate numerical methods proposed for weather prediction and climate modeling, and will be used to further verify that our methods indeed perform well on these problems in comparison with other currently adopted numerical methods such as the spectral transform method. Special attention will be paid to the spatial convergence behaviour of the numerical solution, and its sensitivity, if any, at the poles.

Given their computational intensity, weather prediction problems are perfect candidates for parallel implementation. Therefore, it is our goal to develop numerical methods that are scalable on massively parallel machines. Based on finite-element schemes, our methods lead to sparse matrices and therefore generate relatively little global communication, compared to the spectral transform methods which give rise to dense matrices. A parallel version of our code will be developed, and then tested with one of the problems in the NCAR test set that is identified as an efficiency benchmark for assessing the performance of parallel algorithms.

The next logical step beyond the shallow water equations test problem is to build a primitive equation dynamical core. A primitive equation dynamical core differs from the shallow water model in that the former is three-dimensional, includes temperature and also viscosity and hence allows turbulent flows [17]. Though the shallow water model includes many important characteristics present in more comprehensive atmospheric models, it is insufficient in part because it includes only deterministic cases. A primitive equation dynamical core, on the other hand, includes turbulent cascade in which dissipation is an important component. The Held-Suarez test [18] and/or the Boer-Denis [3] test may be used to determine the stability and accuracy of the methods, and the sensitivity to resolution, timestep and adaptive timesteps.

Appendix A

The Discrete Operators

In this appendix, we present the explicit forms of the quadratic spline Galerkin (QSG) and the quadratic spline collocation (QSC) operators, as well as their eigenvectors and the associated eigenvalues. Throughout, biperiodic boundary conditions are assumed. Let $\imath \equiv \sqrt{-1}$. Let the following vectors ϑ_k and $\hat{\vartheta}_k$ in the λ-direction be defined by

$$\vartheta_k = \left(e^{\imath k j \Delta\lambda}\right)_{j=0}^{N_\lambda - 1}, \quad \hat{\vartheta}_k = \left(e^{\imath k (j+\frac{1}{2})\Delta\lambda}\right)_{j=0}^{N_\lambda - 1} \tag{A.1}$$

where $\Delta\lambda = 2\pi/N_\lambda$ and $k = 0, \cdots, N_\lambda - 1$. Similarly in the θ-direction, we define

$$\vartheta'_l = \left(e^{\imath l j \Delta\theta}\right)_{j=0}^{N_\theta - 1}, \quad \hat{\vartheta}'_l = \left(e^{\imath l (j+\frac{1}{2})\Delta\theta}\right)_{j=0}^{N_\theta - 1} \tag{A.2}$$

where $\Delta\theta = 2\pi/N_\theta$ and $l = 0, \cdots, N_\theta - 1$. Note that $\hat{\vartheta}_k = e^{\imath k \Delta\lambda/2}\vartheta_k$, and similarly that $\hat{\vartheta}'_l = e^{\imath k \Delta\theta/2}\vartheta'_l$. These vectors are useful in deriving the eigenvalues of the linear operators considered in this appendix.

A.1 The Quadratic Spline Galerkin Method

A.1.1 The Matrices

The matrices associated with the QSG method can be obtained by analytically computing the inner products of the quadratic spline basis functions defined in Section 3.1.1. With biperiodic boundary conditions, the mass matrices are found to be:

$$
\begin{aligned}
P_{i,j} &= \frac{1}{\Delta\lambda}\int_{\lambda_0}^{\lambda_{N_\lambda}} \beta_j^P(\lambda)\beta_i^P(\lambda)d\lambda, \quad Q_{k,l} = \frac{1}{\Delta\theta}\int_{\theta_0}^{\theta_{N_\theta}} \beta_l^P(\theta)\beta_k^P(\theta)d\theta \\
\Rightarrow P,\ Q &= \frac{1}{120}\begin{bmatrix} 66 & 26 & 1 & & & 1 & 26 \\ 26 & 66 & 26 & 1 & & & 1 \\ 1 & 26 & 66 & 26 & 1 & & \\ & & & \vdots & & & \\ & & & 1 & 26 & 66 & 26 & 1 \\ 1 & & & & 1 & 26 & 66 & 26 \\ 26 & 1 & & & & 1 & 26 & 66 \end{bmatrix} \\
P_{i,j}^{\Delta\to\hat{\Delta}} &= \frac{1}{\Delta\lambda}\int_{\lambda_0}^{\lambda_{N_\lambda}} \beta_j^P(\lambda)\hat{\beta}_i^P(\lambda)d\lambda, \quad Q_{k,l}^{\Delta\to\hat{\Delta}} = \frac{1}{\Delta\theta}\int_{\theta_0}^{\theta_{N_\theta}} \beta_l^P(\theta)\hat{\beta}_k^P(\theta)d\theta \\
\Rightarrow P^{\Delta\to\hat{\Delta}},\ Q^{\Delta\to\hat{\Delta}} &= \frac{1}{3840}\begin{bmatrix} 1682 & 1682 & 237 & 1 & & & 1 & 237 \\ 237 & 1682 & 1682 & 237 & 1 & & & 1 \\ 1 & 237 & 1682 & 1682 & 237 & 1 & & \\ & & & \vdots & & & & \\ & & 1 & 237 & 1682 & 1682 & 237 & 1 \\ 1 & & & 1 & 237 & 1682 & 1682 & 237 \\ 237 & 1 & & & 1 & 237 & 1682 & 1682 \\ 1682 & 237 & 1 & & & 1 & 237 & 1682 \end{bmatrix}
\end{aligned}
$$

for $i, j = 1, \cdots, N_\lambda$ and $k, l = 1, \cdots, N_\theta$. We have also $P^{\hat{\Delta}\to\Delta} = (P^{\Delta\to\hat{\Delta}})^T$ and $Q^{\hat{\Delta}\to\Delta} = (Q^{\Delta\to\hat{\Delta}})^T$. The first derivative matrices are defined below:

$$
P_{\lambda i,j} = \frac{1}{\Delta\lambda}\int_{\lambda_0}^{\lambda_{N_\lambda}} \beta_j^{P'}(\lambda)\beta_i^P(\lambda)d\lambda, \quad Q_{\theta k,l} = \frac{1}{\Delta\theta}\int_{\theta_0}^{\theta_{N_\theta}} \beta_l^{P'}(\theta)\beta_k^P(\theta)d\theta
$$

$$\Rightarrow P_\lambda,\ Q_\theta \quad = \quad \frac{1}{24\Delta s}\begin{bmatrix} 0 & 10 & 1 & & & & -1 & -10 \\ -10 & 0 & 10 & 1 & & & & -1 \\ -1 & -10 & 0 & 10 & 1 & & & \\ & & & \vdots & & & & \\ & & & -1 & -10 & 0 & 10 & 1 \\ 1 & & & & -1 & -10 & 0 & 10 \\ 10 & 1 & & & & -1 & -10 & 0 \end{bmatrix}$$

$$P_{\lambda}{}^{\Delta\to\hat\Delta}_{i,j} \quad = \quad \frac{1}{\Delta\lambda}\int_{\lambda_0}^{\lambda_{N_\lambda}} \beta_j^{P'}(\lambda)\hat\beta_i^{P}(\lambda)d\lambda, \quad Q_{\theta}{}^{\Delta\to\hat\Delta}_{k,l} = \frac{1}{\Delta\theta}\int_{\theta_0}^{\theta_{N_\theta}} \beta_l^{P'}(\theta)\hat\beta_k^{P}(\theta)d\theta$$

$$\Rightarrow P_\lambda^{\Delta\to\hat\Delta},\ Q_\theta^{\Delta\to\hat\Delta} \quad = \quad \frac{1}{384\Delta s}\begin{bmatrix} -154 & 154 & 75 & 1 & & & -1 & -75 \\ -75 & -154 & 154 & 75 & 1 & & & -1 \\ -1 & -75 & -154 & 154 & 75 & 1 & & \\ & & & \vdots & & & & \\ & & -1 & -75 & -154 & 154 & 75 & 1 \\ 1 & & & -1 & -75 & -154 & 154 & 75 \\ 75 & 1 & & & -1 & -75 & -154 & 154 \\ 154 & 75 & 1 & & & -1 & -75 & -154 \end{bmatrix}$$

for $i,j = 1,\cdots,N_\lambda$ and $k,l = 1,\cdots,N_\theta$, whereas $P_\lambda^{\hat\Delta\to\Delta} = -(P_\lambda^{\Delta\to\hat\Delta})^T$ and $Q_\theta^{\hat\Delta\to\Delta} = -(Q_\theta^{\Delta\to\hat\Delta})^T$. In the above definitions, $\Delta s = \Delta\lambda$ for the P-matrices and $\Delta\theta$ for the Q-matrices. Finally, the stiffness matrices have the following form:

$$P_{\lambda\lambda i,j} \quad = \quad \frac{1}{\Delta\lambda}\int_{\lambda_0}^{\lambda_{N_\lambda}} \beta_j^{P''}(\lambda)\beta_i^{P}(\lambda)d\lambda, \quad Q_{\theta\theta k,l} = \frac{1}{\Delta\theta}\int_{\theta_0}^{\theta_{N_\theta}} \beta_l^{P''}(\theta)\beta_k^{P}(\theta)d\theta$$

$$\Rightarrow P_{\lambda\lambda},\ Q_{\theta\theta} \quad = \quad \frac{1}{6\Delta s^2}\begin{bmatrix} -6 & 2 & 1 & & & & 1 & 2 \\ 2 & -6 & 2 & 1 & & & & 1 \\ 1 & 2 & -6 & 2 & 1 & & & \\ & & & \vdots & & & & \\ & & & 1 & 2 & -6 & 2 & 1 \\ 1 & & & & 1 & 2 & -6 & 2 \\ 2 & 1 & & & & 1 & 2 & -6 \end{bmatrix}$$

for $i, j = 1, \cdots, N_\lambda$ and $k, l = 1, \cdots, N_\theta$.

A.1.2 Spectral Properties

Below we give the form of the eigenvalues of P, P_λ and $P_{\lambda\lambda}$. Note that with biperiodic boundary conditions, both ϑ_k and $\hat{\vartheta}_k$, defined in (A.1), are eigenvectors of P, P_λ and $P_{\lambda\lambda}$. The eigenvalue p_k for P corresponding to both ϑ_k and $\hat{\vartheta}_k$ is

$$\begin{aligned} p_k &= \frac{1}{120}\left[2\cos(2k\Delta\lambda) + 52\cos(k\Delta\lambda) + 66\right] \\ &= \frac{1}{60}\left\{\left[1 - 8\sin^2\left(\frac{k\Delta\lambda}{2}\right)\left(1 - \sin^2\left(\frac{k\Delta\lambda}{2}\right)\right)\right] + 26\left[1 - 2\sin^2\left(\frac{k\Delta\lambda}{2}\right)\right] + 33\right\} \\ &= \frac{1}{15}\left[15 - 15\sin^2\left(\frac{k\Delta\lambda}{2}\right) + 2\sin^4\left(\frac{k\Delta\lambda}{2}\right)\right] \qquad \text{(A.3)} \end{aligned}$$

while that for P_λ is

$$\begin{aligned} p_{\lambda k} &= \frac{\imath}{24\Delta\lambda}\left[2\sin(2k\Delta\lambda) + 20\sin(k\Delta\lambda)\right] \\ &= \frac{\imath}{24\Delta\lambda}\left\{8\sin\left(\frac{k\Delta\lambda}{2}\right)\cos\left(\frac{k\Delta\lambda}{2}\right)\left[1 - 2\sin^2\left(\frac{k\Delta\lambda}{2}\right)\right] + 40\sin\left(\frac{k\Delta\lambda}{2}\right)\cos\left(\frac{k\Delta\lambda}{2}\right)\right\} \\ &= \imath\frac{2}{3\Delta\lambda}\sin\left(\frac{k\Delta\lambda}{2}\right)\cos\left(\frac{k\Delta\lambda}{2}\right)\left[3 - \sin^2\left(\frac{k\Delta\lambda}{2}\right)\right] \qquad \text{(A.4)} \end{aligned}$$

and that for $P_{\lambda\lambda}$ is

$$\begin{aligned} p_{\lambda\lambda k} &= \frac{1}{6\Delta\lambda^2}\left[2\cos(2k\Delta\lambda) + 4\cos(k\Delta\lambda) - 6\right] \\ &= \frac{1}{3\Delta\lambda^2}\left\{1 - 8\sin^2\left(\frac{k\Delta\lambda}{2}\right)\left(1 - \sin^2\left(\frac{k\Delta\lambda}{2}\right)\right) + 2\left[1 - 2\sin^2\left(\frac{k\Delta\lambda}{2}\right)\right] - 3\right\} \end{aligned}$$

$$= \frac{4}{3\Delta\lambda^2}\sin^2\left(\frac{k\Delta\lambda}{2}\right)\left[-3+2\sin^2\left(\frac{k\Delta\lambda}{2}\right)\right] \quad \text{(A.5)}$$

Similarly, ϑ_l' and $\hat{\vartheta}_l'$ are the eigenvectors of Q, Q_θ and $Q_{\theta\theta}$, and the corresponding eigenvalues, denoted by q_l, q_{θ_l} and $q_{\theta\theta_l}$, respectively, are similar to p_l, p_{λ_l} and $p_{\lambda\lambda_l}$, respectively.

The eigenvectors ϑ_l' and $\hat{\vartheta}_l'$ satisfy the following relations with the staggering matrices:

$$\begin{aligned} P^{\Delta\to\hat{\Delta}}\vartheta_k &= (e^{\imath k\frac{\Delta\lambda}{2}}p_k^{\rightarrow})\vartheta_k = p_k^{\rightarrow}\hat{\vartheta}_k, \quad P^{\hat{\Delta}\to\Delta}\hat{\vartheta}_k = (e^{-\imath k\frac{\Delta\lambda}{2}}p_k^{\rightarrow})\hat{\vartheta}_k = p_k^{\rightarrow}\vartheta_k \\ P_\lambda^{\Delta\to\hat{\Delta}}\vartheta_k &= (e^{\imath k\frac{\Delta\lambda}{2}}p_{\lambda_k}^{\rightarrow})\vartheta_k = p_{\lambda_k}^{\rightarrow}\hat{\vartheta}_k, \quad P_\lambda^{\hat{\Delta}\to\Delta}\hat{\vartheta}_k = (e^{-\imath k\frac{\Delta\lambda}{2}}p_{\lambda_k}^{\rightarrow})\hat{\vartheta}_k = p_{\lambda_k}^{\rightarrow}\vartheta_k \end{aligned} \quad \text{(A.6)}$$

where

$$\begin{aligned} p_k^{\rightarrow} &= \frac{1}{3840}\cdot 2\left[\cos\left(\frac{5k\Delta\lambda}{2}\right)+237\cos\left(\frac{3k\Delta\lambda}{2}\right)+1682\cos\left(\frac{k\Delta\lambda}{2}\right)\right] \\ &= \frac{1}{120}\cos\left(\frac{k\Delta\lambda}{2}\right)\left[120-60\sin^2\left(\frac{k\Delta\lambda}{2}\right)+\sin^4\left(\frac{k\Delta\lambda}{2}\right)\right] \quad \text{(A.7)} \\ p_{\lambda_k}^{\rightarrow} &= \imath\frac{2}{\Delta\lambda}\left[\sin\left(\frac{5k\Delta\lambda}{2}\right)+75\sin\left(\frac{3k\Delta\lambda}{2}\right)+154\sin\left(\frac{k\Delta\lambda}{2}\right)\right] \\ &= \imath\frac{32}{\Delta\lambda}\sin\left(\frac{k\Delta\lambda}{2}\right)\left[24-20\sin^2\left(\frac{k\Delta\lambda}{2}\right)+\sin^4\left(\frac{k\Delta\lambda}{2}\right)\right] \quad \text{(A.8)} \end{aligned}$$

The matrices $Q^{\Delta\to\hat{\Delta}}$, $Q^{\hat{\Delta}\to\Delta}$, $Q_\theta^{\Delta\to\hat{\Delta}}$ and $Q_\theta^{\hat{\Delta}\to\Delta}$ satisfy relations similar to (A.6), and the corresponding scalars, $q_l^{\rightarrow}$ and $q_{\theta_l}^{\rightarrow}$, are similar to $p_l^{\rightarrow}$ and $p_{\lambda_l}^{\rightarrow}$, respectively.

A.2 The Quadratic Spline Collocation Method

A.2.1 The Matrices

The matrices associated with the QSC method have narrower bandwidths than those of their QSG counterparts. With biperiodic boundary conditions, the mass matrices in the λ- and θ-directions are

$$P_{i,j} = \beta_j^P(\tau_{\lambda_i}), \quad Q_{k,l} = \beta_l^P(\tau_{\theta_k})$$

$$\Rightarrow P,\ Q = \frac{1}{8}\begin{bmatrix} 6 & 1 & & & 1 \\ 1 & 6 & 1 & & \\ & \vdots & & & \\ & & 1 & 6 & 1 \\ 1 & & & 1 & 6 \end{bmatrix}$$

$$P^{\Delta\to\hat{\Delta}}_{i,j} = \beta^P_j(\hat{\tau}_{\lambda_i}), \quad Q^{\Delta\to\hat{\Delta}}_{k,l} = \beta^P_l(\hat{\tau}_{\theta_k})$$

$$\Rightarrow P^{\Delta\to\hat{\Delta}},\ Q^{\Delta\to\hat{\Delta}} = \frac{1}{2}\begin{bmatrix} 1 & 1 & & & \\ & 1 & 1 & & \\ & & \vdots & & \\ & & & 1 & 1 \\ 1 & & & & 1 \end{bmatrix}$$

for $i, j = 1, \cdots, N_\lambda$ and $k, l = 1, \cdots, N_\theta$. Moreoever, $P^{\hat{\Delta}\to\Delta} = (P^{\Delta\to\hat{\Delta}})^T$ and $Q^{\hat{\Delta}\to\Delta} = (Q^{\Delta\to\hat{\Delta}})^T$. The first derivative matrices are defined by:

$$P_{\lambda_{i,j}} = \beta^{P'}_j(\tau_{\lambda_i}), \quad Q_{\theta_{k,l}} = \beta^{P'}_l(\tau_{\theta_k})$$

$$\Rightarrow P_\lambda,\ Q_\theta = \frac{1}{2\Delta s}\begin{bmatrix} 0 & 1 & & & -1 \\ -1 & 0 & 1 & & \\ & & \vdots & & \\ & & -1 & 0 & 1 \\ 1 & & & -1 & 0 \end{bmatrix}$$

$$P^{\Delta\to\hat{\Delta}}_{\lambda_{i,j}} = \beta^{P'}_j(\tau_{\hat{\lambda}_i}), \quad Q^{\Delta\to\hat{\Delta}}_{\theta_{k,l}} = \beta^{P'}_l(\hat{\tau}_{\theta_k})$$

$$\Rightarrow P^{\Delta\to\hat{\Delta}}_\lambda,\ Q^{\Delta\to\hat{\Delta}}_\theta = \frac{1}{\Delta s}\begin{bmatrix} -1 & 1 & & & \\ & -1 & 1 & & \\ & & \vdots & & \\ & & & -1 & 1 \\ 1 & & & & -1 \end{bmatrix}$$

for $i, j = 1, \cdots, N_\lambda$ and $k, l = 1, \cdots, N_\theta$, where $\Delta s = \Delta\lambda$ for the P-matrices and $\Delta\theta$ for the Q-matrices. Also, $P_\lambda^{\hat{\Delta}\to\Delta} = -(P_\lambda^{\Delta\to\hat{\Delta}})^T$ and $Q_\theta^{\hat{\Delta}\to\Delta} = -(Q_\theta^{\Delta\to\hat{\Delta}})^T$. Finally, the stiffness matrices are

$$
\begin{aligned}
P_{\lambda\lambda_{i,j}} &= \beta_j^{P''}(\tau_{\lambda_i}), \quad Q_{\theta\theta_{k,l}} = \beta_l^{P''}(\tau_{\theta_k}) \\
\Rightarrow P_{\lambda\lambda},\ Q_{\theta\theta} &= \frac{1}{\Delta s^2}\begin{bmatrix} -2 & 1 & & & 1 \\ 1 & -2 & 1 & & \\ & \vdots & & & \\ & & 1 & -2 & 1 \\ 1 & & & 1 & -2 \end{bmatrix}
\end{aligned}
$$

A.2.2 Spectral Properties

The spectral properties of the above matrices are summarized in this section. As in the QSG case, the vectors ϑ_k and $\hat{\vartheta}_k$ are eigenvectors of P, P_λ and $P_{\lambda\lambda}$. The associated eigenvalues, denoted by p_k, p_{λ_k} and $p_{\lambda\lambda_k}$, corresponding to both ϑ_k and $\hat{\vartheta}_k$, are [6]

$$
\begin{aligned}
p_k &= \frac{1}{8}\left[2\cos(k\Delta\lambda) + 6\right] \\
&= 1 - \frac{1}{2}\sin^2\left(\frac{k\Delta\lambda}{2}\right) && \text{(A.9)} \\
p_{\lambda_k} &= \frac{1}{2\Delta\lambda} 2\imath \sin(k\Delta\lambda) \\
&= \imath\frac{2}{\Delta\lambda}\sin\left(\frac{k\Delta\lambda}{2}\right)\cos\left(\frac{k\Delta\lambda}{2}\right) && \text{(A.10)} \\
p_{\lambda\lambda_k} &= \frac{1}{\Delta\lambda^2}\left[2\cos(k\Delta\lambda) - 2\right] \\
&= -\frac{4}{\Delta\lambda^2}\sin^2\left(\frac{k\Delta\lambda}{2}\right) && \text{(A.11)}
\end{aligned}
$$

The matrices $P^{\Delta\to\hat{\Delta}}$, $P^{\hat{\Delta}\to\Delta}$, $P_\lambda^{\Delta\to\hat{\Delta}}$ and $P_\lambda^{\hat{\Delta}\to\Delta}$ satisfy (A.6) with $p_k^{\rightarrow}$ and $p_{\lambda_k}^{\rightarrow}$ defined below:

$$
\begin{aligned}
p_k^{\rightarrow} &= \cos\left(\frac{k\Delta\lambda}{2}\right) && \text{(A.12)} \\
p_{\lambda_k}^{\rightarrow} &= \imath\frac{2}{\Delta\lambda}\sin\left(\frac{k\Delta\lambda}{2}\right) && \text{(A.13)}
\end{aligned}
$$

Similar results can be obtained in the θ-dimension.

A.3 The One-Step Optimal Quadratic Spline Collocation Method

A.3.1 The Matrices

Perturbed first derivative operators are defined in the one-step OQSC method. In the λ-direction,

$$
\begin{aligned}
P'_\lambda &= \left(I - \frac{\Delta\lambda^2}{24}\Lambda'_\lambda\right) P_\lambda \\
&= P_\lambda - \frac{\Delta\lambda^2}{24} \cdot \frac{1}{\Delta\lambda^2}
\begin{bmatrix}
-2 & 1 & & & & 1 \\
1 & -2 & 1 & & & \\
 & & \vdots & & & \\
 & & & 1 & -2 & 1 \\
1 & & & 1 & -2 &
\end{bmatrix}
\cdot \frac{1}{2\Delta\lambda}
\begin{bmatrix}
0 & 1 & & & & -1 \\
-1 & 0 & 1 & & & \\
 & & \vdots & & & \\
 & & & -1 & 0 & 1 \\
1 & & & & -1 & 0
\end{bmatrix} \\
&= P_\lambda - \frac{1}{48\Delta\lambda}
\begin{bmatrix}
0 & -2 & 1 & & & -1 & 2 \\
2 & 0 & -2 & 1 & & & -1 \\
-1 & 2 & 0 & -2 & 1 & & \\
 & & \vdots & & & & \\
 & & -1 & 2 & 0 & -2 & 1 \\
1 & & & -1 & 2 & 0 & -2 \\
-2 & 1 & & & -1 & 2 & 0
\end{bmatrix} \\
P_\lambda'^{\Delta\to\hat{\Delta}} &= \left(I + \frac{\Delta\lambda^2}{12}\Lambda'_\lambda\right) P_\lambda^{\Delta\to\hat{\Delta}}
\end{aligned}
$$

$$= P_\lambda^{\Delta\to\hat\Delta} + \frac{\Delta\lambda^2}{12}\cdot\frac{1}{\Delta\lambda^2}\begin{bmatrix} -2 & 1 & & & & 1 \\ 1 & -2 & 1 & & & \\ & & \vdots & & & \\ & & & 1 & -2 & 1 \\ 1 & & & & 1 & -2 \end{bmatrix}\cdot\frac{1}{\Delta\lambda}\begin{bmatrix} -1 & 1 & & & \\ & -1 & 1 & & \\ & & \vdots & & \\ & & & -1 & 1 \\ 1 & & & & -1 \end{bmatrix}$$

$$= P_\lambda^{\Delta\to\hat\Delta} + \frac{1}{12\Delta\lambda}\begin{bmatrix} 3 & -3 & 1 & & & & -1 \\ -1 & 3 & -3 & 1 & & & \\ & -1 & 3 & -3 & 1 & & \\ & & & \vdots & & & \\ & & & -1 & 3 & -3 & 1 \\ 1 & & & & -1 & 3 & -3 \\ -3 & 1 & & & & -1 & 3 \end{bmatrix}$$

and $P_\lambda'^{\hat\Delta\to\Delta} = -\left(P_\lambda'^{\Delta\to\hat\Delta}\right)^T$. Perturbed operators in the θ-direction are defined similarly.

A.3.2 Spectral Properties

The perturbed operators satisfy equations similar to (A.6) with $p_k'^{\to}$ and $p_{\lambda_k}'^{\to}$ defined as follows:

$$\begin{aligned} p'_{\lambda_k} &= p_{\lambda_k} - \frac{\imath}{48\Delta\lambda}\left(2\sin(2k\Delta\lambda) - 4\sin(k\Delta\lambda)\right) \\ &= \imath\frac{2}{\Delta\lambda}\sin\left(\frac{k\Delta\lambda}{2}\right)\cos\left(\frac{k\Delta\lambda}{2}\right)\left[1+\frac{1}{6}\sin^2\left(\frac{k\Delta\lambda}{2}\right)\right] \\ p'^{\to}_{\lambda_k} &= p^{\to}_{\lambda_k} + \frac{\imath}{12\Delta\lambda}\left(2\sin(k\Delta\lambda) - 6\sin\left(\frac{k\Delta\lambda}{2}\right)\right) \\ &= \imath\frac{1}{6\Delta\lambda}\sin\left(\frac{k\Delta\lambda}{2}\right)\left[9+2\cos\left(\frac{k\Delta\lambda}{2}\right)\right] \end{aligned}$$

In the θ-direction, $q_l'^{\to}$ and $q_{l_\theta}'^{\to}$ are defined similarly.

Bibliography

[1] G. K. Batchelor. *An Introduction to Fluid Dynamics*. Cambridge University Press, 1992.

[2] J. R. Bates and A. McDonald. Multiply-upstream, semi-Lagrangian advection schemes: analysis and application to a multi-level primitive equation model. *Monthly Weather Review*, 110:1831–1842, 1982.

[3] G. J. Boer and B. Denis. Numerical convergence of the dynamics of a gcm. Workshop on Test Cases for Dynamics Cores of Atmospheric General Circulation Models, June 1996.

[4] John P. Boyd. Equatorial solitary waves. Part I: Rossby solitons. *Journal of Physical Oceanography*, 10:1699–1717, November 1980.

[5] John P. Boyd. The nonlinear equatorial Kelvin wave. *Journal of Physical Oceanography*, 10:1–11, January 1980.

[6] C. C. Christara. Quadratic spline collocation methods for elliptic partial differential equations. *BIT*, 34(1):33–61, 1994.

[7] Christina C. Christara and Barry Smith. Multigrid and multilevel methods for quadratic spline collocation. *BIT*, 37(4):781–803, 1997.

[8] Anthanasia Constas. Fast Fourier transform solvers for quadratic spline collocation. M.Sc. Thesis, Department of Computer Science, University of Toronto, Toronto, Ontario, Canada, 1996.

[9] Jean Côté. Variable resolution techniques for weather prediction. *Meteorology and Atmospheric Physics*, 63:31–38, 1997.

[10] Jean Côté, Jean-Guy Desmarais, Sylvie Gravel, André Méthot, Alain Patoine, Michel Roch, and Andrew Staniforth. The operational CMC-MRB Global Environment Multiscale (GEM) model. Part II: Results. *Monthly Weather Review*, 126:1397–1416, June 1998.

[11] Jean Côté, Sylvie Gravel, André Méthot, Alan Patoine, Michel Roch, and Andrew Staniforth. The operational CMC-MRB Global Environmental Multiscale (GEM) model. Part I: Design considerations and formulation. *Monthly Weather Review*, 126:1373–1395, June 1998.

[12] Jean Côté and Andrew Staniforth. A two-time-level semi-Lagrangian semi-implicit scheme for spectral methods. *Monthly Weather Review*, 116:2003–2012, August 1988.

[13] Jean Côté and Andrew Staniforth. An accurate and efficient finite-element global model of the shallow water equations. *Monthly Weather Review*, 118:2707–2717, 1990.

[14] Carl de Boor. *A Practical Guide to Splines.* New York: Springer-Verlag, 1978.

[15] Dale R. Durran. *Numerical Methods for Wave Equations in Geophysical Fluid Dynamics.* New York: Springer, 1999.

[16] Francis X. Giraldo and Beny Neta. Stability analysis for Eulerian and semi-Lagrangian finite element methods of the advection-diffusion equation. *Computers and Mathematics with Applications*, 38(2):97–112, 1997.

[17] George J. Haltiner and Roger T. Williams. *Numerical Prediction and Dynamic Meteorology*. John Wiley and Sons, 1980.

[18] Isaac Held and Max J. Suarez. A proposal for the intercomparison of the dynamical cores of atmospheric general circulation models. *Bulletin of American Meteorological Society*, pages 1825–1830, 1994.

[19] James R. Holton. *An Introduction to Dynamic Meteorology*. San Diego Academic Press, 1992.

[20] E. N. Houstis, C. C. Christara, and J. R. Rice. Quadratic-spline collocation methods for two-point boundary value problems. *International Journal for Numerical Methods in Engineering*, 26:935–952, 1988.

[21] Mohamed Iskandarani, Dale B. Haidvogel, and John P. Boyd. A staggered spectral element model with application to the ocean shallow water equations. *International Journal for Numerical Methods in Fluids*, 20:393–414, 1995.

[22] Hong Ma. A spectral element basin model for the shallow water equations. *Journal of Computational Physics*, 109:133–149, 1992.

[23] M. J. Marsden. Quadratic spline interpolation. *Bulletin of American Mathematics Society*, 30:903–906, 1974.

[24] A. McDonald. Accuracy of multiply-upstream, semi-Lagrangian advective schemes. *Monthly Weather Review*, 112:1267–1275, 1984.

[25] K. S. Ng. Quadratic spline collocation methods for systems of elliptic PDEs. M.Sc. Thesis, Department of Computer Science, University of Toronto, Toronto, Ontario, Canada, 67 pgs., April 2000.

[26] Harold Ritchie. Semi-Lagrangian advection on a Gaussian grid. *Monthly Weather Review*, 115:608–619, 1987.

[27] André Robert. A stable numerical integration scheme for the primitive meteorological equations. *Atmosphere-Ocean*, 19(1):35–46, 1981.

[28] Daniel T. Le Roux, Charles A. Lin, and Andrew Staniforth. A semi-implicit semi-Lagrangian finite-element shallow-water ocean model. *Monthly Weather Review*, 126:1931–1951, July 1998.

[29] R. D. Russell and L. F. Shampine. A collocation method for boundary value problems. *Numerische Mathematik*, 19:1–28, 1972.

[30] Andrew Staniforth and Herschel Mitchell. A semi-implicit finite-element barotropic model. *Monthly Weather Review*, pages 154–169, February 1977.

[31] Andrew Staniforth and Clive Temperton. Semi-implicit semi-Lagrangian integration schemes for barotropic finite-element regional model. *Monthly Weather Review*, 111:2078–2090, November 1986.

[32] Paul N. Swarztrauber. Spectral transform methods for solving the shallow-water equations on the sphere. *Monthly Weather Review*, 124:730–743, April 1996.

[33] Monique Tanguay, André Robert, and René Laprise. A semi-implicit semi-Lagrangian fully compressible regional forecast model. *Monthly Weather Review*, 118:1970–1980, October 1990.

[34] S. Thomas, J. Côté, and A. Staniforth. A semi-implicit semi-Lagrangian shallow-water model for massively parallel processors. Manuscript, 1993.

[35] D. L. Williamson and R. Laprise. Numerical approximations for global atmospheric general circulation models. *Numerical Modelling of the Global Atmosphere in the Climate System*, 2000.

[36] David L. Williamson, John B. Drake, James J. Hack, Rudiger Jakob, and Paul N. Swarztrauber. A standard test set for numerical approximations to the shallow water

equations in spherical geometry. *Journal of Computational Physics*, 102(1):211 – 224, 1992.